GOLD AND SILVER NANOPARTICLES: CHARACTERIZATION OF THEIR INTERESTING OPTICAL PROPERTIES AND THE MECHANISM OF THEIR PHOTOCHEMICAL FORMATION

A Dissertation
Presented to
The Academic Faculty

by

Susie Eustis

In Partial Fulfillment
of the Requirements for the Degree
Doctor of Philosophy in the
School of Chemistry and Biochemistry
College of Science

Georgia Institute of Technology
August 2006

GOLD AND SILVER NANOPARTICLES: CHARACTERIZATION OF THEIR INTERESTING OPTICAL PROPERTIES AND THE MECHANISM OF THEIR PHOTOCHEMICAL FORMATION

Approved by:

Dr. Mostafa A. El-Sayed, Advisor
School of School of Chemistry and Biochemistry
Georgia Institute of Technology

Dr. Z.L. Wang
School of Material Science and Engineering
Georgia Institute of Technology

Dr. Thomas Orlando
School of School of Chemistry and Biochemistry
Georgia Institute of Technology

Dr. Robert Whetten
School of Chemistry and Biochemistry
Georgia Institute of Technology

Dr. Joe Perry
School of School of Chemistry and Biochemistry
Georgia Institute of Technology

Date Approved: May 10,2006

To my mother who listened to my ideas, offered suggestions, and always me gave her time, energy, and encouragement.

ACKNOWLEDGEMENTS

I wish to thank my Advisor, Dr. Mostafa A. El-Sayed, the whole laser dynamics laboratory and the staff of the School of Chemistry and Biochemistry at Georgia Tech. I also wish to thank all my friends and family.

TABLE OF CONTENTS

LIST OF TABLES

LIST OF FIGURES

SUMMARY

This thesis has been divided into three parts. The first part provides a description of the properties of polydispersed gold nanorod solutions. The second part describes the photochemical synthesis of metal nanoparticles using benzophenone as a photosensitizer. The last part presents the mechanism of photochemical reduction of tetrachloroauric(III) acid and tetrabromoauric(III) acid solutions in ethylene glycol. Elaborations of the experimental results are presented below.

An introduction to metal nanoparticles describing the synthetic strategies to generate nanoparticles, the origin of the optical properties, and many applications of the optical and catalytic properties are presented. There is a large electromagnetic field created on the surface of metal nanoparticles that can be utilized to enhance the optical absorption, fluorescence, and scattering on the nanoscale.

Some synthetic techniques to generate metal nanoparticles are described. The challenges and successful strategies for the synthesis of high quality samples are presented. Kinetic control is observed in the chemical seeding technique, where the temperature of the growth solution is of great importance to generate desired nanorods. The absorption coefficient of gold nanorods of high aspect ratio are determined and compared to previous values. This synthetic method is used for nanorods samples in further experiments.

Using the absorption spectrum of the gold nanorods generated by the chemical seeding technique, a method is developed to determine the aspect ratio distribution of the sample referred to as the Gold Nanorod Optical Modeling Equations (GNOME) method.

The observed inhomogeneously broadened longitudinal plasmon resonance absorption spectrum is fitted with a distribution of homogeneously broadened absorption spectra of different aspect ratios calculated using Gans equation. The sensitivity of the longitudinal plasmon resonance to the aspect ratio makes this technique an ideal candidate to determine properties of the polydispersed gold nanorod solutions synthesized. This method also provides a fast, easy, and inexpensive method of determining the average aspect ratio and the distribution of gold nanorods in solution without the need for TEM analysis.

The fluorescence spectra of five different solutions of nanorods along with the theoretical calculation of the predicted emission of these rods are compared. The emission of the high aspect ratio nanorods decreases in intensity, contrary to what was reported previously. The decrease of the fluorescence is due to a decrease in the overlap between the interband transition, which is responsible for the fluorescence emission and the longitudinal plasmon resonance absorption, which is responsible for the enhancement. The theoretical equations for the enhancement factor of the fluorescence emission are presented with the inclusion of the intrinsic emission of bulk gold. The use of the aspect ratio distribution obtained from the GNOME method described above are critical to obtain a reasonable agreement between the theoretical predictions and the experimental results.

The size and shape distributions of nanoparticles resulting from photothermal melting of low and high aspect ratio gold nanorods after exposure to fs laser irradiation are determined. It was predicted by Lord Rayleigh that nanorods of aspect ratio >4.5 melt to form multiple particles instead of melting to form a single sphere. All rods

investigated (aspect ratio 3, 5, 5.5 and 6) are observed to melt into spheres with a slight reduction in the number of atoms from that of the parent rod. It is also observed that a similar percentage of atoms are lost from all nanorods examined. Since the laser wavelength is kept constant at 800nm for all of these samples, nanorods, which have absorption near this wavelength, are melting in each sample due to the overlap of the longitudinal plasmon resonance with the laser wavelength. Although the average aspect ratio of different samples changes, many of the nanorods that melt have the same aspect ratio regardless of the average aspect ratio of a given solution due to photoselection. The large polydispersity of each of these samples also contributes to the difficulty in determining if high aspect ratio nanorods melt to form multiple particles in solution. Other factors such as the effect of capping material and ablation processes could increase the aspect ratio at which the rods would melt to form multiple nanoparticles.

The photosensitization with benzophenone to generate metal nanoparticles is described. Benzophenone (BP) is used as a photosensitizer in aqueous solution. This allows photoreduction of gold and silver ions in different environments. The light source and size of the nanoparticles formed are investigated. A fs laser is used as the light source and is found to give narrower plasmon resonance absorptions and particle distributions than the cw mercury lamp. Twenty nanometer particles are generated at short irradiation times and low laser powers. As the time of irradiation or the intensity of the light increases, the nanoparticles begin to absorb the incident irradiation, and fragment to generate large populations of small nanoparticles.

The effect of different forms of silica is investigated on the synthesis of gold and silver nanoparticles. Silica films can be used as a carrier for the BP, allowing the BP to

be introduced immediately before irradiation, and removed afterwards, allowing a minimal amount of BP to diffuse into the aqueous solution. This method leads to a controlled reduction, and larger stability of nanoparticles. Silica powders can be used as a transport agent to remove the metal ions from solution by attaching BP to silica powder. The silica powder to which metal nanoparticles are attached can then be removed by centrifugation. Silica films with silver ions or gold ions imbedded can be photoreduced when in contact with a BP-alcohol solution. This allows generation of conducting silica films, or stable supports for silver and gold nanoparticles used for catalysis.

The absorption spectrum of tetrachloroauric(III) acid in water and alcohol solutions is measured. Hydrolysis is only observed in the aqueous solution at high pH's. The hydrogen-binding environment of the solvent affects the absorption spectrum of tetrachloroauric(III) acid. The number of bromide ions attached to a gold ion in mixed bromo-chloroauric(III) acid is also calculated from the absorption spectrum.

The results of the photochemical reduction of tetrachloroauric(III) acid are presented as the solvent is changed from water to ethylene glycol. The disproportionation of metastable chloroauric acid intermediates and the reduction by ethylene glycol are important to the formation of gold nanoparticles. The maximum rate of gold nanoparticle formation is found at 0.40 mole fraction of ethylene glycol in ethylene glycol-water mixed solvent. This suggests that two conflicting effects of ethylene glycol take place in the reaction. The glycol is able to reduce the excited state of the gold molecule, but because of the high viscosity of the solvent and with the diffusion limited disproportionation of $Au^{(1+)}Cl_2^-$ a maximum rate of nanoparticle formation is found at 0.40 mole fraction ethylene glycol.

The investigation of the replacement of chloride ions with bromide ions in tetrachloroauric(III) acid is presented. When tetrabromoauric(III) acid is used, gold nanoparticle formation is not observed. This is suggested to be due to the steric effects of the bromide ions during the diffusion controlled disproportionation reactions that produce gold atoms, which form the nanoparticles. If silver ions are added to the tetrachloroauric(III) acid or tetrabromoauric(III) acid solutions, formation of gold nanoparticles is accelerated. This is explained by the removal of the halide ions formed during the disproportionation reactions. This leads to a shift in the equilibria involving these reactions that increase the concentration of atomic gold responsible for the nanoparticle formation.

CHAPTER 1

INTRODUCTION TO NOBLE METAL NANOPARTICLES[†]

Abstract

An introduction to the field of noble metal nanoparticles is presented with a description of how the particles are created, the scientific procedures used to observe the surface plasmon resonance absorption, and current applications. New properties are observed on the nanoscale due to the lack of symmetry at the interface and electron confinement that do not scale linearly with size. The origin of the surface plasmon resonance is explored and synthesis procedures of nanoparticles are detailed. A number of applications are presented. Nanoparticle catalysts lower the activation energy of the reaction, and thus increase the rate of reaction and the yield of the desired products with small amounts of material. Applications of metal nanoparticles generally take advantage of the electromagnetic field enhancement of noble metal nanoparticles resulting from the surface plasmon oscillations.

Introduction

Noble metal nanoparticles show brilliant colors due to the surface plasmon resonance absorption. The examination of the surface plasmon resonance absorption is part of a large ongoing research field to investigate properties on the nanometer scale.[1, 2] The color of metal nanoparticles is found to depend on the shape and size of the nanoparticle and dielectric constant of the surrounding medium, leading to many studies

[†] Eustis, S.; El-Sayed, M. A., Why Gold Nanoparticles Are More Precious than Pretty Gold: Noble Metal Surface Plasmon Resonance and its Enhancement of the Radiative and Nonradiative Properties of Nanocrystals of Different Shapes. *Chem. Soc. Rev.* **2006,** 35, (3), 209-217.

on their synthesis and applications. Studies seek to identify the characteristics of nanoparticles, contributing to the basic science in a manner that creates the ability to use nanoparticles for many applications. Table 1-1 shows a collection of recent review articles and the techniques and concepts covered in these reviews.

Table 1-1: *Some useful review articles in the field of noble metal nanoparticles*

Topic	Articles					
General Reviews	Intro[1, 2]	Intro, synthesis assembly and applications[3]	Shape based[4]	Optical and electronic[5-7]	Photocatalytic and photochemical[8]	Core-shell optical properties[9]
Synthesis	Seeded[10]	Dendrimer intro level[11]	Dendrimer[12]	Wires, rods, belts and tubes[13]	Reverse micelle[14, 15]	
Separation	Super critical fluid[16]					
Lithography	Conventional[17]	Unconventional[18]				
Uses	Nanosphere lithography[19]	Intro to Raman[20]	Comprehensive review of Raman[21]	Single Molecule SERS[22]	Biodiagnostics[23]	Biological uses[24, 25]
Uses (cont.)	Fluorescence enhancement and quenching[26]	Fluorescence effects[27]	Functionalization[28]	Optical componets[29]	Shape catalysis[30]	
Assemblies	Intro[31]	Clusters[32]	On electrodes[33]	Synthesis and applications[34, 35]	Waveguides[36]	
Theory	Absorption and DDA of anisotropic nanoparticle[37]	Optical properties by shape and size[38]	Bulk[39]			

Nanotechnology

The study of atoms and molecules is the conventional field of chemistry. An atom measures about 1 angstrom, or 10^{-10} meters. Studies in the late 19th and 20th century established that the nanometer (nm), or 10^{-9} meters, represents a collection of a few atoms or molecules. Properties of bulk substances of micrometer sizes or larger have been studied for years by solid state physicists and material scientists and are currently well understood.

Materials on the 1-100nm scale have shown that on this size scale the properties of a material become dependent on its size and shape. New properties develop on the nanoscale due to the lack of symmetry at the interface or to electron confinement that does not scale linearly with size. Thus, the nanometer scale (1-100nm) incorporates collections of atoms or molecules, whose properties are neither those of the individual constituents nor those of the bulk. On this scale, many of the atoms are still located on the surface, or one layer removed from the surface, as opposed to the interior.

The interface between substances is just now beginning to be understood. New properties are observed on this scale due to the interface that is not observed in the bulk or individual atoms. Since the properties depend on the size of the structure, instead of just the nature of the material, reliable and continual change can be achieved using a single material. Quantum dots of CdSe of different sizes have differing emission maxima across the whole visible region,[40, 41] and gold and silver nanostructures have absorption across most of the visible region.[1, 2, 42, 43]

The nanometer scale is also interesting in biological systems.[23-25] Many proteins are ~10's of nm in size. Since structures can be accurately designed on the nanometer

scale they can be incorporated into biological systems, due to the similar size scales. Biological systems are complex, with synthesis, structure, and function all rarely understood in detail. The ability to rationally design structures on the same size as biological molecules generates the ability to probe and modify biological systems. Furthermore, biological systems are used to build up nanomaterials of specific shape and function. Nanostructures are being used as drug delivery agents, labeling agents, sensors, and to enhance electromagnetic fields.

Nanotechnology for life sciences represents an attempt to address problems ranging from painful and inefficient drug delivery to the need for faster medical diagnosis and analysis. Quantum dots have been used in medical imaging with the ability to differentiate many different areas of a cell with a single excitation source. They have advantages over traditional fluorescent dyes that they are more photostable than conventional dyes, and the same chemistry can be used to modify different colors for entry into the biological sample.

The field of nanotechnology has received attention with the number of publications of gold and silver nanoparticles growing exponentially, as shown in Figure 1-1. The major publications in this area have appeared in the Journal of Physical Chemistry B, Journal of the American Chemical Society and Langmuir. Nano Letters has also published a large number of letters in this field since its conception in 2001. The number of patent applications and symposium articles for the Materials Research Society (MRS), the American Chemical Society (ACS) and Advanced Materials also represent a large number of the publications every year on noble metal nanoparticles. The recent

growth in the number of publications observed in Figure 1-1 is due to the recognition of the new and changing properties on the nanoscale.

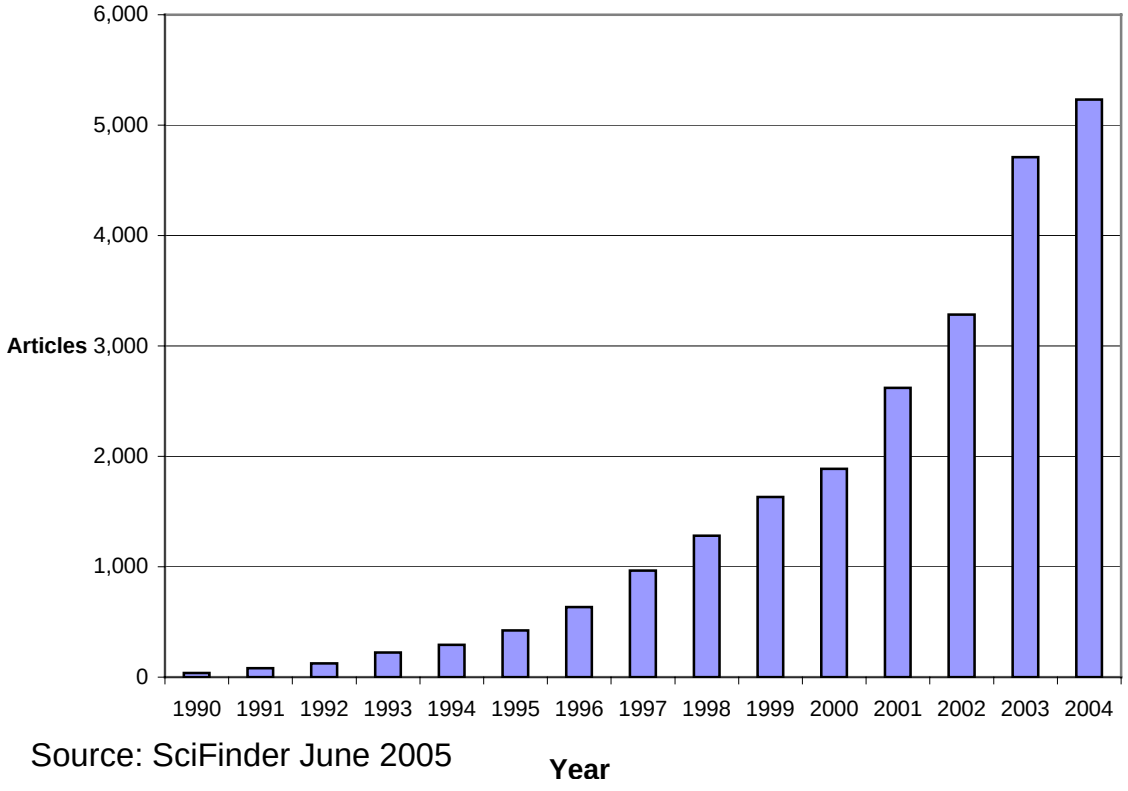

Figure 1-1: *Plot of the number of articles published on gold and silver nanoparticles since 1990.*

Discoveries have led to the observation that new properties exist when the size of materials is on the nanoscale due to electronic confinement in semi-conductors and surface effects in metals. The nanoparticle literature has been and continues to be dominated by synthetic papers. The difficulty in generating the desired size, shape, and monodisperisty of nanoparticles continues to press the need for new and refined synthetic techniques. Generation of the desired chemical and physical interfaces to interact with target molecules also require the need for many different synthetic techniques of generating metal nanoparticles. The percent (and also number) of papers describing the

applications of nanoparticles has increased as nanoparticles are better understood and more researchers are finding useful applications for the nanoparticles. (Source: SciFinder Scholar v. 2004, accessed June 2005.) Thus, the synthesis of nanoparticles continues to be an active area of research as new and improved synthetic techniques are developed, expanding the use of nanoparticles. This increase in the available nanoparticles generates an increase in the number of applications, driving the potential for great advances in every day life due to nanotechnology. One of the hottest areas for nanoparticle use is in biological systems, due to their potential application in medicine.

Semiconductor Nanoparticle Quantum Confinement

In semiconductors the nanoscale becomes important due to the quantum confinement of the electrons.[41] As the particle size decreases below the Bohr radius of the semiconductor material used, the electron becomes more confined in the particle.[41] This leads to an increase in the band gap energy. Furthermore the valence and conduction bands break into quantized energy levels.[41] The study by Bawendi,[40] where CdSe spherical nanoparticles of various sizes are generated illustrates the macroscopic realization of quantized energy levels. The band gap emission shown in Figure 1-2 is observed to shift through the entire visible region, from red emission for the largest particles, to blue emission for the smallest clusters.

The significance of nanoscale quantum confinement of the electrons provides visualization of the shift in the characteristics of the material depending on the size of the nanoparticles. Electrons are not as free to move, creating new samples that hold promise for new applications.

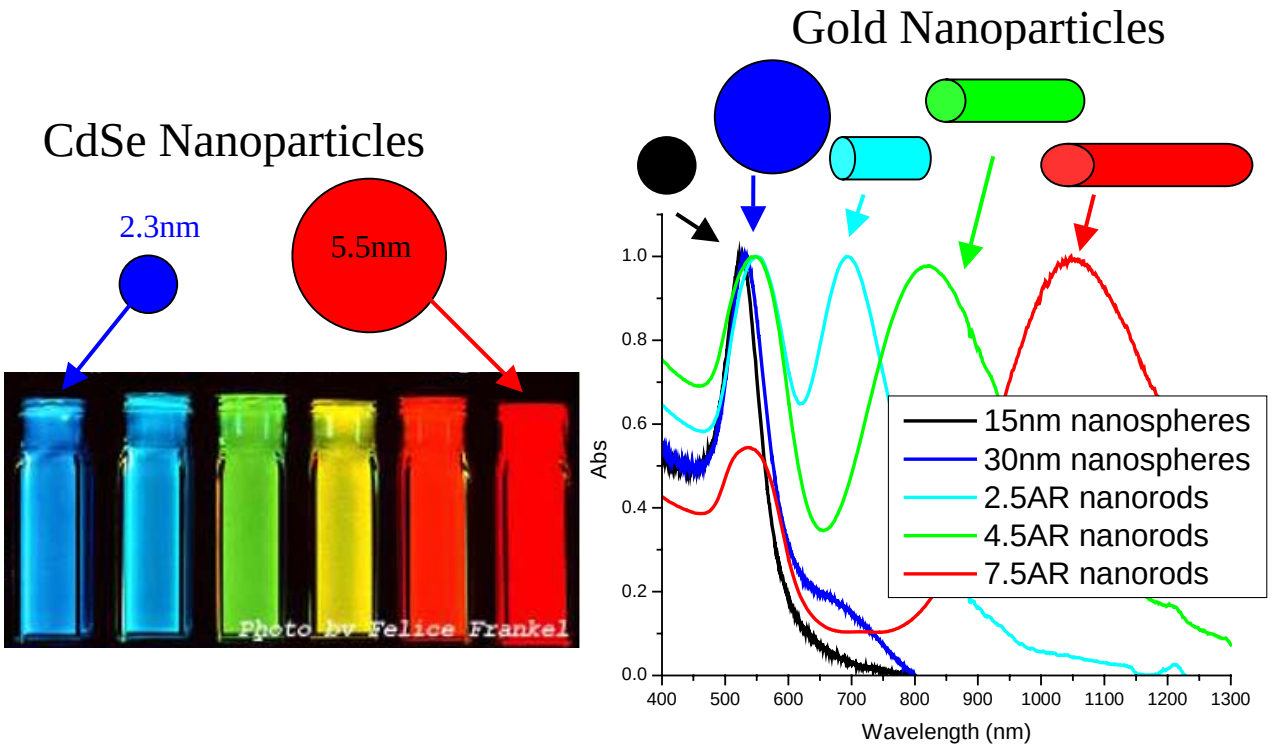

Figure 1-2: *Fluorescence emission of (CdSe)ZnS quantum dots of various sizes*[40] *(*Reproduced with permission from *J. Phys. Chem. B* **1997**, *101,* 9463-9475. Copyright 1997 Am. Chem. Soc.) *and gold nanoparticles absorption of various sizes and shapes.*

Noble Metal Nanoparticles

Methods have long been known to generate beautifully colored glass for cathedrals by adding gold to generate burgundy, red, or purple glass.[3] Faraday[44] attributed this color to very finely divided colloidal gold, or gold nanoparticles. As the size or shape of the nanoparticle changes, the observed color also changes. Gold nanospheres have a characteristic red color, while silver nanospheres are yellow. The color is due to the collective oscillation of the electrons in the conduction band, known as the surface plasmon oscillation. More details of the origin of this plasmon resonance are described in the next section. The oscillation frequency is usually in the visible region for gold and silver giving rise to the strong surface plasmon resonance absorption. This

means that the origins of properties on the nanoscale are different for metal nanoparticles than for semiconductor nanoparticles.

Figure 1-2 shows the difference in the optical properties of metal and semiconductor nanoparticles. With the CdSe semiconductor nanoparticles, a simple change in size alters the optical properties of the nanoparticles. When metal nanoparticles are enlarged, their optical properties change only slightly as observed for the different samples of gold nanospheres in Figure 1-2. However, when an anisotropy is added to the nanoparticle the optical properties of the nanoparticles can change dramatically. Many applications became possible because of the enhancement of the surface electric field on the metal nanoparticles surface.

The plasmon resonance absorption of gold nanoparticles has an absorption coefficient orders of magnitude larger than strongly absorbing dyes. Anisotropic shapes have plasmon resonance absorptions that are even stronger, leading to increased detection sensitivity. Metal nanoparticles generate enhanced electromagnetic fields that affect the local environment. These electromagnetic fields are significantly stronger than observed from the bulk material. The fields determined by the geometry of the nanoparticle enhance fluorescence of the metal, the Raman signal of a molecule on the surface, and the scattering of light.

The origin of the plasmon resonance and its applications presented in the following sections introduce the importance of nanoparticle properties and current applications. The optical properties of noble metal nanoparticles lead to many uses as sensing and imaging techniques. Mirkin and co-workers[23] have pioneered the use of DNA in assembling and studying their interaction and their application in colorometric

detection of biological targets based on the binding events of target DNA. Nanoparticle use in the field of photonics[45] relates to exciting extensions of existing optical technology with control of dimensions on the nanometer scale.

Origin of Surface Plasmon Resonance in Noble Metal Nanoparticles

Free electrons in the metal (d electrons in silver and gold) travel through the material. The mean free path in gold and silver is ~50nm. In particles smaller than ~50nm, no scattering is expected from the bulk. This means interactions with the surface dominate. When the wavelength of light is much larger than the nanoparticle size it sets up standing resonance conditions as represented in Figure 1-3. Light in resonance with the surface plasmon oscillation causes the free-electrons in the metal to oscillate. As the wave front of the light passes, the electron density in the particle is polarized to one surface and oscillates in resonance with the light's frequency causing a standing oscillation. The resonance condition is determined from absorption and scattering spectroscopy and is found to depend on the shape, size, and dielectric constants of both the metal and the surrounding material. This is referred to as the surface plasmon resonance, since it is located at the surface. As the shape or size of the nanoparticle changes, the surface geometry changes, causing a shift in the electric field density on the surface. This causes a change in the oscillation frequency of the electrons, generating different cross-sections for the optical properties including absorption and scattering.

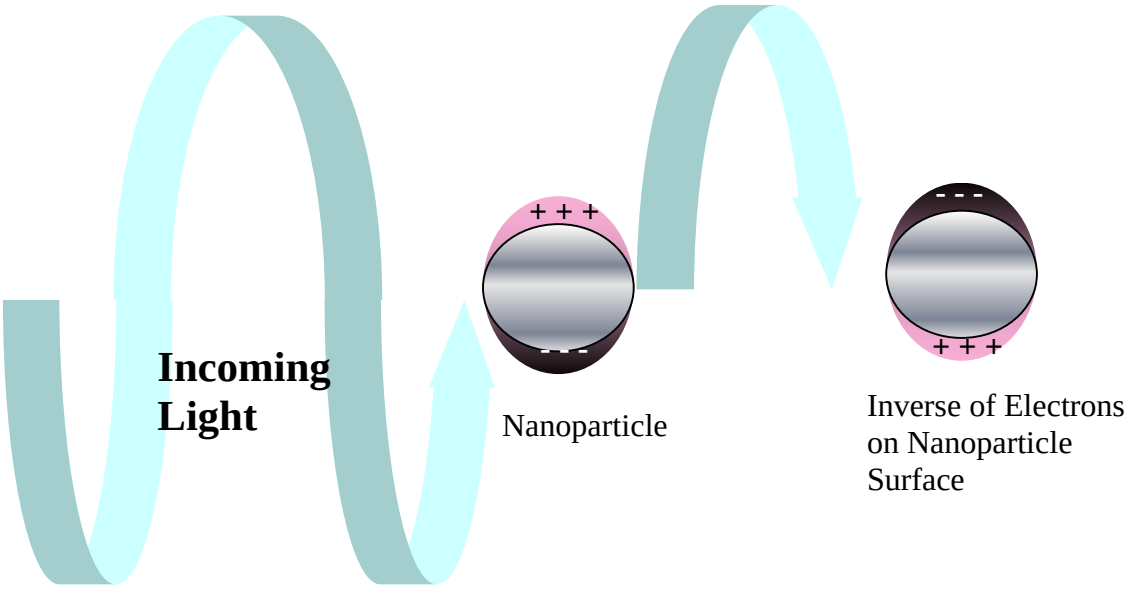

Figure 1-3: *Origin of surface plasmon resonance due to coherent interaction of the electrons in the conduction band with electromagnetic field*

The interaction of the metal nanoparticles can be described by Maxwell's equations and was solved for the case of spherical nanoparticles by Mie.[46] The total extinction and scattering efficiency Q_{ext} and Q_{sca} for a homogenous sphere are expressed in the following infinite series:

$$Q_{ext} = \frac{2}{x^2}\sum_{n=1}^{\infty}(2\varepsilon+1)\mathrm{Re}\left[a_n + b_n\right] \qquad (1.1)$$

$$Q_{sca} = \frac{2}{x^2}\sum_{n=1}^{\infty}(2\varepsilon+1)\left[a_n^2 + b_n^2\right] \qquad (1.2)$$

$$Q_{abs} = Q_{ext} - Q_{sca} \qquad (1.3)$$

$$a_n = \frac{m\psi_n(mx)\psi_n'(x) - \psi_n(x)\psi_n'(mx)}{m\psi_n(mx)\xi_n'(x) - m\xi_n(x)\psi_n'(mx)} \qquad (1.4)$$

$$b_n = \frac{\psi_n(mx)\psi_n'(x) - m\psi_n(x)\psi_n'(mx)}{\psi_n(mx)\xi_n'(x) - m\xi_n(x)\psi_n'(mx)} \qquad (1.5)$$

where ε is the refractive index of the metal, ε_m is the refractive index of the surrounding medium, m is the ratio of the refractive index of the sphere and the surrounding medium ($m = \varepsilon/\varepsilon_m$), R is the radius of the sphere, λ is the wavelength of light, x is the size parameter ($x = 2\pi n_m R/\lambda$), ψ_n and ξ_n are the Riccati-Bessel functions and the prime represents first differentiation with respect to the argument in parentheses. These expressions have been solved in the dipole approximation for spherical nanoparticles much smaller than the wavelength of light (<20nm) where only the dipole contributes to the absorption by the nanoparticle.[7, 46-48]

$$Q_{abs} = \frac{18\pi V \varepsilon_m^{3/2}}{\lambda} \times \frac{\varepsilon_2(\lambda)}{\left[\varepsilon_1(\lambda) + 2\varepsilon_m\right]^2 + \varepsilon_2(\lambda)^2} \qquad (1.6)$$

where V is the volume of the nanoparticle, ε_m is the dielectric constant of the surrounding medium, λ is the wavelength of light, and the dielectric constant of the metal is expressed in the complex form as a function of the wavelength of light, where $\varepsilon(\lambda) = \varepsilon_1(\lambda) + i\varepsilon_2(\lambda)$. This allows the calculation of the expected absorption and scattering spectra of small spherical metal nanoparticles.

Changing the dielectric constant of the surrounding material has an effect on the oscillation frequency due to the varying ability of the surface to accommodate electron charge density from the nanoparticles.[49] The expected shift in the absorption spectrum with changing medium dielectric constant (ε_m) can be calculated using equation 6. Changing the solvent changes the dielectric constant, but the capping material is most important in determining the shift of the plasmon resonance due to the local nature of its effect on the surface of the nanoparticle. Chemically bonded molecules can be detected by the observed change they induce in the electron density on the surface, which results

in a shift in the surface plasmon absorption maximum. This is the basis for the use of noble metal nanoparticles as sensitive sensors.

Mie[46] originally calculated the surface plasmon resonance by solving Maxwell's equations for small spheres interacting with an electromagnetic field. Gan[50, 51] was able to extend this theory to apply to ellipsoidal geometries. Modern methods using the discrete dipole approximation (DDA)[37, 38, 52] allows one to calculate the surface plasmon resonance absorption for arbitrary geometries. Calculation of the longitudinal plasmon resonance for gold nanorods generates an increase in the intensity and wavelength maximum as the aspect ratio (=length divided by width) increases.[1, 2, 5-7, 53-55] The plasmon resonance can be tuned across the visible region by changing the aspect ratio. [1, 2, 5-7, 53-55] The increase in the intensity of the surface plasmon resonance absorption leads to an enhancement of the electric field, as exploited in many applications described in detail in the following sections.

Many shapes of noble metal nanoparticles have been synthesized.[4, 10, 13, 15, 37, 42, 43, 56-62] Nanorods[5-7, 10, 63-66] have attracted the most attention, due to the ease of preparation, the large number of synthetic methods available, the high monodispersity possible, and the rational control over the aspect ratio, which is primarily responsible for the change in their optical properties. The two plasmon resonances[1] of nanorods are due to the transverse oscillation of the electrons around 520nm for gold and the longitudinal plasmon resonance at longer wavelengths as shown for various aspect ratios in Figure 1-2. The transverse surface plasmon resonance does not depend on the aspect ratio and is at the same wavelength as the plasmon resonance of spheres. The longitudinal surface plasmon resonance increases with larger aspect ratios. The

anisotropy has been shown to generate large control over the optical absorbance for all shapes generated.[38] Triangular nanoparticles have been generated by photochemical means[42, 43, 67] and chemical growth.[56-61] Arrays of triangular nanoparticles can also be synthesized with nanosphere lithography.[68] The edges and corners are very important with triangular nanoparticles. Snipping of the edges produces a visible blue shift in the plasmon resonance,[43] which can be modeled theoretically.[37, 38] Disks also display a similar plasmon resonance absorption dependence on their aspect ratio.[15]

Synthesis

Synthesis techniques to generate metal nanoparticles depend on isolation of small amounts of a material. There are two general strategies to obtain materials on the nanoscale.[24] The bottom up method is one where the atoms (produced from reduction of ions) are assembled to generate nanostructures. The top down method is where material is removed from the bulk material, leaving only the desired nanostructures. Common top down techniques are photolithography and electron beam lithography (generation of the mask). Top down techniques suffer from the need to remove large amounts of material. More detailed information of the synthesis techniques for metal nanoparticles used in the scope of this thesis are discussed in Chapter 2.

Bottom up techniques suffer from poor monodispersity due to the need to arrest growth at the same point for all the nanoparticles. Photolithography is limited by the diffraction limit in the size resolution of features currently of around 60nm, as it is based on the wavelength of the lasers available. As new techniques develop in producing laser pulse with shorter wavelengths, smaller nanostructures can be made by these techniques.

Electron beam lithography is not limited by resolution constraints. Instrumentation using this technology can produce nanostructures smaller than 10nm. However, commercial instrumentation is expensive. Both of these techniques are only able to create a 2-dimenional structure in a single step. Current research in multi-photon photolithography applied to soft materials[69] is working to remove both the size and the dimensional restrictions.

Nanosphere lithography[68], being a bottom up technique, is an inexpensive synthetic procedure to generate arrays of noble metal nanoparticles. A monolayer of closely packed monodisperse polystyrene spheres having sizes that are hundreds of micrometers in diameter is deposited onto a substrate that acts as a template for metal deposition. Metal is then deposited onto and in between the spheres using thermal evaporation to create particles in the voids of the polystyrene spheres. The polystyrene spheres can then be dissolved in organic solvents leaving an array of triangular shaped metal nanoparticles on the substrate as observed in Figure 1-4. This generates monodisperse, uncapped nanoparticles in geometric arrays over a large surface area of the substrate. Nanosphere lithography has generated large amounts of attention due to its ease of replication and high monodispersity of samples generated, both across one sample, and multiple trials. This technique is limited in absorption intensity due to the presence of only a monolayer of nanoparticles. However, the fact that prismatic particles have sharp corners, the absorption enhancement is so great that only ten thousand particles give excellent absorption on a microspectrometer.[70] Recently, Haes et. al. [71] have been able to release the triangular nanoparticles into solution by adding surfactant and sonicating the sample to remove the particles from the substrate to form isolated

particles or dimer pairs of triangular nanoparticles. Nanosphere lithography is being used to make sensors based on the position of the absorption maximum of the surface plasmon resonance. Due to the ease of fabrication, functionalization, and low cost per sample, this technique is useful in generating disposable units that can be used as sensors in many applications.

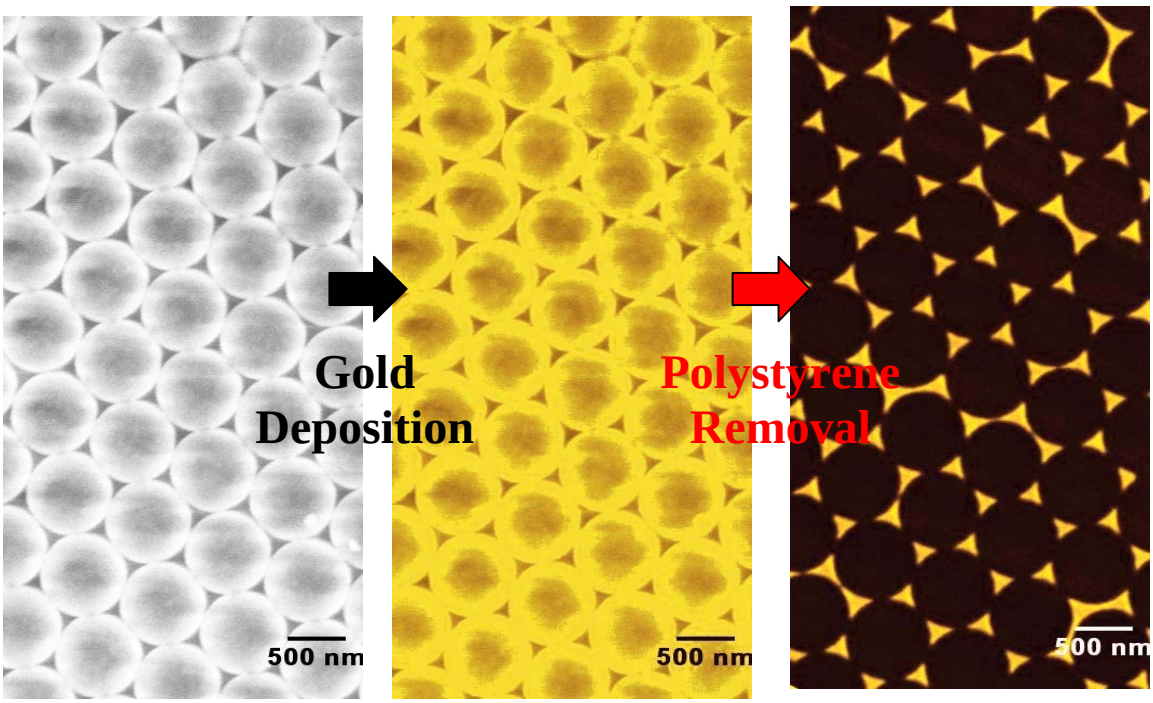

Figure 1-4: *Deposition of polystyrene spheres on substrate, thermal evaporation of bulk gold and removal of polystyrene spheres to leave triangular gold nanoparticles.*[72] Reproduced with permission from "Huang, Wenyu; Qian, Wei; El-Sayed, Mostafa. A, Optically detected coherent picosecond lattice oscillations in two dimensional arrays of gold nanocrystals of different sizes and shapes induced by femtosecond laser pulses" Proc. SPIE Int. Soc. Opt. Eng. 2005, 5927, 592701.

Bottom up techniques include templating,[73] chemical,[14, 57, 58, 60, 65, 74-76] electrochemical,[64, 77, 78] sonochemical,[79, 80] thermal[81-85] and photochemical reduction[42, 43, 63, 67, 86-96] have been used to generate nanoparticles.[3, 10] Bottom up synthesis techniques usually employ an agent to stop growth of the particle at the nanoscale.[8] Capping

materials, such as a surfactant or polymer are used in this technique to prevent aggregation and precipitation of the metal nanoparticles out of solution. Choice of the reduction technique, time, and capping material determine the size and shape of the nanoparticles generated. Spheres,[3, 10, 14, 15, 74, 75, 97] rods,[10, 63-66] cubes,[58, 76, 83, 84] disks,[15, 98-100] wires,[81, 82, 85] tubes, [13] branched,[37, 58, 62] triangular prisms,[37, 42, 43, 56-58, 60, 89, 101] and tetrahedral[67, 76, 85] nanoparticles have been generated in gold, silver and platinum with various reduction techniques and capping materials.

The amounts of nanoparticles synthesized by these techniques are usually small and the resulting particles are slightly different on every run. Many factors can affect the synthesis of nanoparticles, such as nucleation centers, temperature and humidity generating experimental challenges to generate narrow distributions of desired nanoparticles. Gold and silver nanoparticles are now commercially available both preconjugated and conjugated to popular analytes, but caution should be exercised as the samples will vary from batch to batch and could be contaminated by the chemicals used in the synthetic procedure. Choice of solvent and surface chemistry often narrow the possible synthetic techniques for the desired processes.

Generation of spherical gold nanoparticles is commonly carried out by the citrate reduction method[3] reported by Turkevitch[74] in 1951. Gold salt and citrate are stirred in water, while the temperature, the ratio of gold to citrate, and the order of addition of the reagents control the size distribution of gold nanospheres generated. Small metal clusters have been generated in dendrimers.[11, 12]

There are a large number of synthetic methods of generating nanorods[5-7, 10, 63-66] available providing rational control over the aspect ratio, which is primarily responsible

for the change in optical properties. It is this change in optical properties that makes the nanorods more desirable than nanospheres.

The seeding technique[10] is a popular method for generation of large spherical and non-spherical nanoparticles . A chemical reducing agent is used, where small, generally spherical nanoparticles are first generated and then added to a growth solution with more metal ions and surfactant to induce anisotropic growth. The seeds are generated with a strong reducing agent, such as sodium borohydride. The growth solution employs a weaker reducing agent (often ascorbic acid) to reduce the metal salt to an intermediate state so that only catalyzed reduction on the nanoparticle surface is allowed. Growth is believed to be due to kinetic conditions, limiting the control over size and shape. Proper seed, salt, and stabilizer concentrations are adjusted to generate nanorods. Counter ions and additives have also been found to play a role in directing growth and the final shape of nanoparticles obtained.[102] Nanorod growth is proposed to be due to a steric interaction of the stabilizer forming bilayer structures along the long axis of the nanorod to allow growth only along the short axis.[10] Having a seed with facets that are ready for growth is necessary to form anisotropic particles.

Two-phase reactions have been extensively used and studied to produce nanoparticles for generation of very small nanoparticles (1-5nm) with narrow disperisty.[3, 97, 103-108] The particles are stabilized by a gold-thiol bond. Samples generated with the two-phase method are stable for long periods of time when dry and can easily be redispersed in many organic solvents. In synthesis, the gold salt is first transferred to the organic phase using a suitable surfactant. Then sodium borohydride is added to the aqueous phase. The formation of nanoparticles is monitored by the generation of the

orange to deep brown color in the organic phase. The ratio of gold to surfactant and the reaction temperature control particle size and dispersity. This synthetic procedure is often referred to as generating monolayer-protected clusters (MPCs) due to the monolayer coverage of the sulfur groups and the small size of nanoparticles generated. Many improvements to this synthesis procedure have been reported[3] to generate small monodisperse gold nanoparticles.

Inverse micelles[14, 15] have been used to generate many different sizes and shapes of nanoparticles. Inverse micelles use surfactants to create small pockets of a water phase in an organic solvent, where the surfactant has a polar group that faces the aqueous phase, and the tail faces the organic phase. Adding water will linearly affect the size of the micelle generated,[14] leading to an increase in the size of the nanoparticles generated. The key to generating single crystal, monodisperse nanoparticles in inverse micelles is to use a metal salt conjugated to the surfactant prior to the addition of the reducing agent. The inverse micelles allow for exchange between different water volumes, generating good monodispersity of nanoparticles, and can be used for many different materials.[14]

Applications of Noble Metal Nanoparticles

Catalysis

Catalysis drives many reactions, with the ability to lower the activation energy of the reaction, and thus increases the rate of reaction and the yield of the desired products. The use of nanoparticles as catalysts has increased as nanoparticle properties and reactions are better understood. The possibility of using less material and having different properties for different shapes of nanoparticles is very attractive. Nanoparticle catalysis has been investigated for both homogeneous (catalyst and reactants are both in

solution) and heterogeneous (catalyst supported on a substrate) systems. A recent review has many of the references important for current research into nanocatalysis.[30]

Small clusters are also found to be very catalytically active, even for materials that display very limited reactivity on the bulk scale.[109, 110] For example, bulk gold is considered a noble metal, and is very un-reactive in the bulk state. However, small clusters of gold are found to be catalytically active. Many possible explanations have been proposed[109, 110] for the difference in reactivity between clusters and bulk gold. They include the electronic and chemical properties of nanoparticles or the shape, size and oxidation state of the nanoparticles. The surface support is also suggested to be responsible for the catalytic activity.[109] The crystal structure of gold has also been proposed to be important in the catalytic properties. This demonstrates new properties for nanoparticles, which are unexpected based on bulk behavior since bulk gold has no catalytic activity, and clusters are efficient catalysts, generating further interest in nanomaterials as new functionality is present on the nanoscale.

Applications Based on the Enhanced Optical Properties of Nanoparticles

a. Absorption

Haes et.al.[68] have used the surface plasmon resonance from an array of silver nanoparticles created by nanosphere lithography to detect the interaction of amyloid β-derived diffusible ligands (ADDL) and anti-ADDL antibody, believed to be important in Alzheimer's disease. Nanosphere lithrography[19] generates a triangular array of nanoparticles, which has a plasmon resonance whose frequency is very sensitive to the dielectric constant of the surrounding material, due to the sharp edges of the triangular nanoparticles. The gold nanoprisms were functionalized to bind to ADDLs on the

exposed surface of the nanoparticles. The substrate is then exposed to varying concentrations of anti-ADDL and a shift in the plasmon resonance absorption is detected to varying degrees linked to the concentration. The binding constant of the anti-ADDL and ADDL can be determined with this technique.[68] Thus, the surface plasmon resonance absorption is a powerful detection technique for species of interest. The nanoparticles can be functionalized to observe only the molecules of interest[19] and the absorption of desired molecules can be observed by a shift in the plasmon resonance absorption (i.e. a change in the color).

b. Fluorescence of Chromophores in Close Proximity

Metal nanoparticles have an effect on molecular chromophores in close proximity to the surface, as well as their intrinsic fluorescence. The effect on chromophore fluorescence in close proximity to the surface of metal nanoparticles is due to the strong electromagnetic field generated at the surface of metal nanoparticles.[26, 27] Chromophores within ~5nm of the surface of the metal nanoparticle have their fluorescence quenched while chromophores at distances of ~10nm or greater have their fluorescence enhanced up to 100-fold. Chromophores within 5nm of the surface interact electronically with the surface to donate the excited electrons to the metal, thus quenching the fluorescence by non-radiative pathways available in the metal nanoparticle. However, as the distance is increased the electric field is still strong enough to enhance the fluorescence probability, but the nanoparticle is not able to interact directly with the electrons of the metal. Thus, the fluorescence of molecular fluorophores can be increased by attaching chromophores via long linkers to the surface of metal nanoparticles.

c. Nanoparticle Fluorescence

The weak intrinsic fluorescence of noble bulk metals (quantum yield ~10^{-10}) resulting from the electronic interband transition was discovered in 1969.[111] Recent research has shown that nanoparticles have enhanced fluorescence emission over the bulk, particularly in small clusters[112] or nanorods.[53, 113] Nanorods also have enhanced emission over bulk metal and nanospheres, due to the large enhancement of the longitudinal plasmon resonance.[5-7, 53, 113] Clusters[112] and nanorods[53, 113] have an emission that shifts wavelengths as the size or aspect ratio increases, respectively. For nanorods, the longitudinal plasmon resonance enhances the radiative cross section of the interband transition of bulk gold leading to shifting emission wavelengths and intensities depending on the overlap between the two transitions.[53, 113] The observed emission of gold nanorods is presented in Figure 1-5a with quantum yields of 10^{-4}-10^{-5}.[53] The emission wavelength increases as the aspect ratio of the nanorod is increased.

Emission of gold[112] and silver[114] clusters is highly tunable by small changes in the number of atoms in the cluster. Zheng et.al. [112] characterize the gold cluster fluorescence with emission and excitation maxima, quantum yields, and lifetimes. The emission and excitation spectra of the different size clusters are presented in Figure 1-5b. As the number of atoms in the cluster increase the emission wavelength redshifts.[112] High quantum yields are observed, especially for the smallest cluster (Au_5) at 70%.[112] The narrow and tunable emission of the gold clusters make them attractive as energy transfer pairs used to measure distance and interactions of many types of molecules.

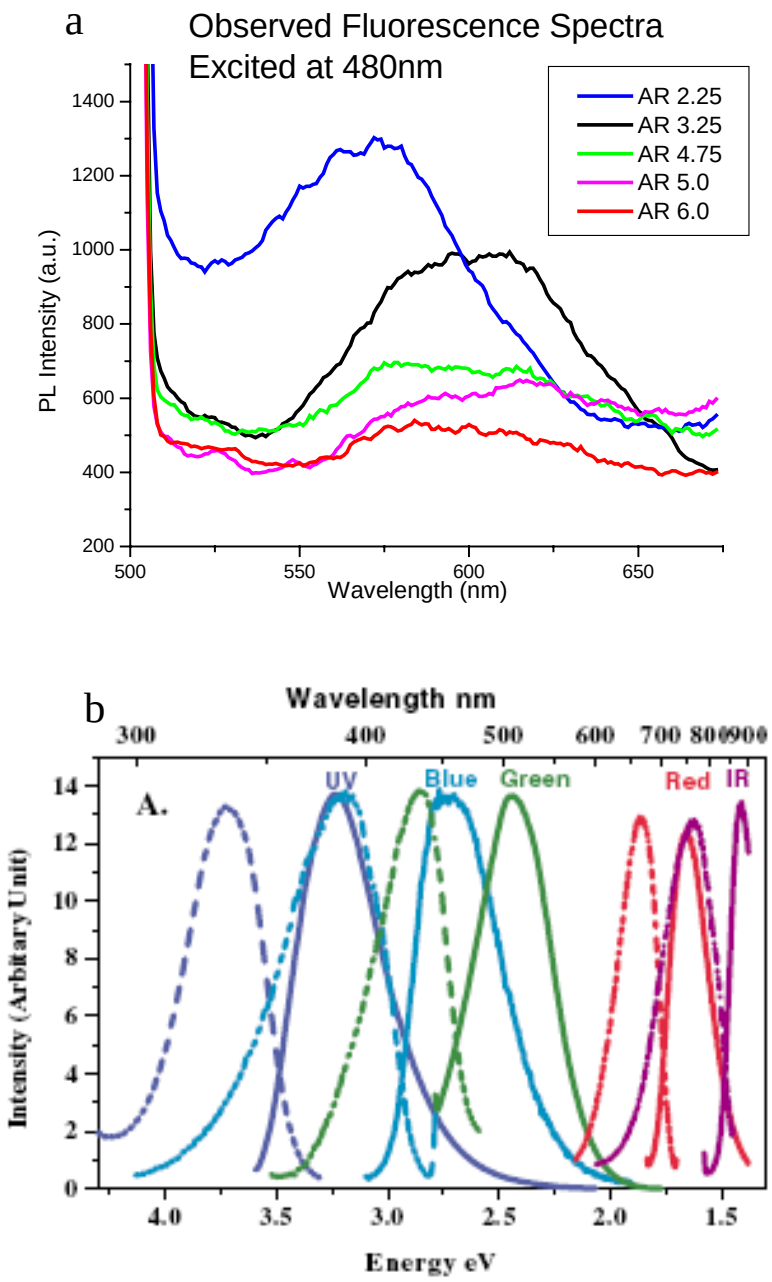

Figure 1-5: *a) Experimentally observed emission spectra from gold nanorods excited at 480nm.*[53]*. Reproduced with permission from J. Phys. Chem.B* ***2005****, 109, 16350-16356. Copyright 2005 Am. Chem. Soc. b) Emission from gold clusters.*[112] Reprinted Figure 1a with permission from J. Zheng, C. Zhang, and R. M. Dickson, *Phys. Rev. Lett.*, **93**, 077402, 2004. Copyright 2004 by the American Physical Society.

d. Enhanced Rayleigh (Mie) Scattering

The enhanced scattering cross section due to surface field effects can be used as a powerful technique to image biological systems. Gold nanoparticle surface plasmon resonance scattering is predicted in the Mie equations and is found to increase as the size of the nanoparticle increases. By conjugating gold nanoparticles to anit-EGFR antibody, El-Sayed et.al.[115] are able to distinguish between cancer and non-cancer cells from the strong scattering images of the gold nanoparticles conjugated to antibodies that binds only to the cancer, but not to the non-cancer cells. This scattering is observed from a simple optical microscope. They obtain a 600% greater binding ratio to the cancerous cells than to non-cancerous cells, enabling detection of cancerous cells by observing the scattered light on a dark field microscope. Figure 1-6 shows the scattering obtained with gold nanoparticles non-specifically adsorbed on the surface (a-c) and gold nanoparticles with anti-EGFR (d-f) antibodies specifically bound to the cancerous cells but not to the non-cancerous cells. Because of this difference the band shape and the surface plasmon absorption maximum are found to be different and this can thus be used as to differentiate cancerous cells. These results show that gold nanoparticles have enormous power as a diagnostic tool. Not only can changes in the surface plasmon resonance absorbance be detected to determine the adsorbed species in chemical, biochemical, sensing, and medical fields, but also the scattering signal can be used in imaging techniques to observe different binding with functionalized nanoparticles.

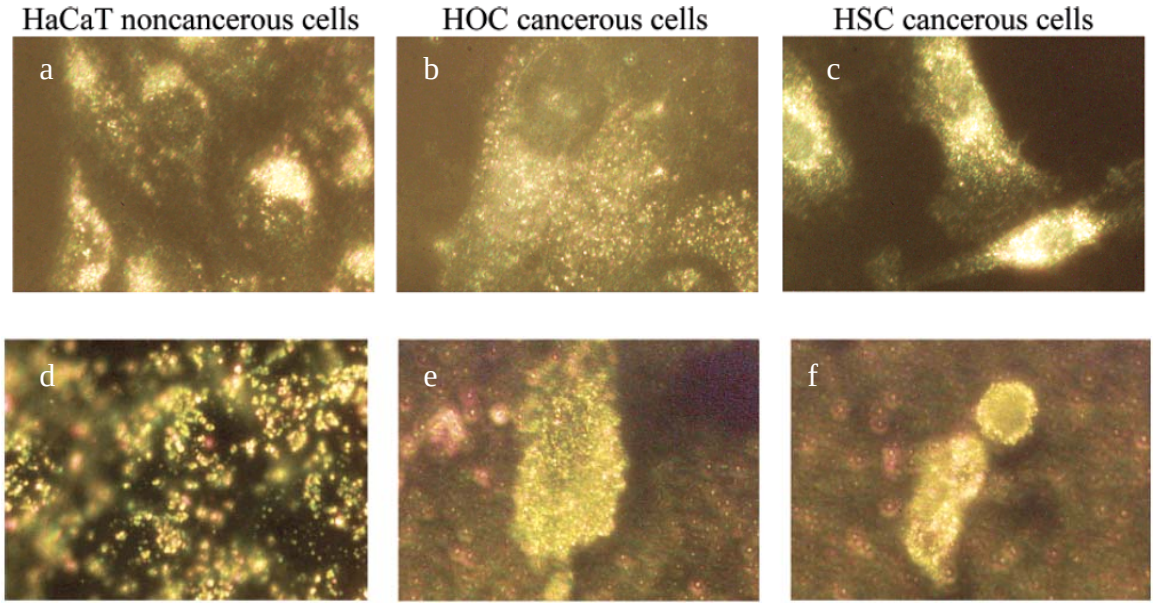

Figure 1-6: *Light scattering of cell labeled with (a-c) gold nanoparticles and (d-f) anti-EGFR coated gold nanoparticles. The anti-EGFR coated gold nanoparticles bind specifically to the cancerous cells, while all other gold nanoparticles are non-specifically bound. (a&d) nonmalignant epithelial cell line HaCaT (human keratinocytes), (b&d) malignant epithelial cell lines HOC 313 clone 8 (human oral squamous cell carcinoma) (c&f) malignant epithelial cell lines HSC 3 (human oral squamous cell carcinoma)*[115] *Reproduced with permission from Nano Lett.* ***2005****, 5, 829-834. Copyright 2005 Am. Chem. Soc.*

e. Surface Enhanced Raman Scattering (SERS) of Adsorbed Molecules

An effect was observed in the early 70's when molecules deposited on rough noble metal surfaces showed greatly enhanced Raman scattering.[20] Rough surfaces are decorated with nanoparticle shapes with surface plasmon oscillations. This effect has come to be known as surface enhanced Raman scattering (SERS).[21] Recently, nanoparticle research has shown that aggregates of nanoparticles are able to give the largest enhancement.[116] The origin of this effect has been the subject of intense debate. Prevailing theories attribute the origin of the SERS signal as a "hot spot" at the junction of two or more particles.[22, 116, 117] Nanorods are observed to have higher SERS signals

than spheres, [118, 119] due to the higher electric field generated at the tips of the nanorod.[37] SERS is being developed as a powerful diagnostic tool.[22, 116, 117] Large enhancement is available along with chemical information.

There are two effects[120, 121] which have been considered to account for this enhancement of the Raman signal: chemical enhancement[120] and electromagnetic field enhancement.[121] The chemical effect analysis states that the nature of the molecule determines the enhancement factor. Different signal strengths are observed on the same substrate with different chemicals. However, the bonding strength will affect the amount of molecules bound and in contact with the substrate and the time it spends in a given "hot spot." Thus it is difficult to determine if the chemical effect is simply a bonding time in a high electromagnetic field determined by sample geometry. The electromagnetic field enhancement mechanism attributes this effect to the local field strength generated by the surface plasmon oscillations.[121] Nanoparticles are observed to generate moderate signals, while aggregates generate much larger enhancement, suggesting that it is the interaction of multiple particles that generates large Raman enhancement. The electromagnetic field of a given geometry of the metal structures can be calculated.[37] Large electromagnetic fields are predicted to increase at the junction of two nanoparticles or as the radius of curvature increases, such as sharp points of a triangle. Rough surfaces have many random geometries with which to enhance Raman signals, but nanoparticles offer the opportunity to study the enhancement in accurately designed systems.

An intense background signal is also observed in all SERS specta.[20] This background blinks with the SERS signal. This background signal has been attributed to

the emission of the metal surface, enhanced by the roughness of the surface.[117, 122, 123] This signal has also been attributed to a metal-substrate charge interaction leading to emission.[124-127]

Summary

Synthesis of gold nanorods depends on techniques to isolate and stabilize particles. There are two general strategies to obtain materials on the nanoscale: The bottom up method is where the atoms are assembled from individual molecules. The top down method is where material is removed from the bulk material, leaving only the desired nanostructures. Synthetic techniques continue to evolve leading to improved control over the size and shape of the particles generated. Elucidating the properties of noble metal nanoparticles follows and accompanies the ability to synthesize materials. The optical properties and intense electromagnetic fields generated by the nanoparticles make these particles very attractive for sensing, diagnostics, and photothermal therapeutic applications in many areas. The change in color of the nanoparticles to signal adsorption or bonding of a certain molecule to the surface can be easily detected. The enhancement of both Rayleigh and Raman signals leads to the ability to gather imaging and chemical information at many levels. Diagnostic measurements can be obtained that were previously unattainable in a diagnostic setting. Changing properties simply by changing the size or shape of the nanoparticle creates many attractive opportunities to investigate old materials with the new properties. New structures are sure to emerge with characteristics central to development of new applications in every industry including electronics, materials science, healthcare, manufacturing, packaging, and telecommunications.

Scope of the Dissertation

In an attempt to further the understanding of nanoscience, the synthesis, optical and catalytic properties of gold and silver nanoparticles are investigated. There are three sections, one that describes investigations into the optical properties of gold nanorods, and two photochemical investigations into the synthesis of gold and silver nanoparticles.

The synthesis of high aspect ratio gold nanorods is described as used for further study. A useful technique referred to as the gold nanorod optical modeling equations (GNOME) is developed that determines the distribution of nanorods from absorption models that are based on the Gans equation for the absorption of a single species of nanorod. The fluorescence and the response to laser irradiation of high aspect ratio nanorods are examined and compared to previously reported results on shorter aspect ratios.

The first photochemical system involves the use of benzophenone as a photosensitizer to reduce silver and gold. The influence of irradiation source, time, and power are investigated. The mechanism of reduction by benzophenone and alcohol is refined. Silica power, film and colloidal particles are added to this system to control introduction and removal of starting and finished materials, and stabilization of metal nanoparticles for use as catalysts.

The second photochemical method involves the direct reduction of gold in alcohol solutions. The absorption of gold chloride shows the presence of this species in solution. At low pHs used in these experiments the hydrolysis equilibrium can be safely ignored in all solutions. The red shift of the absorption spectrum when the solvent is changed from water to ethylene glycol is explained by the difference in the hydrogen binding between

the two solvents. This absorption is excited with a lamp source and the mechanism of formation of gold nanoparticles is presented based on the absorption spectra. The effect of replacing chloride with bromide is also investigated. Brief descriptions of the chapters in this thesis are presented below.

Chapter 2 presents the synthesis techniques to generate gold nanorods. The ability to generate high aspect ratio (5-7) nanorods in high yield in investigated. The challenges and details important for high quality samples are presented. Kinetic control is observed in all growth conditions, with great importance on the temperature of the growth solution to generate the desired nanoparticles. The absorption coefficient of gold nanorods of high aspect ratio are determined and compared to previous values.

In Chapter 3, a method is presented to determine the aspect ratio distribution of the synthesized nanorod samples. The longitudinal plasmon absorption is modeled using Gans theory for a composite of homogeneously broadened rods of different aspect ratios. The sensitivity of the longitudinal plasmon resonance to the aspect ratio makes it an ideal candidate to determine properties of the solution. This method allows fast, easy, and inexpensive determination of the aspect ratio maximum and distribution of gold nanorods while in solution without the need for TEM analysis.

Chapter 4 presents the fluorescence of 5 different solutions of nanorods along with the theoretical calculation of the predicted emission of these rods. The emission of high aspect ratio nanorods decreases in intensity, contrary to what was reported previously. This chapter goes through the theory for the predicted emission and incorporates the intrinsic emission of the bulk gold to the enhancement factor for each aspect ratio. The fits to the aspect ratio distribution obtained from Chapter 3 are

important in obtaining a reasonable agreement between the theoretical predictions and the experimental results.

Chapter 5 describes the photothermal melting of high aspect ratio gold nanorods after exposure to fs laser irradiation. As the aspect ratio increases, structures are expected to melt to form multiple particles instead of melting to form a single sphere as reported previously. All rods investigated (aspect ratio 3, 5 and 6) were observed to decrease slightly in the number of atoms lost from the rod volume to the sphere volume, with similar percent of atoms lost in all rod solutions. As the laser wavelength was kept constant through all of these samples, the same aspect ratio nanorods are melting in each case due to the overlap of the longitudinal plasmon resonance with the laser wavelength. The larger polydispersity of each of these samples also contributes to the difficulty in determining if high aspect ratio nanorods melt to form multiple particles in solution with a capping material.

The photosensitization is described in Chapter 6 and 7. Benzophenone (BP) is used as a photosensitizer in aqueous solution. This allows photoreduction of gold and silver in various different environments. In Chapter 6 the light source and size of the nanoparticles formed are investigated. The fs laser used as the light source was found to give narrower plasmon resonance absorptions and particle distributions than the cw mercury lamp. Twenty nanometer particles are generated at short irradiation times, and low laser powers. As the time of irradiation or the intensity increase, the nanoparticles begin to absorb the incident irradiation, and fragment to generate large populations of small nanoparticles.

Chapter 7 investigates the effect of different forms of silica on the synthesis of gold and silver nanoparticles. Silica films can be used as a carrier for the BP, allowing the BP to be introduced immediately before irradiation, and removed afterwards, with very little BP allowed to diffuse into the aqueous solution, leading to a control over size reactions, and larger stability of particles generated with this method. Silica powders can be used as a method to remove metal ions from solution by attaching BP to the powder, and irradiating the solution followed by removal of the silica powder with metal nanoparticles by centrifugation. Silica films with silver ions or gold ions imbedded can be photoreduced when in contact with a BP-alcohol solution. This allows generation of conducting silica films, or stable supports for silver or gold nanoparticles used for catalysis.

Chapter 8 introduces the absorption of gold chloride in water and alcohol solutions. Hydrolysis is only observed in the aqueous solution at low pH's. The hydrogen-binding environment of the solvent affects the absorption spectrum of gold chloride. The number of bromide ions attached to a gold ion is also calculated from the absorption spectrum.

Chapter 9 presents the results of the photochemical reduction as the solvent is shifted from water to ethylene glycol. The maximum rate of gold nanoparticle formation is found at 0.40 mole fraction ethylene glycol, suggesting that two conflicting effects of ethylene glycol take place in this reaction. The glycol is able to reduce the excited state of the gold molecule, but it is also a vicious solvent, with the disproportionation of $Au^{(1+)}Cl_2^-$ being diffusion limited, leading to the observed maximum in the rate of

nanoparticle formation. The effect of saturating the solution with different gasses is also observed to affect the rate of formation of gold nanoparticles.

Chapter 10 investigates replacing the chloride ions in the starting material with bromide ions. When the gold bromide complex is used, gold nanoparticle formation is not observed. This is due to the steric repulsion of the bromide ions due to their larger size than the chloride ions. The effect of silver ions increases the rate of formation of gold nanoparticles when gold-chloride complex is used, and generates gold nanoparticles when gold-bromide is used. The effect of the silver ion is suggested to be assisting in heterogeneous nucleation and removing the extra halide ions from solution to drive the formation of gold nanoparticles.

References

1. El-Sayed, M. A., Some interesting properties of metals confined in time and nanometer space of different shapes. *Acc. Chem. Res.* **2001,** 34, (4), 257-264.

2. Eustis, S.; El-Sayed, M. A., Why Gold Nanoparticles Are More Precious than Pretty Gold: Noble Metal Surface Plasmon Resonance and its Enhancement of the Radiative and Nonradiative Properties of Nanocrystals of Different Shapes. *Chem. Soc. Rev.* **2006,** 35, (3), 209-217.

3. Daniel, M.-C.; ; Astruc, D.; , Gold Nanoparticles: Assembly, Supramolecular Chemistry, Quantum-Size-Related Properties, and Applications toward Biology, Catalysis, and Nanotechnology *Chem. Rev.* **2004,** 104, (1), 293-346.

4. Burda, C.; Chen, X.; Narayanan, R.; El-Sayed, M. A., Chemistry and Properties of Nanocrystals of Different Shapes *Chem. Rev.* **2005,** 105, (4), 1025-1102.

5. Link, S.; El-Sayed, M. A., Spectral properties and relaxation dynamics of surface plasmon electronic oscillations in gold and silver nanodots and nanorods. *J. Phys. Chem. B* **1999,** 103, (40), 8410-8426.

6. Link, S.; El-Sayed, M. A., Shape and size dependence of radiative, non-radiative and photothermal properties of gold nanocrystals. *Int. Rev. Phys. Chem.* **2000,** 19, (3), 409-453.

7. Link, S.; El-Sayed, M. A., Optical Properties and Ultrafast Dynamics of Metallic Nanocrystals. *Annu. Rev. Phys. Chem.* **2003,** 54, 331-366.

8. Kamat, P. V., Photophysical, photochemical and photocatalytic aspects of metal nanoparticles. *J. Phys. Chem. B* **2002,** 106, (32), 7729-7744.

9. Schärtl, W., Crosslinked Spherical Nanoparticles with Core-Shell Topology. *Adv. Mater.* **2000,** 12, (24), 1899-1908.

10. Murphy, C. J.; Sau, T. K.; Gole, A. M.; Orendorff, C. J. G., J.; Gou, L.; Hunyadi, S. E.; Li, T., Anisotropic Metal Nanoparticles: Synthesis, Assembly, and Optical Applications *J. Phys. Chem. B* **2005,** 109, (29), 13857-13870.

11. Crooks, R. M.; ; Zhao, M.; ; Sun, L.; ; Chechik, V.; ; Yeung, L. K.; , Dendrimer-Encapsulated Metal Nanoparticles: Synthesis, Characterization, and Applications to Catalysis *Acc. Chem. Res.* **2001,** 34, (3), 181-190.

12. Scott, R. W. J.; Wilson, O. M.; Crooks, R. M., Synthesis, Characterization, and Applications of Dendrimer-Encapsulated Nanoparticles *J. Phys. Chem. B* **2005,** 109, (2), 692-704.

13. Xia, Y.; Yang, P.; Sun, Y.; Wu, Y.; Mayers, B.; Gates, B.; Yin , Y.; Kim , F.; Yan, H., One-Dimensional Nanostructures: Synthesis, Characterization, and Applications. *Adv. Mater.* **2003,** 15, (5), 353 - 389.

14. Pileni, M. P., Nanosized Particles Made in Colloidal Assemblies. *Langmuir* **1997,** 13, (13), 3266-3276.

15. Pileni, M. P., The role of soft colloidal templates in controlling the size and shape of inorganic nanocrystals. *Nature Mater.* **2003,** 2, (3), 145-150.

16. Shah, P. S.; ; Hanrath, T.; ; Johnston, K. P.; ; Korgel, B. A.; , Nanocrystal and Nanowire Synthesis and Dispersibility in Supercritical Fluids *J. Phys. Chem. B* **2004,** 108, (28), 9574-9587.

17. Wallraff, G. M.; ; Hinsberg, W. D.; , Lithographic Imaging Techniques for the Formation of Nanoscopic Features *Chem. Rev.* **1999,** 99, (7), 1801-1821.

18. Xia, Y.; Rogers, J. A.; Paul, K. E.; Whitesides, G. M., Unconventional Methods for Fabricating and Patterning Nanostructures *Chem. Rev.* **1999,** 99, (7), 1823-1848.

19. Haynes, C. L.; Van Duyne, R. P., Nanosphere Lithography: A Versatile Nanofabrication Tool for Studies of Size-Dependent Nanoparticle Optics. *J. Phys. Chem. B* **2001,** 105, (24), 5599-5611.

20. Campion, A.; Kambhampati, P., Surface-enhanced Raman scattering. *Chem. Soc. Rev.* **1998,** 27, (4), 241-250.

21. Kneipp, K.; Kneipp, H.; Itzkan, I.; Dasari, R. R.; Feld, M. S., Ultrasensitive Chemical Analysis by Raman Spectroscopy *Chem. Rev.* **1999,** 99, (10), 2957-2976.

22. Nie, S.; Emory, S. R., Probing Single Molecules and Single Nanoparticles by Surface-Enhanced Raman Scattering. *Science* **1997,** 275, (5303), 1102-1106.

23. Rosi, N. L.; ; Mirkin, C. A.; , Nanostructures in Biodiagnostics *Chem. Rev.* **2005,** 105, (4), 1547-1562.

24. Shenhar, R.; Rotello, V. M., Nanoparticles: Scaffolds and Building Blocks. *Acc. Chem. Res.* **2003,** 36, (7), 549-561.

25. Katz, E.; Willner, I., Integrated Nanoparticle-Biomolecule Hybrid Systems: Synthesis, Properties, and Applications. *Angew. Chem. Int. Ed.* **2004,** 43, (45), 6042-6108.

26. Lakowicz, J.; Geddes, C.; Gryczynski, I.; Malicka, J.; Gryczynski, Z.; Aslan, K.; Lukomska, J.; Matveeva, E.; Zhang, J.; Badugu, R.; Huang, J., Advances in Surface-Enhanced Fluorescence. *J. Fluorescence* **2004,** 14, (4), 425-441.

27. Thomas, K. G.; ; Kamat, P. V.; , Chromophore-Functionalized Gold Nanoparticles *Acc. Chem. Res.* **2003,** 36, (12), 888-898.

28. Shon, Y. S.; Choo, H., Organic reactions of monolayer-protected metal nanoparticles. *C.R. Chimie* **2003,** 6, 1009-1018.

29. Hutter, E.; Fendler, J. H., Exploitation of Localized Surface Plasmon Resonance. *Adv. Mater.* **2004,** 16, (19), 1685 - 1706.

30. Narayanan, R.; El-Sayed, M. A., Catalysis with Transition Metal Nanoparticles in Colloidal Solution: Nanoparticle Shape Dependence and Stability *J. Phys. Chem. B* **2005,** 109, (26), 12663-12676.

31. Sastry, M.; Rao, M.; Ganesh, K. N., Electrostatic Assembly of Nanoparticles and Biomacromolecules *Acc. Chem. Res.* **2002,** 35, (10), 847-855.

32. Whetten, R. L.; Shafigullin, M. N.; Khoury, J. T.; Schaaff, T. G.; Vezmar, I.; Alvarez, M. M.; Wilkinson, A., Crystal Structures of Molecular Gold Nanocrystal Arrays *Acc. Chem. Res.* **1999,** 32, (5), 397-406.

33. Shipway, A. N.; Lahav, M.; Willner, I., Nanostructured Gold Colloid Electrodes. *Adv. Mater.* **2000,** 12, (13), 993-998.

34. Pileni, M. P.; , Nanocrystal Self-Assemblies: Fabrication and Collective Properties *J. Phys. Chem. B* **2001,** 105, (17), 3358-3371.

35. Rao, C. N. R.; Kulkarni, G. U.; Thomas, P. J., Metal Nanoparticles and their Assemblies. *Chem. Soc. Rev.* **2000,** 29, 27-35.

36. Maier, S. A.; Brongersma, M. L.; Kik, P. G.; Meltzer, S.; Requicha, A. A. G.; Atwater, H. A., Plasmonics - A Route to Nanoscale Optical Devices. *Adv. Mater.* **2001,** 13, (19), 1501-1505.

37. Hao, E.; Schatz, G.; Hupp, J., Synthesis and Optical Properties of Anisotropic Metal Nanoparticles. *J. Fluorescence* **2004,** 14, (4), 331-341.

38. Kelly, K. L.; Coronado, E.; Zhao, L. L.; Schatz, G. C., The Optical Properties of Metal Nanoparticles: The Influence of Size, Shape, and Dielectric Environment *J. Phys. Chem. B* **2003,** 107, (3), 668-677.

39. Pyykkö, P., Theoretical Chemistry of Gold. *Angew. Chem. Int. Ed.* **2004,** 43, (34), 4412-4456.

40. Dabbousi, B. O.; Rodriguez-Viejo, J.; Mikulec, F. V.; Heine, J. R.; Mattoussi, H.; Ober, R.; Jensen, K. F.; Bawendi, M. G., (CdSe)ZnS Core-Shell Quantum Dots: Synthesis and Characterization of a Size Series of Highly Luminescent Nanocrystallites *J. Phys. Chem. B* **1997,** 101, (46), 9463-9475.

41. El-Sayed, M. A., Small is different: Shape-, size-, and composition-dependent properties of some colloidal semiconductor nanocrystals. *Acc. Chem. Res.* **2004,** 37, (5), 326-333.

42. Jin, R. C.; Cao, Y. C.; Hao, E. C.; Metraux, G. S.; Schatz, G. C.; Mirkin, C. A., Controlling anisotropic nanoparticle growth through plasmon excitation. *Nature* **2003,** 425, (6957), 487-490.

43. Jin, R. C.; Cao, Y. W.; Mirkin, C. A.; Kelly, K. L.; Schatz, G. C.; Zheng, J. G., Photoinduced conversion of silver nanospheres to nanoprisms. *Science* **2001,** 294, (5548), 1901-1903.

44. Faraday, M., The Bakerian Lecture: Experimental Relations of Gold (and Other Metals) to Light. *Philos. Trans. R. Soc. London, Ser. A* **1857,** 147, 145-181.

45. Prasad, P. N., *NANOPHOTONICS*. John Wiley & Sons, Inc.: Hopoken, New Jersey, USA, 2004.

46. Mie, G., Beitrage zur Optik truber Medien, speziell kolloidaler Metallosungen. *Ann. Phys.* **1908,** 25, 377-445.

47. Kreibig, U.; Vollmer, M., *Optical Properties of Metal Clusters*. Springer: Berlin, 1995; Vol. 25, p 532.

48. van de Hulst, H. C., *Light Scattering by Small Particles* Dover Publications 1981; p 470.

49. Mulvaney, P., Surface Plasmon Spectroscopy of Nanosized Metal Particles. *Langmuir* **1996,** 12, 788-800.

50. Gans, R. v., Uber die Form ultramikroskopischer Goldteilchen. *Ann. Phys.* **1912,** 37, 881-900.

51. Gans, R. v., Uber die Form Ultramikroskopischer Silberteilchen. *Ann. Phys.* **1915,** 47, 270-284.

52. Brioude, A.; Jiang, X. C.; Pileni, M. P., Optical Properties of Gold Nanorods: DDA Simulations Supported by Experiments. *J. Phys. Chem. B* **2005,** 109, (27), 13138-13142.

53. Eustis, S.; El-Sayed, M. A., The Aspect Ratio Dependence of the Enhanced Fluorescence Intensity of Gold Nanorods: Experimental and Simulation Study. *J. Phys. Chem. B* **2005,** 109, (34), 16350-16356.

54. Link, S.; El-Sayed, M. A., Simulation of the Optical Absorption Spectra of Gold Nanorods as a Function of Their Aspect Ratio and the Effect of the Medium Dielectric Constant (Addition/Correction). *J. Phys. Chem. B* **2005,** 109, (20), 10531-104532.

55. Link, S.; Mohamed, M. B.; El-Sayed, M. A., Simulation of the optical absorption spectra of gold nanorods as a function of their aspect ratio and the effect of the medium dielectric constant. *J. Phys. Chem. B* **1999,** 103, (16), 3073-3077.

56. Millstone, J. E.; Park, S.; Shuford, K. L.; Qin, L.; Schatz, G. C.; Mirkin, C. A., Observation of a Quadrupole Plasmon Mode for a Colloidal Solution of Gold Nanoprisms *J. Am. Chem. Soc.* **2005,** 127, (15), 5312-5313.

57. Metraux, G. S.; Mirkin, C. A., Rapid Themal Synthesis of Silver Nanoprisms with Chemically Tailorable Thickness. *Adv. Mater.* **2005,** 17, (4), 412-415.

58. Sau, T. K.; Murphy, C. J., Room Temperature, High-Yield Synthesis of Multiple Shapes of Gold Nanoparticles in Aqueous Solution *J. Am. Chem. Soc.* **2004,** 126, (28), 8648-8649.

59. Metraux, G. S.; Cao, Y. C.; Jin, R. C.; Mirkin, C. A., Triangular nanofrarnes made of gold and silver. *Nano Letters* **2003,** 3, (4), 519-522.

60. Chen, S.; Carroll, D. L., Synthesis and Characterization of Truncated Triangular Silver Nanoplates *Nano Lett.* **2002,** 2, (9), 1003-1007.

61. Shankar, S. S.; Rai, A.; Ankamwar, B.; Singh, A.; Ahmad, A.; Sastry, M., Biological synthesis of triangular gold nanoprisms. *Nature Mater.* **2004,** 3, (7), 482–488.

62. Chen, S.; Wang, Z. L.; Ballato, J.; Foulger, S. H.; Carroll, D. L., Monopod, Bipod, Tripod, and Tetrapod Gold Nanocrystals *J. Am. Chem. Soc.* **2003,** 125, (52), 16186-16187.

63. Kim, F.; Song, J. H.; Yang, P., Photochemical Synthesis of Gold Nanorods *J. Am. Chem. Soc.* **2002,** 124, (48), 14316-14317.

64. Yu, Y. Y.; Chang, S. S.; Lee, C. L.; Wang, C. R. C., Gold Nanorods: Electrochemical Synthesis and Optical Properties. *J. Phys. Chem. B* **1997,** 101, (34), 6661-6664.

65. Busbee, B. D.; Obare, S. O.; Murphy, C. J., An Improved Synthesis of High-Aspect-Ratio Gold Nanorods. *Adv. Mater.* **2003,** 15, (5), 414-416.

66. Jana, N. R.; Gearheart, L.; Murphy, C. J., Wet Chemical Synthesis of Silver Nanorods and Nanowires of Controllable Aspect Ratio. *Chem. Commun.* **2001**, 617-618.

67. Kim, F.; Connor, S.; Song, H.; Kuykendall, T.; Yang, P. D., Platonic gold nanocrystals. *Angew. Chem. Int. Ed.* **2004,** 43, (28), 3673-3677.

68. Haes, A. J.; Hall, W. P.; Chang, L.; Klein, W. L.; Van Duyne, R. P., A localized surface plasmon resonance biosensor: First steps toward an assay for Alzheimer's disease. *Nano Lett.* **2004,** 4, (6), 1029-1034.

69. Yu, T.; Ober, C. K.; Kuebler, S. M.; Zhou, W.; Marder, S. R.; Perry, J. W., Chemically-amplified positive resist system for two-photon three-dimensional lithography. *Adv. Mater.* **2003,** 15, (6), 517-521.

70. Huang, W.; ; Qian, W.; ; El-Sayed, M. A.; , Coherent Vibrational Oscillation in Gold Prismatic Monolayer Periodic Nanoparticle Arrays *Nano Lett.* **2004,** 4, (9), 1741-1747.

71. Haes, A. J.; ; Zhao, J.; ; Zou, S.; ; Own, C. S.; ; Marks, L. D.; ; Schatz, G. C.; ; Van Duyne, R. P.; , Solution-Phase, Triangular Ag Nanotriangles Fabricated by Nanosphere Lithography *J. Phys. Chem. B* **2005,** 109, (22), 11158-11162.

72. Huang, W.; Qian, W.; El-Sayed, M. A. In *Optically detected coherent picosecond lattice oscillations in two dimensional arrays of gold nanocrystals of different sizes and shapes induced by femtosecond laser pulses*, Plasmonics: Metallic Nanostructures and Their Optical Properties III, San Diego, CA, USA, 2005; SPIE: San Diego, CA, USA, 2005; p 592701.

73. Foss, C. A., Jr. ; Hornyak, G. L.; Stockert, J. A.; Martin, C. R., Template-Synthesized Nanoscopic Gold Particles: Optical Spectra and the Effects of Particle Size and Shape. *J. Phys. Chem.* **1994,** 98, (11), 2963-2971.

74. Turkevich, J.; Stevenson, P. C.; Hillier, J., A study of the nucleation and growth processes in the synthesis of colloidal gold. *Discuss. Faraday Soc.* **1951,** 11, 55-75.

75. Jana, N. R.; Gearheart, L.; Murphy, C. J., Seeding Growth for Size Control of 5-40nm Diameter Gold Nanoparticles. *Langmuir* **2001,** 17, (22), 6782-6786.

76. Ahmadi, T. S.; Wang, Z. L.; Green, T. C.; Henglein, A.; El-Sayed, M. A., Shape-Controlled Synthesis of Colloidal Platinum Nanoparticles. *Science* **1996,** 272, 1924-1926.

77. Yin, B.; Ma, H.; Wang, S.; Chen, S., Electrochemical Synthesis of Silver Nanoparticles under Protection of Poly(N-vinylpyrrolidone) *J. Phys. Chem. B* **2003,** 107, (34), 8898-8904.

78. Bonet, F.; Guery, C.; Guyomard, D.; Urbina, R. H.; Tekaia-Elhsissen, K.; Tarascon, J.-M., Electrochemical reduction of noble metal compounds in ethylene glycol. *Int. J. Inorg. Mater.* **1999,** 1, 47-51.

79. Su, C.-H.; Wu, P.-L.; Yeh, C.-S., Sonochemical Synthesis of Well-Dispersed Gold Nanoparticles at the Ice Temperature *J. Phys. Chem. B* **2003,** 107, (51), 14240-14243.

80. Caruso, R. A.; Ashokkumar, M.; Grieser, F., Sonochemical Formation of Gold Sols *Langmuir* **2002,** 18, (21), 7831-7836.

81. Sun, Y. G.; Yin, Y. D.; Mayers, B. T.; Herricks, T.; Xia, Y. N., Uniform silver nanowires synthesis by reducing AgNO3 with ethylene glycol in the presence of seeds and poly(vinyl pyrrolidone). *Chem. Mater.* **2002,** 14, (11), 4736-4745.

82. Sun, Y.; Xia, Y., Large-Scale Synthsis of Uniform Silver Nanowires Through a Soft, Self-Seeding, Polyol Process. *Adv. Mater.* **2002,** 14, (11), 833-837.

83. Jin, R.; Egusa, S.; Scherer, N. F., Thermally-Induced Formation of Atomic Au Clusters and Conversion into Nanocubes *J. Am. Chem. Soc.* **2004,** 126, (32), 9900-9901.

84. Sun, Y. G.; Xia, Y. N., Shape-controlled synthesis of gold and silver nanoparticles. *Science* **2002,** 298, (5601), 2176-2179.

85. Wiley, B.; Herricks, T.; Sun, Y. G.; Xia, Y. N., Polyol synthesis of silver nanoparticles: Use of chloride and oxygen to promote the formation of single-crystal, truncated cubes and tetrahedrons. *Nano Lett.* **2004,** 4, (9), 1733-1739.

86. Eustis, S.; Hsu, H.-Y.; El-Sayed, M. A., Gold Nanoparticle Formation from Photochemical Reduction of Au3+ by Continuous Excitation in Colloidal Solutions. A Proposed Molecular Mechanism *J. Phys. Chem. B* **2005,** 109, (11), 4811-4815.

87. Esumi, K.; Suzuki, A.; Aihara, N.; Usui, K.; Torigoe, K., Preparation of Gold Colloids with UV Irradiation Using Dendrimers as Stabilizer. *Langmuir* **1998,** 14, 3157-3159.

88. Maillard, M.; Huang, P.; Brus, L., Silver Nanodisk Growth by Surface Plasmon Enhanced Photoreduction of Adsorbed [Ag+] *Nano Lett.* **2003,** 3, (11), 1611-1615.

89. Callegari, A.; Tonti, D.; Chergui, M., Photochemically Grown Silver Nanoparticles with Wavelength-Controlled Size and Shape. *Nano Lett.* **2003,** 3, (11), 1565-1568.

90. Weaver, S.; Taylor, D.; Gale, W.; Mills, G., Photoinitiated Reversible Formation of Small Gold Crystallites in Polymer Gels. *Langmuir* **1996,** 12, (20), 4618-4620.

91. Bronstein, L.; Chernyshov, D.; Valetsky, P.; Tkachenko, N.; Lemmetyinen, H.; Hartmann, J.; Forster, S., Laser photolysis formation of gold colloids in block copolymer micelles. *Langmuir* **1999,** 15, (1), 83-91.

92. Leontidis, E.; Kleitou, K.; Kyprianidou-Leodidou, T.; Bekiari, V.; Lianos, P., Gold colloids from cationic surfactant solutions. 1. Mechanisms that control particle morphology. *Langmuir* **2002,** 18, (9), 3659-3668.

93. Han, M. Y.; Quek, C. H., Photochemical synthesis in formamide and room-temperature Coulomb staircase behavior of size-controlled cold nanoparticles. *Langmuir* **2000,** 16, (2), 362-367.

94. Zhou, Y.; Wang, C. Y.; Zhu, Y. R.; Chen, Z. Y., A Novel Ultraviolet Irradiation Technique for Shape-Controlled Synthesis of Gold Nanoparticles at Room Temperature. *Chem. Mater.* **1999,** 11, 2310-2312.

95. Zhou, Y.; Yu, S. H.; Wang, C. Y.; Li, X. G.; Zhu, Y. R.; Chen, Z. Y., A Novel Ultraviolet Irradiation Photoreduction Technique for the Preparation of Single-Crystal Ag Nanorods and Ag Dendrites. *Adv. Mater.* **1999,** 11, (10), 850-852.

96. Yonezawa, Y.; Kawabata, I.; Sato, T., Photochemical Formation of Colloidal Gold Particles in Chitosan Films. *Ber. Bunsen-Ges. Phys. Chem.* **1996,** 100, (1), 39-45.

97. Brust, M.; Walker, M.; Bethell, D.; Schiffrin, D.; Whyman, R., Synthesis of Thiol-derivatised Gold Nanoparticles in a Two-phase Liquid-Liquid System. *J. Chem. Soc., Chem. Comm.* **1994**, 801-802.

98. Chen, S.; Carroll, D. L., Silver Nanoplates: Size Control in Two Dimensions and Formation Mechanisms *J. Phys. Chem. B* **2004,** 108, (18), 5500-5506.

99. Chen, S.; Fan, Z.; Carroll, D. L., Silver Nanodisks: Synthesis, Characterization, and Self-Assembly *J. Phys. Chem. B* **2002,** 106, (42), 10777-10781.

100. Millard, M.; Giorgio, S.; Pileni, M. P., Silver Nanodisks. *Adv. Mater.* **2002,** 14, (15), 1084-1086.

101. Pastoriza-Santos, I.; ; Liz-Marzan, L. M.; , Synthesis of Silver Nanoprisms in DMF *Nano Lett.* **2002,** 2, (8), 903-905.

102. Filankembo, A.; Giorgio, S.; Lisiecki, I.; Pileni, M. P., Is the Anion the Major Parameter in the Shape Control of Nanocrystals? . *J. Phys. Chem. B* **2003,** 107, (30), 7492-7500.

103. Brust, M.; Bethell, D.; Kiely, C. J.; Schiffrin, D. J., Self-Assembled Gold Nanoparticle Thin Film with Nonmetallics Optical and Electronic Properites. *Langmuir* **1998,** 14, (19), 5425-5429.

104. Brust, M.; Schiffrin, D. J.; Bethell, D.; Kiely, C. J., Novel gold-dithiol nano-networks with non-metallic electronic properties. *Adv. Mater.* **1995,** 7, (9), 795-797.

105. Brust, M.; Fink, J.; Bethell, D.; Schiffrin, D. J.; Kiely, C., Synthesis and reactions of functionalised gold nanoparticles. *J. Chem. Soc., Chem. Comm.* **1995**, 1655-1656.

106. Yee, C. K.; Jordan, R.; Ulman, A.; White, H.; King, A.; Rafailovich, M.; Sokolov, J., Novel One-Phase Synthesis of Thiol-Functionalized Gold, Palladium, and Iridium Nanoparticles Using Superhydride. *Langmuir* **1999,** 15, (10), 3486-3491.

107. Chen, S.; Templeton, A. C.; Murray, R. W., Monolayer-Protected Cluster Growth Dynamics. *Langmuir* **2000,** 16, (7), 3543-3548.

108. Frenkel, A. I.; Nemzer, S.; Pister, I.; Soussan, L.; Harris, T.; Sun, Y.; Rafailovich, M. H., Size-controlled synthesis and characterization of thiol-stabilized gold nanoparticles. *J. Chem. Phys.* **2005,** 123, (18), 18470/1-6.

109. Chen, M. S.; Goodman, D. W., The Structure of Catalytically Active Gold on Titania. *Science* **2004,** 306, (5694), 252-255.

110. Valden, M.; Lai, X.; Goodman, D. W., Onset of Catalytic Activity of Gold Clusters on Titania with the Appearance of Nonmetallic Properties. *Science* **1998,** 281, (5383), 1647-1650.

111. Mooradian, A., Photoluminescence of Metals. *Phys. Rev. Lett.* **1969,** 22, (3), 185-187.

112. Zheng, J.; Zhang, C.; Dickson, R. M., Highly Fluorescent, Water-Soluble, Size-Tunable Gold Quantum Dots. *Phys. Rev. Lett.* **2004,** 93, (7), 077402.

113. Mohamed, M. B.; Volkov, V.; Link, S.; El-Sayed, M. A., The 'lightning' gold nanorods: fluorescence enhancement of over a million compared to the gold metal. *Chem. Phys. Lett.* **2000,** 317, (6), 517-523.

114. Zheng, J.; Dickson, R. M., Individual Water-Soluble Dendrimer-Encapsulated Silver Nanodot Fluroescence. *J. Am. Chem. Soc.* **2002,** 124, (47), 13982-13983.

115. El-Sayed, I. H.; Huang, X.; El-Sayed, M. A., Surface Plasmon Resonance Scattering and Absorption of anti-EGFR Antibody Conjugated Gold Nanoparticles in Cancer Diagnostics: Applications in Oral Cancer *Nano Lett.* **2005,** 5, (5), 829-834.

116. Lu, H. P., Site-specific Raman spectroscopy and chemical dynamics of nanoscale interstitial systems. *J. Phys. Cond. Matter* **2005,** 17, (7), R333-R335.

117. Jiang, J.; Bosnick, K.; Maillard, M.; Brus, L., Single Molecule Raman Spectroscopy at the Junctions of Large Ag Nanocrystals. *J. Phys. Chem. B* **2003,** 107, 9964-9972.

118. Nikoobakht, B.; El-Sayed, M. A., Surface-enhanced Raman scattering studies on aggregated gold nanorods. *J. Phys. Chem. A* **2003,** 107, (18), 3372-3378.

119. Nikoobakht, B.; Wang, J. P.; El-Sayed, M. A., Surface-enhanced Raman scattering of molecules adsorbed on gold nanorods: off-surface plasmon resonance condition. *Chem. Phys. Lett.* **2002,** 366, (1-2), 17-23.

120. Moskovits, M., Surface-enhanced spectroscopy. *Rev. Mod. Phys.* **1985,** 57, (3), 783-826.

121. Moskovits, M., Surface roughness and the enhanced intensity of Raman scattering by molecules adsorbed on metals. *J. Chem. Phys.* **1978,** 69, (9), 4159-4161

122. Jian, Z.; Liqing, H.; Yongchang, W.; Yimin, L., Fluorescence spectrum properties of gold nanochains. *Physica E* **2004,** 25, (1), 114-118.

123. Michaels, A. M.; Nirmal, M.; Brus, L., Surface Enhanced Raman Spectroscopy of Individual Rhodamine 6G Molecules on Large Ag Nanocrystals. *J. Am. Chem. Soc.* **1999,** 121, (43), 9932-9939.

124. Persson, B. N. J.; Baratoff, A., Theory of Photon Emission in Electron Tunneling to Metallic Particles. *Phys. Rev. Lett.* **1992,** 68, (21), 3224-3227.

125. Birke, R. L.; Lombardi, J. R.; Gersten, J. I., Observation of a Continuum in Enhanced Raman Scattering from a Metal-Solution Interface. *Phys. Rev. Lett.* **1979,** 43, (1), 71-75.

126. Lombardi, J. R.; Birke, R. L.; Lu, T.; Xu, J., Charge-transfer theory of surface enhanced Raman spectroscopy: Herzberg-Teller contributions. *J. Chem. Phys.* **1986,** 84, (8), 4171-4180.

127. Adrian, F. J., Charge Transfer effects in surface-enhanced Raman scattering. *J. Chem. Phys.* **1982,** 77, (11), 5302-5314.

PART I: INVESTIGATIONS INTO THE PROPERTIES OF POLYDISPERSED SOLUTIONS OF GOLD NANORODS WITH DIFFERENT ASPECT RATIOS

CHAPTER 2

GOLD NANOROD SYNTHESIS: PROCEDURE AND CHALLENGES

Abstract

In the synthesis of gold nanorods it is important to obtain a narrow distributions with high aspect ratios. The experimental techniques of the chemical seeding technique is used, where the temperature is the most important parameter in controlling nanorod growth due to the kinetic control of the reaction. The absorption coefficients of high aspect ratio nanorods are 2.10×10^9 for aspect ratio 5 and 2.27×10^9 for aspect ratio 6.4. History and cleanliness of the glassware as well as temperature and humidity are also important factors affecting nucleation, and particles obtained.

Introduction

Metal Nanospheres

Many different synthesis techniques have been published to generate gold and silver spheres. One of the best-known techniques was described by Turkivech[1-3] where an aqueous solution is brought to a boil and sodium citrate is used as both the capping material and the reduction agent. The order of addition of the metal salt, and sodium citrate as well as the temperature, mole ratio citrate to metal salt, and volume of solution determine the size of the nanoparticles generated.[1-3] This synthesis is easy, quick, reproducible, and generates monodisperse population of nanoparticles around 20nm in diameter.[1-3] This synthesis is widely used to generate metal nanoparticles for many systems, where 20nm is a desirable diameter, or as a seed for further growth. The use of

sodium citrate as the capping material allows easy surface modification for a variety of applications. The narrow dispersion in the sizes of the nanoparticles is desirable for many applications. Sodium citrate is a weak reducing agent, which does not reduce the metal ions at room temperature. Thus the strength of the reducing agent is controlled by the temperature of the solution.

Another synthesis of metal nanospheres uses γ-irradiation to reduce of a solution of gold cyanide[4-7] or silver perchlorate[8] solution. This synthesis can also be used to enlarge previously formed nanoparticles, while maintaining or even improving the size distribution.[4-6, 8] To improve the speed and yield of nanoparticles generated, seeds from the reduction with citrate are added before reduction from the Turkivech[1-3] method. This reduction technique involves an aqueous solution of gold cyanide or silver perchlorate in methanol, saturated with nitrous oxide, irradiated with γ-irradiation until all of the metal ions have been reduced.[4-6, 8] Silver solutions also contain sodium citrate to stabilize the nanoparticles.[4-6, 8] This synthesis technique has the ability to produce gold or silver nanospheres with excellent size distributions from 20nm-100nm in diameter with no surface stabilizing agent, allowing further surface modification.

A very popular technique of generating small gold nanoparticles has been reported by Brust et. al.[9-12] The technique is often referred to as creating monolayer protected clusters (MCPs) due to the formation of a monolayer of thiol molecules on the surface of the gold nanoparticles. These particles are extremely stable due to the strength of the gold-thiol bond. A two-phase system is used where the gold ion is first transferred to the organic phase by employing a phase transfer agent (typically tetraoctylammonium bromide).[9-12] Then sodium borohydride is used to reduce the gold ions. This reduction is

accomplished slowly, when the gold ions from the organic phase come in contact with the sodium borohydride from the aqueous phase, the gold is reduced.[9-12] Then thiols can be used to protect the gold ions after they are reduced.[9-12] This technique is able to grow clusters around 1.5nm diameter that are very stable.[9-12] These nanoparticles can also be formed without addition of a thiol by using toluene for the organic phase solvent.[11] A similar one phase synthesis was developed by Yee et. al.[13] The one phase synthesis also used thiol molecules to protect small gold clusters leading to similar particles while removing the phase transfer step.[13] These methods have been used by numerous researchers and investigate the properties of these MCPs.[14, 15] Polymers can also be used to generate nanoparticles on the same size range.[16]

Stronger reducing agents have also been used to generate gold and silver nanospheres. These methods face similar challenges in the need to balance nucleation, stabilization and termination of the growth process. The seed particles used to enlarge or form anisotropic shapes have narrow size distributions and weak capping materials. Reducing agents used include sodium borohydride,[17-21] formamide,[22] tetrakis(hydroxymethyl)phosphonium chloride (THPC),[23] sucrose,[24] and glucose[25] to form gold and silver nanospheres.

One general method for thermal reduction of various metals to form monodisperse populations of nanoparticles is the polyol process.[26-42] Ethylene glycol is a viscous solvent slowing down diffusion, and is capable of providing reducing species, without the need for a separate reducing agent.[28-30] The polyol process uses very high temperatures ($160^{o}C - 280^{o}C$) to achieve reduction of the metal ions.[28-30]

Recently, photochemical reduction methods have been developed to produce metal nanoparticles.[4, 7, 43-78] Various different approaches are used in photochemical reduction such as use of a photosensitizer,[43-47] use of dendrimers as stabilizers,[48, 49] or placement of metal salts in polymer films[46, 50-59] or glasses.[60-63] Light has also been used to modify the shape of nanoparticles.[55, 61, 64-67] The solvent is sometimes used to reduce the excited metal ions.[68-71]

Other techniques to reduction gold and silver ions to form nanoparticles are sonochemical,[79-81] electrochemical,[82-84] and in supercritical fluids.[85] These reaction techniques are varied, generating different products. The stabilizing materials are as varied as the reduction technique.[79-85]

Two synthetic methods to reversibly form and dissolve silver nanoparticles have been described previously.[20, 86] The color of the solution oscillates from yellow to colorless as the nanoparticles form and dissolve in solution.[20, 86] One method involved the laser fragmentation of the nanoparticles to atoms, followed by the coalescence of the atoms to reform nanoparticles.[86] The other method involved the reaction of O_2 with active sodium borohydride to dissolve the silver nanoparticles, only to be regenerated in the absence of O_2.[20]

Due to the precise concentrations and volumes for most nanoparticle synthesis schemes, scaling up is a large problem to be solved before they are used on large scales. To obtain gold nanoparticles in a continuous fashion, conditions for a microreactor are reported[87] to obtain many batches of nanoparticle synthesis with narrow dispersions. Another resent report has generated gold, silver and copper nanoparticles on the gram scale using ammonium salts for stabilization in organic solvents.[88]

Metal Nanorods

Gold nanorods are of particular interest due to the large number of synthetic techniques and the ability to tune the optical properties from the middle of the visible spectra to the near IR.[89-93] Many mechanisms of anisotropic growth have been proposed,[93-107] but there still remains some challenges is determining the overall mechanism, due to the kinetic nature of the growth, and the number of different parameters that impact the process.

Gold and silver nanorods have been synthesized previously. Preparation techniques included chemical reduction to form gold nanorods,[18, 93-96, 108-113] silver nanowires,[34, 114, 115] and silver nanorods.[17, 116] Template directed growth of template gold nanorods[117, 118] and nanoporous gold nanowires[119] has been achieved. Gold nanorods have also been grown directly on surfaces [100, 120, 121] as well as deposited on surfaces by layer by layer deposition[122] or by spin coating.[123] Photochemical methods have also been reported to generate gold nanorods.[48, 98, 99, 103, 104, 113, 124] High yield and monodisperstiy gold nanorod solutions are obtained from the electrochemical synthesis described by Yu et. al.[125] More details of the electrochemical procedure are presented by Reetz and Helbig.[126, 127]

Many photochemical methods have described the synthesis gold nanorods.[48, 98, 99, 103, 104, 113, 124] Early attempts employed hexadecyltrimethylammonium chloride (CTAC) (no silver or Br were present in solution), generating large polydispersity and low yields.[48] The photochemical reaction was reported to start by photoreduction of the surfactants.[98] Later studies showed that the aspect ratio generated was dependent on the amount of silver ions added.[103] Early stages of nanorod formation have gold and silver

alloy formation suggesting that AgBr is photoreduced to initiate rod formation.[103] The intensity and wavelength are important in the photochemical synthesis of gold nanorods where a high intensity of 300nm light is found to improve the yield of nanorods compared to 254nm irradiation.[104] By combining the photochemical and chemical reduction techniques Niidome et. al.[113] were able to quickly form monodisperse populations of gold nanorods.

The mechanism is still debated for the formation of gold nanorods. Many possible mechanisms have been proposed due to interaction of the seed,[94-96] surfactant,[93, 96-100] additional ions,[93, 94, 96, 101-105] solution volume,[106] and temperature.[107] The structure of gold nanorods has been determined to have 5 faces (100) or (110) along the length and 10 (111) faces on the ends,[108, 121] similar to that of silver.[116] The silver content of gold nanorods has been quantitated to try to elucidate the role of silver in the formation of gold nanorods.[102] Only a small percentage of the silver (<5%) in the solution is part of the final gold nanorods.[102] Silver is predicted to be adsorbed on the gold (110) planes of the gold nanorods, allowing growth along the [100] direction.[94, 102] The effect of the anion in the solution on the shape control of nanoparticles has also been investigated. Filankembo et. al.[101, 105] have shown that the counter ion is able to affect the shape of nanoparticle generated by its ability to bind with specific faces of the metal surface. Growth of nanorods on surfaces have found that the chain length of the surfactant tail can disrupts the rod growth.[100]

Many of the nanorods prepared for use in studies of future chapters were based on the work of Jana et. al.[111, 112] and Nikoobakht and El-Sayed[18] using the chemical reduction method. In this method,[18, 93, 95, 108-113] first seed solutions are generated with a

strong reducing agent, followed by preparation of a growth solution with a weaker reducing agent to generate gold nanorods. Silver is added to the solution to increase the aspect ratio of the nanorods obtained.

Due to the large number of synthetic techniques available for generation of gold nanorods,[17, 18, 34, 48, 93, 95, 96, 98-100, 103, 104, 108-121, 124, 125] many of the properties and applications have been reported. The elastic constants of gold nanorods have been determined by time resolved spectroscopy of the breathing modes.[128] The optical properties of individual gold nanorods have been probed.[129] Imaging of single nanorod plasmon rods is possible with near field microscopy.[123] The optical properties have been modeled in Chapter 3 to obtain the size distribution of gold nanoparticles in solution. The fluorescence emission of nanoparticles has been reported,[130, 131] and further investigated in Chapter 4. Self-assemblies of gold nanorods has been observed.[132] The electrical properties of nanoporous gold nanowires has been investigated by Ji and Searson.[119] Huang et. al.[133] use gold nanorods for molecular imaging and photothermal cancer therapy.

While many reports have been published on the synthesis of gold nanorods,[17, 18, 34, 48, 93, 95, 96, 98-100, 103, 104, 108-121, 124, 125] the details to obtain the desired nanorod distribution prove more illusive than would appear from the literature. Precise concentrations of starting materials, mixing, and temperature are all important parameters in the synthesis of gold nanorods. Repeating synthesis from literature reports was largely unsuccessful with concentrations as published. Repeating synthesis from previous group members was also unsuccessful in obtaining similar solutions. Changes to procedure and concentrations were necessary to obtain gold nanoparticles. This chapter describes the

synthesis conditions, and concentrations with many details to enable repetition of this synthesis. The optical properties and melting of the rods produced here are discussed in future chapters.

Other Nanoshapes

Recently there have been many synthesis techniques describing the generation of flat nanoparticles of gold and silver.[36, 109, 134-145] They have been referred to as nanoprisms,[134-139] nanodisks,[140-143] and nanoplates.[36, 109, 144, 145] Although these names seem to suggest a different structure, the particles generated are very similar. They mainly consist of flat triangular nanoparticles with different degrees of truncation of their corners. Thus the particles with the least truncation appear to have three corners, while those with the most truncation have six corners. The method of synthesis is widely varied suggesting that there is an inherent stability of these flat structures due to surface energy constraints, and proper growth rates are the most important factor to obtain the desired structure. These shapes resemble structures observed on the micron scale[146] and the shape of silver crystals after photoreduction of silver halide by light irradiation.

One of the synthesis techniques where the mechanism is understood was reported by Xia et. al.[31, 32, 34-42] They use the polyol reduction procedure where a solution of the metal salt and PVP are heated in ethylene glycol to reduce the metal ion. By controlling the temperature and the gaseous environment they control the rate of nucleation and the rate of oxidation of the metal nanoparticles.[32, 35, 40, 42] By carefully adjusting parameters they can create a system where the nanoparticles are selectively etched until only single crystal shapes remain, allowing monodispersity in the size and shape of the nanoparticles

created. [32, 35, 40, 42] Thus to obtain shapes other than spherical, often a species to slow down reduction and a species to stabilize the desired product are introduced.[32, 36, 37, 42]

Many other shapes have been reported by various researchers.[37, 109, 147-150] They include cubes,[109, 147] bipyramids,[37] branched[148, 149] and "tadpole" shapes.[150] The synthesis conditions and reactant concentrations determine the shape generated.[37, 109, 147-150]

Experimental

Chemical Synthesis

The seed solution consists of 5mL 0.2M hexadecyltrimethylammonium bromide (CTAB) mixed with 5mL of 0.0005M $HAuCl_4$. Growth is initiated by addition of 0.6mL of ice cold 0.01M $NaBH_4$ while the solution was stirring. A fresh seed is needed for a good synthesis. Seed solutions were more reproducible when the stir bar had not been cleaned with aqua regia prior to seed synthesis. This suggests that a very small amount of seed on a stir bar allows seeding of a new seed solution. The age of the seed solution is important for use in nanorod growth. This solution should be kept warm (~26^{o}C) and uncovered for 5-40 minutes before use. Seeds older than this will decrease the aspect ratio of the nanorods generated.

Growth solutions are made up with mixtures of CTAB and benzyldimethylammonioum chloride hydrate (BDAC) as stabilizers, which are sonoicated and heated until the solution became clear. In a test tube , 200μL of 0.004M $AgNO_3$ is added to insure rod formation, 4.5mL of 0.001M $HAuCl_4$ and 0.5mL water are added to the solution. Fifty-four microliters of 0.1M ascorbic acid were added to the growth solution as a reducing agent. Twelve micro liters of seed solution are then added to the growth solution to generate nanorods. A temperature controlled circulating pump

with a jacketed beaker is used for the first 4 hours after addition of seed solution to control solution temperature. The geometry of the test tube was used to facilitate mixing by inverting the tube, with parafilm top, which was removed immediately after mixing.

The age of the stock solutions is important in nanoparticle synthesis. The surfactant solutions should be less than two weeks old, and solid BDAC should be stored in the refrigerator for longer stability. Silver nitrate stock solution should be less than one month old. Silver nitrate solutions get cloudy as they age, and should never be used if they appear cloudy. Tetrachloroauric(III) acid stock solution can be used until gold deposits are observed on the bottom of the solution (~3 months). The water should be added to the sodium borohydride ~10-15 minutes (1-2 hours is acceptable) before use. One-tenth molar sodium borohydride is made up first, followed by dilution to 0.01M sodium borohydride after 0.1M solution has lots of bubbles due to the reaction of the sodium borohydride with water. This solution is cooled on ice for 3-5 minutes before use. For optimal growth conditions, the ascorbic acid solution should have the water added immediately before addition to the growth solutions. The sodium borohydride and ascorbic acid solutions should not be used after one day, and growth solutions (without seed addition) should also be fresh for optimal results.

The day of a synthesis, the stock solutions are prepared, and the surfactant solutions are heated. Fresh samples of the reducing agents are massed out, and stored in sealed vessels. The temperature bath is turned on and stabilized at a given temperature. After all of the solutions have been prepared, and all of the surfactant has been dissolved by heating, the seed solution is prepared and left in warm water until the growth solution is ready. The growth solution is prepared with special attention taken to use a graduated

cylinder, and kept warm so that the viscosity remains low, and the surfactant remains in solution. After addition of each component, parafilm is placed over the top and the tube is inverted. The seed solution is then added directly to the solution by placing the pipette in the solution, and quickly removed. The growth solutions are left undisturbed for more than 4 hours.

The gold nanorods are prepared by a slightly modified technique as described previously by this group.[18] Briefly, a seed solution is generated by adding ice cold $NaBH_4$ to a solution of $HAuCl_4$ and hexadecyltrimethylammonium bromide (CTAB). The solution was kept at 25^{o}C for a few minutes before use. A brownish yellow color was observed in all seed solutions used. The growth solution contained 5mL of a solution of 0.20m CTAB and 0.25m benzyldimethylammonioum chloride hydrate (BDAC), which is added to 0.20mL of 4.0mM $AgNO_3$. Then 5.0mL of 0.90mM of $HAuCl_4$ is added and 54μL of 0.10M ascorbic acid. Twelve microliters of seed solution is then added to the solution, which is left undisturbed for 4 hours for the nanorods to grow. Kinetic growth conditions determine the aspect ratio of the nanorods generated, with narrower widths in the higher aspect ratio samples. All growth solutions have similar concentrations with temperature and humidity determining the aspect ratio generated.

To obtain the absorption coefficient of gold nanorods the concentration of gold in solution was then analyzed by Midwest Laboratories Inc by Inductively Coupled Argon Plasma (ICAP) after 3 days of dialysis.

Electrochemical Synthesis

The electrochemical method was previously reported by Yu et. al.[125] In this synthesis 0.08M hexadecyltrimethylammonium bromide (CTAB) is dissolved in 25mL of water. Then 0.083g tetraoctylammonium bromide (TOAB) is dissolved in 1.0mL acetone. The two solutions are then mixed and sonicated at an elevated temperature (~44^{o}C) to form a clear solution. A current of 3mA (2.2V) is applied across a gold sacrificial anode and a platinum cathode. A silver metal plate is inserted into the solution to provide silver ions in the solution. The reaction is allowed to proceed under heat and sonication for 45 minutes. This method generates nanorods with longitudinal plasmon maximums around 745nm corresponding to an aspect ratio of 4. The aspect ratio can be varied by the amount of the silver plate in the solution and the ratio of CTAB to TOAB in solution. The optical absorption spectrum of a solution of nanorods from this synthesis is seen in Figure 2.

The electrodes for this reaction are cleaned prior to the reaction each day. First the electrodes are sanded with fine grit sand paper for electronic electrodes. Then the electrodes gold and platinum electrodes are cleaned in 10% nitric acid for 10 minutes. Then all 3 electrodes are washed in water with sonication for 10 minutes. The water is replaced, and the electrodes are sonicated two more times. The yield of the first synthesis is lower than subsequent syntheses due to the small concentration of nanoparticles present from the first synthesis. The electrodes and glass vial are not cleaned between syntheses on a given day to keep some nucleation seeds.

Results and Discussion

Many different nanorods solutions were made by the chemical seeding technique. Absorption spectra and TEM images of a few samples are seen in Figure 2-1, where the temperature was modified to change the aspect ratio of the sample. The importance of temperature in this reaction is observed due to the kinetic nature of the synthesis. Solutions have been slightly modified from literature[18, 93, 95, 108-113] by adjusting the surfactant concentration, and gold concentration. Holding the temperature constant and at 26^{o}C was found to be paramount in obtaining high aspect ratio nanorods. The nanorods generated by this method differ slightly in length and width depending on the exact conditions of the day. The optical absorption spectrum of gold nanorods has two peaks with the first one being the transverse plasmon is seen at 550nm. The longitudinal plasmon absorption is observed between 600nm and 1100nm depending on the aspect ratio. The plasmon resonance from the spheres present as impurities is also seen around 515nm. This synthesis is affected by many parameters including the time between addition of varying reagents as well as the temperature of the solution and the humidity.

The ends of the nanorods can also change with the synthesis conditions. Previous studies[96, 109] have shown "bone" structure forming on the ends of nanorods for various reaction conditions. These "bone" structures with large deposits of gold on the end of the nanorods are observed in solutions with larger concentrations of gold ions. Thus it is expected that as the reaction is slowing down, or after it has completed, the gold ions continue to be reduced on the surface of the rod, but imperfect capping at the corners is observed to generate nanorods with larger ends.

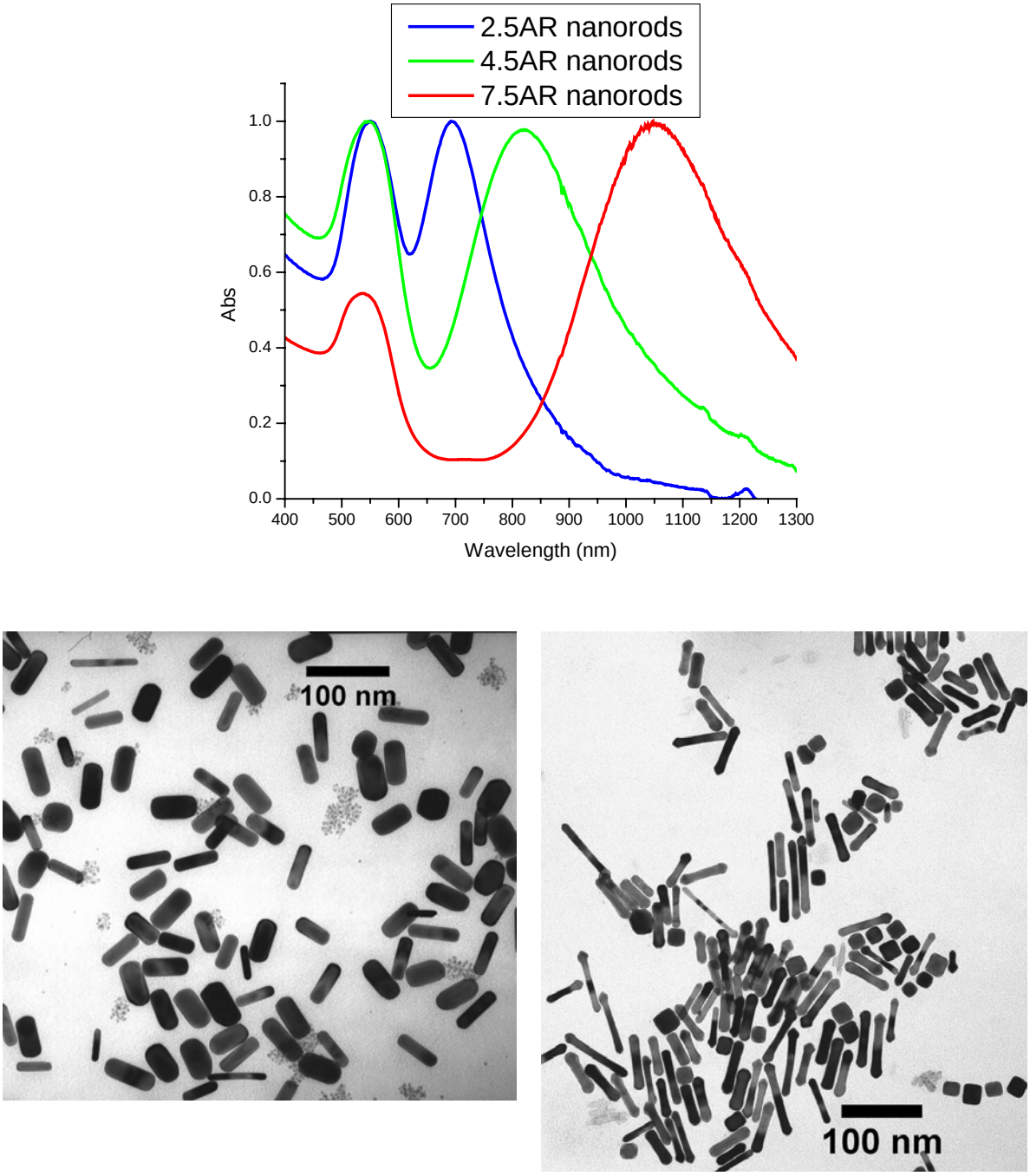

Figure 2-1: *a) Absorption spectra of gold nanorods synthesized by the chemical seeding technique. b) TEM image of nanorod sample Au630 with an aspect ratio of 2.5 c) TEM image of a sample Au880 with an aspect ratio of 4.5*

One synthesis procedure was reported[110] for high aspect ratio nanorods (4-18) in the literature. However, reproducing this synthesis technique did not generate the high yield of nanorods reported. Nanorods were only generated in very low yields (<10%), and the optical absorption of the longitudinal plasmon resonance is in the near infrared, and is out of the range of laser wavelengths in this lab, and thus not of particular interest for optical applications discussed here. This method involves removing the nanoparticles from the bottom of the solution a day after the synthesis. The geometry of the reaction vessel as well as precise hand eye coordination is required to remove only high aspect ratio nanorods, without the solution, or excess surfactant present in the reaction vessel. The longitudinal plasmon resonance absorption of the higher aspect ratio rods is in the same region as water, therefore the water must be removed before accurate absorption measurements can be obtained.

The electrochemical synthesis is difficult to reproduce. In order to obtain gold nanorods the solution must be optically clear, by dissolving TOAB in acetone. Acetone has also been shown to be important in forming gold nanoparticles, and its concentration is delicate. Enough acetone must be added to form a single phase, inducing TOAB to dissolve in aqueous solution. However, if more acetone is added, it reduces everything in solution, and no nanorods are formed. The surface of the electrodes is also important to generate nanoparticles by the electrochemical synthesis. The optical absorption spectrum and a TEM image of an electrochemically generated gold nanorods are shown in Figure 2-2.

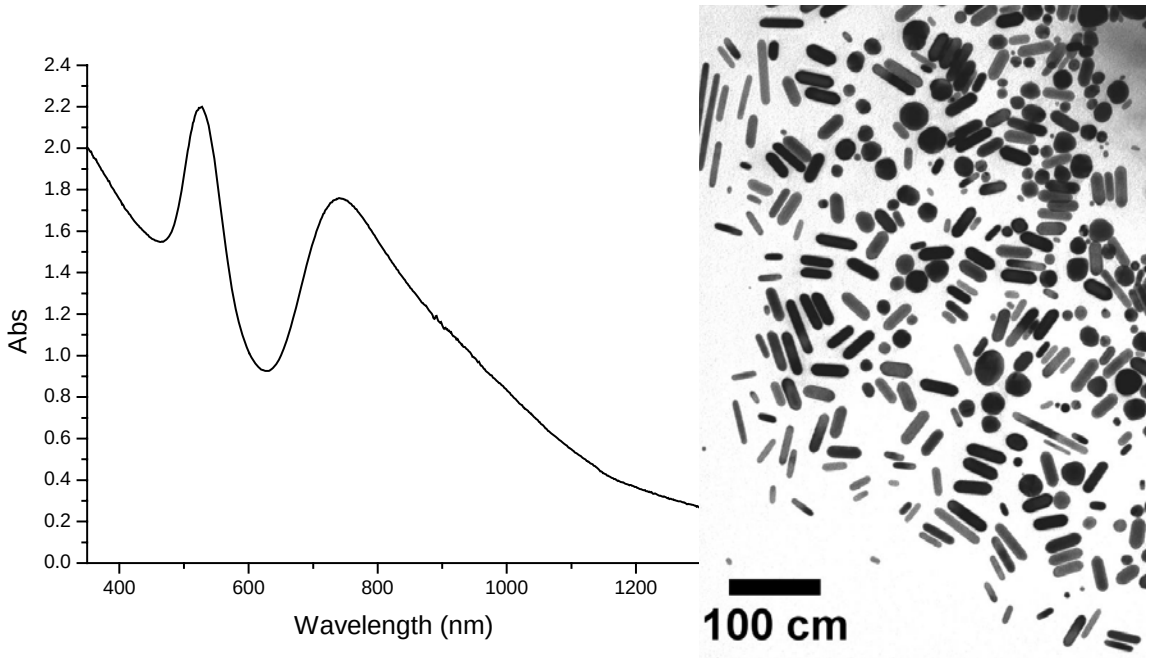

Figure 2-2: *Absorption spectra of gold nanorods synthesized with the electrochemical method (Plasmon max at 740nm) and TEM image of sample*

To obtain the concentrations of nanorods in solutions directly from absorption measurements, the molar absorptivity or the molar absorption coefficient was determined for two chemically synthesized nanorods. The molar absorption coefficient is a measure of the amount of light that one particle absorbs at any wavelength. Thus the molar absorption coefficient is determined for these two samples at the maximum wavelength of the longitudinal plasmon resonance. The two chemical nanorod samples were first dialyzed to remove any excess gold salt still present after synthesis or small nanoparticles not observable in TEM. The samples were then imaged by TEM and the length (L) and width (W) of the nanorods was determined by counting at least 250 nanorods. The volume (V_{rods}) was calculated of each rod was calculated assuming for a cylinder with two hemispherical end caps as follows.

$$V_{rods} = \pi L\left(\frac{W}{2}\right)^2 + \frac{4}{3}\pi\left(\frac{W}{2}\right)^3 \qquad (2.1)$$

The TEM images are also analyzed to determine the percentage of the sample that is nanorods as used later in the calculation. The data for the aspect ratio and percentage of nanorods can be seen in Table 2-1. Inductively Coupled Argon Plasma (ICAP) is used to analyze the concentration of gold in solution after dialysis. The concentration of nanorods could then be calculated by the following equation.

$$c_{NR} = \frac{c_{Au} * \%_{rods}}{\rho_{Au} * V_{rods}} \qquad (2.2)$$

Where ρ_{Au} is the density of bulk gold (59 atoms/nm^3), c_{Au} is the concentration of gold atoms as determined by ICAP, $\%_{rods}$ is the percentage rods in the sample from TEM. The average volume (V_{rods}) calculated from equation1 of the nanorods from TEM analysis is used. The molar extinction coefficient can then be determined using Beer's law.

$$A = \varepsilon l c_{NR} \qquad (2.3)$$

Where A is the absorbance at that wavelength, ε is the molar absorption coefficient, *l* is the path length (1cm for all experiments shown here) and c_{NR} is the concentration of nanorods in solution. The absorbance of each sample can be seen in Figure 2-3. The molar absorption coefficient was found to be 2.10x10^9 M^{-1}cm^{-1} at 880nm for aspect ratio 5.0 sample Au900, and 2.27x10^9 M^{-1}cm^{-1} at 1030nm for aspect ratio 6.4 sample Au1000 as seen in Table 1. These numbers are similar to those published previously for lower aspect ratios. [102, 151-153] Orendroff and Murphy[102] report the molar absorption coefficient of the longitudinal plasmon resonance to vary linearly from 2.5x10^9 M^{-1}cm^{-1} to 5.5x10^9 M^{-1}cm^{-1} for aspect ratios 2.0 to 4.5. Nikoobakht reports (p. 219) [151] molar absorption coefficient at the maximum plasmon resonance to be 1x10^8 to 4x10^9 from aspect ratios 2.6 to 8.5 with a plateau behavior as the aspect ratio increases. Liao and Hafner[152] report

an absorption coefficient of $4.4 \times 10^9\ M^{-1}cm^{-1}$ for 15nm by 50nm gold nanorods. These values will be further investigated in Chapter 3.

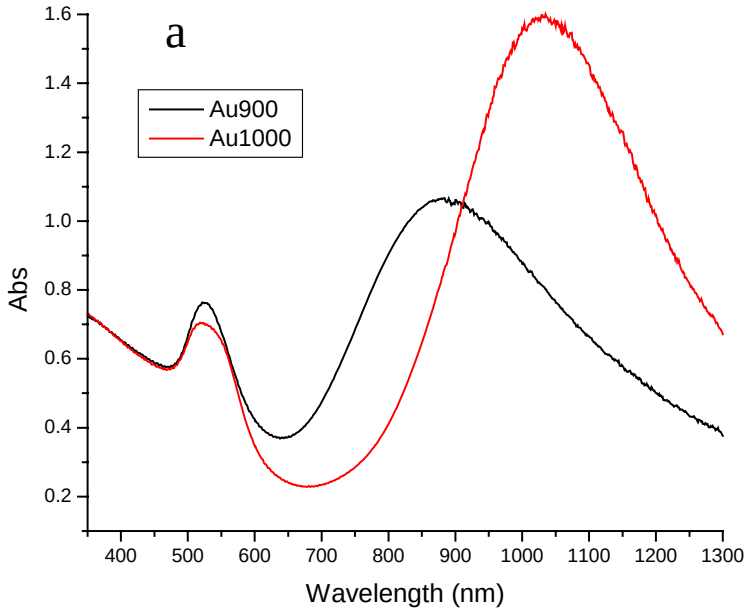

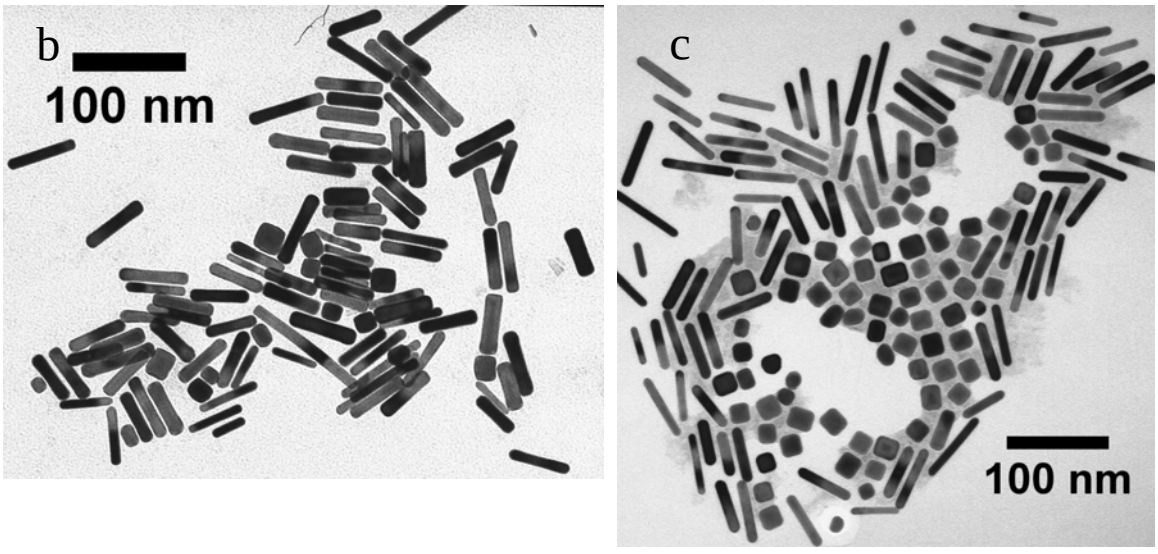

Figure 2-3: *a) Absorption spectra of nanorods for gold nanorod absorption coefficient b) TEM image of sample Au900 and c) TEM image of sample Au1000. Samples were dialyzed for at least 3 days.*

Table 2-1: *Rods used for ε analysis size population data and shape percentages as calculated from TEM images.*

Absorption Coefficient of Nanorods

Sample	AR	Length (nm)	Width (nm)	V (nm^3)	% rods	C_{NR} [M]	ε
Au900	5.0	52.5	11.2	6280	0.73	5.06E-10	2.10E+09
Au1000	6.4	57.3	9.2	4300	0.81	7.01E-10	2.27E+09

References

1. Turkevich, J.; Garton, G.; Stevenson, P. C., The color of colloidal gold. *J. Colloid Sci.* **1954,** 9, (Supplement 1), 26-35.

2. Turkevich, J.; Stevenson, P. C.; Hillier, J., A study of the nucleation and growth processes in the synthesis of colloidal gold. *Discuss. Faraday Soc.* **1951,** 11, 55-75.

3. Turkevich, J., Colloidal Gold. Part I. *Gold Bull.* **1985,** 18, (3), 86-91.

4. Henglein, A., Radiolytic preparation of ultrafine colloidal gold particles in aqueous solution: Optical spectrum, controlled growth, and some chemical reactions. *Langmuir* **1999,** 15, (20), 6738-6744.

5. Henglein, A.; Meisel, D., Radiolytic control of the size of colloidal gold nanoparticles. *Langmuir* **1998,** 14, (26), 7392-7396.

6. Mosseri, S.; Henglein, A.; Janata, E., Reduction of $Au(CN)_2^-$ In Aqueous Solution. Formation of Nonmetallic Clusters and Colloidal Gold. *J. Phys. Chem.* **1989,** 93, (18), 6791-6795.

7. Gachard, E.; Remita, H.; Khatouri, J.; Keita, B.; Nadjo, L.; Belloni, J., Radiation-induced and chemical formation of gold clusters. *New. J. Chem.* **1998**, 1257-1265.

8. Henglein, A.; Giersig, M., Formation of Colloidal Silver Nanoparticles: Capping Action of Citrate. *J. Phys. Chem. B* **1999,** 103, (44), 9533-9539.

9. Brust, M.; Bethell, D.; Kiely, C. J.; Schiffrin, D. J., Self-Assembled Gold Nanoparticle Thin Film with Nonmetallics Optical and Electronic Properites. *Langmuir* **1998,** 14, (19), 5425-5429.

10. Brust, M.; Walker, M.; Bethell, D.; Schiffrin, D.; Whyman, R., Synthesis of Thiol-derivatised Gold Nanoparticles in a Two-phase Liquid-Liquid System. *J. Chem. Soc., Chem. Comm.* **1994**, 801-802.

11. Brust, M.; Schiffrin, D. J.; Bethell, D.; Kiely, C. J., Novel gold-dithiol nano-networks with non-metallic electronic properties. *Adv. Mater.* **1995,** 7, (9), 795-797.

12. Brust, M.; Fink, J.; Bethell, D.; Schiffrin, D. J.; Kiely, C., Synthesis and reactions of functionalised gold nanoparticles. *J. Chem. Soc., Chem. Comm.* **1995**, 1655-1656.

13. Yee, C. K.; Jordan, R.; Ulman, A.; White, H.; King, A.; Rafailovich, M.; Sokolov, J., Novel One-Phase Synthesis of Thiol-Functionalized Gold, Palladium, and Iridium Nanoparticles Using Superhydride. *Langmuir* **1999,** 15, (10), 3486-3491.

14. Chen, S.; Templeton, A. C.; Murray, R. W., Monolayer-Protected Cluster Growth Dynamics. *Langmuir* **2000,** 16, (7), 3543-3548.

15. Frenkel, A. I.; Nemzer, S.; Pister, I.; Soussan, L.; Harris, T.; Sun, Y.; Rafailovich, M. H., Size-controlled synthesis and characterization of thiol-stabilized gold nanoparticles. *J. Chem. Phys.* **2005,** 123, (18), 18470/1-6.

16. Hussain, I.; Graham, S.; Wang, Z.; Tan, B.; Sherrington, D. C.; Rannard, S. P.; Cooper, A. I.; Brust, M., Size-Controlled Synthesis of Near-Monodisperse Gold Nanoparticles in the 1-4 nm Range Using Polymeric Stabilizers. *J. Am. Chem. Soc.* **2005,** 127, (47), 16398-16399.

17. Jana, N. R.; Gearheart, L.; Murphy, C. J., Wet Chemical Synthesis of Silver Nanorods and Nanowires of Controllable Aspect Ratio. *Chem. Commun.* **2001**, 617-618.

18. Nikoobakht, B.; El-Sayed, M. A., Preparation and growth mechanism of gold nanorods (NRs) using seed-mediated growth method. *Chem. Mater.* **2003,** 15, (10), 1957-1962.

19. Zhang, Z.; Han, M., Template-directed growth from small clusters into uniform silver nanoparticles. *Chem. Phys. Lett.* **2003,** 374, (1-2), 91-94.

20. Pal, T.; Sau, T. K.; Jana, N. R., Reversible formation and dissolution of silver nanoparticles in aqueous surfactant media. *Langmuir* **1997,** 13, (6), 1481-1485.

21. Yonezawa, T.; Onoue, S. Y.; Kimizuka, N., Preparation of Highly Positively Charged Silver Nanoballs and Their Stability. *Langmuir* **2000,** 16, (12), 5218-5220.

22. Sarkar, A.; Kapoor, S.; Mukherjee, T., Preparation, Characterization, and Surface Modification of Silver Nanoparticles in Formamide. *J. Phys. Chem. B* **2005,** 109, (16), 7698-7704.

23. Duff, D. G.; Baiker, A.; Edwards, P. P., A New Hydrosol of Gold Clusters. !. Formation and Particle Size Variation. *Langmuir* **1993,** 9, (9), 2301-2309.

24. Qi, Z.; Zhou, H.; Matsuda, N.; Honma, I.; Shimada, K.; Takatsu, A.; Kato, K., Characterization of Gold Nanoparticles Synthesized Using Sucrose by Seeding Formation in the Solid Phase and Seeding Growth in Aqueous Solution. *J. Phys. Chem. B* **2004,** 108, (22), 7006-7011.

25. Raveendran, P.; Fu, J.; Wallen, S. L., Completely "Green" Synthesis and Stabilization of Metal Nanoparticles. *J. Am. Chem. Soc.* **2003,** 125, (46), 13940-13941.

26. Bonet, F.; Delmas, V.; Grugeon, S.; Urbina, R. H.; Silvert, P. Y.; Tekaia-Elhsissen, K., Synthesis of monodisperse Au, Pt, Pd, Ru and Ir nanoparticles in ethylene glycol. *Nanostruct. Mater.* **1999,** 11, (8), 1277-1284.

27. DucampSanguesa, C.; HerreraUrbina, R.; Figlarz, M., Synthesis and Characterization of Fine and Monodisperse Silver Particles of Uniform Shape. *J. Solid State Chem.* **1992,** 100, (2), 272-280.

28. Fievet, F.; Lagier, J. P.; Blin, B.; Beaudoin, B.; Figlarz, M., Homogeneous and Heterogeneous Nucleations in the Polyol Process for the Preparation of Micron and Sub-Micron Size Metal Particles. *Solid State Ionics* **1989,** 32-3, 198-205.

29. Kim, F.; Connor, S.; Song, H.; Kuykendall, T.; Yang, P. D., Platonic gold nanocrystals. *Angew. Chem. Int. Ed.* **2004,** 43, (28), 3673-3677.

30. Silvert, P. Y.; Tekaiaelhsissen, K., Synthesis of Monodisperse Submicronic Gold Particles by the Polyol Process. *Solid State Ionics* **1995,** 82, (1-2), 53-60.

31. Sun, Y. G.; Xia, Y. N., Shape-controlled synthesis of gold and silver nanoparticles. *Science* **2002,** 298, (5601), 2176-2179.

32. Wiley, B.; Herricks, T.; Sun, Y. G.; Xia, Y. N., Polyol synthesis of silver nanoparticles: Use of chloride and oxygen to promote the formation of single-crystal, truncated cubes and tetrahedrons. *Nano Lett.* **2004,** 4, (9), 1733-1739.

33. Bonet, F.; Guery, C.; Guyomard, D.; Urbina, R. H.; Tekaia-Elhsissen, K.; Tarascon, J.-M., Electrochemical reduction of noble metal compounds in ethylene glycol. *Int. J. Inorg. Mater.* **1999,** 1, 47-51.

34. Sun, Y. G.; Yin, Y. D.; Mayers, B. T.; Herricks, T.; Xia, Y. N., Uniform silver nanowires synthesis by reducing AgNO3 with ethylene glycol in the presence of seeds and poly(vinyl pyrrolidone). *Chem. Mater.* **2002,** 14, (11), 4736-4745.

35. Xia, Y.; Rogers, J. A.; Paul, K. E.; Whitesides, G. M., Unconventional Methods for Fabricating and Patterning Nanostructures *Chem. Rev.* **1999,** 99, (7), 1823-1848.

36. Sun, Y.; Mayers, B.; Xia, Y., Transformation of Silver Nanospheres into Nanobelts and Triangular Nanoplates through a Thermal Process. *Nano Lett.* **2003,** 3, (5), 675-679.

37. Wiley, B. J.; Xiong, Y.; Li, Z. Y.; Yin, Y.; Xia, Y., Right Bipyramids of Silver: A New Shape Derived from Single Twinned Seeds. *Nano Lett.* **2006**.

38. Sun, Y.; Mayers, B. T.; Xia, Y., Template-Engaged Replacement Reaction: A One-Step Approach to the Large-Scale Synthesis of Metal Nanostructures with Hollow Interiors. *Nano Lett.* **2002,** 2, (5), 481-485.

39. Sun, Y.; Xia, Y., Increased Sensitivity of Surface Plasmon Resonance of Gold Nanoshells Compared to That of Gold Solid Colloids in Response to Environmental Changes. *Anal. Chem.* **2002,** 74, (20), 5297-5305.

40. Sun, Y.; Xia, Y., Mechanistic Study on the Replacement Reaction between Silver Nanostructures and Chloroauric Acid in Aqueous Medium. *J. Am. Chem. Soc.* **2004,** 126, (12), 3892-3901.

41. Sun, Y.; Mayers, B.; Xia, Y., Metal Nanostructures with Hollow Interiors. *Adv. Mater.* **2003,** 15, (7-8), 641-646.

42. Lee, Y. T.; Im, S. H.; Wiley, B.; Xia, Y., Quick Formation of Single-Crystals Nanocubes of Silver Through Dual Functions of Hydrogen Gas in Polyol Synthesis. *Chem. Phys. Lett.* **2005,** 411, 479-483.

43. Mandal, M.; Ghosh, S. K.; Kundu, S.; Esumi, K.; Pal, T., UV photoactivation for size and shape controlled synthesis and coalescence of gold nanoparticles in micelles. *Langmuir* **2002,** 18, (21), 7792-7797.

44. Kapoor, S., Preparation, characterization, and surface modification of silver particles. *Langmuir* **1998,** 14, (5), 1021-1025.

45. Kometani, N.; Doi, H.; Asami, K.; Yonezawa, Y., Laser flash photolysis study of the photochemical formation of colloidal Ag nanoparticles in the presence of benzophenone. *Phys. Chem. Chem. Phys.* **2002,** 4, 5142-5147.

46. Korchev, A. S.; Bozack, M. J.; Slaten, B. L.; Mills, G., Polymer-initiated photogeneration of silver nanoparticles in SPEEK/PVA films: Direct metal photopatterning. *J. Am. Chem. Soc.* **2004,** 126, (1), 10-11.

47. Eustis, S.; Krylova, G.; Eremenko, A.; Smirnova, N.; Schill, A. W.; El-Sayed, M. A., Growth and fragmentation of silver nanoparticles in their synthesis with a fs laser and CW light by photo-sensitization with benzophenone. *Photochem. Photobio. Sci.* **2005,** 4, (1), 154-159.

48. Esumi, K.; Suzuki, A.; Aihara, N.; Usui, K.; Torigoe, K., Preparation of Gold Colloids with UV Irradiation Using Dendrimers as Stabilizer. *Langmuir* **1998,** 14, 3157-3159.

49. Zhou, Y.; Yu, S. H.; Wang, C. Y.; Li, X. G.; Zhu, Y. R.; Chen, Z. Y., A Novel Ultraviolet Irradiation Photoreduction Technique for the Preparation of Single-Crystal Ag Nanorods and Ag Dendrites. *Adv. Mater.* **1999,** 11, (10), 850-852.

50. Zhao, C. J.; Qu, S. L.; Qiu, J. R.; Zhu, C. S., Photoinduced formation of colloidal Au by a near-infrared femtosecond laser. *J. Mater. Res.* **2003,** 18, (7), 1710-1714.

51. Hirose, T.; Omatsu, T.; Sugiyama, M.; Inasawa, S.; Koda, S., Au-nano-particles production by pico-second ultra-violet laser deposition in Au-ion doped PMMA film. *Chem. Phys. Lett.* **2004,** 390, (1-3), 166-169.

52. Malone, K.; Weaver, S.; Taylor, D.; Cheng, H.; Sarathy, K. P.; Mills, G., Formation Kinetics of Small Gold Crystallites in Photoresponsive Polymer Gels. *J. Phys. Chem. B* **2002,** 106, (30), 7422-7431.

53. Stellacci, F.; Bauer, C. A.; Meyer-Friedrichsen, T.; Wenseleers, W.; Alain, V.; Kuebler, S. M.; Pond, S. J. K.; Zhang, Y.; Marder, S. R.; Perry, J. W., Laser and Electron-Beam Induced Growth of Nanoparticles for 2D and 3D Metal Patterning. *Adv. Mater.* **2002,** 14, (3), 194-198.

54. Mayer, A.; Antonietti, M., Investigation of polymer-protected noble metal nanoparticles by transimssion electron microscopy: control of particle morphology and shape. *Colloid Polym. Sci.* **1998,** 276, 769-779.

55. Zhou, Y.; Wang, C. Y.; Zhu, Y. R.; Chen, Z. Y., A Novel Ultraviolet Irradiation Technique for Shape-Controlled Synthesis of Gold Nanoparticles at Room Temperature. *Chem. Mater.* **1999,** 11, 2310-2312.

56. Korchev, A. S.; Shulyak, T. S.; Slaten, B. L.; Gale, W. F.; Mills, G., Sulfonated Poly(Ether Ether Ketone)/Poly(Vinyl Alcohol) Sensitizing System for Solution Photogeneration of Small Ag, Au, and Cu Crystallites. *J. Phys. Chem. B* **2005,** 109, (16), 7733-7745.

57. Gaddy, G. A.; Korchev, A. S.; McLain, J. L.; Slaten, B. L.; Steigerwalt, E. S.; Mills, G., Light-Induced Formation of Silver Particles and Clusters in Crosslinked PVA/PAA Films. *J. Phys. Chem. B* **2004,** 108, (39), 14850-14857.

58. Gaddy, G. A.; McLain, J. L.; Korchev, A. S.; Slaten, B. L.; Mills, G., Kinetics of Silver Particle Photogeneration in Crosslinked PVA/PAA Films. *J. Phys. Chem. B* **2004,** 108, (39), 14858-14865.

59. Monti, O. L. A.; Fourkas, J. T.; Nesbitt, D. J., Diffraction-limited photogeneration and characterization of silver nanoparticles. *J. Phys. Chem. B* **2004,** 108, (5), 1604-1612.

60. Qu, S.; Zhao, C.; Jiang, X.; Fang, G.; Gao, Y.; Zeng, H.; Song, Y.; Qiu, J.; Zhu, C.; Hirao, K., Optical nonlinearities of space selectively precipitated Au nanoparticles inside glasses. *Chem. Phys. Lett.* **2003,** 368, (3-4), 352-358.

61. Jiang, X.; Qiu, J.; Zeng, H.; Zhu, C.; Hirao, K., Laser-controlled dissolution of gold nanoparticles in glass. *Chem. Phys. Lett.* **2004,** 391, 91-94.

62. Zhang, J.; Worley, J.; Denommee, S.; Kingston, C.; Jakubek, Z. J.; Deslandes, Y.; Post, M.; Simard, B.; Braidy, N.; Botton, G. A., Synthesis of Metal Alloy Nanoparticles in Solution by Laser Irradiation of a Metal Powder Suspension. *J. Phys. Chem. B* **2003,** 107, (29), 6920-6923.

63. Qiu, J.; Jiang, X.; Zhu, C.; Shirai, M.; Si, J.; Jiang, N.; Hirao, K., Manipulation of Gold Nanoparticles inside Transparent Materials. *Angew. Chem. Int. Ed.* **2004,** 43, 2230-2234.

64. Jin, R. C.; Cao, Y. C.; Hao, E. C.; Metraux, G. S.; Schatz, G. C.; Mirkin, C. A., Controlling anisotropic nanoparticle growth through plasmon excitation. *Nature* **2003,** 425, (6957), 487-490.

65. Jin, R. C.; Cao, Y. W.; Mirkin, C. A.; Kelly, K. L.; Schatz, G. C.; Zheng, J. G., Photoinduced conversion of silver nanospheres to nanoprisms. *Science* **2001,** 294, (5548), 1901-1903.

66. Callegari, A.; Tonti, D.; Chergui, M., Photochemically Grown Silver Nanoparticles with Wavelength-Controlled Size and Shape. *Nano Lett.* **2003,** 3, (11), 1565-1568.

67. Podlipensky, A. V.; Grebenev, V.; Seifert, G.; Graener, H., Ionization and photomodification of Ag nanoparticles in soda-lime glass by 150 fs laser irradiation: a luminescence study. *J. Luminescence* **2004,** 109, 135-142.

68. Hada, H.; Yonezawa, Y.; Yoshida, A.; Kurakake, A., Photoreduction of silver ion in aqueous and alcoholic solutions *J. Phys. Chem.* **1976,** 80, (25), 2728-2731.

69. Eustis, S.; Hsu, H.-Y.; El-Sayed, M. A., Gold Nanoparticle Formation from Photochemical Reduction of Au3+ by Continuous Excitation in Colloidal

Solutions. A Proposed Molecular Mechanism *J. Phys. Chem. B* **2005,** 109, (11), 4811-4815.

70. Kartuzhanskii, A. L.; Studzhinskii, O. P.; Plachenov, B. T.; Sokolova, I. V., Photoolysis of Tetrachloroaurate Anions. *J. Appl. Chem. USSR* **1986,** 59, (11), 2265-2268.

71. Studzhinskii, O. P.; Kartuzhanskii, A. L.; Plachenov, B. T., Photoreduction of Tetrachloroaurate Ions in Isopropyl Alcohol. *J. Gen. Chem. USSR* **1985,** 55, (3), 597-600.

72. Bronstein, L.; Chernyshov, D.; Valetsky, P.; Tkachenko, N.; Lemmetyinen, H.; Hartmann, J.; Forster, S., Laser photolysis formation of gold colloids in block copolymer micelles. *Langmuir* **1999,** 15, (1), 83-91.

73. Han, M. Y.; Quek, C. H., Photochemical synthesis in formamide and room-temperature Coulomb staircase behavior of size-controlled cold nanoparticles. *Langmuir* **2000,** 16, (2), 362-367.

74. Longenberger, L.; Mills, G., Formation of Metal Particles in Aqueous-Solutions by Reactions of Metal-Complexes with Polymers. *J. Phys. Chem.* **1995,** 99, (2), 475-478.

75. Kurihara, K.; Kizling, J.; Stenius, P.; Fendler, J. H., Laser and Pulse Radiolytically Induced Colloidal Gold Formation in Water and in Water-in-Oil Microemulsions. *J. Am. Chem. Soc.* **1983,** 105, (9), 2574-2579.

76. Yonezawa, Y.; Kawabata, I.; Sato, T., Photochemical Formation of Colloidal Gold Particles in Chitosan Films. *Ber. Bunsen-Ges. Phys. Chem.* **1996,** 100, (1), 39-45.

77. Leontidis, E.; Kleitou, K.; Kyprianidou-Leodidou, T.; Bekiari, V.; Lianos, P., Gold colloids from cationic surfactant solutions. 1. Mechanisms that control particle morphology. *Langmuir* **2002,** 18, (9), 3659-3668.

78. Wilcoxon, J. P.; Williamson, R. L.; Baughman, R., Optical Properties of Gold Colloids Formed in Inverse Micelles. *J. Chem. Phys.* **1993,** 98, (12), 9933-9950.

79. Caruso, R. A.; Ashokkumar, M.; Grieser, F., Sonochemical Formation of Gold Sols *Langmuir* **2002,** 18, (21), 7831-7836.

80. Su, C.-H.; Wu, P.-L.; Yeh, C.-S., Sonochemical Synthesis of Well-Dispersed Gold Nanoparticles at the Ice Temperature *J. Phys. Chem. B* **2003,** 107, (51), 14240-14243.

81. Okitsu, K.; Ashokkumar, M.; Grieser, F., Sonochemical Synthesis of Gold Nanoparticles: Effects of Ultrasound Frequency. *J. Phys. Chem. B* **2005,** 109, (44), 20673-20675.

82. Huang, S.; Ma, H.; Zhang, X.; Yong, F.; Feng, X.; Pan, W.; Wang, X.; Wang, Y.; Chen, S., Electrochemical Synthesis of Gold Nanocrystals and Their 1D and 2D Organization. *J. Phys. Chem. B* **2005,** 109, (42), 19823-19830.

83. Liu, Y. C.; Chuang, T. C., Synthesis and Characterization of Gold/Polypyrrole Core-Shell Nanocomposites and Elemental Gold Nanoparticles Based on the Gold-Containing Nanocomplexes Prepared by Electrochemical Methods in Aqueous Solutions. *J. Phys. Chem. B* **2003,** 107, (45), 12383-12386.

84. Yin, B.; Ma, H.; Wang, S.; Chen, S., Electrochemical Synthesis of Silver Nanoparticles under Protection of Poly(N-vinylpyrrolidone) *J. Phys. Chem. B* **2003,** 107, (34), 8898-8904.

85. McLeod, M. C.; McHenry, R. S.; Beckman, E. J.; Roberts, C. B., Synthesis and Stabilization of Silver Metallic Nanoparticles and Premetallic Intermediates in Perfluoropolyether/CO_2 Reverse Micelle Systems. *J. Phys. Chem. B* **2003,** 107, (12), 2693-2700.

86. Pyatenko, A.; Yamaguchi, M.; Suzuki, M., Laser Photolysis of Silver Colloid Prepared by Citric Acid Reduction Method. *J. Phys. Chem. B* **2005,** 109, (46), 21608-21611.

87. Wagner, J.; Kohler, J. M., Continuous Synthesis of Gold Nanoparticles in a Microreactor. *Nano Lett.* **2005,** 5, (4), 685-691.

88. Jana, N. R.; Peng, X., Single-Phase and Gram-Scale Routes toward Nearly Monodisperse Au and Other Noble Metal Nanocrystals. *J. Am. Chem. Soc.* **2003,** 125, (47), 14280-14281.

89. El-Sayed, M. A., Some interesting properties of metals confined in time and nanometer space of different shapes. *Acc. Chem. Res.* **2001,** 34, (4), 257-264.

90. Eustis, S.; El-Sayed, M. A., Why Gold Nanoparticles Are More Precious than Pretty Gold: Noble Metal Surface Plasmon Resonance and its Enhancement of the Radiative and Nonradiative Properties of Nanocrystals of Different Shapes. *Chem. Soc. Rev.* **2006,** 35, (3), 209-217.

91. Link, S.; El-Sayed, M. A., Simulation of the Optical Absorption Spectra of Gold Nanorods as a Function of Their Aspect Ratio and the Effect of the Medium Dielectric Constant (Addition/Correction). *J. Phys. Chem. B* **2005,** 109, (20), 10531-104532.

92. Link, S.; Mohamed, M. B.; El-Sayed, M. A., Simulation of the optical absorption spectra of gold nanorods as a function of their aspect ratio and the effect of the medium dielectric constant. *J. Phys. Chem. B* **1999,** 103, (16), 3073-3077.

93. Murphy, C. J.; Sau, T. K.; Gole, A. M.; Orendorff, C. J. G., J.; Gou, L.; Hunyadi, S. E.; Li, T., Anisotropic Metal Nanoparticles: Synthesis, Assembly, and Optical Applications *J. Phys. Chem. B* **2005,** 109, (29), 13857-13870.

94. Liu, M. Z.; Guyot-Sionnest, P., Mechanism of Silver(I)-Assisted Growth of Gold Nanorods and Bipyramids. *J. Phys. Chem. B* **2005,** 109, (47), 22192-22200.

95. Gole, A.; Murphy, C. J., Seed-Mediated Synthesis of Gold Nanorods: Role of the Size and Nature of the Seed. *Chem. Mater.* **2004,** 16, (19), 3633-3640.

96. Sau, T. K.; Murphy, C. J., Seeded High Yield Synthesis of Short Au Nanorods in Aqueous Solution. *Langmuir* **2004,** 20, (15), 6414-6420.

97. Nikoobakht, B.; El-Sayed, M. A., Evidence for bilayer assembly of cationic surfactants on the surface of gold nanorods. *Langmuir* **2001,** 17, (20), 6368-6374.

98. Torigoe, K.; Esumi, K., Preparation of colloidal gold by photoreduction of tetracyanoaurate(1-)-cationic surfactant complexes *Langmuir* **1992,** 8, (1), 59-63.

99. Esumi, K.; Hara, J.; Aihara, N.; Usui, K.; Torigoe, K., Preparation of Anisotropic Gold Particles Using a Gemini Surfactant Template. *J. Colloid Interface Sci.* **1998,** 208, 578-581.

100. Liao, H.; Hafner, J. H., Monitoring Gold Nanorod Synthesis on Surfaces. *J. Phys. Chem. B* **2004,** 108, (50), 19276-19280.

101. Filankembo, A.; Giorgio, S.; Lisiecki, I.; Pileni, M. P., Is the Anion the Major Parameter in the Shape Control of Nanocrystals? . *J. Phys. Chem. B* **2003,** 107, (30), 7492-7500.

102. Orendorff, C. J.; Murphy, C., J., Quantitation of Metal Content in the Silver-Assisted Growth of Gold Nanorods. *J. Phys. Chem. B* **2006,** 110, (9), 3990-3994.

103. Kim, F.; Song, J. H.; Yang, P., Photochemical Synthesis of Gold Nanorods *J. Am. Chem. Soc.* **2002,** 124, (48), 14316-14317.

104. Miranda, O. R.; Ahmadi, T. S., Effects of Intensity and Energy of CW UV Light on the Growth of Gold Nanorods. *J. Phys. Chem. B* **2005,** 109, (33), 15724-15734.

105. Filankembo, A.; Pileni, M. P., Is the Template of Self-Colloidal Assemblies the Only Factor That Controls Nanocrystal Shapes? *J. Phys. Chem. B* **2000,** 104, (25), 5865-5868.

106. Chen, H. M.; Peng, H. C.; Liu, R. S.; Asakura, K.; Lee, C. L.; Lee, J. F.; Hu, S. F., Controlling the Length and Shape of Gold Nanorods. *J. Phys. Chem. B* **2005,** 109, (42), 19553-19555.

107. Pérez-Juste, J.; Liz-Marzán, L. M.; Carnie, S.; Chan, D. Y. C.; Mulvaney, P., Electric-Field-Directed Growth of Gold Nanorods in Aqueous Surfactant Solutions. *Adv. Funct. Mater.* **2004,** 14, (6), 571-579.

108. Johnson, C. J.; Dujardin, E.; Davis, S. A.; Murphy, C. J.; Mann, S., Growth and form of gold nanorods prepared by seed-mediated, surfactant-directed synthesis. *J. Mater. Chem.* **2002,** 12, 1765 - 1770.

109. Sau, T. K.; Murphy, C. J., Room Temperature, High-Yield Synthesis of Multiple Shapes of Gold Nanoparticles in Aqueous Solution *J. Am. Chem. Soc.* **2004,** 126, (28), 8648-8649.

110. Busbee, B. D.; Obare, S. O.; Murphy, C. J., An Improved Synthesis of High-Aspect-Ratio Gold Nanorods. *Adv. Mater.* **2003,** 15, (5), 414-416.

111. Jana, N. R.; Gearheart, L.; Murphy, C. J., Wet Chemical Synthesis of High Aspect Ratio Cylindrical Gold Nanorods. *J. Phys. Chem. B* **2001,** 105, (19), 4065-4067.

112. Jana, N. R.; Gearheart, L.; Murphy, C. J., Seed-Mediated Growth Approach for Shape-Controlled Synthesis of Spheroidal and Rod-like Gold Nanoparticles Using a Surfactant Template. *Adv. Mater.* **2001,** 13, (18), 1389-1393.

113. Niidome, Y.; Nishioka, K.; Kawaski, H.; Yamada, S., Rapid synthesis of gold nanorods by the combination of chemical reduction and photoirradiation processes; morphological changes depending on the growing processes. *Chem. Commun.* **2003**, 2376-2377.

114. Y. Sun, Y. X., Large-Scale Synthesis of Uniform Silver Nanowires Through a Soft, Self-Seeding, Polyol Process. *Advanced Materials* **2002,** 14, (11), 833-837.

115. Caswell, K. K.; Bender, C. M.; Murphy, C. J., Seedless, Surfactantless Wet Chemical Synthesis of Silver Nanowires. *Nano Lett.* **2003,** 3, (5), 667-669.

116. Chen, H.; Gao, Y.; Zhang, H.; Liu, L.; Yu, H.; Tian, H.; Xie, S.; Li, J., Transmission-Electron-Microscopy Study on Fivefold Twinned Silver Nanorods. *J. Phys. Chem. B* **2004,** 108, (32), 12038-12043.

117. Martin, C. R., Membrane-Based Synthesis of Nanomaterials. *Chem. Mater.* **1996,** 8, (8), 1739-1746.

118. Thurn-Albrecht, T.; Schotter, J.; Kästle, G. A.; Emley, N.; Shibauchi, T.; Krusin-Elbaum, L.; Guarini, K.; Black, C. T.; Tuominen, M. T.; Russell, T. P., Ultrahigh-Density Nanowire Arrays Grown in Self-Assembled Diblock Copolymer Templates *Science* **2000,** 290, (5499), 2126 - 2129.

119. Ji, C.; Searson, P. C., Synthesis and Characterization of Nanoporous Gold Nanowires. *J. Phys. Chem. B* **2003,** 107, (19), 4494-4499.

120. Wei, Z.; Mieszawska, A. J.; Zamborini, F. P., Synthesis and Manipulation of High Aspect Ratio Gold Nanorods Grown Directly on Surfaces. *Langmuir* **2004,** 20, (11), 4322-4326.

121. Wei, Z.; Zamborini, F. P., Directly Monitoring the Growth of Gold Nanoparticle Seeds into Gold Nanorods. *Langmuir* **2004,** 20, (26), 11301-11304.

122. Niidome, Y.; Takahashi, H.; Urakawa, S.; Nishioka, K.; Yamada, T., Immobilization of Gold Nanorods on the Glass Substrate by the Electrostatic Interactions for Localized Plasmon Sensing. *Chem. Lett.* **2004,** 33, (4), 454-455.

123. Imura, K.; Nagahara, T.; Okamoto, H., Imaging of Surface Plasmon and Ultrafast Dynamics in Gold Nanorods by Near-Field Microscopy. *J. Phys. Chem. B* **2004,** 108, (42), 16344-16347.

124. Esumi, K.; Nawa, M.; Aihara, N.; Usui, K., Growth of rodlike Au/Pt particles in cationic micelles by UV irradiation. *New J. Chem.* **1998**, 719-720.

125. Yu, Y. Y.; Chang, S. S.; Lee, C. L.; Wang, C. R. C., Gold Nanorods: Electrochemical Synthesis and Optical Properties. *J. Phys. Chem. B* **1997,** 101, (34), 6661-6664.

126. Reetz, M. T.; Helbig, W., Size-Selective Synthesis of Nanostructured Transition Metal Clusters *J. Am. Chem. Soc.* **1994,** 116, (16), 7401-7402.

127. Reetz, M. T.; Helbig, W.; Quaiser, S. A.; Stimming, U.; Breuer, N.; Vogel, R., Visualization of Surfactants on Nanostructured Palladium Clusters by a Combination of STM and High-Resolution TEM. *Science* **1995,** 267, 367-369.

128. Hu, M.; Hillyard, P.; Hartland, G. V.; Kosel, T.; Perez-Juste, J.; Mulvaney, P., Determination of the Elastic Constants of Gold Nanorods Produced by Seed Mediated Growth. *Nano Lett.* **2004,** 4, (12), 2493-2497.

129. Sonnichsen, C.; Alivisatos, A. P., Gold Nanorods as Novel Nonbleaching Plasmon-Based Orientation Sensors for Polarized Single-Particle Microscopy. *Nano Lett.* **2005,** 5, (2), 301-304.

130. Eustis, S.; El-Sayed, M. A., The Aspect Ratio Dependence of the Enhanced Fluorescence Intensity of Gold Nanorods: Experimental and Simulation Study. *J. Phys. Chem. B* **2005,** 109, (34), 16350-16356.

131. Mohamed, M. B.; Volkov, V.; Link, S.; El-Sayed, M. A., The 'lightning' gold nanorods: fluorescence enhancement of over a million compared to the gold metal. *Chem. Phys. Lett.* **2000,** 317, (6), 517-523.

132. Nikoobakht, B.; Wang, Z. L.; El-Sayed, M. A., Self-assembly of gold nanorods. *J. Phys. Chem. B* **2000,** 104, (36), 8635-8640.

133. Huang, X.; El-Sayed, I. H.; Qian, W.; El-Sayed, M. A., Cancer Cell Imaging and Photothermal Therapy in the Near-Infrared Region by Using Gold Nanorods. *J. Am. Chem. Soc.* **2006,** 128, (6), 2115-2120.

134. Millstone, J. E.; Park, S.; Shuford, K. L.; Qin, L.; Schatz, G. C.; Mirkin, C. A., Observation of a Quadrupole Plasmon Mode for a Colloidal Solution of Gold Nanoprisms *J. Am. Chem. Soc.* **2005,** 127, (15), 5312-5313.

135. Metraux, G. S.; Mirkin, C. A., Rapid Themal Synthesis of Silver Nanoprisms with Chemically Tailorable Thickness. *Adv. Mater.* **2005,** 17, (4), 412-415.

136. Metraux, G. S.; Cao, Y. C.; Jin, R. C.; Mirkin, C. A., Triangular nanofrarnes made of gold and silver. *Nano Letters* **2003,** 3, (4), 519-522.

137. Shankar, S. S.; Rai, A.; Ankamwar, B.; Singh, A.; Ahmad, A.; Sastry, M., Biological synthesis of triangular gold nanoprisms. *Nature Mater.* **2004,** 3, (7), 482–488.

138. Pastoriza-Santos, I.; ; Liz-Marzan, L. M.; , Synthesis of Silver Nanoprisms in DMF *Nano Lett.* **2002,** 2, (8), 903-905.

139. He, R.; Qian, X.; Yin, J.; Zhu, Z., Preparation of polychrome silver nanoparticles in different solvents. *J. Mater. Chem.* **2002,** 12, 3783-3786.

140. Chen, S.; Fan, Z.; Carroll, D. L., Silver Nanodisks: Synthesis, Characterization, and Self-Assembly *J. Phys. Chem. B* **2002,** 106, (42), 10777-10781.

141. Maillard, M.; Huang, P.; Brus, L., Silver Nanodisk Growth by Surface Plasmon Enhanced Photoreduction of Adsorbed [Ag+] *Nano Lett.* **2003,** 3, (11), 1611-1615.

142. Maillard, M.; Giorgio, S.; Pileni, M. P., Silver Nanodisks. *Adv. Mater.* **2002,** 14, (15), 1084-1086.

143. Hao, E.; Kelly, K. L.; Hupp, J. T.; Schatz, G. C., Synthesis of Silver Nanodisks Using Polystyrene Mesospheres as Templates. *J. Am. Chem. Soc.* **2002,** 124, (51), 15182-15183.

144. Chen, S.; Carroll, D. L., Synthesis and Characterization of Truncated Triangular Silver Nanoplates *Nano Lett.* **2002,** 2, (9), 1003-1007.

145. Chen, S.; Carroll, D. L., Silver Nanoplates: Size Control in Two Dimensions and Formation Mechanisms *J. Phys. Chem. B* **2004,** 108, (18), 5500-5506.

146. Kan, C.; Zhu, X.; Wang, G., Single-Crystalline Gold Microplates: Synthesis, Characterization, and Thermal Stability. *J. Phys. Chem. B* **2006,** 110, (10), 4651-4656.

147. Jin, R.; Egusa, S.; Scherer, N. F., Thermally-Induced Formation of Atomic Au Clusters and Conversion into Nanocubes *J. Am. Chem. Soc.* **2004,** 126, (32), 9900-9901.

148. Chen, S.; Wang, Z. L.; Ballato, J.; Foulger, S. H.; Carroll, D. L., Monopod, Bipod, Tripod, and Tetrapod Gold Nanocrystals *J. Am. Chem. Soc.* **2003,** 125, (52), 16186-16187.

149. Hao, E.; Bailey, R. C.; Schatz, G. C.; Hupp, J. T.; Li, S., Synthesis and Optical Properties of "Branched" Gold Nanocrystals. *Nano Lett.* **2004,** 4, (2), 327-330.

150. Hu, J.; Zhang, Y.; Liu, B.; Liu, J.; Zhou, H.; Xu, Y.; Jiang, Y.; Yang, Z.; Tian, Z. Q., Synthesis and Properties of Tadpole-Shaped Gold Nanoparticles. *J. Am. Chem. Soc.* **2004,** 126, (31), 9470-9471.

151. Nikoobakht, B. Synthesis, characterization and self-assembly of gold nanorods and surface-enhanced Raman studies. Georgia Institute of Technology, Atlanta, GA, 2003.

152. Liao, H.; Hafner, J. H., Gold Nanorod Bioconjugates. *Chem. Mater.* **2005,** 17, (18), 4636-4641.

153. Nikoobakht, B.; Wang, J. P.; El-Sayed, M. A., Surface-enhanced Raman scattering of molecules adsorbed on gold nanorods: off-surface plasmon resonance condition. *Chem. Phys. Lett.* **2002,** 366, (1-2), 17-23.

CHAPTER 3

DETERMINATION OF THE ASPECT RATIO DISTRIBUTION OF GOLD NANORODS IN SOLUTION FROM A THEORETICAL FIT OF THE OBSERVED INHOMOGENEOUSLY BROADENED LONGITUDINAL PLASMON RESONANCE ABSORPTION SPECTRUM[‡]

Abstract

The determination of the statistical distribution of aspect ratios of a nanorod solution is desirable for experimentally synthesized solutions. The traditional method of using TEM images for size determination gives statistically incorrect values due to distortions introduced by TEM sample preparation and by difficulties in counting a sufficiently large number of rods. In the present work we propose a method to obtain the aspect ratio distribution using the observed longitudinal surface plasmon resonance absorption spectrum of gold nanorods in solution referred to as Gold Nanorod Optical Modeling Equations (GNOME). The observed inhomogeneously broadened spectrum is fitted with a collection of homogeneously broadened spectra of nanorods each with a specific aspect ratio and population contribution using Gans extension of Mie theory. The fit generates an aspect ratio distribution for the rods in solution from which the median value and the statistical distribution are determined. This method is statistically

[‡] The following article has been submitted to J. Appl. Phys. After it is published, it will be found at Eustis, S.; El-Sayed, M. A., Determination of the Aspect Ratio Statistical Distribution of Gold Nanorods in Solution from a Theoretical Fit of the Observed Inhomogeneously Broadened Longitudinal Plasmon Resonance Absorption Spectrum. *J. Appl. Phys* **2006,** Submitted.

more accurate, more convenient and less expensive than the traditional method of TEM analysis on a solid substrate.

Introduction

The optical properties of noble metal nanoparticles are of great interest due to the potential uses of the strong surface plasmon resonance absorption and scattering in the visible region of the electromagnetic spectrum.[1-4] This strong absorption leads to the enhancement in the electromagnetic field near the surface leading to enhancement of the absorption as well as the Raman and Rayleigh (Mie) scattering processes.[3, 4] Gold nanorods have two plasmon resonance absorptions, one due to the transverse oscillation of electrons around 520nm regardless of aspect ratio. The other absorption is much stronger and is due to the longitudinal oscillation of the electrons, whose wavelength maximum depends on the aspect ratio (length divided by width) of the nanorod. The resonances are due to a collective oscillation of the free electrons through the metal, which depend on the boundary conditions.

Nanorod synthesis by bottom up methods in solution use the electrochemical reduction method,[5-8] the seeded method with chemical reduction,[9-17] or the photochemical reduction method.[17-23] The resulting rods usually have a broad distribution of aspect ratios with a broad longitudinal plasmon absorption. The determination of the aspect ratios produced in a given synthesis is presently carried out by determining the aspect ratio of a few hundred nanorods in a few representative TEM images prepared by evaporating drops of the solution on a solid substrate. Both the sample preparation and the limited selection of a few images to determine the average size of the nanorods often lead to statically incorrect and irreproducible values. Furthermore, while TEM is an

essential instrument to the field of nanotechnology, allowing the physical imaging of structures on the nanoscale, its use is slow, costly, and requires long analysis times, due to the limited ability of software to recognize and distinguish nanoparticles from background effects. Non-spherical nanoparticles are more troublesome than spherical ones to be analyzed with software such as Image J[24] due to the increasing overlapping of different particles and the differing intensities due to twinning defects of nanorods.

The desire to characterize solution samples by optical absorption is attractive, as it is fast, easy, cheap, and non-destructive. The longitudinal plasmon resonance of gold nanorods is very sensitive to the aspect ratio. The bottom up technique of nanoparticle synthesis frequently produces polydispersed samples that have dispersion in the values of the nanorod aspect ratios. This gives rise to an inhomogeneously broadened absorption spectrum. This means that the observed inhomogeneous absorption spectrum is the result of the contribution of a number of overlapping homogeneously broadened spectra each having a specific aspect ratio.

The longitudinal plasmon resonance absorption of homogeneously broadened samples (i.e. samples with rods of a single aspect ratio) have been successfully modeled by Link et. al.[25-27] using Gans[28] extension of Mie's theory[29] and by the discrete dipole approximation (DDA).[30-32] For nanorods, these two methods agree well with one another,[30] allowing the simpler of the two (Gans model) to be used. However, these methods have yet to be applied to determine the distribution of the aspect ratio for synthesized samples in solution, which is a very useful parameter experimentally.

In the present work we show the determination of the aspect ratio distribution of a gold nanorod sample in solution from its absorption spectrum referred to as Gold

Nanorod Optical Modeling Equations (GNOME). The absorption spectrum is fitted to the calculated spectra of a collection of nanorods where each different aspect ratio has its own contribution. The aspect ratio distribution is determined from the fit and the contributions of each aspect ratio.

The distributions determined from the TEM images are not found to reproduce the observed longitudinal plasmon resonance absorption spectra of the samples due to the limited number of rods measured and the environmental change of the nanoparticle (from solution to solid support) which is necessary for TEM measurement. The absorption spectra measure the bulk solution properties and determine the properties of the nanorods in solution. Modeling of absorption spectrum of experimental samples has only been applied to samples previously characterized by transmission electron microscopy (TEM) for determination of the optical properties of different shapes.[25-27, 30-32]

Experimental

The gold nanorods are prepared by the chemical seeding technique described previously.[10, 16, 33-35] Briefly, a seed solution is generated by adding ice cold $NaBH_4$ to a solution of $HAuCl_4$ and hexadecyltrimethylammonium bromide (CTAB). The solution is kept at 25^{o}C for a few minutes before use. A brownish yellow color is observed in all seed solutions used. The growth solution contains 5mL of a solution of 0.20*m* CTAB and 0.25*m* benzyldimethylammonioum chloride hydrate (BDAC), which is added to 0.20mL of 4.0mM $AgNO_3$. Then 5.0mL of 0.90mM $HAuCl_4$ is added and 54μL of 0.10M ascorbic acid. Twelve microliters of seed solution is then added to the solution, which is left undisturbed for 4 hours for the nanorods to grow. Kinetic growth conditions determine the aspect ratio of the nanorods generated, with narrower widths in the higher

aspect ratio samples. The optical absorbance spectra are recorded on a Shimadzu UV-3101-PC UV-Vis-NIR scanning spectrometer. A JEOL100 transmission electron microscope (TEM) an accelerating voltage of 100kV at The Center for Nanostructure Characterization and Fabrication at Georgia Tech with is used for TEM characterization of experimental samples.

Theoretical Calculations

Absorption spectra of gold nanorods have been modeled previously by Link et. al.[25-27] They apply Gans[28] extension of Mie's theory[29] to calculate the absorption spectra of gold nanorods of different aspect ratios and medium dielectric constants. The absorption coefficient, γ, can be calculated in the dipole approximation (which should hold for these samples) as follows.

$$\gamma = \frac{2\pi NV\varepsilon_m^{3/2}}{3\lambda}\sum_J \frac{(1/P_J^2)\varepsilon_2}{\left(\varepsilon_1 + \frac{1-P_J}{P_J}\varepsilon_m\right)^2 + \varepsilon_2^2} \qquad (3.1)$$

where: $P_A = \frac{1-e^2}{e^2}\left[\frac{1}{2e}\ln\left(\frac{1+e}{1-e}\right)-1\right]$

$P_B = P_C = \frac{1-P_A}{2}$ and

$e = \sqrt{1-\left(\frac{W}{L}\right)^2}$

P_A, P_B and P_C are the shape factors as a function of e, which is a function of the inverse of the aspect ratio (=L/W), λ is the wavelength, ε_m is the dielectric constant of the medium (1.77 for all the samples), $\varepsilon = \varepsilon_1 + i\,\varepsilon_2$ is the complex dielectric constant of the metal, N is

the number of particles per unit volume, L is the length of the nanorod, W is the width of the nanorod, and $V=(4/3)\pi L(W/2)^2$ is the volume of the nanorod.

The shape factor used by Boyd and Shen[36-38], A, can be used in place of the shape factor, P_J.

$$A = \left[1 - \frac{\xi Q_1^{'}(\xi)}{Q_1(\xi)}\right]^{-1} \qquad (3.2)$$

$$\xi = \left[1 - \left(\frac{W}{L}\right)^2\right]^{-1/2}$$

$$Q_1(\xi) = \left(\frac{\xi}{2}\right)\ln\left[\frac{\xi+1}{\xi-1}\right] - 1$$

$$Q_1^{'}(\xi) = \frac{dQ_1(\xi)}{d\xi}$$

These two factors are very similar, but the calculated absorption spectrum resembled the experimental results more closely using A. Using equation 3.2 for A in place of P_J, thereby calculating only the longitudinal plasmon resonance of the nanorod, equation 1 can be simplified to the following equation:

$$\gamma = \frac{2\pi NV\varepsilon_m^{3/2}}{3\lambda}\frac{(\varepsilon_2 / A^2)}{\left(\varepsilon_1 + \frac{1-A}{A}\varepsilon_m\right)^2 + \varepsilon_2^2} \qquad (3.3)$$

Equation 3.3 is used to calculate the absorption coefficient of the homogeneously broadened spectra of the nanorods. The absorption coefficient is calculated for each aspect ratio between 1.5 and 9, every 0.25 to model absorption spectra of nanorod samples. Each aspect ratio is multiplied by the frequency representing the contribution of rods of that aspect ratio present to fit the absorption spectrum observed for the sample.

The sum of these calculated spectra times their respective frequency is fitted to the longitudinal plasmon resonance absorption by adjusting the frequency of each aspect ratio to match the experimentally observed absorption spectra. This distribution of aspect ratios is expected to represent the bulk properties of the samples.

Calculation Methods

To model the absorption spectrum and obtain the aspect ratio distribution, an Excel file with many worksheets is created for all calculations for each experimental sample. The theoretical calculation section presents the equations and definitions of the parameters used to determine the absorption. Figure 3-1 shows a representative scheme for the Excel file used for each experimental sample. The first worksheet of the Excel file contains all of the sample parameters, including aspect ratio, length, width, volume, ξ, $Q_1(\xi)$, $Q_1'(\xi)$, the medium dielectric constant, and the frequency factor of each aspect ratio in the sample (for fits to experimental data). All derivates are preformed using Origin 7 (OriginLab Co. 2002). To insure that all rods have the same volume, only the aspect ratio and the volume are used to obtain the dimensions of nanorods.

An aspect ratio worksheet is created for each aspect ratio studied between 1.5 and 9, every 0.25, shown pictorially in Figure 3-1. These worksheets contain the dielectric data from Johnson and Christy[39] with the wavelength in the first column. (The number of data points for the dielectric constant has been increased using Origin 7 to connect their data points, and read from the screen.) The data from the sample parameters is linked at the top of the aspect ratio worksheet to the sample parameters worksheet for easy access. Finally, equation 3 for the absorption coefficient can be used to calculate the intensity.

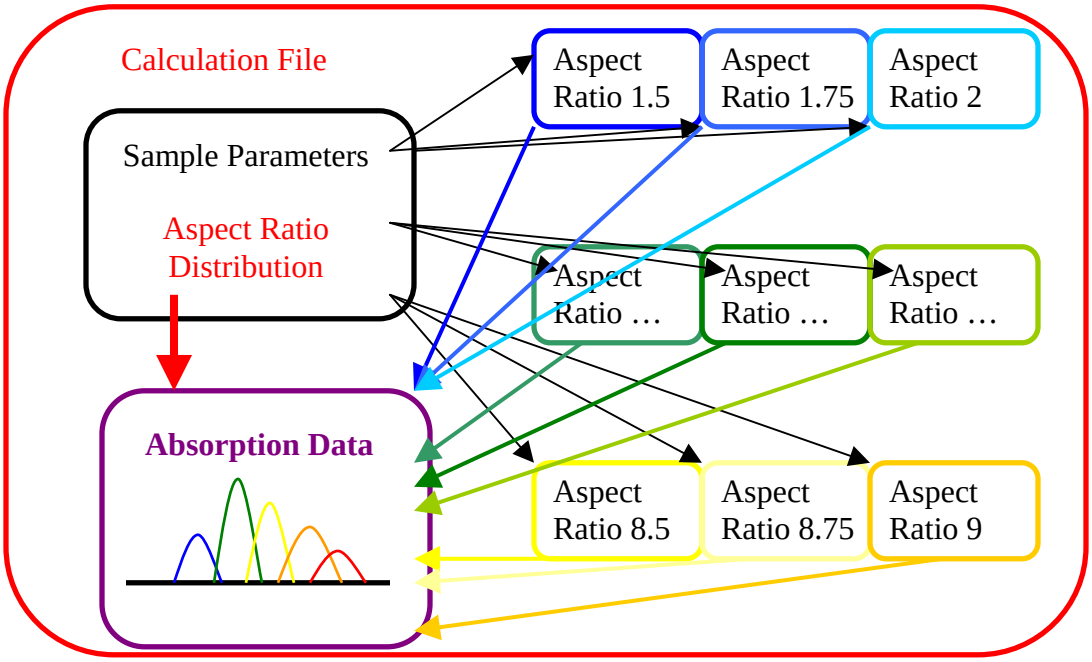

Figure 3-1: *Diagram of the excel file used to calculate the absorption spectra of the different aspect ratio and their distribution used to model the experimental absorption spectra.*

A new worksheet is then created with only the absorption data for each aspect ratio (from equating to the cell in the aspect ratio's worksheet). The absorption calculated is multiplied by the frequency factor from the sample parameters page. The sum of all the aspect ratios is obtained by summing the intensity contribution from the individual aspect ratios over all aspect ratios modeled at each wavelength. The sum is normalized using the maximum function in Excel to determine the absorption maximum of the sum column. A separate column is divided by the maximum (every wavelength divided by that one cell) to automatically obtain a normalized spectrum of the calculated absorption. The experimental data is added to this same worksheet by insuring that the wavelengths data is the same by multiplying it by the wavelengths from the dielectric

data (x data) with every "y" value equal to 1 in Origin 7. This allows visual comparison of experimental and calculated results.

Results

The longitudinal absorption spectrum of gold nanorods depends on the aspect ratio of the rod.[25-27] This absorption can be used as a measure of the aspect ratio of the sample, removing the need for TEM analysis. The absorption coefficients for unit volume nanorods of different aspect ratios are plotted in Figure 3-2. The volume of a given nanorod and the number of particles per unit volume are then multiplied by the value of the unit volume absorption coefficient presented here to obtain the experimentally comparable absorption coefficient. The plasmon resonance shifts to the red as the aspect ratio is increased, similar to previous reports. As the aspect ratio increases, the intensity of the absorption coefficient increases due to the larger degree of anisotropy of the particle. The width of the longitudinal plasmon resonance is also found to increase as the aspect ratio increases, leading to the need to model the whole absorption spectrum of the nanorods. Modeling only the peak absorption wavelength does not generate information about the distribution of the aspect ratio or the polydispersity, which is important in relating the properties of different experimental samples.

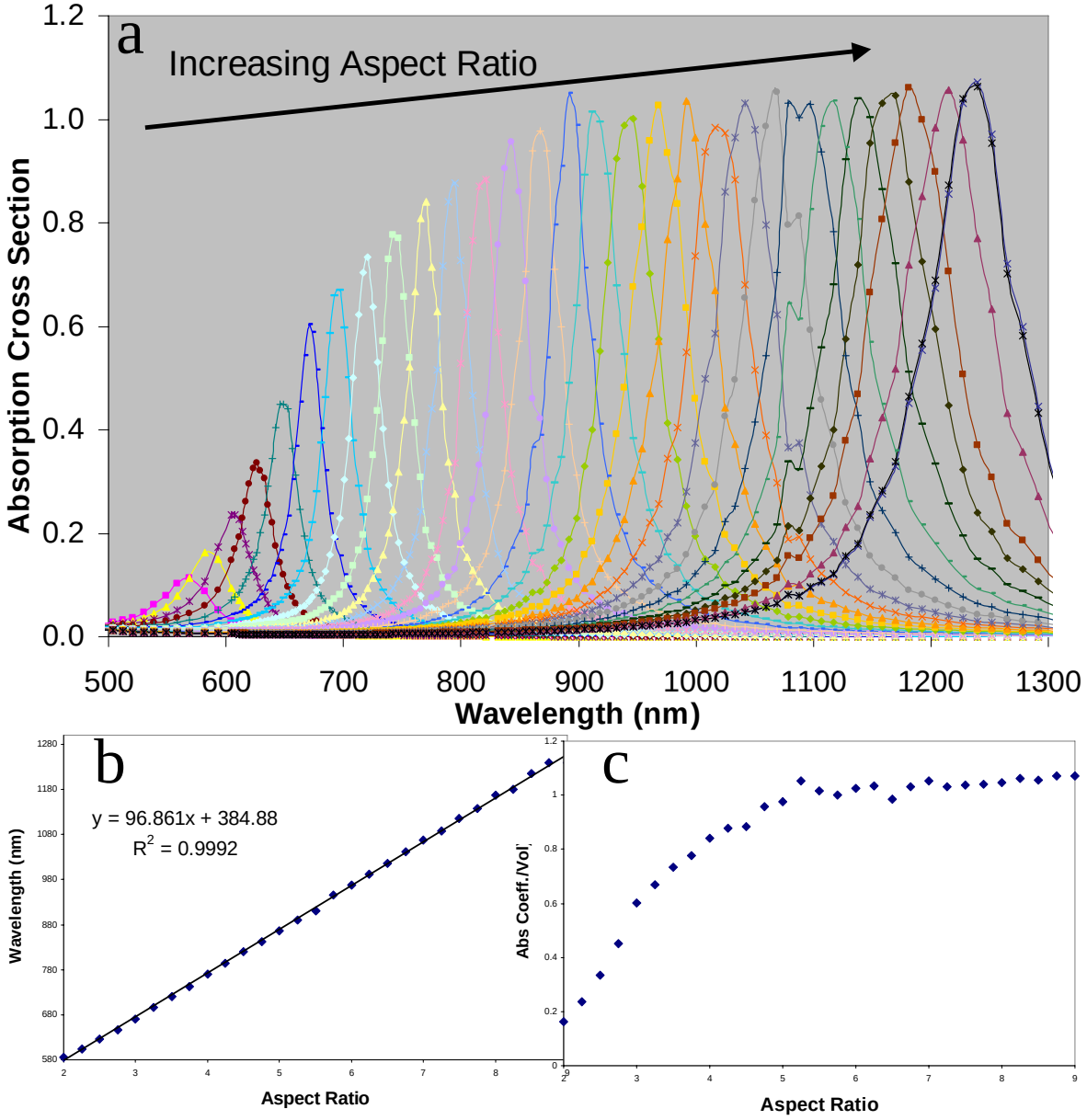

***Figure 3-2**: a) Longitudinal plasmon resonance absorption cross section calculated for different aspect ratios using Gans' Equation. The calculated dependence of b) wavelength maximum, and c) absorption coefficient on the aspect ratio*

Figure 3-2b and 3-2c show the maximum longitudinal plasmon resonance intensity and wavelength, respectively as calculated from equation 3 for a nanorod of unit volume. The results show a linear increase in the maximum of the longitudinal plasmon resonance intensity and wavelength as the aspect ratio is increased, as reported previously.[27, 30] As the aspect ratio continues to increase, the plasmon resonance wavelength continues to shift to longer wavelength. The equation obtained from fitting the wavelength maximum as a function of aspect ratio with ε_m=1.77 is:

$$\lambda_{max}=96.9AR + 384.9 \qquad (3.4)$$

This is similar to that reported previously.[27, 30] While the wavelength maximum continues to shift linearly with increasing aspect ratio, the intensity reaches a saturation value at an aspect ratio around 5. The maximum occurs at a value of 1, showing that all of the electrons involved in the dipole transition are moving the maximum effective distance at this aspect ratio. Increasing the aspect ratio of a nanorod with a constant volume does not increase the size of the induced dipole moment, μ=QL, even though the length (L) is longer, the charge density (Q) is less. Thus the strength of the dipole remains the same even as the aspect ratio increases for a constant volume nanorod as observed by the constant intensity for high aspect ratio nanorods.

In order to fit the experimentally observed gold nanorod solution spectra, the calculated longitudinal plasmon absorption spectra shown in Figure 3-2 are used. A frequency term reflecting the contribution of a certain aspect ratio nanorod to the observed spectrum is introduced for each aspect ratio calculated. This frequency will represent the aspect ratio distribution of the sample. Therefore the sum of the calculated longitudinal plasmon absorptions of each aspect ratio times its frequency factor is fit to

match the experimental longitudinal plasmon absorption. In order to compare the experimental absorption with the calculated spectra, both are normalized. The frequency terms of the different aspect ratios can then be modified by hand until the spectra overlay. In the future, a fitting algorithm can be applied to obtain the best fit to the absorption spectrum. An example of the experimental spectra along with the calculated and summed spectra is shown in Figure 3-3 for sample Au850, which has a median aspect ratio of 4.75. The contribution from each aspect ratio is shown by the other curves underneath this spectrum. The broadening of the absorption spectra is noticed on the red side of the longitudinal plasmon absorption spectra where a larger number of aspect ratios contribute to the absorption than on the blue side. This leads to the gap between the sum of the

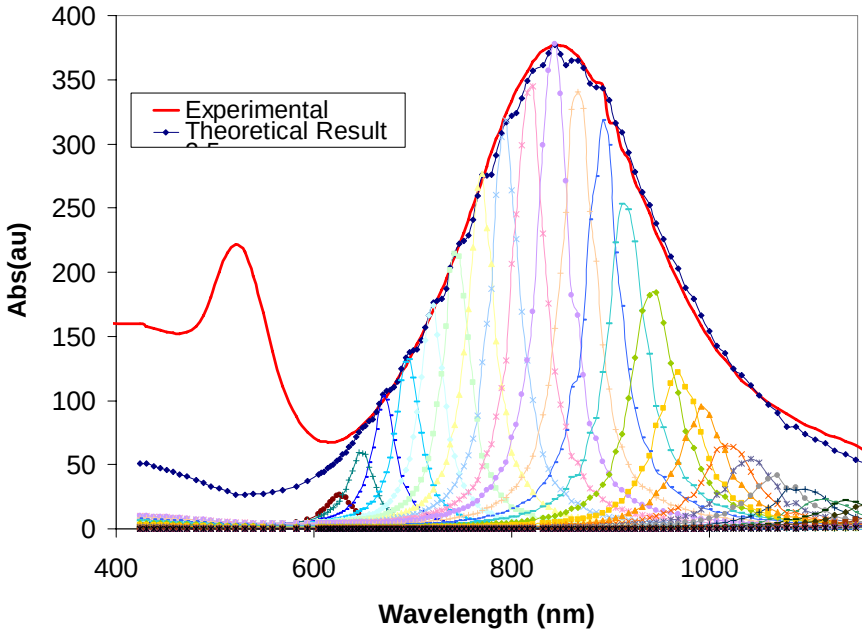

Figure 3-3: *The fit of the observed longitudinal absorption band of gold nanorods to the sum of the theoretically calculated homogeneously broadened absorption spectra of rods of different aspect ratios generating the aspect ratio distribution.*

components to give the theoretical result and the individual components observed in Figure 3-3.

The transverse plasmon is not calculated in these equations, as it is insensitive to the aspect ratio. Both the transverse plasmon resonance of gold nanorods and the plasmon resonance of gold nanospheres are present at 520nm. Thus any absorption modeling of the transverse plasmon must take into account both the spheres and the rods present in the solution. The absorption of gold spheres at 520 nm is relatively insensitive to changes in the diameter from 5-20nm.[40] Changes in the width of gold nanorods are expected to slightly modify the position of transverse plasmon resonance, but similar to gold spheres the shift is expected to be small. Thus due to the absorption of gold spheres and rods and the relative insensitivity to width of the transverse plasmon, the longitudinal plasmon resonance is chosen for fitting while the transverse plasmon is ignored. This suggests that the ability to predict the shape and size distribution is much more accurate for anisotropic shapes, due to the large changes observed in the optical absorption spectrum with small changes in the size or shape. This allows us to ignore the presence of other shapes that have their absorption at different wavelengths.

Equation 3.3 shows that the absorption coefficient is directly proportional to the volume of the nanorod. The volume in this calculation has been set to unity so that the calculated absorption coefficient can be multiplied by the volume and the number of electrons to obtain results to compare with experimental samples. Keeping the volume constant enables comparison of the cross section for different aspect ratios.

The volume, though assumed to be constant in these calculations, is a scalar quantity in the equations implying that it can be multiplied by the result at any time.

More importantly, due to the mechanism of growth, an increase in the aspect ratio results from an increase in the length and a smaller decrease in the width. The equations for the aspect ratios (AR) and volume (V_r) of each rod are calculated according to the following equations:

$$AR = \frac{L}{W} \tag{3.5}$$

$$V_r = \frac{4}{3}\pi\left(\frac{W}{2}\right)^2 L = \frac{\pi}{3}W^3 AR \tag{3.6}$$

where L is the length and W is the width of the nanorod. Thus one might expect that as the aspect ratio increases the volume would also increase. However, this is only true if the width of the rods remains constant. Other synthetic techniques generate nanorods with a constant length[5-7] or a constant width.[5-8] The chemical seeding synthesis is a kinetic process where both the length and width change with the aspect ratio. Analysis of the volumes and aspect ratios for nanorods obtained from TEM results show that each sample had an average volume that did not vary with the aspect ratio showing that similar amounts of gold are present in each nanorod. Thus, the higher aspect ratio nanorods formed from the seeded synthesis have narrower widths and longer lengths, leading to a similar volume for all nanorods in a given sample. The volume does not need to be compared between different samples as it only affects the intensity, which is normalized for each experimental sample. If a relationship is noticed between the volume and aspect ratio of rods made in a synthetic method as noticed in the electrochemical method,[5-8] a volume factor can be introduced to insure proper scaling with the aspect ratio. Thus the nanorod aspect ratio and volume are not related for samples grown with the seeded method.

Comparison of Optical and TEM Method

This study used TEM to authenticate the method used here and obtain general information about the nanorod dimensions. In order to compare the aspect ratio distribution obtained by the optical method and the TEM imaging, we measured TEM images of the nanorods used in the optical studies. These are shown in Figure 3-4.

The aspect ratio distributions obtained from fitting of the absorption spectra of 5 experimental samples are shown in Figure 3-5a along with the fits obtained from TEM analysis (dotted lines) (Figure 3-5b) of these same samples. The aspect ratio distributions for samples Au630 and Au900 from the fit to the optical absorption are similar to the TEM results. However, the aspect ratio distributions generated for samples Au700, Au850, and Au1000 are significantly different from the two methods.

To evaluate the aspect ratio distribution obtained from the fit to the absorption spectra, the optical absorption of the five experimental samples are shown in Figure 3-5c. This is then compared to the absorption spectra calculated from equation 3.3 and multiplied by aspect ratio distribution obtained from TEM. The modeled absorption spectrum using the distribution obtained from the TEM analysis (dotted lines) of these same samples are shown in Figure 3-5d. Some of the optical fits agree well with the TEM results (Au 630, Au900), while others are not as good, similar to the agreement between TEM and optically determined aspect ratio distributions. For samples Au700, Au850, and Au1000 the fits from TEM do not match the position of the experimental absorption maximum, nor the width of the experimental absorption spectrum. Since the method presented here involves modifying the size distribution until the optical

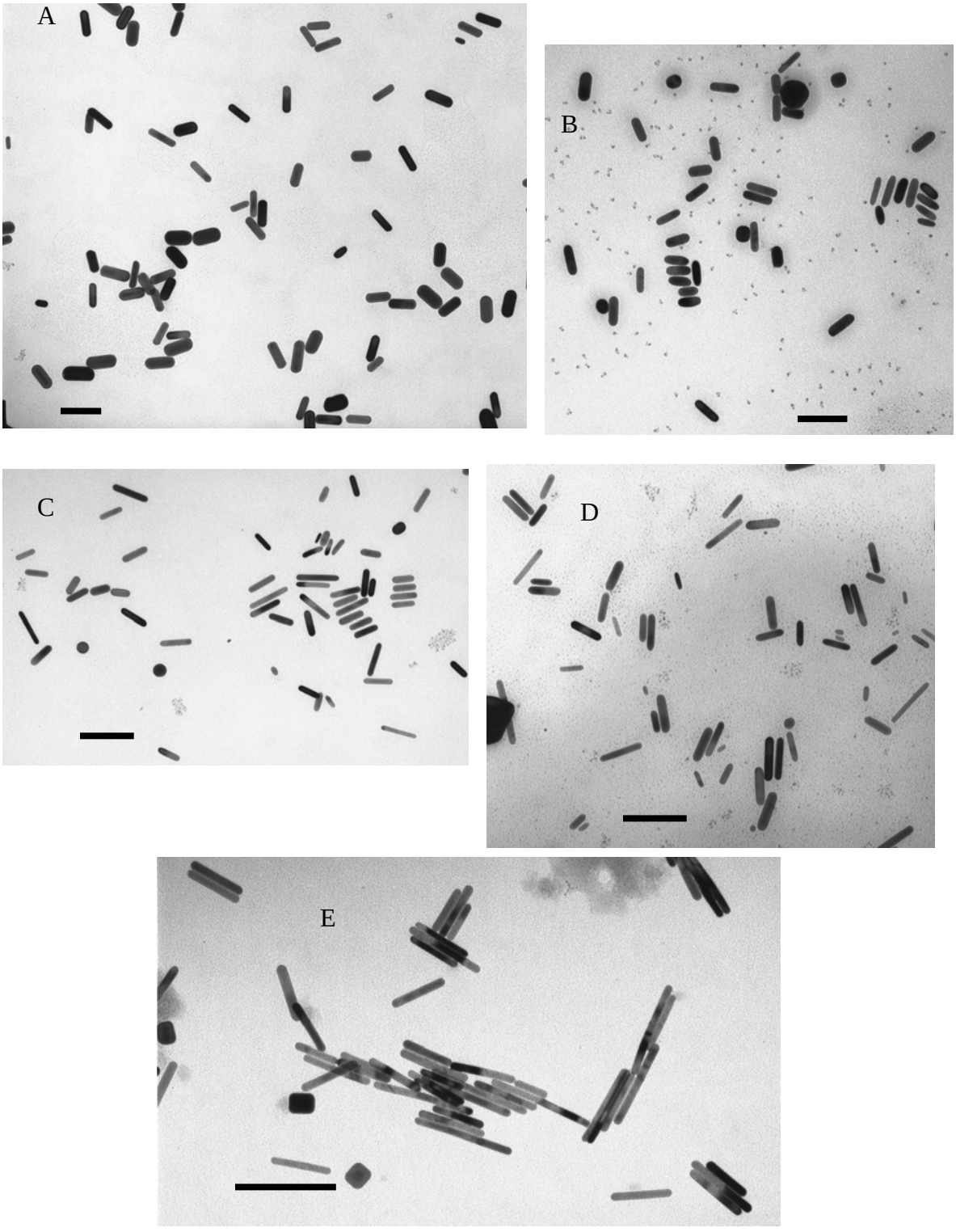

Figure 3-4: *TEM images of gold nanorods used in absorption studies A) Au630, B) Au700, C) Au 850, D) Au900, and E) Au1000. All scale bars represent 100nm. Reproduced with permission from J. Phys. Chem.B* ***2005****, 109, 16350-16356. Copyright 2005 Am. Chem. Soc.*

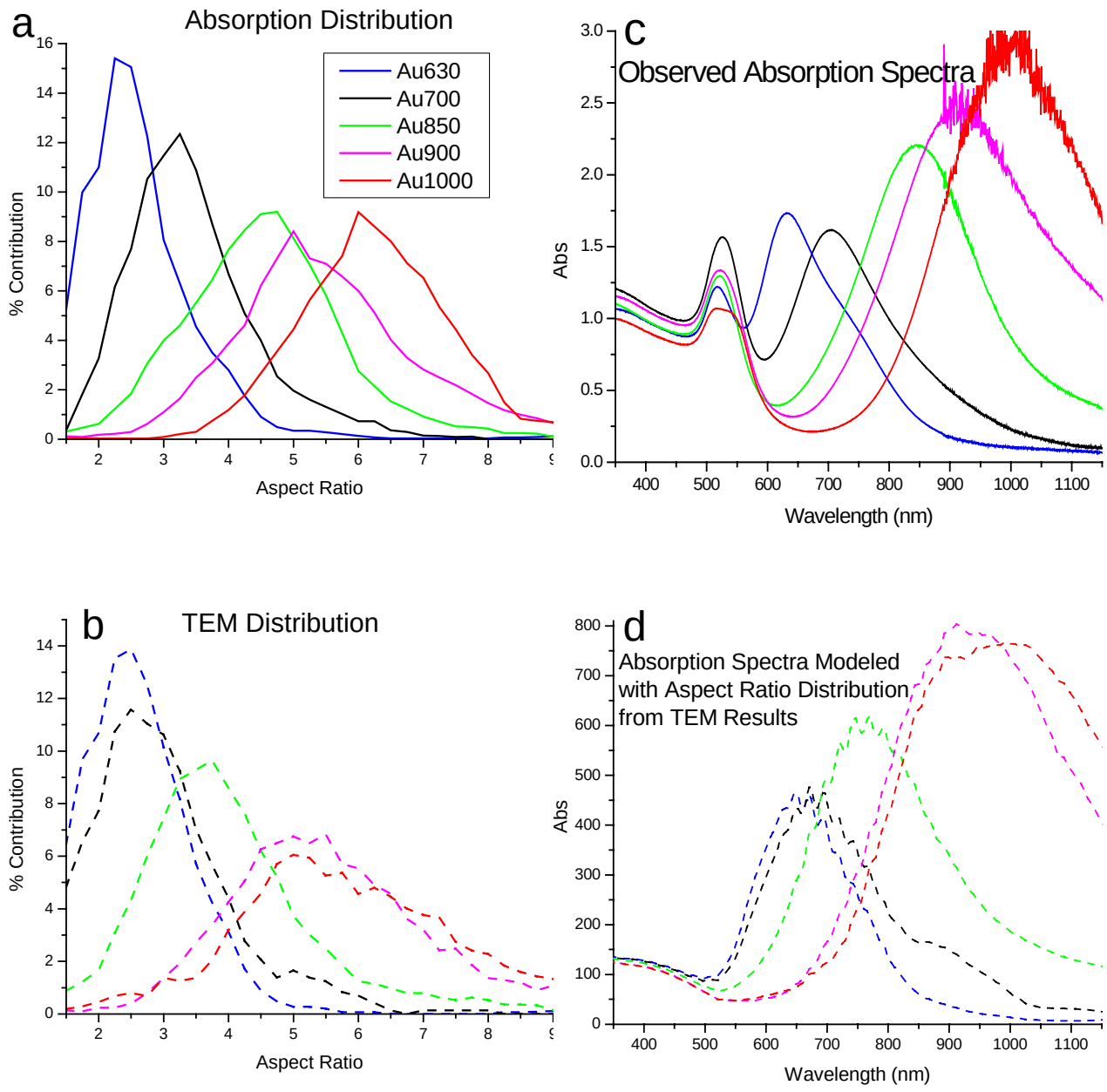

Figure 3-5: *The aspect ratio distributions obtained from fits to the longitudinal plasmon resonance (solid lines)(a) and TEM results (dotted lines)(b). Longitudinal absorption spectrum from experimental observations (solid lines)(c) and the calculated absorption spectrum using Gans equation and aspect ratio distributions from TEM results (dotted lines)(d).*

absorption is matched, no significant differences between the experimental absorption and the fitted absorption spectra are observed as shown in Figure 3-3 for sample Au850. Fitting the absorption spectrum of the sample by the technique presented here improves the sample distribution obtained for the sample over TEM results as it probes a macroscopic volume of the sample, allowing many nanorods to be probed at the same time. The error associated with the optical fit is much smaller than the error in the distribution obtained from TEM analysis. This is due to the ability to probe macroscopic volumes at the same time with the optical technique and the large variation in the longitudinal plasmon resonance with small changes in the aspect ratio leading to a unique fit to the longitudinal plasmon resonance with the optical technique.

The use of the optical properties offers an attractive alternative to TEM analysis. While TEM is extremely valuable for characterization of the shapes made in a synthesis procedure, the optical method enables a practical method to determine the aspect ratio distribution without TEM. Thus the technique presented here allows for easy, strait forward determination of not only the average aspect ratio of a sample of nanorods in solution, but also the distribution from an optical absorption spectrum. This is useful as a quick determination of the aspect ratio and the quality of a sample, without the need for TEM analysis of every sample.

Acknowledgments: The authors wish to thank Dr. Stephan Link for insightful discussions and wish to acknowledge the financial support of the National Science Foundation, Chemistry Division Grant No. 0240380.

References

1. Link, S.; El-Sayed, M. A., Shape and size dependence of radiative, non-radiative and photothermal properties of gold nanocrystals. *Int. Rev. Phys. Chem.* **2000,** 19, (3), 409-453.

2. Kamat, P. V., Photophysical, photochemical and photocatalytic aspects of metal nanoparticles. *J. Phys. Chem. B* **2002,** 106, (32), 7729-7744.

3. El-Sayed, M. A., Some interesting properties of metals confined in time and nanometer space of different shapes. *Acc. Chem. Res.* **2001,** 34, (4), 257-264.

4. Eustis, S.; El-Sayed, M. A., Why Gold Nanoparticles Are More Precious than Pretty Gold: Noble Metal Surface Plasmon Resonance and its Enhancement of the Radiative and Nonradiative Properties of Nanocrystals of Different Shapes. *Chem. Soc. Rev.* **2006,** 35, (3), 209-217.

5. Martin, C. R., Membrane-Based Synthesis of Nanomaterials. *Chem. Mater.* **1996,** 8, (8), 1739-1746.

6. Thurn-Albrecht, T.; Schotter, J.; Kästle, G. A.; Emley, N.; Shibauchi, T.; Krusin-Elbaum, L.; Guarini, K.; Black, C. T.; Tuominen, M. T.; Russell, T. P., Ultrahigh-Density Nanowire Arrays Grown in Self-Assembled Diblock Copolymer Templates *Science* **2000,** 290, (5499), 2126 - 2129.

7. Ji, C.; Searson, P. C., Synthesis and Characterization of Nanoporous Gold Nanowires. *J. Phys. Chem. B* **2003,** 107, (19), 4494-4499.

8. Yu, Y. Y.; Chang, S. S.; Lee, C. L.; Wang, C. R. C., Gold Nanorods: Electrochemical Synthesis and Optical Properties. *J. Phys. Chem. B* **1997,** 101, (34), 6661-6664.

9. Johnson, C. J.; Dujardin, E.; Davis, S. A.; Murphy, C. J.; Mann, S., Growth and form of gold nanorods prepared by seed-mediated, surfactant-directed synthesis. *J. Mater. Chem.* **2002,** 12, 1765 - 1770.

10. Sau, T. K.; Murphy, C. J., Room Temperature, High-Yield Synthesis of Multiple Shapes of Gold Nanoparticles in Aqueous Solution *J. Am. Chem. Soc.* **2004,** 126, (28), 8648-8649.

11. Busbee, B. D.; Obare, S. O.; Murphy, C. J., An Improved Synthesis of High-Aspect-Ratio Gold Nanorods. *Adv. Mater.* **2003,** 15, (5), 414-416.

12. Jana, N. R.; Gearheart, L.; Murphy, C. J., Wet Chemical Synthesis of High Aspect Ratio Cylindrical Gold Nanorods. *J. Phys. Chem. B* **2001,** 105, (19), 4065-4067.

13. Jana, N. R.; Gearheart, L.; Murphy, C. J., Seed-Mediated Growth Approach for Shape-Controlled Synthesis of Spheroidal and Rod-like Gold Nanoparticles Using a Surfactant Template. *Adv. Mater.* **2001,** 13, (18), 1389-1393.

14. Nikoobakht, B.; El-Sayed, M. A., Preparation and growth mechanism of gold nanorods (NRs) using seed-mediated growth method. *Chem. Mater.* **2003,** 15, (10), 1957-1962.

15. Gole, A.; Murphy, C. J., Seed-Mediated Synthesis of Gold Nanorods: Role of the Size and Nature of the Seed. *Chem. Mater.* **2004,** 16, (19), 3633-3640.

16. Murphy, C. J.; Sau, T. K.; Gole, A. M.; Orendorff, C. J. G., J.; Gou, L.; Hunyadi, S. E.; Li, T., Anisotropic Metal Nanoparticles: Synthesis, Assembly, and Optical Applications *J. Phys. Chem. B* **2005,** 109, (29), 13857-13870.

17. Niidome, Y.; Nishioka, K.; Kawaski, H.; Yamada, S., Rapid synthesis of gold nanorods by the combination of chemical reduction and photoirradiation processes; morphological changes depending on the growing processes. *Chem. Commun.* **2003**, 2376-2377.

18. Esumi, K.; Suzuki, A.; Aihara, N.; Usui, K.; Torigoe, K., Preparation of Gold Colloids with UV Irradiation Using Dendrimers as Stabilizer. *Langmuir* **1998,** 14, 3157-3159.

19. Kim, F.; Song, J. H.; Yang, P., Photochemical Synthesis of Gold Nanorods *J. Am. Chem. Soc.* **2002,** 124, (48), 14316-14317.

20. Miranda, O. R.; Ahmadi, T. S., Effects of Intensity and Energy of CW UV Light on the Growth of Gold Nanorods. *J. Phys. Chem. B* **2005,** 109, (33), 15724-15734.

21. Torigoe, K.; Esumi, K., Preparation of colloidal gold by photoreduction of tetracyanoaurate(1-)-cationic surfactant complexes *Langmuir* **1992,** 8, (1), 59-63.

22. Esumi, K.; Hara, J.; Aihara, N.; Usui, K.; Torigoe, K., Preparation of Anisotropic Gold Particles Using a Gemini Surfactant Template. *J. Colloid Interface Sci.* **1998,** 208, 578-581.

23. Esumi, K.; Nawa, M.; Aihara, N.; Usui, K., Growth of rodlike Au/Pt particles in cationic micelles by UV irradiation. *New J. Chem.* **1998**, 719-720.

24. ImageJ is a public domain Java image processing program inspired by NIH Image. The source code is freely available. Watershead plugin and other plugins also available. http://rsb.info.nih.gov/ij/ Date Accessed (5/23/06).

25. Link, S.; Mohamed, M. B.; El-Sayed, M. A., Simulation of the optical absorption spectra of gold nanorods as a function of their aspect ratio and the effect of the medium dielectric constant. *J. Phys. Chem. B* **1999,** 103, (16), 3073-3077.

26. Yan, B.; Yang, Y.; Wang, Y., Comment on "Simulation of the Optical Absorption Spectra of Gold Nanorods as a Function of Their Aspect Ratio and the Effect of the Medium Dielectric Constant" *J. Phys. Chem. B* **2003,** 107, (34), 9159-9159.

27. Link, S.; El-Sayed, M. A., Simulation of the Optical Absorption Spectra of Gold Nanorods as a Function of Their Aspect Ratio and the Effect of the Medium Dielectric Constant (Addition/Correction). *J. Phys. Chem. B* **2005,** 109, (20), 10531-104532.

28. Gans, R. v., Uber die Form Ultramikroskopischer Silberteilchen. *Ann. Phys.* **1915,** 47, 270-284.

29. Mie, G., Beitrage zur Optik truber Medien, speziell kolloidaler Metallosungen. *Ann. Phys.* **1908,** 25, 377-445.

30. Brioude, A.; Jiang, X. C.; Pileni, M. P., Optical Properties of Gold Nanorods: DDA Simulations Supported by Experiments. *J. Phys. Chem. B* **2005,** 109, (27), 13138-13142.

31. Sosa, I. O.; Noguez, C.; Barrera, R. G., Optical Properties of Metal Nanoparticles with Arbitrary Shapes. *J. Phys. Chem. B* **2003,** 107, (26), 6269-6275.

32. Kelly, K. L.; Coronado, E.; Zhao, L. L.; Schatz, G. C., The Optical Properties of Metal Nanoparticles: The Influence of Size, Shape, and Dielectric Environment *J. Phys. Chem. B* **2003,** 107, (3), 668-677.

33. Eustis, S.; El-Sayed, M. A., The Aspect Ratio Dependence of the Enhanced Fluorescence Intensity of Gold Nanorods: Experimental and Simulation Study. *J. Phys. Chem. B* **2005,** 109, (34), 16350-16356.

34. Nikoobakht, B. Synthesis, characterization and self-assembly of gold nanorods and surface-enhanced Raman studies. Georgia Institute of Technology, Atlanta, GA, 2003.

35. Sau, T. K.; Murphy, C. J., Seeded High Yield Synthesis of Short Au Nanorods in Aqueous Solution. *Langmuir* **2004,** 20, (15), 6414-6420.

36. Boyd, G. T.; Yu, Z. H.; Shen, Y. R., Photoinduced Luminescence From the Noble-Metals and Its Enhancement On Roughened Surfaces. *Phys. Rev. B* **1986,** 33, (12), 7923-7936.

37. Boyd, G. T.; Rasing, T.; Leite, J. R. R.; Shen, Y. R., Local-Field Enhancement on Rough Surfaces of Metals, Semimetals, and Semiconductors with the Use of Optical 2nd-Harmonic Generation. *Phys. Rev. B* **1984,** 30, (2), 519-526.

38. Chen, C. K.; Heinz, T. F.; Ricard, D.; Shen, Y. R., Surface-Enhanced 2nd-Harmonic Generation and Raman-Scattering. *Phys. Rev. B* **1983,** 27, (4), 1965-1979.

39. Johnson, P. B.; Christy, R. W., Optical Constants of the Noble Metals. *Phys. Rev. B* **1972,** 6, (12), 4370-4379.

40. Link, S.; El-Sayed, M. A., Size and temperature dependence of the plasmon absorption of colloidal gold nanoparticles. *J. Phys. Chem. B* **1999,** 103, (21), 4212-4217.

CHAPTER 4

THE ASPECT RATIO DEPENDENCE OF THE ENHANCED FLUORESCENCE INTENSITY OF GOLD NANORODS: EXPERIMENTAL AND SIMULATION STUDY[§]

Abstract:

Experimental observations and theoretical treatments are carried out for the band shape and relative intensity of the emission from gold nanorods of various aspect ratios in the range between 2.25 (1.5 theory) and 6.0 (9 theory). The calculation of the fluorescence spectra requires knowledge of the nanorod size distribution, the shape dependent enhancement factors and the band shape of the un-enhanced fluorescence spectrum. The size distribution is determined from the fit of the observed inhomogeneously broadened absorption spectrum for each of the nanorod samples synthesized to the sum of the calculated homogeneously broadened spectra of nanorods of different aspect ratios using Gans model referred to as Gold Nanorod Optical Modeling Equations (GNOME). The theory by Boyd and Shen is used to calculate the enhanced interband fluorescence spectra of the previously observed weak emission of bulk gold for each synthesized sample. In order to compare theory to the observed nanorod fluorescence spectra, which suffer from self-absorption, the calculated nanorod fluorescence spectra are corrected to take account of this effect using the observed

[§] Reproduced with permission from Eustis, S.; El-Sayed, M. A., The Aspect Ratio Dependence of the Enhanced Fluorescence Intensity of Gold Nanorods: Experimental and Simulation Study. *J. Phys. Chem. B* **2005,** 109, (34), 16350-16356. Copyright 2005 American Chemical Society.

absorption spectra. The comparison between the observed and calculated fluorescence band shapes is found to be acceptable.

Introduction:

The optical properties of noble metal nanoparticles are of great interest due to the strong surface plasmon resonance absorption in the visible region of the electromagnetic spectrum.[1, 2] This strong absorption leads to the enhancement in the electromagnetic field near the surface leading to enhancement of Raman and Rayleigh scattering processes. Gold nanorods have two plasmon resonance absorptions, one due to the transverse oscillation of electrons around 520nm regardless of aspect ratio. The other absorption is due to the longitudinal oscillation of the electrons, which depends on the aspect ratio of the nanorod. The resonances are due to a collective oscillation of the free electrons through the metal, which depends on the boundary conditions.

Bulk gold fluorescence, first observed by Mooradian in 1969,[3] is very weak with a quantum yield of 10^{-10}. Fluorescence emission of gold nanorods with a quantum yield of 10^{-3}-10^{-4} was first reported in 2000 by Mohamed et. al.[4] Recent research has produced a number of reports of fluorescence enhancement in nanoparticles[4-17] as well as a background emission believed to be fluorescence in SERS.[18-23] Gold nanoclusters fluoresce in the visible and near IR with quantum yields[5-9, 16] of up to 10^{-3}. Emission from gold clusters was first observed[5] in 1998, by Wilcoxon et. al. where small gold clusters were found to fluoresce with quantum efficiencies in the 10^{-4} - 10^{-5} range. Recently emission from a single species of gold clusters has been identified.[8-10] The emission wavelength changes with the size of the cluster, with Au_8 emits light below 500nm,[9] and Au_{28} emits light above 800nm.[8] Blinking has also been observed in single-

molecule studies in both gold and silver on the second time scale.[12, 17] Two-photon-induced photoluminescence (PL) spectrum of a single gold nanorod excited at 780nm has been reported by Imura et. al.[24]

Experimental and theoretical results published by Shen and Boyd [25-27] ascribe the emission of noble metals to the band structure of the metal. Large enhancement in emission on roughened metal surfaces was attributed to local enhancement in the field around the surface of the metal. This same enhancement is observed in SERS activity.[28] The emission is attributed to a recombination between the electrons and holes in the interband recombination.

Previous studies[4, 15] of this group were able to use a theoretical model to place an upper bound on the lifetime of the fluorescence emission from gold nanorods as a function of the aspect ratio. Large enhancement in fluorescence emission was found for electrochemically synthesized rods over spheres with quantum yields of 10^{-4} –10^{-5}. Experimentally, the emission wavelength increased linearly with aspect ratio, and the enhancement factor was found to increase linearly with the square of the aspect ratio.[4] Theoretically the enhancement of the emission from nanorods was modeled using a lighting rod effect to account for the enhancement of the electric field near the surface of the nanorods.[4, 15] The upper bound on the lifetime was determined to be 50 fs, and is likely related to the dynamics of the holes created in the d-bands immediately after irradiation.[15]

This chapter presents an extension of the previous research looking at high aspect ratio nanorods made by a new synthetic technique and extending the theoretical model. This chapter shows that at higher aspect ratios, the enhancement decreases, and broadens

due to the diminishing coupling between the longitudinal plasmon resonance oscillation and the interband transition. Emission is not observed at the wavelengths predicted in the previous theoretical model[4] due to the importance of the wavelength region of bulk gold emission.

Experimental

The gold nanorods are prepared by the chemical seeding technique described in Chapter 2. Briefly, a seed solution is generated by adding ice cold $NaBH_4$ to a solution of $HAuCl_4$ and hexadecyltrimethylammonium bromide (CTAB). The solution was kept at 25^{o}C for a few minutes before use. A brownish yellow color was observed in all seed solutions used. The growth solution contained 5mL of a solution of 0.20m CTAB and 0.25m benzyldimethylammonioum chloride hydrate (BDAC), which is added to 0.20mL of 4.0mM $AgNO_3$. Then 5.0mL of 0.90mM of $HAuCl_4$ is added and 54μL of 0.10M ascorbic acid. Twelve microliters of seed solution is then added to the solution, which is left undisturbed for 4 hours for the nanorods to grow. Kinetic growth conditions determine the aspect ratio of the nanorods generated, with narrower widths in the higher aspect ratio samples.

The optical absorbance spectra were recorded on a Shimadzu UV-3101-PC UV-Vis-NIR scanning spectrometer. Fluorescence measurements were taken on a PTI Model C60 steady-state spectrometer. Average volume was determined from TEM images using 100kV on JEOL100 transmission electron microscope (TEM) using Image Pro Plus v.4.5 to determine the length and width of nanorods. Models of absorption spectra obtained in chapter are used to determine the aspect ratio distribution for the calculations

of the fluorescence emission due to the bulk average represented in the absorption and emission spectra.

Theoretical calculations are preformed similar to those in Chapter 3. The equations can be added to the aspect ratio worksheet, and a new worksheet is created to collect the predicted emission for each aspect ratio, analogously to that created for the absorption calculation.

Experimental Results

Figure 4-1a shows the optical absorption of the samples used in this experiment. The optical absorption spectra in Figure 4-1a exhibit the same behavior Link et. al.[29-31] described theoretically where as the aspect ratio of the nanorod increases the longitudinal plasmon resonance increases in wavelength and intensity for a given concentration of nanorods. Figure 4-1b shows the fluorescence emission from the gold nanorods after excitation with 480nm light. As the average aspect ratio increases from 2.25 (Au630) to 3.25 (Au700) the emission red shifts from 575nm to 600nm. At higher aspect ratios, the emission remains centered around 600nm, but decreases in intensity. The quantum yield is 10^{-4}. The fluorescence shown in Figure 4-1b are similar to the previous emission spectra observed for gold nanorods,[4] but emission intensities are observed to decrease instead of increasing. The previous report was limited to samples with longitudinal plasmon resonances below 800nm.[4] As the longitudinal plasmon resonance (and the aspect ratio) increases further the emission intensity decreases. The growth methods for the two studies are different; chemical vs. electrochemical reduction, using different surfactants to stabilize the surface of the gold nanorod during growth. Furthermore, the electrochemical method produces rods having single crystals. The seed growth method

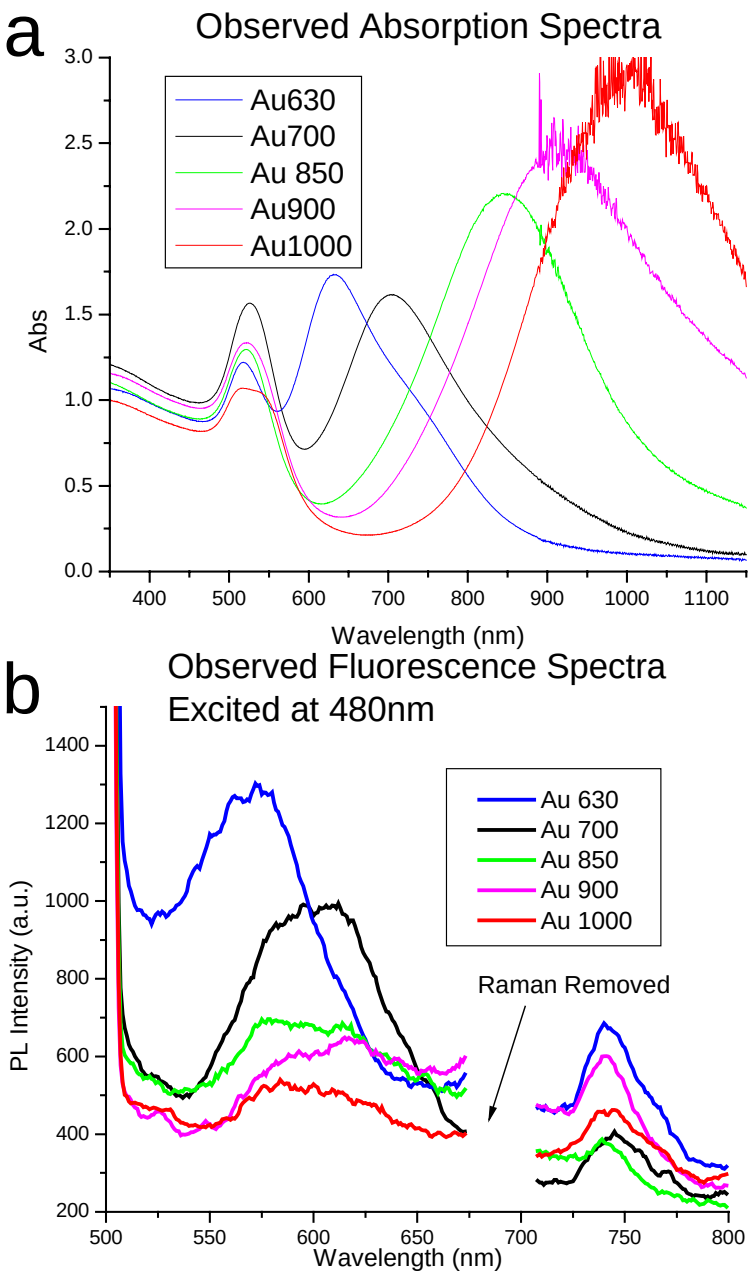

Figure 4-1: *a) Absorption spectra of gold nanorods. b) Fluorescence spectra of gold nanorods upon 480nm excitation.*

generates nanorods with more defects as the aspect ratio increases. By observing the similarity between the observed fluorescence it can be said that the fluorescence is due to the gold nanorods in solution and is not affected by differing surfactants.

Figure 4-2 presents the emission spectrum for sample Au630 after excitation with 407nm-437nm light. Raman bands are easily identified, besides being relatively sharp, they shift with changing the excitation wavelength. The fluorescence band maxima do not change with changing the excitation wavelength. Thus in Figure 4-2, the emission bands at 575nm and 730nm remain constant, while a Raman band is observed shifting from 585nm to 625nm upon changing the excitation wavelength from 407-437nm. The inset further confirms this analysis by converting the x-axis to Δ wavenumbers. The Raman scattering is observed at a constant shift of 7,000cm^{-1} from the incident wavelength. This energy is too high for the fundamental of any molecular vibration, and could be due to an enhanced electronic transition or an enhanced overtone of OH or NH vibration.

The quantum yield of these nanorods was measured relative to Rhodamine 6G (0.9) and is found to be on the order of the 10^{-4}. This suggests that the nanorods have an observed lifetime which is 10^{-4} times smaller that that of Rhodamine 6G, which is ~10^{-9}s, i.e. ~10^{-9} s x 10^{-4} = ~ 10^{-13}s. This is consistent with a previous attempt[15] to measure the nanorod lifetime, which was found to be less than 50fs. This suggests that the observed nanorod fluorescence lifetime is dominated by rapid (<50fs) non-radiative processes, and does not measure the radiative lifetime of the emission.

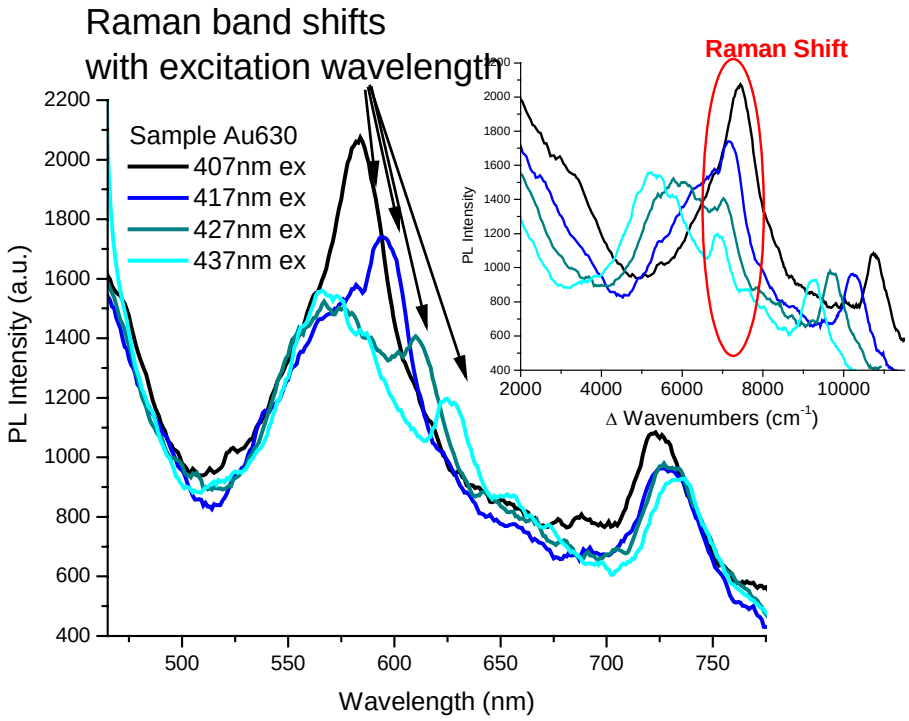

Figure 4-2: *Emission spectra of samples Au630 with different excitation wavelengths. Inset: same data, with the x-axis converted to Δ wavenumbers.*

Theoretical Calculation

In order to simulate the enhanced fluorescence emission of the gold nanorod samples presented here, the absorption spectrum is modeled to obtain the aspect ratio distributions using the GNOME method as shown in Chapter 3. The aspect ratio distributions determined from TEM results did not give good agreement with the observed emission due to the limited statistics (~200 nanorods per sample), and the change of state of the nanoparticle environment (liquid to solid support) necessary for TEM analysis. The absorption spectra are a measure of the bulk solution properties, as are the fluorescence emission spectra.

The emission spectrum is then calculated by first calculating the enhancement factors for gold nanorods, often referred to as the "Lightning Rod Effect" according to Shen and Boyd[25-27] as reported by Mohamed et. al.[4] This enhancement factor is multiplied by the aspect ratio distribution determined from the previous chapter. This enhancement factor is then multiplied by the emission of bulk gold measured by Mooradian[3] as suggested in the equations presented by Shen and Boyd.[25-27] When theoretical predictions for this emission[32] are used in place of experimental data, the emission at higher wavelengths is found to be overestimated, and does not fit the observed spectra. For a closer agreement with experimental data, the self-absorption of the solution is taken into account by subtracting the experimental absorption spectra from the predicted emission spectra. The corrected band shapes of the different emission spectra simulated in this manner are found to be in good agreement with that observed. The details of these calculations are given below and the results of these calculations are presented in Figure 4-6.

The absorption and emission of gold nanorods were calculated using a structure factor to model the shape of the nanorod. Similarly to the absorption calculated in Chapter 3, the fluorescence can be calculated using similar equations as presented there. Boyd and Shen[25-27] have proposed a model for emission enhancement for gold nanorods. Their theory is based on a local field factor L(ω), which is given by the dimensions of a hemispheroid of length a and width b (aspect ratio = a/b) and the dielectric constant of gold is obtained from Johnson and Christy.[33]

$$L(\omega) = L_{LR}\left[\frac{\varepsilon(\omega)}{\varepsilon_m} - 1 + L_{LR}\left(1 + \frac{i4\pi^2 V(1-\varepsilon(\omega))\varepsilon_m^{1/2}}{3\lambda^3}\right)\right]^{-1} \qquad (4.1)$$

where: $L_{LR} = A^{-1}$

$$A = \left[1 - \frac{\xi Q_1^{'}(\xi)}{Q_1(\xi)}\right]^{-1}$$

$$\xi = \left[1 - \left(\frac{b}{a}\right)^2\right]^{-1/2}$$

$$Q_1(\xi) = \left(\frac{\xi}{2}\right)\ln\left[\frac{\xi+1}{\xi-1}\right] - 1$$

$$Q_1^{'}(\xi) = \frac{dQ_1(\xi)}{d\xi}$$

λ is the wavelength, ε_m is the dielectric constant of the medium, and $V=(4/3)\pi a(b/2)^2$ is the volume of the nanorod. The emitted luminescence is given by:

$$P_{1sph}(\omega, a/b, V) = \beta_1 2^4 |E_o|^2 V\left[L^2(\omega_1)L^2(\omega_2)\right] \qquad (4.2)$$

where $L^2(\omega_1)$ is the local-field factor at the excitation wavelength and $L^2(\omega_2)$ is the local-field factor at the emission wavelength, $|E_o|^2$ is the incident electric field, and β_1 is a proportionality constant including the intrinsic luminescence spectrum of gold. The average volume of sample nanorods (as determined from TEM) was used for all the calculations of the emission enhancement.

Mohamed et. al.[4] previously reported the calculated results of $|L(\omega_1)^2L(\omega_2)^2|$ as a function of aspect ratio as given by Equation 4.2. The results from this equation for the enhancement of gold nanorods $|L(\omega_1)^2L(\omega_2)^2|$, fail to account for the observed rapid decrease in the emission of gold nanorods at higher aspect ratio and the theory vastly overestimates the emission wavelength maximum for rods of aspect ratio 6.0 predicted at 970nm. Mohamed et. al.[4] previously reported only an increase in the intensity as the

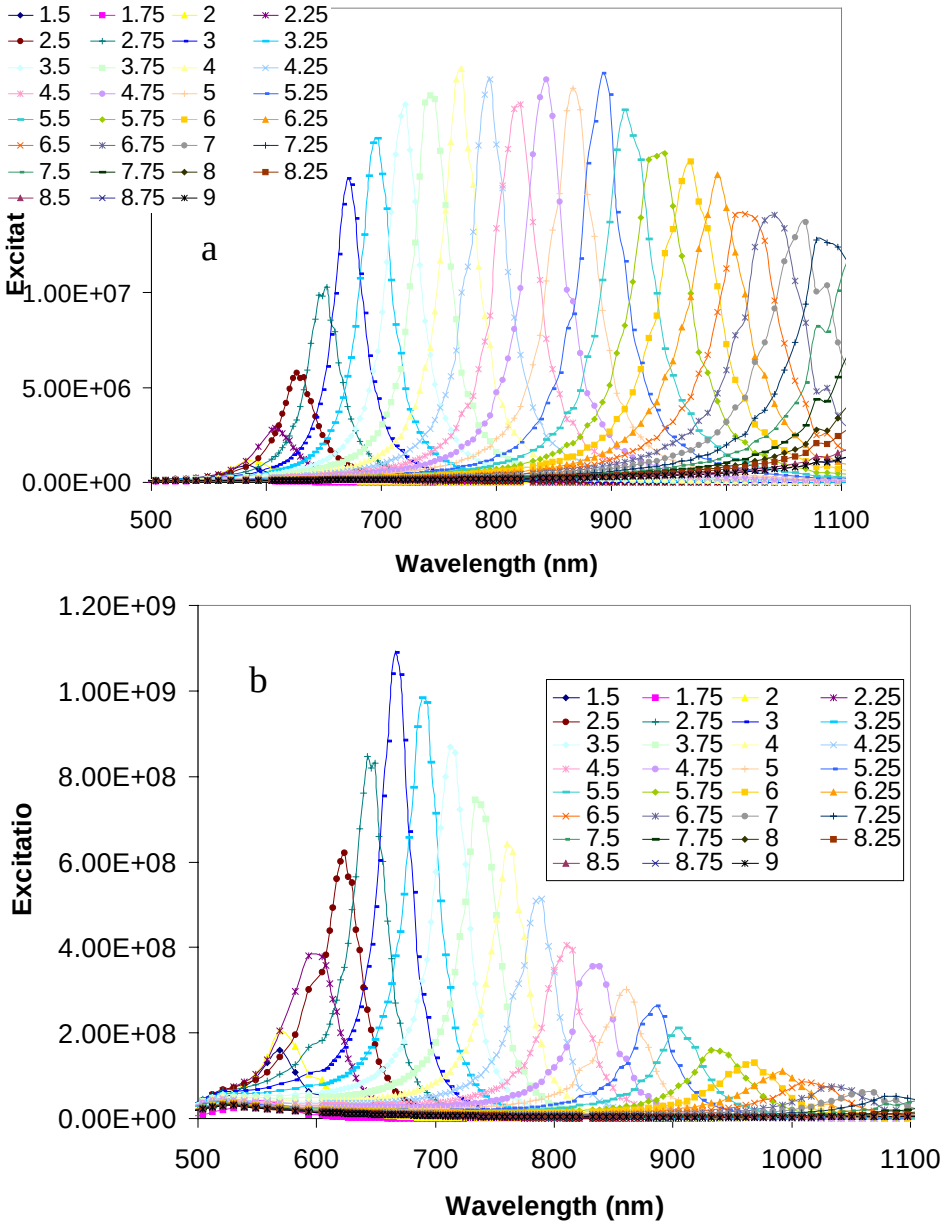

Figure 4-3 *a) Simulated fluorescent enhancement $|L(\omega_1)^2 L(\omega_2)^2|$ for aspect ratios 1.5-9. b) Simulated fluorescence enhancement $|L(\omega_1)^2 L(\omega_2)^2|$ times the emission spectrum β_1 predicted by Apell.*[32]

aspect ratio was increased. If higher aspect ratios are plotted than previously studied (shown in Figure 4-3a) the intensity of the enhancement factor is observed to decrease as the aspect ratio further increases. This decrease is due to the increase in the separation of the excitation wavelength and the longitudinal surface plasmon resonance spectrum as the aspect ratio of the nanorod is increased.

Thus, the intrinsic luminescence of bulk gold must be incorporated into this model, or β_1 should be incorporated. A theory has been proposed by Apell[32] describing the fluorescence emission as a coupling between the optical properties of gold and the transitions of its d electrons. This theory predicts that the when the longitudinal plasmon resonance is around the d orbital transitions the emission is enhanced. The differential luminescence scattering power as a function of the emitted and scattered photons, $d^2P^0/d\Omega d\omega_2$, was modeled using the equation:

$$\frac{d^2P^0}{d\Omega d\omega_2} \cong \frac{\omega_2}{\alpha(\omega_1)+\alpha(\omega_2)} \cdot \frac{|t_2|^2}{n_2^2+k_2^2} \cdot D_2^0(\omega_2) \qquad (4.3)$$

with

$$D_2^0 \approx \int_{E_F-\omega_1}^{E_F-\omega_2} dE\left[\zeta_d^<(E)\right]^2 \qquad (4.4)$$

where $\zeta_d^<$ is the density of states of the filled d orbitals from Kupratakuln [34] fitted and integrated with Origin 7 (OriginLab Co.), n and k are the dielectric constant of gold from Johnson and Christy[33], $|t_2|^2$ is the transmission factor is for light with polarization perpendicular to the surface, and $\alpha(\omega)$ is the absorption at the exciting and emission wavelength. This theory leads to the interpretation that the observed enhanced emission arises from the d orbital transitions and the reflection and absorption constants of gold.

These results are compared to the fluorescence emission determined by Mooradian[3] as shown in Figure 4-4.

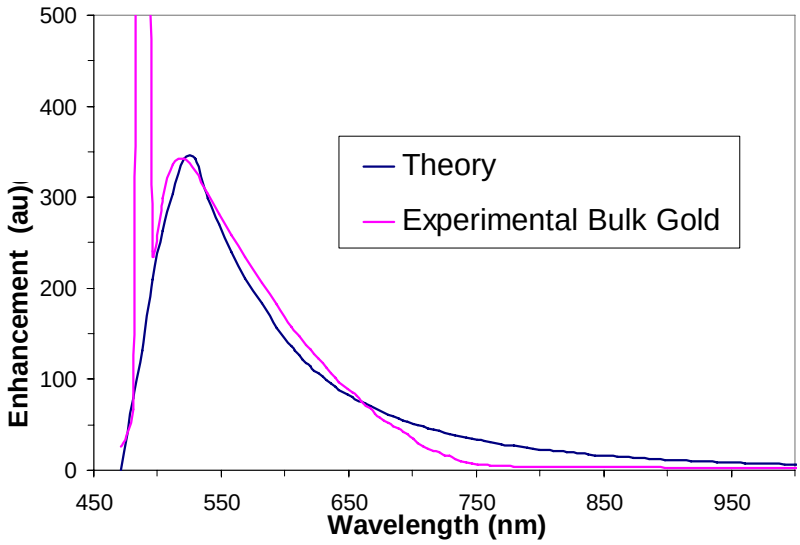

Figure 4-4: *Emission spectra of bulk gold from Mooradian experimental data and Apell's theory.*

It should be noted that this theory overestimates the emission above 700nm, and as a result it is not a good equation to use to determine the corrected emission. This effect is observed in Figure 4-3b as the aspect ratio increases, the intensity decreases. However, large enhancement in the fluorescence emission of high aspect ratio nanorods is still calculated that is not observed experimentally. While the results in Figure 4-3b are closer to experimental results than Figure 4-3a, the long wavelength component still overestimates the experimental results in Figure 4-1b. This is similar to the overestimation of the fluorescence observed in Figure 4-4 of experimental emission by Apell's equations. This difference could be due to a failure of the equation, or to the limited ability to calculate the density of states in this energy region. Thus the

experimental results of Moordian[3] were tabulated and used as β_1 in equation. 4.2 to calculate the emission spectra.

In order to compare the calculated spectra with the observed ones, self-absorption has to be taken into account. The self-absorption of the nanorod emission due to absorption by the plasmon resonance absorption before reaching the detector is taken into account by subtracting the experimental absorption spectrum (which includes the transverse and longitudinal plasmon resonance) from the calculated emission spectrum. The experimental absorption spectrum was multiplied by 10,000,000 to account for the differences between theoretical calculations and experimental intensities. Since we are interested in band shapes, the absolute intensities are not important; in fact their units are different.

To graphically explore the enhancement of the emission of gold nanorods the interband absorption is calculated by the methods reported in Pinchuk et. al.[35] The Drude model calculates the complex dielectric constants of a material to be expressed as follows:

$$\varepsilon(\omega) = 1 - \frac{\omega_p^2}{\omega + i\gamma\omega} + \chi^{ib}(\omega) \qquad (4.5)$$

where ω is the frequency, ω_p is the plasmon frequency of the conducting electrons, γ is the rate of electron collisions, and $\chi^{ib}(\omega)$ is the interband susceptibility (a complex number) that contributes to the dielectric constant of noble metal nanoparticles above a characteristic wavelength. The values of ω_p = 9.1and γ = 0.014 are obtained from Pinchuk et. al.[35]

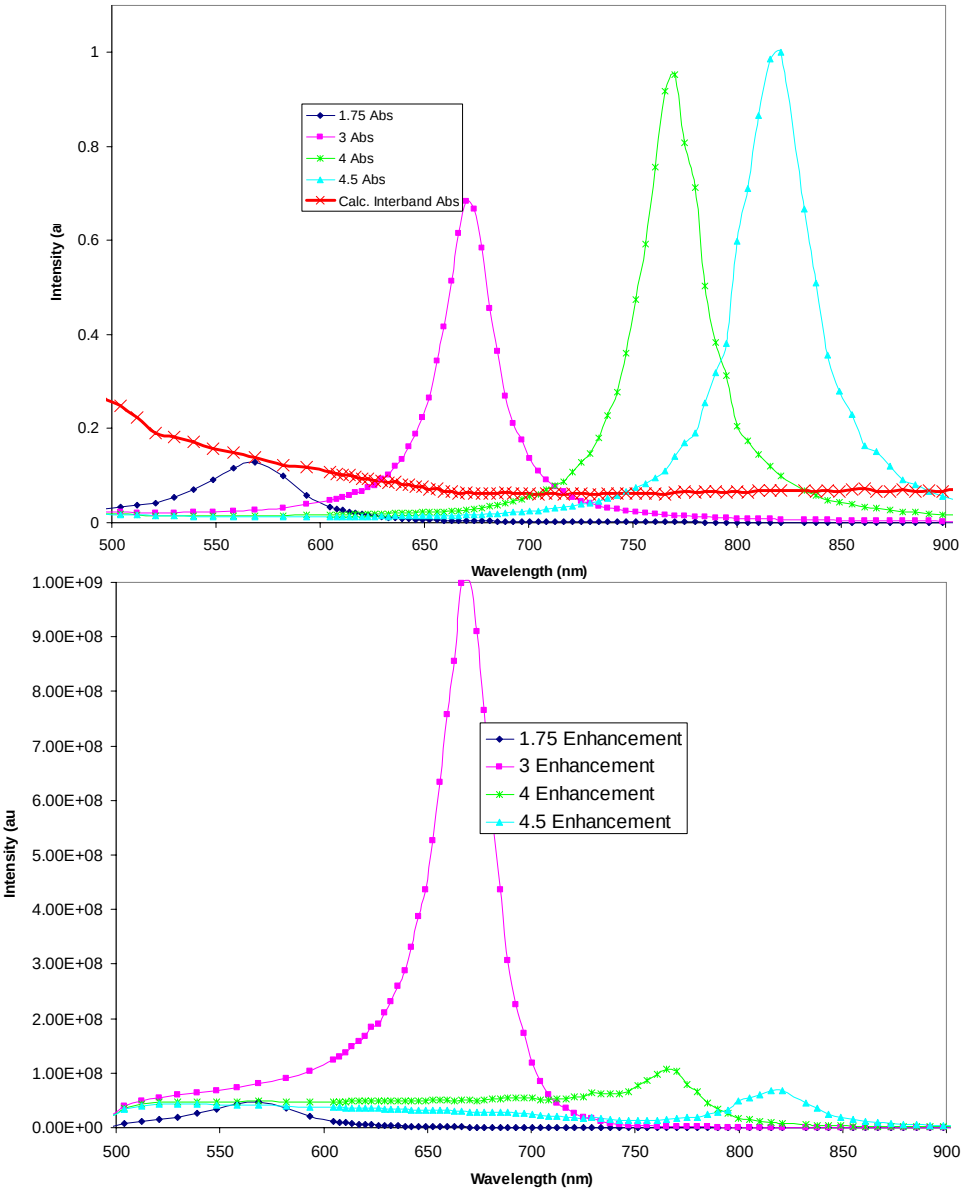

Figure 4-5: *a)Overlap of the interband transition with the longitudinal plasmon resonance of different aspect ratios. b)Predicted fluorescence for different aspect ratios.*

The calculated interband transition is shown with calculated longitudinal plasmon resonance absorptions of gold nanoparticles of different aspect ratios in Figure 4-5. The interband fluorescence emission of gold nanorods is calculated from the emission of the interband transition of bulk gold times the square of the enhancement factor, which depends on the intensity of the longitudinal plasmon resonance.[25, 36] Only those samples where the longitudinal surface plasmon overlaps with the interband transition will have enhanced fluorescence. However, the emission depends on the square of the longitudinal plasmon resonance, so the larger the absorption cross-section of the nanorod, the larger the enhancement. As the aspect ratio increases, the cross-section increases for a given volume of nanorod.[29-31] This leads to the observed effect where the maximum emission intensity is expected for an aspect ratio of 3 shown in Figure 4-5.

Discussion

The calculated fluorescence emission spectra presented in Figure 4-6b is the compilation of the calculated enhancement factor from the Boyd and Shen[25-27] equation 4.2 using 470nm excitation, aspect ratio distribution results from the calculated fit of the observed absorption spectrum using the method described in Chapter 3, the observed emission of bulk gold from Mooradian,[3] and the self-absorption correction using the observed absorption spectra. These results are then compared to the experimental results in Figure 4-1b and in Table 4-1. Using the absorption spectra as a model for the aspect ratio distribution generates reasonable agreement with experimentally observed emission, especially after self-absorption has been corrected. Both absorption and emission examine a macroscopic volume of the sample in solution, and generate an averaged

signal across the sample. The emission spectra calculated in Figure 4-6b resemble the observed emission in Figure 4-1b in shape and shifting emission wavelength. The calculated values of the emission wavelength maxima obtained theoretically are slightly red shifted from those observed experimentally, but this difference is much less than that presented by Mohamed et. al.[4] due to the incorporation of the fluorescence spectra of bulk gold in the present treatment. (For AR of 5.4, their calculated emission maximum is 725nm compared to 588 nm for their observed maximum).[4] The decease in the intensity is due to the decrease in the emission of bulk gold as the wavelength increases as related to the density of states of the d-band in gold. Samples Au630 and Au700 are observed to fluoresce at their minimum absorption as observed in Figure 4-1a and 4-1b, generating larger observed emission intensities. Erroneous results are obtained before self-absorption is taken into account. The emission for samples Au850, Au900, and Au1000 are predicted to be above 750nm, but the plasmon resonance becomes more intense at higher aspect ratios and the emission of bulk gold decreases at 700nm, leading to the observed emission cut-off at ~750nm.

Table 4-1: *Comparison of experiment and theory. The experimental position of the longitudinal plasmon resonance absorption maximum, the enhanced emission wavelength maximum for gold nanorods and its relative intensity in the present study are compared to the values obtained theoretically for the calculated median aspect ratio that is obtained from the fit of the absorption spectrum.*

Experimental Samples				From Theory		
Sample	Plasmon Max(nm)	Emission Max (nm)	Emission Intensity (norm)	Aspect Ratio	Emission Max (nm)	Emission Intensity (norm)
Au630	630	572	1.00	2.25	635	1.00
Au700	705	597	1.08	3.25	660	1.00
Au850	845	598	0.44	4.75	667	0.43
Au900	900	615	0.54	5.00	673	0.18
Au1000	995	-	0.23	6.00	-	0.10

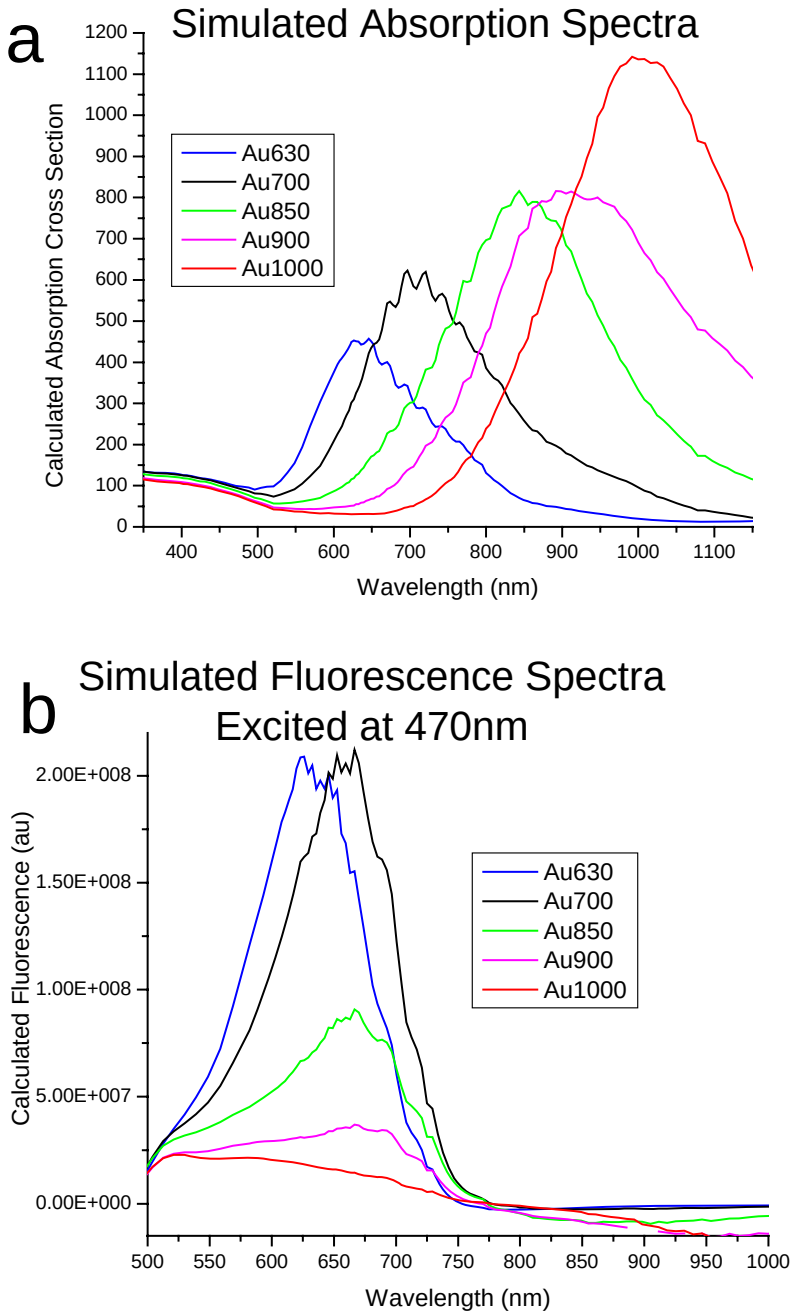

Figure 4-6: *a) Calculated absorption spectra of samples fit to experimental data in Figure 4-1a by adjusting the aspect ratio distribution. b) Calculated emission spectra of nanorod samples excited at 470nm. (See text for method of calculation.)*

The detector used for this experiment does not have sensitivity above 800nm, but by observing the calculated emission spectra in Figure 4-6b, the gold is predicted to have much less emission above this wavelength due to the limitation of the spectral width of the emission spectrum of the bulk metal. It is important to take into account the emission of bulk gold into the equation when larger aspect ratios are used due to the limited emission from bulk gold at higher wavelengths. It is also important to notice, that the theory for predicting bulk gold emission also overestimates the emission at longer wavelengths. Thus, the theory presented here is able to predict the observed results, where the emission wavelength stops shifting for higher aspect ratio nanorods due to the limits imposed by the emission spectrum of bulk gold. These results can be interpreted using the theoretical models presented here to show that as the aspect ratio increases and as the longitudinal plasmon resonance absorption shifts away from the interband transition (as reflected by its fluorescence of the bulk gold), the enhancement decreases. This shows that as the aspect ratio continues to increase, the enhancement does not continue to increase as suggested by previous results.

The results suggest that large interband enhanced fluorescence from gold nanorods will be limited to those with aspect ratios for which the longitudinal surface plasmon absorption band is overlapping with the interband absorption and fluorescence bands. The previously determined quantum yield by Mohamed et al.[4] for these rods and its increase with aspect ratio in the spectral region of overlap are due to the increase in the absorption cross-section of the surface plasmon absorption and larger overlap of the bands of the bulk metal as the aspect ratio increases. In that case the overlap between the interband absorption and the surface plasmon absorption increase as the aspect ratio

increases and the fluoresce emission enhancement increases, leading to the predicted and observed increase in the quantum yield by Mohamed et al.[4] Within the broad interband absorption, as the aspect ratio increase, the surface plasmon absorption band shifts to longer wavelength which causes the enhanced fluorescence spectrum maximum to shift to longer wavelength, as shown and predicted in the previous studies. As the surface plasmon absorption overlaps with the emission spectral wavelength region, the amount of the overlap becomes important in determining the emission enhancement. In the current study, the longitudinal surface plasmon absorption band moves to longer wavelength than the bulk fluorescence spectrum by increasing the aspect ratio, leading to a decrease in the enhancement, as predicted and observed.

Comments on the 740nm Emission

An emission was observed at ~740nm in all of the rods as well as the spheres with different surfactants, which suggests it is a property of the metal nanoparticles. Similar emission was also observed from thin metal films of gold (experimental result). Thus this emission is not specific to the shape in contrast to the other emission around 600nm, which is observed to be enhanced for nanorods specifically. The 740nm emission was not observed for solutions not containing gold nanoparticles. The theory presented in this paper predicts that emission at 740nm corresponds to an aspect ratio of 3.75, which is unlikely to be present in a sample of spheres, thus this emission is not attributed to shape enhanced emission. In Figure 4-6b, the emission spectra calculated displays a decrease almost to the baseline by 750nm, due to the decrease of the emission of bulk gold in the near-IR, and does not predict a separate emission at 740nm as is observed experimentally.

In order to gain more insight into the origin of this near-IR emission we tried to examine its intensity dependence on the aspect ratio. In order to determine accurate relative intensities, the self-absorption of the different samples are corrected and given in Table 4-2. The experimentally observed emission intensity and the theoretically calculated absorption cross-section at 740nm are presented. The absorption cross section is normalized to the minimum value of 1. Then the experimentally observed emission intensity is multiplied by the absorption cross-section normalization to obtain the corrected relative emission intensity. This shows that the emission observed is enhanced by the surface plasmon resonance, or the largest absorption cross-section at 740nm leads to the largest emission intensity, after self-absorption has been taken into account. Thus the sample with the plasmon resonance furthest from 740nm, Au1000, has the least emission intensity after self-absorption correction. Samples that have the same absorption cross-section have similar emission, even though the maximum plasmon resonance absorption are on opposite energy sides of the emission. Thus, explanations of the origin of this emission should include the sensitivity of the absorption of the sample due to the plasmon resonance, as a mechanism to enhance the near-IR emission.

Table 4-2: *Intensity of absorption taken from theoretical calculations at 740nm, and the maximum intensity of the second emission are presented. The experimental fluorescence is then corrected for self-absorption.*

	Absorbance: Theory		Fluroescence: Experiment	
Sample	Int. at 740nm (au)	Normalized	Int. at 740nm (au)	Int. Corrected (au)
Au630	245	2.6	686	1788
Au700	564	6.0	376	2262
Au850	453	4.8	380	1833
Au900	245	2.6	601	1566
Au1000	93.8	1.0	460	460

Several proposed sources of this emission are given previously. Similar emission is also observed by Li et. al.[37] where very high aspect ratio (16) nanorods emit a bright fluorescence at 743nm when excited at 690nm. A similar emission is observed by Jian et. al.,[38] attributed to aggregate emission. Beversluis et. al.[39] also observe a separate emission in the IR that increases around 720nm, which displays different dependences, and cannot be explained by the same mechanism as the visible emission. Au_{23} has been shown to have emission around this wavelength,[10] so it is possible that this emission is due to small clusters present in solution. Reports suggest that the band edge of gold is around 1.7eV (730nm).[32, 40] This would suggest that the emission observed at 740nm could be band edge emission due to the recombination of electrons enhanced by the surface plasmon transition. This emission could also be the background emission present in SERS spectra.[18-23] The background spectrum is only observed with the SERS signal when both the rough metal surface and molecule are in contact,[18, 19] and is believed to be due to a metal-molecule charge transfer interaction.[20-23] This background emission was previously observed to be independent of size and shape of the nanoparticle,[41] but related to both the metal and adsorbed molecule. Thus, the emission at 740nm could be due a

state created by adsorption of a molecule (or oxygen) on the surface of the nanorods (or nanospheres).

References

1. Link, S.; El-Sayed, M. A., Shape and size dependence of radiative, non-radiative and photothermal properties of gold nanocrystals. *Int. Rev. Phys. Chem.* **2000,** 19, (3), 409-453.

2. Kamat, P. V., Photophysical, photochemical and photocatalytic aspects of metal nanoparticles. *J. Phys. Chem. B* **2002,** 106, (32), 7729-7744.

3. Mooradian, A., Photoluminescence of Metals. *Phys. Rev. Lett.* **1969,** 22, (3), 185-187.

4. Mohamed, M. B.; Volkov, V.; Link, S.; El-Sayed, M. A., The 'lightning' gold nanorods: fluorescence enhancement of over a million compared to the gold metal. *Chem. Phys. Lett.* **2000,** 317, (6), 517-523.

5. Wilcoxon, J. P.; Martin, J. E.; Parsapour, F.; Wiedenman, B.; Kelley, D. F., Photoluminescence from nanosize gold clusters. *J. Chem. Phys.* **1998,** 108, (21), 9137-9143.

6. Hwang, Y. N.; Jeong, D. H.; Shin, H. J.; Kim, D.; Jeoung, S. C.; Han, S. H.; Lee, J. S.; Cho, G., Femtosecond emission studies on gold nanoparticles. *J. Phys. Chem. B* **2002,** 106, (31), 7581-7584.

7. Huang, T.; Murray, R. W., Visible luminescence of water-soluble monolayer-protected gold clusters. *J. Phys. Chem. B* **2001,** 105, (50), 12498-12502.

8. Link, S.; Beeby, A.; FitzGerald, S.; El-Sayed, M. A.; Schaaff, T. G.; Whetten, R. L., Visible to infrared luminescence from a 28-atom gold cluster. *J. Phys. Chem. B* **2002,** 106, (13), 3410-3415.

9. Zheng, J.; Petty, J. T.; Dickson, R. M., High quantum yield blue emission from water-soluble Au-8 nanodots. *J. Am. Chem. Soc.* **2003,** 125, (26), 7780-7781.

10. Zheng, J.; Zhang, C.; Dickson, R. M., Highly Fluorescent, Water-Soluble, Size-Tunable Gold Quantum Dots. *Phys. Rev. Lett.* **2004,** 93, (7), 077402.

11. Bruzzone, S.; Arrighini, G. P.; Guidotti, C., Some spectroscopic properties of gold nanorods according to a schematic quantum model founded on the dielectric behavior of the electron-gas confined in a box. I. *Chem. Phys.* **2003,** 291, (2), 125-140.

12. Geddes, C. D.; Parfenov, A.; Gryczynski, I.; Lakowicz, J. R., Luminescent blinking of gold nanoparticles. *Chem. Phys. Lett.* **2003,** 380, (3-4), 269-272.

13. Jian, Z.; Yongchang, W.; Qin, W., Fluorescence characteritics of Au colloidal nanoparticles. *Acta photonica sinica* **2003,** 32, (3), 357-360.

14. Maali, A.; Cardinal, T.; Treguer-Delapierre, M., Intrinsic fluorescence from individual silver nanoparticles. *Physica E* **2003,** 17, 559-560.

15. Varnavski, O. P.; Mohamed, M. B.; El-Sayed, M. A.; Goodson, T., III, Relative Enhancement of Ultrafast Emission in Gold Nanorods. *J. Phys. Chem. B* **2003,** 107, (14), 3101-3104.

16. Wang, G.; Huang, T.; Murray, R. W.; Menard, L.; Nuzzo, R. G., Near-IR Luminescence of Monolayer-Protected Metal Clusters. *J. Am. Chem. Soc.* **2005,** 127, (3), 812-813.

17. Geddes, C. D.; Parfenov, A.; Gryczynski, I.; Lakowicz, J. R., Luminescent Blinking from Silver Nanostructures *J. Phys. Chem. B* **2003,** 107, (37), 9989-9993.

18. Jiang, J.; Bosnick, K.; Maillard, M.; Brus, L., Single Molecule Raman Spectroscopy at the Junctions of Large Ag Nanocrystals. *J. Phys. Chem. B* **2003,** 107, 9964-9972.

19. Michaels, A. M.; Nirmal, M.; Brus, L., Surface Enhanced Raman Spectroscopy of Individual Rhodamine 6G Molecules on Large Ag Nanocrystals. *J. Am. Chem. Soc.* **1999,** 121, (43), 9932-9939.

20. Persson, B. N. J.; Baratoff, A., Theory of Photon Emission in Electron Tunneling to Metallic Particles. *Phys. Rev. Lett.* **1992,** 68, (21), 3224-3227.

21. Birke, R. L.; Lombardi, J. R.; Gersten, J. I., Observation of a Continuum in Enhanced Raman Scattering from a Metal-Solution Interface. *Phys. Rev. Lett.* **1979,** 43, (1), 71-75.

22. Lombardi, J. R.; Birke, R. L.; Lu, T.; Xu, J., Charge-transfer theory of surface enhanced Raman spectroscopy: Herzberg-Teller contributions. *J. Chem. Phys.* **1986,** 84, (8), 4171-4180.

23. Adrian, F. J., Charge Transfer effects in surface-enhanced Raman scattering. *J. Chem. Phys.* **1982,** 77, (11), 5302-5314.

24. Imura, K.; Nagahara, T.; Okamoto, H., Plasmon Mode Imaging of Single Gold Nanorods *J. Am. Chem. Soc.* **2004,** 126, (40), 12730-12731.

25. Boyd, G. T.; Yu, Z. H.; Shen, Y. R., Photoinduced Luminescence From the Noble-Metals and Its Enhancement On Roughened Surfaces. *Phys. Rev. B* **1986,** 33, (12), 7923-7936.

26. Boyd, G. T.; Rasing, T.; Leite, J. R. R.; Shen, Y. R., Local-Field Enhancement on Rough Surfaces of Metals, Semimetals, and Semiconductors with the Use of Optical 2nd-Harmonic Generation. *Phys. Rev. B* **1984,** 30, (2), 519-526.

27. Chen, C. K.; Heinz, T. F.; Ricard, D.; Shen, Y. R., Surface-Enhanced 2nd-Harmonic Generation and Raman-Scattering. *Phys. Rev. B* **1983,** 27, (4), 1965-1979.

28. Otto, A.; Mrozek, I.; Grabhorn, H.; Akemann, W., Surface-Enhanced Raman-Scattering. *J. Phys.: Condens. Matter* **1992,** 4, (5), 1143-1212.

29. Link, S.; Mohamed, M. B.; El-Sayed, M. A., Simulation of the optical absorption spectra of gold nanorods as a function of their aspect ratio and the effect of the medium dielectric constant. *J. Phys. Chem. B* **1999,** 103, (16), 3073-3077.

30. Yan, B.; Yang, Y.; Wang, Y., Comment on "Simulation of the Optical Absorption Spectra of Gold Nanorods as a Function of Their Aspect Ratio and the Effect of the Medium Dielectric Constant" *J. Phys. Chem. B* **2003,** 107, (34), 9159-9159.

31. Link, S.; El-Sayed, M. A., Simulation of the Optical Absorption Spectra of Gold Nanorods as a Function of Their Aspect Ratio and the Effect of the Medium Dielectric Constant (Addition/Correction). *J. Phys. Chem. B* **2005,** 109, (20), 10531-104532.

32. Apell, P.; Monreal, R.; Lundqvist, S., Photoluminescence of Noble Metals. *Phys. Scripta.* **1988,** 38, 174-179.

33. Johnson, P. B.; Christy, R. W., Optical Constants of the Noble Metals. *Phys. Rev. B* **1972,** 6, (12), 4370-4379.

34. Kupratakuln, S., Relativistic Electron Band Structure of Gold. *J. Phys. C: Solid State Phys.* **1970,** 3, (2), S109-S119.

35. Pinchuk, A.; Plessen, G. v.; Kreibig, U., Influence of interband electronic transitions on the optical absorption in metallic nanoparticles. *J. Phys. D: Appl. Phys* **2004,** 37, 3133-3139.

36. Eustis, S.; El-Sayed, M. A., The Aspect Ratio Dependence of the Enhanced Fluorescence Intensity of Gold Nanorods: Experimental and Simulation Study. *J. Phys. Chem. B* **2005,** 109, (34), 16350-16356.

37. Li, C. Z.; Male, K. B.; Hrapovic, S.; Loung, J. H. T., Fluorescence properties of gold nanorods and their applicaion for DNA biosensing. *Chem. Commun.* **2005**, 3924-3926.

38. Jian, Z.; Liqing, H.; Yongchang, W.; Yimin, L., Fluorescence spectrum properties of gold nanochains. *Physica E* **2004,** 25, (1), 114-118.

39. Beversluis, M. R.; Bouhelier, A.; Novotny, L., Continuum generation from single gold nanostructures through near-field mediated intraband transitions. *Phys. Rev. B* **2003,** 68, (11), 115433.

40. Alvarez, M. M.; Khoury, J. T.; Schaaff, G.; Shafigullin, M. N.; Vezmar, I.; Whetten, R. L., Optical Absorption Spectra of Nanocrystal Gold Molecules. *J. Phys. Chem. B* **1997,** 101, (19), 3706-3712.

41. Nikoobakht, B. Synthesis, characterization and self-assembly of gold nanorods and surface-enhanced Raman studies. Georgia Institute of Technology, Atlanta, GA, 2003.

CHAPTER 5

PHOTOTHERMAL MELTING OF HIGH ASPECT RATIO NANORODS

Abstract

According to predictions of Lord Rayleigh, nanorods of aspect ratio below 4.5 melt into a single sphere while those with an aspect ratio above 4.5 break apart during melting to form multiple particles. Experimentally, Link and El-Sayed have shown that nanorods of low aspect ratio melt into spheres in 30ps. To test the prediction for high aspect ratio nanorod samples with a median aspect ratio of up to 6, the lifetime of decay of the longitudinal plasmon resonance absorption spectrum due to nanorod melting, and the size distributions of the samples after exposure to femtosecond pulses of appropriate energies are examined. Higher threshold energies (energy required to melt every nanorod in the irradiation volume with one pulse) are observed for high aspect ratio nanorods due to the decrease in the coupling of the longitudinal plasmon resonance and the laser wavelength used. Samples with a median aspect ratio of 6 have a threshold energy of 9μJ while shorter aspect ratio nanorods have a threshold energy of 5μJ. No difference is observed in the size of the nanospheres formed with laser energy. Similar percent of atoms are lost for all aspect ratios observed, thus this study fails to observe the formation of multiple particles. These results are discussed in terms of the large polydispersity of the sample, the effect of the capping material, and the fixed wavelength laser used.

Introduction

The optical properties of gold nanoparticles have been investigated due to their strong absorption, and the dependence on the size and shape of the nanoparticle.[1, 2] Gold nanorods are special with two plasmon resonances observed, one due to the transverse plasmon oscillation along the short axis, and the other along the long axis, referred to as the longitudinal plasmon resonance.[1, 2] As the aspect ratio increases, the longitudinal plasmon resonance red shifts, allowing for the determination of the aspect ratio distribution by optical absorption measurements as shown in Chapter 3 by the GNOME method and previous publications.[3, 4] The optical properties of gold nanorods allow determination of the changes in the size or shape of the nanoparticles by optical absorption measurement. Thus, the optical properties can be thought of as a microscope that allows visualization at the nanoscale by following their absorption spectrum.

Previous researchers have investigated the effect of laser irradiation on gold and silver nanoparticles.[5-21] Metal nanoparticles have been found to be formed,[6-10] fragmented,[6, 7, 10-13] melted,[13-21] and reshaped[13, 15-19, 21] with laser irradiation. By studying the time-dependent properties of the bleach spectrum, electron-phonon relaxation times[18] can be determined. These show that the electronic temperature of metal nanoparticles can be very high as a results of laser excitation.[17] The electronic kinetic energy is transferred into the lattice kinetic energy by electron-phonon interaction and dissipated by phonon-phonon interaction.[17] By varying the energy of the laser, wavelength of excitation and temporal pulse width, the sample is affected differently. Thus melting, fragmentation or atomic ablation can take place.[15-19] The heating ability, and thus the possibility of using gold nanoparticles as nanoheaters has recently been investigated in

ice.[22] Nanorods have also been used as heaters where the laser wavelength is tuned to the longitudinal plasmon resonance of the different aspect ratio to locally increase the temperature.[23]

The laser melting of electrochemically prepared[24] gold nanorods of low aspect ratio (2-4) was studied previously.[15-19, 21] Many different parameters have already been investigated in this system, including the structural changes,[15, 21] the pulse length of the laser irradiation,[16, 17] the power dependence and the frequency dependence.[16, 17, 21] Higher aspect ratio nanorods have also been investigated by Chang et. al.[21] with a nanosecond laser. At the low intensities used in this study,[21] incomplete melting is observed with pregnant or ϕ shaped nanoparticles when the laser irradiation is at the longitudinal plasmon resonance.

Previous studies[15-19] investigated the melting of gold nanorods using a femtosecond laser system. The nanorods investigated previously where chosen to have their longitudinal plasmon resonance absorption maximum at the same wavelength as the laser.[15-19] The intensity and pulse width of the laser are important considerations as higher powers and longer pulses fragment gold nanorods.[16] However, lower energies can selectively remove one size or shape from the sample by choosing the frequency and intensity to match the sample.[16] Laser intensities of 2-30 microjoules are useful for melting nanorods into nanospheres without large amounts of fragmentation. Previously, a threshold energy was determined at which one pulse has enough energy to melt all of the nanorods in the focal volume.[17, 19] This threshold is observed by the absence of hole burning in the longitudinal plasmon resonance and a constant time for the longitudinal plasmon resonance intensity to decrease by 1/e as a function of the laser intensity. The

threshold is determined to be 5μJ for an aspect ratio of 4.1 with 800nm fs laser irradiation.[17, 19] The current study examines the aspect ratio dependence of this threshold energy and the number and sizes of spheres generated after laser irradiation of a nanorod.

The absorption characteristics are shifted by changing the dielectric constant around the nanoparticle or by adjusting the aspect ratio of the nanorod. Previous studies modified the aspect ratio of the samples, until the laser wavelength matched the longitudinal plasmon resonance to selectively heat the nanorods.[15-19, 21] This experiment slightly changes the aspect ratio of the nanorods so that the longitudinal plasmon resonance is slightly shifted from the laser wavelength.

High aspect ratio systems have distinct properties in how they respond to instabilities. Lord Rayleigh[25] predicted in 1879 that particles of higher aspect ratio than 4.5 will break apart into multiple spheres. Lord Rayleigh presented a calculation for the shapes and number of particles formed as a liquid jet is released from a nozzle into air.[25] As the particle breaks apart to form a more thermodynamically stable shape the driving forces modeled by Lord Rayleigh are the surface energy and the energy required for reorganization.[25] The prediction of the instability of structures with aspect ratios larger than 4.5 have been confirmed more recently by Bréchignac et al.[26] where fractal structures are observed to break apart when the aspect ratio is above 4.5. Many previous reports on the melting of gold nanorods with an aspect ratio of ~4, just below this cutoff for instability, have been reported.[15-19, 21] The gold nanorod system is interesting because it offers the possibility of measuring the time scale of this transition using the optical absorbance from the plasmon resonance, which depends on the particle shape. The study presented here examines the photothermal response of high aspect ratio nanorods in

solution and tries to see if they break apart into multiple particles, instead of melting into single spherical particles.

Experimental

Gold nanorods are prepared by the chemical seeding technique described in Chapter 2. Samples are characterized by the maximum wavelength of the longitudinal plasmon resonance, and the aspect ratio distribution is obtained using the GNOME method described in Chapter 3. Laser samples are irradiated with a 100 femtosecond laser pulse from an amplified Ti:Sapphire laser system (Clark-MXR CPA 1000). The fundamental frequency at 800nm is used for irradiation experiments. The sample was placed in a 1cm glass cuvette, with a stir bar. The laser pulses are focused with a short focal length lens, near the bottom of the cuvette, to insure a fresh sample volume for each laser pulse. Two and a half milliliters of solution with a 0.43 optical density at 800nm is used. Absorption spectra are measured on a Shimadzu UV-3103-PC spectrophotometer. For the TEM measurements, a drop of solution is allowed to dry overnight on a carbon coated copper TEM grid (Ted Pella). The samples are imaged at 100kV in the JOEL JEM-100C transmission electron microscope (TEM) to determine the size distributions.

To determine size distributions, optical characterization of the aspect ratio from absorption spectrums described in detail in Chapter 3 and transmission electron microscopy (TEM) are used. The TEM images can be analyzed on magnified prints with a ruler by hand, or on scanned negatives, and analyzed using programs such as Image J.[27] Results from each technique are compared to show that the two methods produce similar results. Computer analysis is faster, enabling the determination of multiple particles at the same time, and reduces chemicals, by the removal of the need to print the negative.

While counting particles by hand requires determining the dimensions of each particle individually, and then entering the size data into the computer. Analysis of images with software removes this need, but programs are bad at identifying particles. Images must have a threshold set, or the minimum gray value that is to be considered a particle, everything else is considered background and is ignored in future analysis. Then the particles must be separated so that the computer does not count multiple particles as a single particle. This was achieved by use of the watershed algorithm, which takes the path predicted for the flow of water through the area, and separates areas predicted to be different. This algorithm is slow and memory intensive, therefore it can only handle part of an image at a time. Alternatively, particles can be separated by hand in the computer file by removing a small amount of the particle in the image. All sizes are tabulated in Microsoft Excel, and the Histogram function is used to bin data. Then Origin 7 (OriginLab Co.) is used to fit the histogram with a Gaussian distribution. The Guassian distributions are used to compare the samples and the different methods of analysis.

Results and Discussion

Laser Melting Dynamics

The samples used in this study have been characterized by the optical absorption GNOME method described previously[4] and in Chapter 3. The longitudinal plasmon resonance absorption is fitted to theoretically obtained absorption of nanorods by obtaining the % of the sample function. Thus the aspect ratio distribution can be obtained from the spectroscopic absorption. The longitudinal plasmon resonance absorption is fit for all of the samples in this study to generate the aspect ratio distribution shown in

Figure 5-1. The aspect ratio increases as the plasmon resonance shifts to the red. Thus the percent of each aspect ratio is shown for all of the samples used in this study.

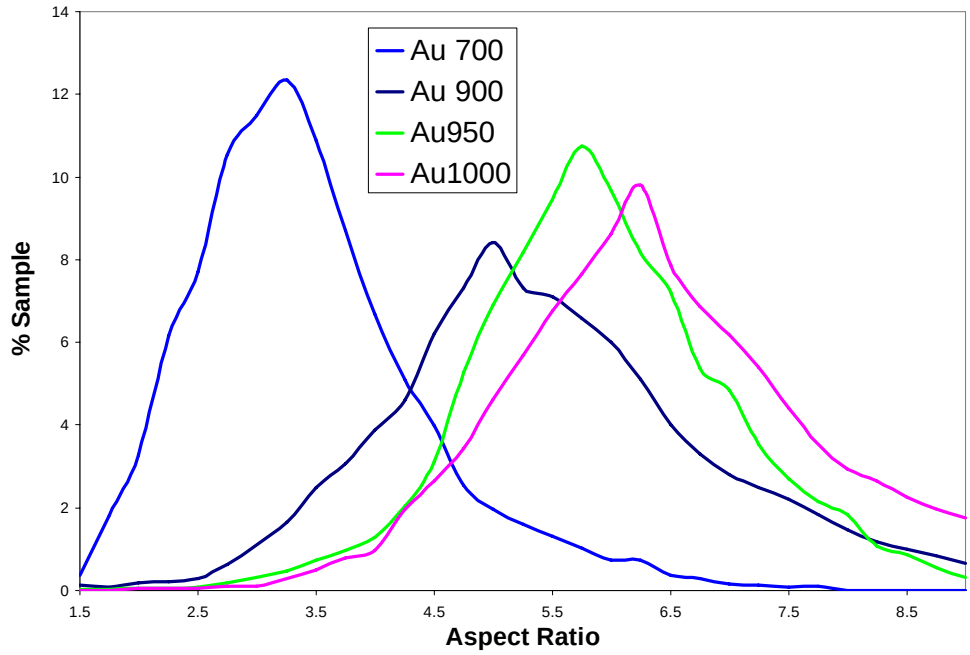

Figure 5-1: *Aspect ratio distributions of the gold nanorod samples used in the photochemical method. Fits are obtained from a fit to the longitudinal plasmon resonance absorption by the GNOME method described previously*[4] *and in Chapter 3.*

The melting of nanorods after exposure to 800nm fs laser irradiation is measured by following the absorption spectrum. The absorption spectra of samples, Au700, Au900 and Au1000 irradiated with laser irradiation are shown in Figure 5-2. The aspect ratio distributions of these samples are shown in Figure 5-1. The longitudinal plasmon resonance of the gold nanorods decreases with laser irradiation for all samples. The presence of "hole burning" is seen in the lower aspect ratio samples at low power. At these conditions the laser energy is able to selectively melt the nanorods with absorption close to the laser wavelength. As the longitudinal plasmon resonance is red shifted due to

increasing aspect ratio of the nanorods, the relative position of the hole burning is observed to blue shift and decrease, due to the fixed laser wavelength. A clear difference in the absorption spectrum is observed for energies above and below the threshold energy. As shown in Figure 5-2a, sample Au700 irradiated with low laser intensity is below the threshold energy, leading to an observed "hole burning" in the longitudinal plasmon resonance because the energy is not enough to couple to the nanorods with higher or lower aspect ratio nanorods as observed previously.[17, 19] At intensities above the threshold, the longitudinal plasmon resonance is seen to decrease at all wavelengths with no optical hole. The decrease in the absorption takes places faster at energies above the threshold. The threshold energy is defined as the energy at which all of the nanorods in the focal volume of the laser are melted with a single laser pulse.[18, 19]

Sample Au1000, with a higher aspect ratio and the longitudinal plasmon resonance absorption maximum at 1018nm is exposed to laser irradiation shown in Figure 5-2e and 5-2f. Below the threshold energy no hole burning is observed in the optical spectra, unlike previous reports[17, 19] and samples Au700 and Au900. Above the threshold energy for sample Au1000 the transition is much faster, and goes to completion after 3 minutes of laser irradiation. The threshold energy is much harder to specify for this sample because of the lack of optical hole burning. However, the longitudinal plasmon resonance is observed to red shift more at lower energies. This is similar to hole burning, in that only those rods with plasmon resonances close to that of the laser irradiation wavelength melt faster, but the laser wavelength is no longer the center of the longitudinal plasmon resonance. The population of nanorods with their longitudinal

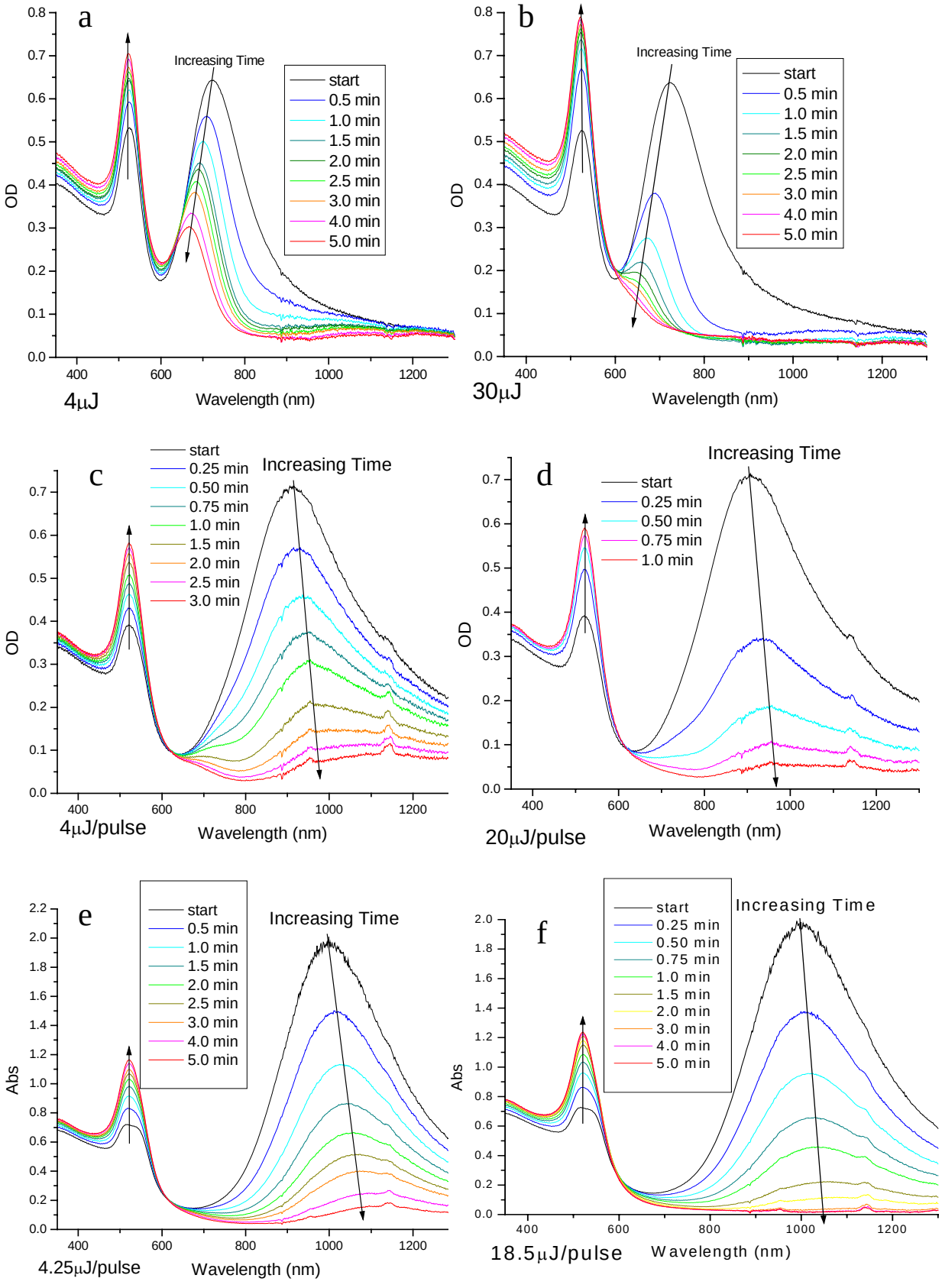
a
Increasing Time
start
0.5 min
1.0 min
1.5 min
2.0 min
2.5 min
3.0 min
4.0 min
5.0 min
OD
Wavelength (nm)
4μJ
b
Increasing Time
start
0.5 min
1.0 min
1.5 min
2.0 min
2.5 min
3.0 min
4.0 min
5.0 min
OD
Wavelength (nm)
30μJ
c
start
0.25 min
0.50 min
0.75 min
1.0 min
1.5 min
2.0 min
2.5 min
3.0 min
Increasing Time
OD
Wavelength (nm)
4μJ/pulse
d
Increasing Time
start
0.25 min
0.50 min
0.75 min
1.0 min
OD
Wavelength (nm)
20μJ/pulse
e
start
0.5 min
1.0 min
1.5 min
2.0 min
2.5 min
3.0 min
4.0 min
5.0 min
Increasing Time
Abs
Wavelength (nm)
4.25μJ/pulse
f
start
0.25 min
0.50 min
0.75 min
1.0 min
1.5 min
2.0 min
3.0 min
4.0 min
5.0 min
Increasing Time
Abs
Wavelength (nm)
18.5μJ/pulse

Figure 5-2: *The absorption spectrum of samples Au700 (a & b), Au900 (c & d) and Au1000 (e & f) during irradiation with 800nm fs laser irradiation, above (b, d and f) and below (a, c and e) the threshold energy. Longitudinal plasmon resonance hole burning is observed at lower laser powers.*

plasmon resonance to the blue of the laser wavelength is very small and does not remain to observe the "hole burning" seen in nanorods with shorter aspect ratios.[17, 19]

The time for the optical density to decrease to 1/e of its initial value is a measure of the transition time of the bulk sample and is referred to as the "lifetime" of the transition.[18, 19] The lifetime was calculated by fitting the decreasing optical density as a function of irradiation time using a single exponential in Microsoft Excel at the laser wavelength, maximum wavelengths at the start of laser irradiation and at the continuous wavelength maximum. The lifetimes for samples Au900 and Au1000 at these wavelengths are shown in Figure 5-3, with the solid curve belonging to sample Au900 and the dashed curve belonging to sample Au1000. The spread between the lifetimes calculated at the different wavelengths shows that at lower energies the laser irradiation cannot couple to all of the nanorods below the threshold energy.

Two different methods are used to determine the threshold energy for each sample. One method to determine the threshold energy is the energy at which the wavelength maximum remains constant during irradiation. The other method to determine the threshold energy is where the lifetime remains relatively constant independent of the laser energy. The red shift of the wavelength maximum after laser exposure irradiation time is tabulated for each sample. The results of both of these methods agree where the threshold energy is 5μJ/pulse for the sample Au900, as seen in Figure 5-3. This is the same threshold reported previously for aspect ratio 4.1 gold

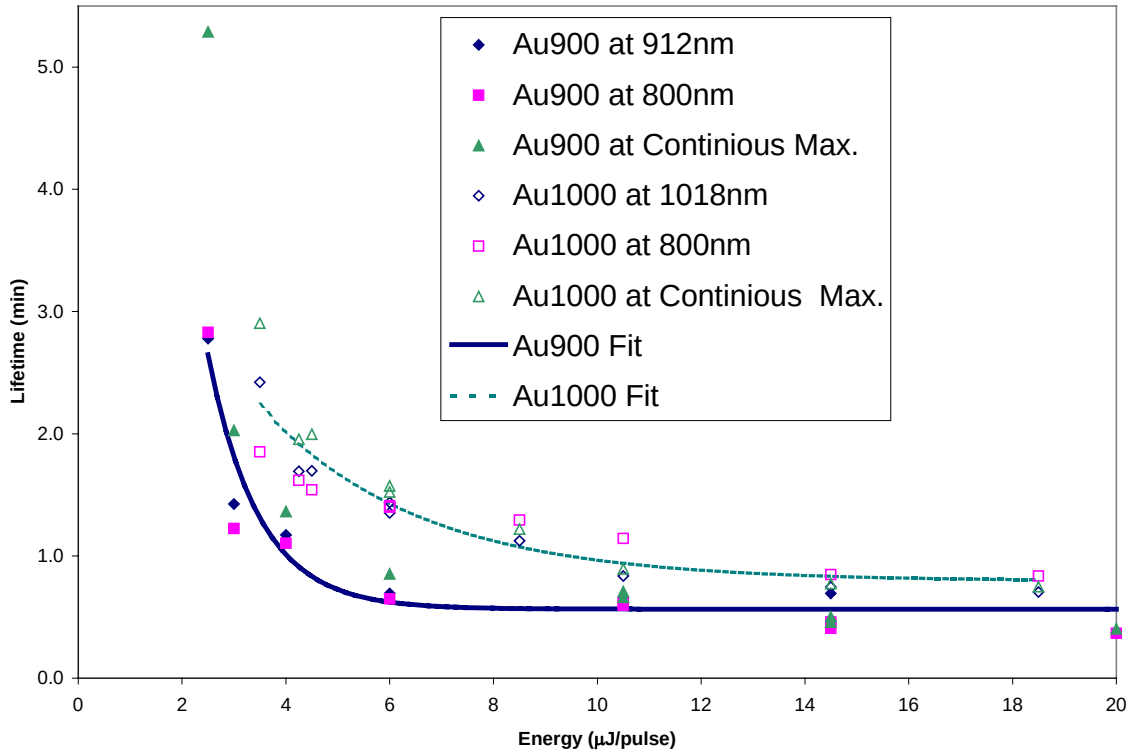

Figure 5-3: *Lifetimes calculated for samples Au900 and Au1000 at different laser powers. The lifetimes are measured at different wavelengths to observe how the plasmon resonance shifts and decreases; 800nm is the laser wavelength, 912nm is samples' Au900 maximum, 1018 is samples' Au1000 maximum, and the maximum intensity as the wavelength maximum red shifts.*

nanorods.[19] The lifetimes are slightly different due to different sample cuvettes. The threshold for Au1000 appears to be around 9µJ/pulse. The lifetimes obtained are slightly longer for Au1000. This might be due to the fact that the longitudinal plasmon resonance is further away from the 800nm excitation wavelength for sample Au1000. Thus more of the longitudinal plasmon resonance band couples closely with the laser irradiation for sample Au900 than sample Au1000. This affects both the threshold energy and the lifetime.

The observed threshold of 5μJ/pulse (with 800nm femtosecond irradiation) for the nanorods prepared by the chemical synthesis is comparable to the threshold energy of nanorods in the electrochemical system examined previously by Link et. al.[15-19]

Analysis of the Size of the Nanoparticles

The nanorods and nanospheres for these experiments were investigated by TEM analysis. The nanorods have been analyzed by determining the size from enlarged TEM prints, and also analyzed by modeling the absorption spectra discussed in Chapter 3. However, the volume is particularly important in this study to obtain the amount of atoms lost during laser irradiation, therefore TEM analysis of the nanorods is used. The nanospheres generated after laser irradiation must be analyzed by TEM statistics. In order to compare the results obtained using the software package Image J to previous reports, the particle diameter statistics generated using enlarged prints and computer results for the three samples are compared. Figure 5-4 shows the data along with the fits for spheres after different powers of laser irradiation. The fits to the data agree closely with each other showing the method of obtaining the information does not affect the size distribution. This data also shows that the size of the spheres generated does not change as a function of laser power.

The TEM results from samples Au900, and Au1000 generated the length and width of many different rods present in the sample. The length (l) and width (w) can then be used to obtain the aspect ratios (AR) and volume (V_r) of each rod according to the following equations.

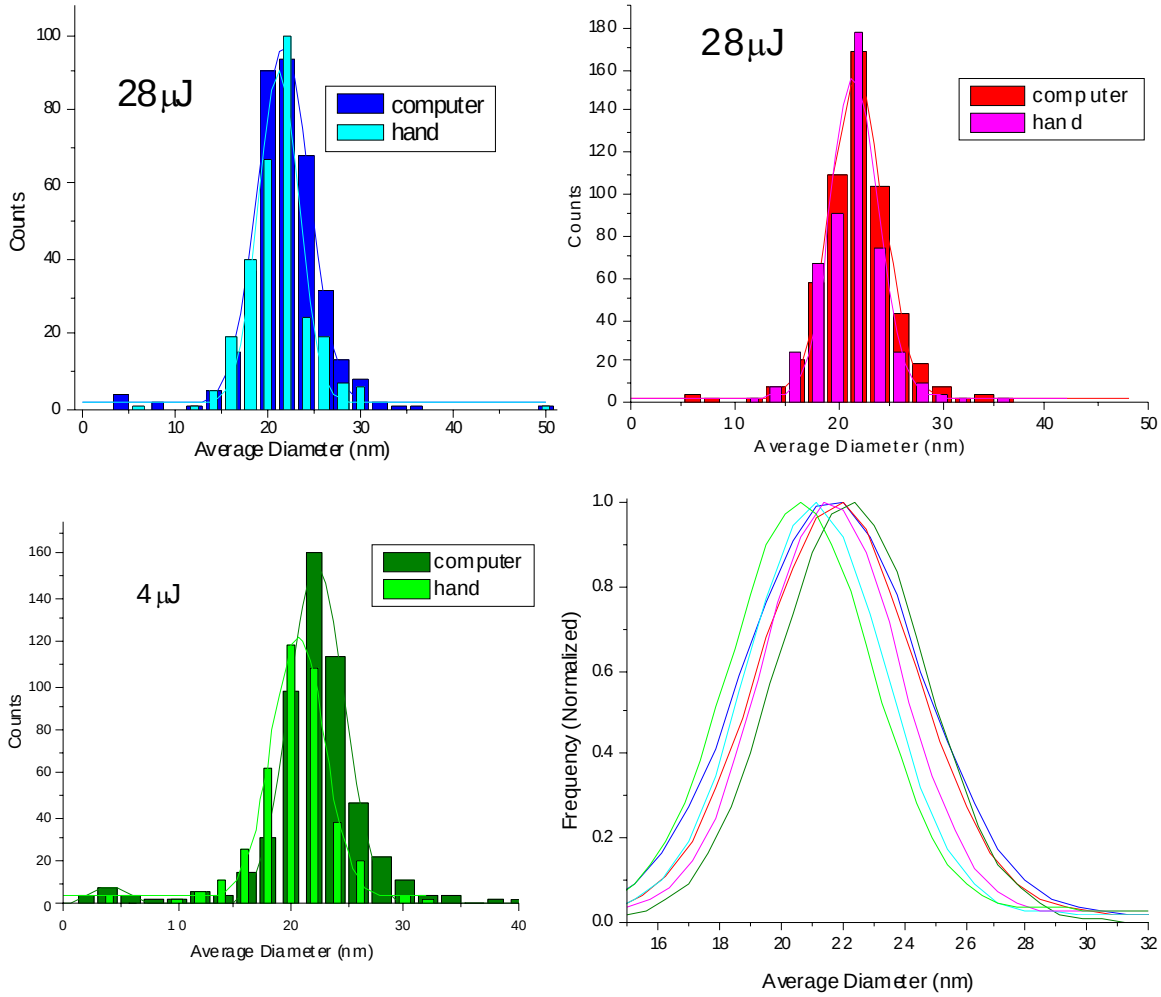

Figure 5-4: *Fits to the average diameter of spheres formed after laser melting of gold nanorods with an 800nm fs laser. The differences between the diameter obtained by counting by hand, and that obtained using Image J[27] are shown for 4μJ, 28μJ (two different samples) and all of the fits.*

$$AR = \frac{l}{w} \tag{5.1}$$

$$V_r = \pi\left(\frac{w}{2}\right)^2 l = \frac{\pi}{4} w^3 AR \tag{5.2}$$

Thus one might expect that as the aspect ratio increases, the volume would also increase. However, this is only true if the width of the rods remains constant as shown in equation 5.2. Figure 5-5 shows the aspect ratio and volume for individual nanorods in sample Au1000 from TEM analysis. As the aspect ratio increases, the average volume remains the same, showing that there is no relationship between the aspect ratio and the volume of the nanorods grown by the seeding chemical synthesis method used here. This is a kinetic growth where all of the nanorods have approximately the same number of atoms reduced. Thus the nanorod aspect ratio and volume are not related for these samples. This however, increases the difficulty in determining if high aspect ratio nanorods break into multiple particles. Even though there are high aspect ratio nanorods present in the sample before irradiation, with only the volume analysis of the products, determining the number of spheres formed from a single nanorod is difficult.

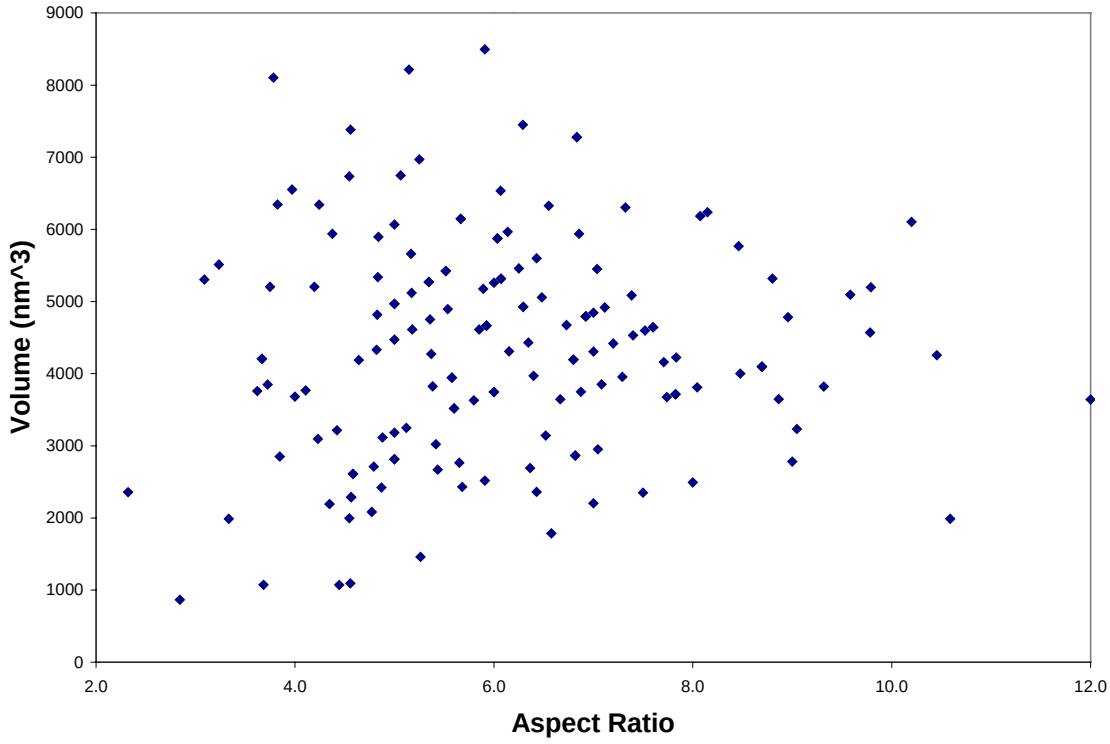

Figure 5-5: *Aspect ratio and volume of individual nanorods from sample Au1000. There is no relationship in this sample between the aspect ratio and the volume as predicted from equation 5.2.*

Number of Spheres Formed From One Nanorod

TEM Analysis

In order to observe the number of particles formed from nanorods after laser exposure the samples are analyzed by TEM. The volume of rods is shown in Figure 5-5 as a function of aspect ratio according the equation 5.2. The average diameter (*d*) of spheres observed after laser irradiation are also obtained from TEM results. The volume (V_{sp}) of the spheres can be calculated from the following equation.

$$V_{sp} = \frac{4}{3}\pi\left(\frac{d}{2}\right)^3 \qquad (5.3)$$

The volumes of the rods and the spheres are fitted to a Gaussian distribution, and the median value is used in further analysis. The median diameter from the Gaussian fits is shown in Figure 5-6 and Table 5-1 as a function of laser power for 4 different samples.

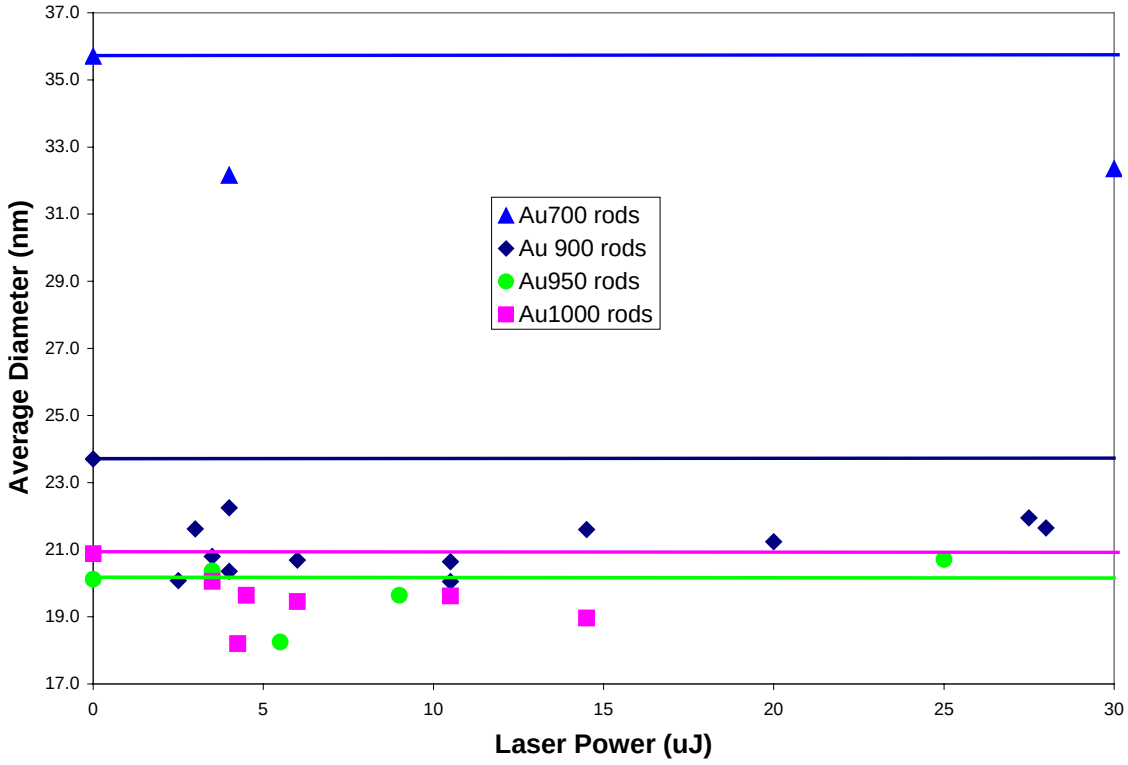

Figure 5-6: *The average diameter of spheres produced after different laser irradiation powers (Solid line represents the calculated average diameter from the volume of the rods) for different nanorod samples*

Table 5-1: *Median aspect ratio and longitudinal absorption wavelength maximum for experimental samples from absorption GNOME modeling presented in Chapter 3*

Sample	Wavelength Maximum (nm)	Median Aspect Ratio
Au700	700	3.25
Au900	912	5
Au950	954	5.75
Au1000	1018	6

No dependence of the average diameter of the sphere produced on the laser power is observed as seen in Figure 5-6 where the average diameter of each sample is plotted. The average diameter at zero power is calculated by assuming that the volume of the rod remains intact through the melting process to from one sphere. As observed in Figure 5-6 the different samples form different sizes of nanospheres due to the different volume of the starting nanorod solutions. The method used to generate nanoparticles for this study employs kinetic growth conditions leading to a different fraction of gold ions reduced per particle in each sample.

Previous results show that a threshold energy is necessary to melt all of the nanoparticles in the irradiation volume with a single laser shot.[19] However, pulses both above and below this energy form the same nanoparticle size as shown in Figure 5-6. This further confirms that the energy provided does not affect the melting process, only the percentage of the sample that melts.

To examine the similarities and differences between the samples presented in Figure 5-6 the percent change of the number of atoms in a nanorod to a nanosphere is calculated for all samples with different laser powers. Then the number of gold atoms in the particles (ρ) is calculated by using the volume of atomic gold[28] of 10.2cm^3/mol to calculate the number of atoms in the rods and the spheres. The % change in the number

of gold atoms in the spheres compared to the number of gold atoms in rod is calculated according to the following equation.

$$\%change = \frac{\frac{V_{sp}}{\rho} - \frac{V_r}{\rho}}{\frac{V_r}{\rho}} * 100 = \frac{V_{sp} - V_r}{V_r} * 100 \qquad (5.4)$$

The % change of each sample is shown in Figure 5-7 as a function of laser power. The percent change of all samples is observed to be in the same range due to the large scatter of the data points from this analysis, even though the samples have different volumes. According to this analysis, most samples show a loss of atoms as the sample is melted. However, the percentage change for low and high aspect ratio nanorods is similar, suggesting that the same behavior is observed for all aspect ratios. Thus, the analysis does not show the rods breaking apart in the solution studies, but the polydispersity was quite large and showed that melting is accompanied by ablation process.

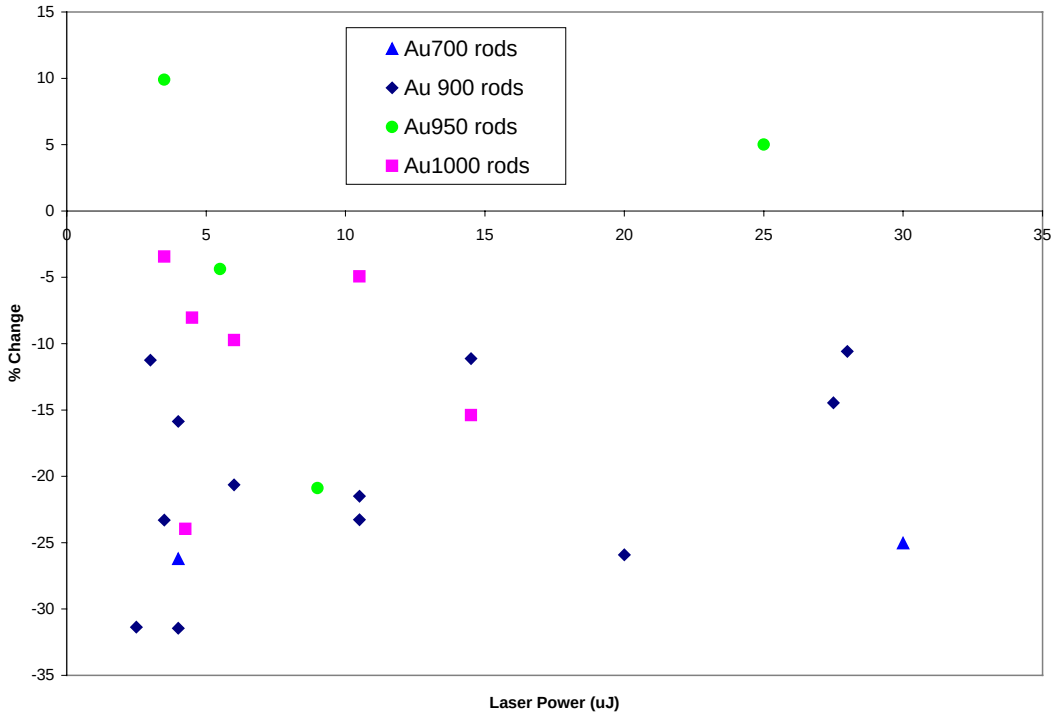

Figure 5-7: *The % change in the average number atoms in the spheres formed after melting of gold nanorods is plotted as a function of laser power for different samples after irradiation with an 800nm fs laser.*

Optical Absorption Analysis

To further investigate the number of spheres produced from the laser melting of gold nanorods, a method based on the optical absorbance is presented. To determine the number of spheres generated from the laser melting of nanorods, the absorbance of each species is compared, using a correction factor for the difference in the optical absorption coefficient. The following equation is used for this determination.

$$\frac{N_{sp}}{N_r}\bullet\frac{\gamma_{sp}}{\gamma_r}=\frac{\Delta(OD)_{sp}}{\Delta(OD)_r};\qquad \frac{N_{sp}}{N_r}=\frac{\Delta(OD)_{sp}}{\Delta(OD)_r}\bullet\frac{\gamma_r}{\gamma_{sp}} \qquad (5.5)$$

where N_{sp} is the number of spheres, N_r is the number of rods, $\Delta(OD)_{sp}$ is the change in the optical density of the plasmon resonance at 522nm, $\Delta(OD)_r$ is the change in the optical density of the longitudinal plasmon resonance at the wavelength maximum durring irradiation. γ_r and γ_{sp} are the absorption coefficients of the nanorods and nanospheres, respectively. The value of the longitudinal plasmon absorption coefficient for the nanorods is obtained from the GNOME modeling the absorption spectrum as described in Chapter 3, with the incorporation of the frequency factors. To determine the absorption coefficient of the spheres in the sample, the Mie[29-32] equation is used.

$$\gamma_{sp} = \frac{18\pi V \varepsilon_m^{3/2}}{\lambda} \bullet \frac{\varepsilon_2}{\left[\varepsilon_1 + 2\varepsilon_m\right]^2 + \varepsilon_2^{\,2}} \qquad (5.6)$$

where V is the volume of the nanoparticle (same as that used for the calculation of the absorption coefficient of the nanorods), ε_m is the dielectric constant of the surrounding medium, λ is the wavelength of light, and the dielectric constant of the metal is expressed in the complex form, where $\varepsilon = \varepsilon_1 + i\varepsilon_2$.

Figure 5-8 shows the number of spheres produced per rod melted during laser irradiation calculated using equation 5.5. Although the values of the N_{sp}/N_r are slightly less than 1, suggesting that the melting of every nanorod does not lead to the formation of a sphere, the value is similar for the different aspect ratios. This implies that the formation of spheres from rods after laser irradiation is similar in all of the samples examined independent of the aspect ratio. No difference is observed as the power of laser irradiation is increased. The different aspect ratios all show the same number of spheres per nanorod melted, as shown in the previous characterization techniques. This technique further confirms that all of the experimental samples have similar behavior.

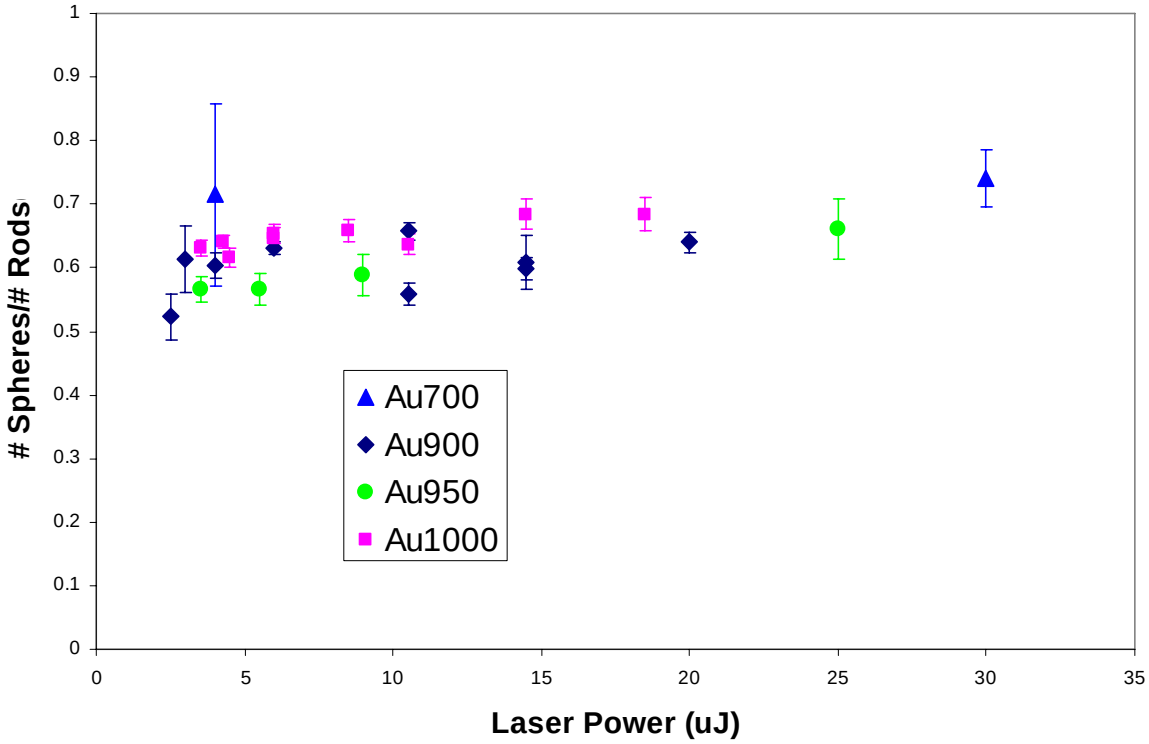

Figure 5-8: *The calculated change in the number of spheres per nanorod from absorption intensities during laser melting*

Discussion of the Number of Spheres Formed From One Nanorod

The diameter analysis (from TEM), % change analysis (from TEM), and optical absorption analysis are used to determine the number of spheres formed by melting a nanorod showed that all of the samples lose a small number atoms and melt into about one sphere regardless of laser power or aspect ratio of the nanorods investigated. Thus, all of the different techniques are all validated, and the conclusion that no significant difference is observed. Therefore this study was unable to determine if higher aspect ratio nanorods melt into multiple particles after exposure to laser irradiation. The GNOME modeling the of the longitudinal plasmon resonance in Chapter 3 shows that the nanorods that absorb around the 800nm laser irradiation have aspect ratios from 4-5.

There is a very similar population of all of these nanorods in all of the samples used in this experiment as shown in Figure 5-1. Since the laser wavelength was not changed with the longitudinal plasmon absorption, the same nanorods are melted in each sample, even though the median aspect ratio of the sample changes. Thus the effect of the laser wavelength may also be influencing which nanorods are melting, due to the fixed laser wavelength in this study.

Thus the data presented above does not necessarily disprove Lord Rayleigh's prediction. The TEM analyses suffer from the need to determine the volume of the nanorod, which is the diameter of the sphere cubed, thus cubing any error in the measurement. In order to obtain good results from an analysis where the dimensions are cubed, a monodisperse sample is necessary. The optical analysis does not suffer from the same need to cube any result, leading to smaller error bars. The optical characterization is an attractive analysis, as no TEM is required to determine the size of the nanoparticles, removing the most time consuming step of analysis. The optical characterization does require modeling of the absorption spectra of both gold nanorods and gold spheres. As these models have already been developed and validated in previous chapters, this is an additional benefit of modeling the absorption spectra of these samples. However, the involvement of ablation processes could interfere in obtaining the correct number of spheres formed from each rod melted .

Another challenge of this study was obtaining nanorod solutions with aspect ratios much larger than 4.5 with no nanorods with aspect ratio less than 4.5. However, the experimental difficulty increases with the aspect ratio of the nanorod generated. I could only obtain samples of aspect ratio 6 repeatedly. Occasionally higher aspect ratio

nanorods were generated, but they were unstable and decreased in aspect ratio quickly. The fact that a large distribution in the aspect ratio and volume of nanorods are obtained increases the complexity of determining the aspect ratio at which the nanorod breaks into multiple particles. While the median aspect ratio of sample Au1000 was around 6, there were still rods present in this sample with an aspect ratio below 4.5 as seen in Figure 5-1. These nanorods will absorb more effectively the exciting laser than the larger ones due to their larger wavelength overlap with the laser wavelength. Thus in all these samples, we are melting rods whose aspect ratio below 5, which absorb strongly the laser excitation wavelength at 800nm.

The presence of the capping material and the solution phase nature of these experiments are much different than those considered by previous theoretical modeling of high aspect ratio structures.[25, 26] The cooling in solution and surface binding of the gold nanorod must also be taken into account, and may increase the aspect ratio required to produce multiple particles predicted by Lord Rayleigh.[25] Previous models used liquid jets[25] or un-stabilized fractals on a glass surface,[26] considering only the minimization of surface energy. Previous studies did not have a surface coating, or a solution, which may explain the difference in the observed result.[25, 26]

In order to form gold nanorods in solution, a strong directing force is necessary to form the highly anisotropic nanorod. This is believed to be induced by the strong bonding of a material (the surfactant, the anion, or the shape directing ion silver) to a crystal facet of the gold nanorod.[33-47] Thus the removal of this surface layer is going to cost energy, and must be included in calculations that predict when a nanorod will break to form 2 or more small nanoparticles instead of a single larger sphere.

Another limiting factor in this study is the overlap of the longitudinal plasmon resonance with the wavelength of the laser. As the longitudinal plasmon resonance absorption shifts into the infrared due to the increasing aspect ratio, the overlap with the laser wavelength decreases. In order to increase the overlap of the plasmon resonance with the laser wavelength an optical parametric amplifier could be used to shift the laser wavelength to keep the overlap the same. If the wavelength of the laser is chosen to overlap with the transverse plasmon resonance instead of the longitudinal plasmon resonance, the nanorod absorbs light from the transverse plasmon resonance and undergoes melting. After melting the nanorods to generate nanospheres, the nanospheres absorb light at the same wavelength as the transverse plasmon resonance of the nanorods. Thus the laser irradiation is able to add energy to the spheres. Then the spheres generated absorb laser irradiation to induce fragmentation. Also, if the sample is polydisperse, all sizes of rods will absorb and melt. This will "wash out" the results of the dependence of melting of rods of different aspect ratios.

These studies have shown that working in solution there is always the polydispersity of the sample to take into account and it can not be determined if the rods are melting into one large sphere or two smaller ones from the data obtained. To get around the polydispersity of solutions, the rod could first be immobilized on the surface[40, 48, 49] before laser irradiation so that single particle experiments can be done to determine if these theoretical predictions hold for the gold nanorod system. These studies were not preformed due to the large polydispersity of these rods on surfaces, [40, 48, 49] and the high aspect ratio of nanorods generated with these methods that are not expected to absorb the laser irradiation at 800nm.

Summary

The threshold energy of nanorods increases with the aspect ratio. However, the size of the nanoparticles formed shows no change with increasing laser power. All of the different methods described here suggest that the laser wavelength must be shifted to probe this prediction as the fixed laser wavelength at 800nm melts the same aspect ratio nanorods regardless of the percentage other nanorods in solution. Thus, all of the nanorods shown here with median aspect ratios from 3-6 melt to form approximately one sphere. Thus all of the methods agree supporting both analyses by TEM and the analysis by optical spectroscopy. Using laser irradiation at the same wavelength as the maximum longitudinal plasmon resonance of higher aspect ratio nanorods could be used to further investigate this system. Binding nanorods to surfaces or directly growing nanorods on surface can also be used to further investigate the number of particles formed from the melting of high aspect ratio systems. The importance of the surface binding and laser fragmentation should be included to determine if that changes the expected aspect ratio when nanorods form multiple particles after destabilization.

Acknowledgement: We wish to acknowledge and the financial support of the National Science Foundation, Division of Material Science Grant No. 0138391

References

1. El-Sayed, M. A., Some interesting properties of metals confined in time and nanometer space of different shapes. *Acc. Chem. Res.* **2001,** 34, (4), 257-264.

2. Eustis, S.; El-Sayed, M. A., Why Gold Nanoparticles Are More Precious than Pretty Gold: Noble Metal Surface Plasmon Resonance and its Enhancement of the Radiative and Nonradiative Properties of Nanocrystals of Different Shapes. *Chem. Soc. Rev.* **2006,** 35, (3), 209-217.

3. Eustis, S.; El-Sayed, M. A., The Aspect Ratio Dependence of the Enhanced Fluorescence Intensity of Gold Nanorods: Experimental and Simulation Study. *J. Phys. Chem. B* **2005,** 109, (34), 16350-16356.

4. Eustis, S.; El-Sayed, M. A., Determination of the Aspect Ratio Statistical Distribution of Gold Nanorods in Solution from a Theoretical Fit of the Observed Inhomogeneously Broadened Longitudinal Plasmon Resonance Absorption Spectrum. *J. Appl. Phys* **2006,** Submitted.

5. Kamat, P. V., Photophysical, photochemical and photocatalytic aspects of metal nanoparticles. *J. Phys. Chem. B* **2002,** 106, (32), 7729-7744.

6. Eustis, S.; Krylova, G.; Eremenko, A.; Smirnova, N.; Schill, A. W.; El-Sayed, M. A., Growth and fragmentation of silver nanoparticles in their synthesis with a fs laser and CW light by photo-sensitization with benzophenone. *Photochem. Photobio. Sci.* **2005,** 4, (1), 154-159.

7. Mafune, F.; Kohno, J. Y.; Takeda, Y.; Kondow, T., Growth of gold clusters into nanoparticles in a solution following laser-induced fragmentation. *J. Phys. Chem. B* **2002,** 106, (34), 8555-8561.

8. Mafune, F.; Kohno, J.; Takeda, Y.; Kondow, T.; Sawabe, H., Formation and size control of sliver nanoparticles by laser ablation in aqueous solution. *J. Phys. Chem. B* **2000,** 104, (39), 9111-9117.

9. Mafune, F.; Kondow, T., Formation of small gold clusters in solution by laser excitation of interband transition. *Chem. Phys. Lett.* **2003,** 372, 199-204.

10. Fujiwara, H.; Yanagida, S.; Kamat, P. V., Visible Laser Induced Fustion and Fragmentation of Thionicotinamide-Capped Gold Nanoparticles. *J. Phys. Chem. B* **1999,** 103, (14), 2589-2591.

11. Kamat, P. V.; Flumiani, M.; Hartland, G. V., Picosecond dynamics of silver nanoclusters. Photoejection of electrons and fragmentation. *J. Phys. Chem. B* **1998,** 102, (17), 3123-3128.

12. Kurita, H.; Takami, A.; Koda, S., Size reduction of gold particles in aqueous solution by pulsed laser irradiation. *Appl. Phys. Lett.* **1998,** 72, (7), 789-791.

13. Takami, A.; Kurita, H.; Koda, S., Laser-induced size reduction of noble metal particles. *J. Phys. Chem. B* **1999,** 103, (8), 1226-1232.

14. Mohamed, M. B.; Ismail, K. Z.; Link, S.; El-Sayed, M. A., Thermal reshaping of gold nanorods in micelles. *J. Phys. Chem. B* **1998,** 102, (47), 9370-9374.

15. Link, S.; Wang, Z. L.; El-Sayed, M. A., How does a gold nanorod melt? *J. Phys. Chem. B* **2000,** 104, (33), 7867-7870.

16. Link, S.; Burda, C.; Mohamed, M. B.; Nikoobakht, B.; El-Sayed, M. A., Laser photothermal melting and fragmentation of gold nanorods: Energy and laser pulse-width dependence. *J. Phys. Chem. A* **1999,** 103, (9), 1165-1170.

17. Link, S.; Burda, C.; Nikoobakht, B.; El-Sayed, M. A., Laser-induced shape changes of colloidal gold nanorods using femtosecond and nanosecond laser pulses. *J. Phys. Chem. B* **2000,** 104, (26), 6152-6163.

18. Link, S.; Burda, C.; Nikoobakht, B.; El-Sayed, M. A., How long does it take to melt a gold nanorod? A femtosecond pump-probe absorption spectroscopic study. *Chem. Phys. Lett.* **1999,** 315, (1-2), 12-18.

19. Link, S.; El-Sayed, M. A., Spectroscopic determination of the melting energy of a gold nanorod. *J. Chem. Phys.* **2001,** 114, (5), 2362-2368.

20. Mohamed, M. B.; Wang, Z. L.; El-Sayed, M. A., Temperature-Dependent Size-Controlled Nucleation and Growth of Gold Nanoclusters. *J. Phys. Chem. A* **1999,** 103, (49), 10255-10259.

21. Chang, S. S.; Shih, C. W.; Chen, C. D.; Lai, W. C.; Wang, C. R. C., The Shape Transition of Gold Nanorods. *Langmuir* **1999,** 15, (3), 701-109.

22. Richardson, H. H.; Hickman, Z. N.; Govorov, A. O.; Thomas, A. C.; Zhang, W.; Kordesch, M. E., Thermooptical Properties of Gold Nanoparticles Embedded in Ice: Characterization of Heat Generation and Melting. *Nano Lett.* **2006,** 6, (4), 783-788.

23. Chou, C. H.; Chen, C. D.; Wang, C. R. C., Highly Efficient, Wavelength-Tunable, Gold Nanoparticle Based Optothermal Nanoconvertors. *J. Phys. Chem. B* **2005,** 109, (22), 11135-11138.

24. Yu, Y. Y.; Chang, S. S.; Lee, C. L.; Wang, C. R. C., Gold Nanorods: Electrochemical Synthesis and Optical Properties. *J. Phys. Chem. B* **1997,** 101, (34), 6661-6664.

25. Rayleigh, On the Instability of Jets. *Proc. London Math. Soc.* **1878,** 10, 4-13.

26. Bréchignac, C.; Cahuzac, P.; Carlier, F.; Colliex, C.; Leroux, J.; Masson, A.; Yoon, B.; Landman, U., Instability Driven Fragmentation of Nanoscale Fractal Islands. *Phys. Rev. Lett.* **2002,** 88, (19), 196103-1-196103-4.

27. ImageJ is a public domain Java image processing program inspired by NIH Image. The source code is freely available. Watershead plugin and other plugins also available. http://rsb.info.nih.gov/ij/ Date Accessed (5/23/06).

28. Oxtoby, D. W.; Freeman, W. A.; Block, T. F., *Chemistry Science of Change*. 3rd ed.; Saunder College Publishing: Fort Worth, 1998.

29. Link, S.; El-Sayed, M. A., Optical Properties and Ultrafast Dynamics of Metallic Nanocrystals. *Annu. Rev. Phys. Chem.* **2003,** 54, 331-366.

30. Kreibig, U.; Vollmer, M., *Optical Properties of Metal Clusters*. Springer: Berlin, 1995; Vol. 25, p 532.

31. van de Hulst, H. C., *Light Scattering by Small Particles* Dover Publications 1981; p 470.

32. Mie, G., Beitrage zur Optik truber Medien, speziell kolloidaler Metallosungen. *Ann. Phys.* **1908,** 25, 377-445.

33. Murphy, C. J.; Sau, T. K.; Gole, A. M.; Orendorff, C. J. G., J.; Gou, L.; Hunyadi, S. E.; Li, T., Anisotropic Metal Nanoparticles: Synthesis, Assembly, and Optical Applications *J. Phys. Chem. B* **2005,** 109, (29), 13857-13870.

34. Liu, M. Z.; Guyot-Sionnest, P., Mechanism of Silver(I)-Assisted Growth of Gold Nanorods and Bipyramids. *J. Phys. Chem. B* **2005,** 109, (47), 22192-22200.

35. Gole, A.; Murphy, C. J., Seed-Mediated Synthesis of Gold Nanorods: Role of the Size and Nature of the Seed. *Chem. Mater.* **2004,** 16, (19), 3633-3640.

36. Sau, T. K.; Murphy, C. J., Seeded High Yield Synthesis of Short Au Nanorods in Aqueous Solution. *Langmuir* **2004,** 20, (15), 6414-6420.

37. Nikoobakht, B.; El-Sayed, M. A., Evidence for bilayer assembly of cationic surfactants on the surface of gold nanorods. *Langmuir* **2001,** 17, (20), 6368-6374.

38. Torigoe, K.; Esumi, K., Preparation of colloidal gold by photoreduction of tetracyanoaurate(1-)-cationic surfactant complexes *Langmuir* **1992,** 8, (1), 59-63.

39. Esumi, K.; Hara, J.; Aihara, N.; Usui, K.; Torigoe, K., Preparation of Anisotropic Gold Particles Using a Gemini Surfactant Template. *J. Colloid Interface Sci.* **1998,** 208, 578-581.

40. Liao, H.; Hafner, J. H., Monitoring Gold Nanorod Synthesis on Surfaces. *J. Phys. Chem. B* **2004,** 108, (50), 19276-19280.

41. Filankembo, A.; Giorgio, S.; Lisiecki, I.; Pileni, M. P., Is the Anion the Major Parameter in the Shape Control of Nanocrystals? . *J. Phys. Chem. B* **2003,** 107, (30), 7492-7500.

42. Orendorff, C. J.; Murphy, C., J., Quantitation of Metal Content in the Silver-Assisted Growth of Gold Nanorods. *J. Phys. Chem. B* **2006,** 110, (9), 3990-3994.

43. Kim, F.; Song, J. H.; Yang, P., Photochemical Synthesis of Gold Nanorods *J. Am. Chem. Soc.* **2002,** 124, (48), 14316-14317.

44. Miranda, O. R.; Ahmadi, T. S., Effects of Intensity and Energy of CW UV Light on the Growth of Gold Nanorods. *J. Phys. Chem. B* **2005,** 109, (33), 15724-15734.

45. Filankembo, A.; Pileni, M. P., Is the Template of Self-Colloidal Assemblies the Only Factor That Controls Nanocrystal Shapes? *J. Phys. Chem. B* **2000,** 104, (25), 5865-5868.

46. Chen, H. M.; Peng, H. C.; Liu, R. S.; Asakura, K.; Lee, C. L.; Lee, J. F.; Hu, S. F., Controlling the Length and Shape of Gold Nanorods. *J. Phys. Chem. B* **2005,** 109, (42), 19553-19555.

47. Pérez-Juste, J.; Liz-Marzán, L. M.; Carnie, S.; Chan, D. Y. C.; Mulvaney, P., Electric-Field-Directed Growth of Gold Nanorods in Aqueous Surfactant Solutions. *Adv. Funct. Mater.* **2004,** 14, (6), 571-579.

48. Wei, Z.; Mieszawska, A. J.; Zamborini, F. P., Synthesis and Manipulation of High Aspect Ratio Gold Nanorods Grown Directly on Surfaces. *Langmuir* **2004,** 20, (11), 4322-4326.

49. Wei, Z.; Zamborini, F. P., Directly Monitoring the Growth of Gold Nanoparticle Seeds into Gold Nanorods. *Langmuir* **2004,** 20, (26), 11301-11304.

PART II: PHOTOCHEMICAL SYNTHESIS WITH BENZOPHENONE AS A PHOTOREDUCER

CHAPTER 6
GROWTH AND FRAGMENTATION OF SILVER NANOPARTICLES IN THEIR SYNTHESIS WITH FEMTOSECOND LASER AND CW LIGHT BY PHOTO-SENSITIZATION WITH BENZOPHENONE[*]

Abstract

The photo-sensitization synthetic technique of making silver nanoparticles using benzophenone is studied using either a laser or a mercury lamp as a light source. The power and irradiation time dependence of the synthesized nanoparticle absorption spectra and their size distribution (as determined by transmission electron microscopy (TEM)) are studied in each method and compared. In the laser synthesis, as either the laser power or the irradiation time increases, the intensity of the surface plasmon resonance absorption at 400nm is found to increase linearly first, followed by a reduction of the red edge of the plasmon resonance absorption band. TEM results showed that in the laser synthesis low powers and short irradiation times produce nanoparticles around 20nm in diameter. Increasing power or irradiation time produces a second population of nanoparticles with average size of 5nm in diameter. These small particles are believed to be formed from the surface ablation of the large particles. The surface plasmon absorption band is found to be narrower (due to a more monodisperse nanoparticle sample) when the nanoparticles are produced with laser irradiation.

Throughout exposure time with the CW lamp, the plasmon resonance absorption band of the particles formed is observed to first grow in intensity, then blue shifts and narrows, and finally red shifts while decreasing in intensity. The TEM results for lamp

[*] Eustis, S.; Krylova, G.; Eremenko, A.; Smirnova, N.; Schill, A. W.; El-Sayed, M. A., Growth and fragmentation of silver nanoparticles in their synthesis with a fs laser and CW light by photo-sensitization with benzophenone. *Photochem. Photobio. Sci.* **2005,** 4, (1), 154-159.

samples showed particle formation and growth, followed by small nanoparticle formation.

The above results are discussed in terms of a mechanism in which, the excited benzophenone forms the ketal radical, which reduces Ag^+ in solution and on the Ag nanoparticle surface. As the time of irradiation or the light energy increases the benzophenone is consumed, which is found to be the limiting reagent in the formation of the silver nanoparticles. This stops the formation of the normal large nanoparticles while their photo-ablation continues, which results in the appearance of the small particles.

Introduction

With the rising importance of nanoparticles, different synthetic methods are being explored to create nanoparticles in solution,[1-4] polymer films,[5-10] and glasses.[11-13] Noble metal nanoparticles have attracted a lot of attention due the plasmon resonance in the visible region which cause these samples to display brilliant colors.[14-20] This plasmon resonance is due to the collective oscillation of electrons in the conduction band,[14-18] which is sensitive to size and shape and the surrounding medium.[19, 20] The plasmon resonance allows size and shape transitions to be monitored simply by following UV/visible absorbance. Silver nanospheres are well known to have a plasmon resonance at 400nm, with the wavelength depending on the size and shape of the nanoparticles. Using photo generation of nanoparticles allows nanoparticles to be studied in various stages of formation by defining the start of particle formation, as the time in which the reaction mixture is first exposed to light. A number of synthetic methods of these nanoparticles have been developed,[1-7, 11-13, 21-25] but little is understood about the mechanism of the growth process.

Recently, photochemical methods have been used to modify and generate metal nanoparticles. Jin et al. [26, 27] have used light to transform silver spheres into prisms by controlling the exposure time and the irradiation wavelength. Lasers have been used to directly excite the ions to form metal nanoparticles in solution through excitation of the interband transition,[28] or excitation of a polymer.[7, 29-31] These methods create on-demand generation of metal nanoparticles, or photoresponsive solutions.

Benzophenone is a well-known photosensitizer that can be excited by UV radiation. It then relaxes to its lowest triplet excited state which can abstract a hydrogen atom from solution to form radicals capable of performing photochemistry.[32-36] The energy level diagram for the excited states of benzophenone from previous studies[32-36] is shown in Figure 6-1. The singlet, triplet states of the benzophenone as well as the states of neutral ketyl radical where BP has abstracted a hydrogen atom to form a ketyl radical, and the anion radical where BP has a negative charge.[32-36]

Benzophenone has been employed as a photosensitizer to form nanoparticles for a variety of metals.[6, 21-25] Kapoor and Mukherjee have formed copper nanoparticles with a narrow size distribution using benzophenone and PVP in solution.[21] The most detailed study presented to date of preparing metal nanoparticles using benzophenone as a photo-sensitizer was preformed by Kometani et al.[22] where laser nanosecond flash photolysis was used to determine the radicals of benzophenone during the formation of silver nanoparticles. Gold nanoparticles have been created using two laser irradiation inside PVA films using BP as the reducing agent.[10] However, no studies have been carried out in which the growth of the nanoparticles is followed by transmission electron microscopy (TEM).

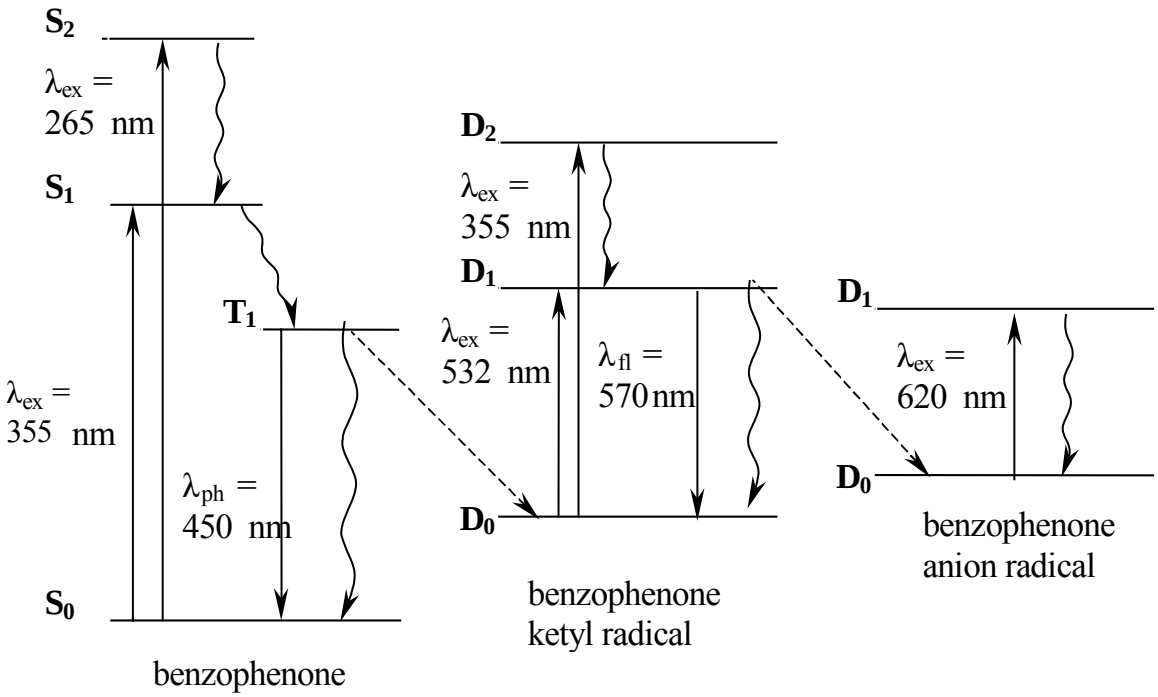

Figure 6-1: *Energy diagram of the energy levels of benzophenone and its radicals with the optical transitions.*

Photochemical methods are attractive for formation of nanoparticles, as reaction conditions can be controlled by light intensity and exposure time. Solutions can be stored until nanoparticles are desired, and light sources are easily attainable. Thus nanoparticles can be generated in an on-demand procedure to ensure fresh samples, or desired placement of samples similar to that described previously.[37] Photochemical methods enable following the reaction mechanism, as intermediates often have absorption spectra in the visible spectra, enabling in-situ monitoring of the reaction.[38]

Femtosecond lasers have enabled the study of ultrafast processes, and allowed distinction between irradiation and subsequent relaxation processes. Previous research showed the difference between melting gold nanorods using a femtosecond and a nanosecond laser.[39, 40] Femtosecond laser studies enabled following the different processes involved in the relaxation of the hot electrons by the lattice (using electron-

phonon processes) and then into the environment (by phonon-phonon process).[41-43] As the nanoparticle is heated rapidly, it can either change its shape by melting or by ablation resulting in the reduction of size due to the continued influx of energy while the particle contains hot electrons. If heating is faster than lattice cooling, mainly melting is observed.[39, 40] As the laser power increases, ablation of metal nanoparticles has been reported.[40, 44-48] The energy density is so high that the atoms dissociate from the nanoparticle and generate small particles in solution that can be capped by the excess stabilizer present in the solution.

The present study examines the optical absorption and TEM of particles formed by irradiation using either the 266nm femtosecond laser or mercury lamp irradiation with a filter to allow 254nm light. After irradiation of aqueous solutions containing Ag^+ and benzophenone as a photo-sensitizer, silver nanoparticles are formed. Initially, linear growth of the optical absorbance of the surface plasmon band was observed. This is followed by sub-linear growth of the surface plasmon absorption as a function of time. TEM analysis revealed that the nanoparticle growth is determined by the irradiation conditions and the stabilizer, followed by ablation or aggregation at longer times of irradiation or higher laser powers for laser growth and with longer times of irradiation for the UV lamp irradiation. Nanoparticle formation and ablation compete to form nanoparticles in solution, thus generating different kinetics as time progresses due to the increase in importance of the ablation process. Aggregation is also found to compete with particle formation after benzophenone has been exhausted.

Experimental

The solution used for irradiation contained benzophenone, stabilizer and metal salt. The femtosecond laser irradiation experiments used solution A1 with $3.3x10^{-5}$M benzophenone (BP) (stock solution of benzophenone is dissolved in isopropyl alcohol), 0.3M isopropyl alcohol (IPA) (total in solution), and $6.0x10^{-4}$M hexadecyltrimethylammonium bromide (CTAB) acting as the stabilizer in water. The solution for mercury lamp irradiation experiments used solution A2 with $3.0x10^{-3}$M benzophenone, 0.3M isopropyl alcohol, and 1mL per 100mL solution of Ludox (Aldrich AS-30) dissolved in water. Both systems used the same solution B containing 0.0043M $AgNO_3$ in water. The final solution contained 2.1mL of A and 0.9mL of B. The sample was placed in a quartz 2mm cylindrical cuvette, and the sample was spun during irradiation. At higher laser powers a ring of silver metal was observed on the inside surface of the cuvette after irradiation, which could be removed with aqua regia. A mercury lamp was used for irradiation in the lamp studies (preformed in Kyiv, Ukraine). Absorption spectra were measured on a Shimadzu UV-3103-PC spectrophotometer. For the TEM measurements, a drop of solution was allowed to dry overnight on a carbon coated copper TEM grid (Ted Pella). The samples were imaged at 100kV in the JOEL JEM-100C transmission electron microscope (TEM) to determine the size distributions. Image J (NIH)[49] was used to determine the size of each nanoparticle. This program enables thresholding images and size determination from images, with many plugins available for image analysis. The watershed plug-in was used occasionally to separate closely spaced nanoparticles prior to analysis. Histograms of the average diameter (major axis and minor axis averaged) were obtained and fit to Gaussian distributions by

Origin 7 SR2 (OriginLab Co.) for three separate spots on each TEM grid and then the fits were averaged for samples from the femtosecond laser. At least 150 particles were counted for each sample, with a thousand particles counted in some cases.

In the limiting reagent experiments, solutions are initially made up the same as above. After 60 minutes of irradiation, a small amount of the solution was removed from the quartz cuvette, the amount given below was added, and then the cuvette was refilled with the removed solution (to around 600μL.) The same cuvette was used for all experiments to ensure constant volume. The solutions added after 60 minutes of irradiation are: 100μL of 0.0043M $AgNO_3$, 36μL of IPA and 36μL of 0.093M BP in IPA. The vials were then shaken, and the spectra were recorded to observe changes due solely to addition of new solutions. Irradiation was then continued with the femtosecond laser system as described above.

Results and Discussion

A. Laser Irradiation

Initially, upon irradiation with UV laser light the solution with benzophenone and silver salt develops a faint yellow color, indicating the appearance of silver nanoparticles. As irradiation continues, the solution continues to darken in color indicating the formation of more nanoparticles as the irradiation is continued. Figure 6-2 shows the absorbance of the silver/BP solution after various irradiation times with a UV femtosecond laser. This shows an increase in intensity of the plasmon resonance for silver spheres at 400nm[19, 20] with increasing laser irradiation. The plasmon resonance absorption red shifts with increasing size and dielectric constant around the particles.

The inset in Figure 6-2 shows the spectra normalized to the maximum absorbance to amplify the changes in the shape of the plasmon resonance absorption band. The shape of the plasmon resonance shifts as irradiation time increases, with the relative contribution from the red edge of the plasmon resonance decreasing. The growth of the optical absorbance from the nanoparticles initially displays linearity as shown in Figure 1b just as described by Kometani et. al.[22] However, after the first hour of irradiation, the absorbance intensity levels off and seems to decrease at longer time while the spectral shape remains constant (as observed in the inset of Figure 6-2) indicating a decrease in the growth rate.

This decrease in the growth rate was explored to determine the limiting reagent of the nanoparticles formation reaction. This limiting reagent is either benzophenone, the silver salt, the alcohol or the capping material. The sample was irradiated for 60 minutes and then a small volume of a solution was added and the absorption was measured for another hour to determine the kinetics of growth as shown in Figure 6-2c. Addition of silver salt to the solution displayed a growth rate as observed in Figure 6-2b with no additional silver salt, implying that silver ions are not the limiting reagent. Addition of IPA did not change the kinetics, thus this small amount of alcohol did not affect the growth of the nanoparticles. Adding larger volumes of IPA to the solution induced aggregation by destabilizing the nanoparticles due to the presence of a shifting phase equilibria in this water/alcohol system.

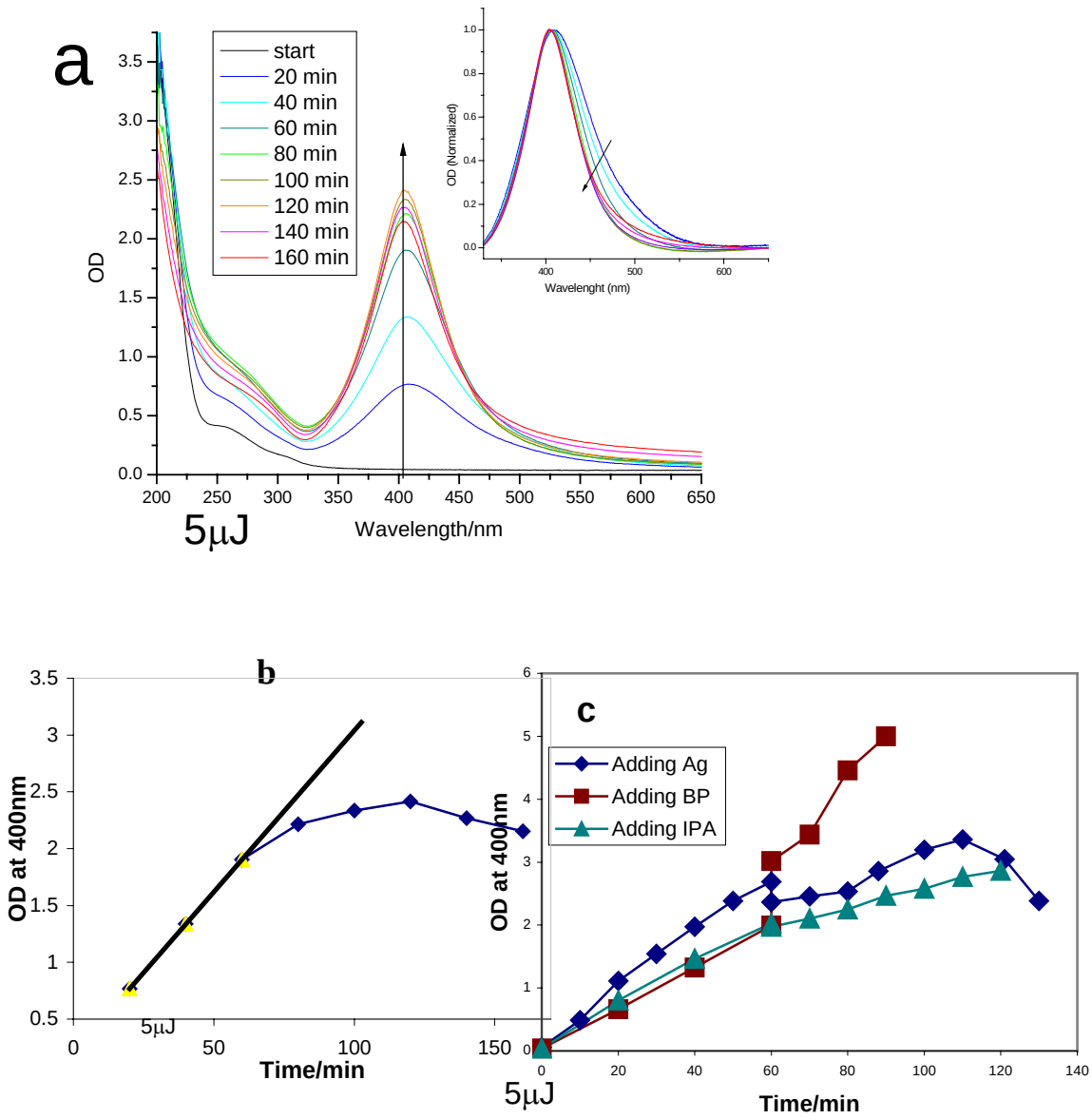

Figure 6-2: *(a) Optical absorbance of silver/benzophenone solution irradiated with 5μJ, 265nm 100 femtosecond laser irradiation for various times as indicated. Inset: Absorbance normalized at the peak intensity to observe changes in shape of optical absorbance as a function of irradiation time. (b) Absorbance of sample at 400nm plotted as a function of the time of irradiation. (c) Absorbance of samples irradiated with 5μJ, 265nm femtosecond laser irradiation at 400nm for 60minutes, followed by addition of $AgNO_3$, IPA or BP (dissolved in IPA) and continued irradiation.*

Adding excess CTAB was able to reduce the effect of additional alcohol by increasing the stabilizing ability of the solution. Increasing the amount of benzophenone in the solution after 60 minutes of irradiation increased the rate of formation of the nanoparticles. These results suggest that benzophenone is the limiting reagent in this synthesis.

We studied the effect of increasing laser power on the absorption spectrum and the size distribution of the silver nanoparticles. Figure 6-3 shows the optical absorbance spectra of the nanoparticles formed at three different powers irradiated for an hour with normalized spectra shown in the inset to observe the changes in shape of the optical spectra. The surface plasmon resonance absorption band narrows and the contribution from the red edge are reduced as the power is increased. This shows that long irradiation times and high laser powers have similar effect on the sample. Higher power produces particles with optical absorbance bands much narrower than those observed from the lamp samples. For the same irradiation time, higher powers generate more nanoparticles as observed by their higher optical absorbance. The higher powers also generate more absorption at 400nm due to selective formation of the smaller nanoparticles as observed in the normalized spectra. TEM is used to follow the formation of nanoparticles at these laser powers.

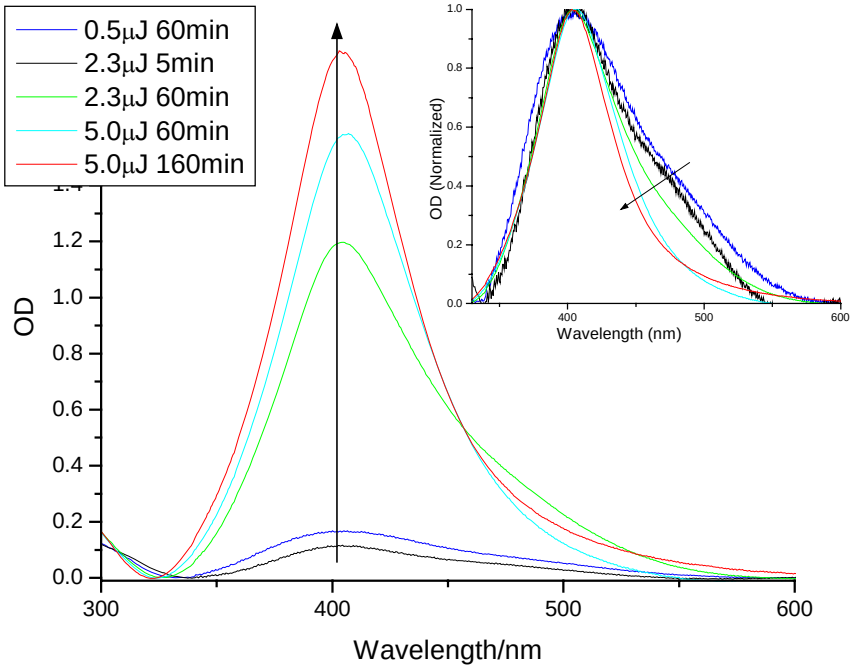

Figure 6-3: *Optical absorbance of silver/benzophenone solutions irradiated with different powers in the femtosecond laser. Inset: Same spectra normalized to observe changes in shape.*

The size of the nanoparticles is a function of laser energy and irradiation time. TEM was used determine the shape of the observed absorption intensity changes with increasing laser power. The size distributions can be seen in Figure 6-4 with the frequency of each size plotted against the average diameter for different irradiation powers. The statistics for each sample with the center, width, and percentage of the width and percentage of large and small spheres are presented in Table 6-1. As the laser energy increases the population of the small spheres increases and ultimately dominates the population. Thus, the shift in the optical absorption band can be understood by the change in the importance of the mechanism for formation of large nanoparticles versus their ablation at high powers of irradiation. The absorption of silver nanoparticles shifts

to the red and increases in width as the size increases due to the free path effect where the electrons collide with the surface of the nanoparticle.[19] Thus, the narrowing of the absorption spectrum as well as the blue shift as the laser power increases suggest that the average size of the silver nanoparticles is smaller. At longer times of irradiation, the amount of benzophenone decreases leading to a decrease in the rate of growth of the large nanoparticles. Meanwhile, as more and more large nanoparticles are formed with time, the rate of their interaction with the laser increases, therefore, the rate of their ablation increases. Thus with increasing irradiation time, the larger nanoparticles decrease in population while that of the small ones increase, as observed.

Table 6-1: *Laser irradiation: energy (0.5, 2.3, and 5μJ) and irradiation time (5, 60 and 160 min) dependence of the average and standard deviation from 3 TEM spots fitted with position of the two centers (xc1, xc2), the widths (w1, w2), and the percent widths (% width1, % width2), of the small (subscript 1) and large nanoparticle (subscript 2) distributions obtained from Gaussian fits to size distribution data for samples from Figure 6-3.*

	0.5μJ	60min	2.3μJ	5min	2.3μJ	60min	5μJ	60min	5μJ	160min
	Avg	Std Dev	Avg	Std Dev	Avg	Std Dev	Avg	Std Dev	Avg	Std Dev
xc1			4.3	0.2	4.2	0.6	4.0	0.5	4.2	0.7
w1			1.4	0.3	2.1	0.4	2.0	1.1	2.2	1.2
% width1			32.9	5.1	49.8	5.3	52.7	32.6	58.8	41.5
xc2	21.1	2.2	19.1	2.3	17.9	2.2	13.2	2.8	29.7	20.2
w2	12.6	4.2	12.0	7.9	15.2	6.0	13.4	4.8	12.0	9.1
% width2	58.9	13.7	60.5	32.9	88.1	46.4	99.6	13.4	73.8	67.1
% small	0.0		25.2		69.6		75.4		80.8	
% large	100.0		74.8	30.0	30.4	11.3	24.6	10.4	19.2	31.3

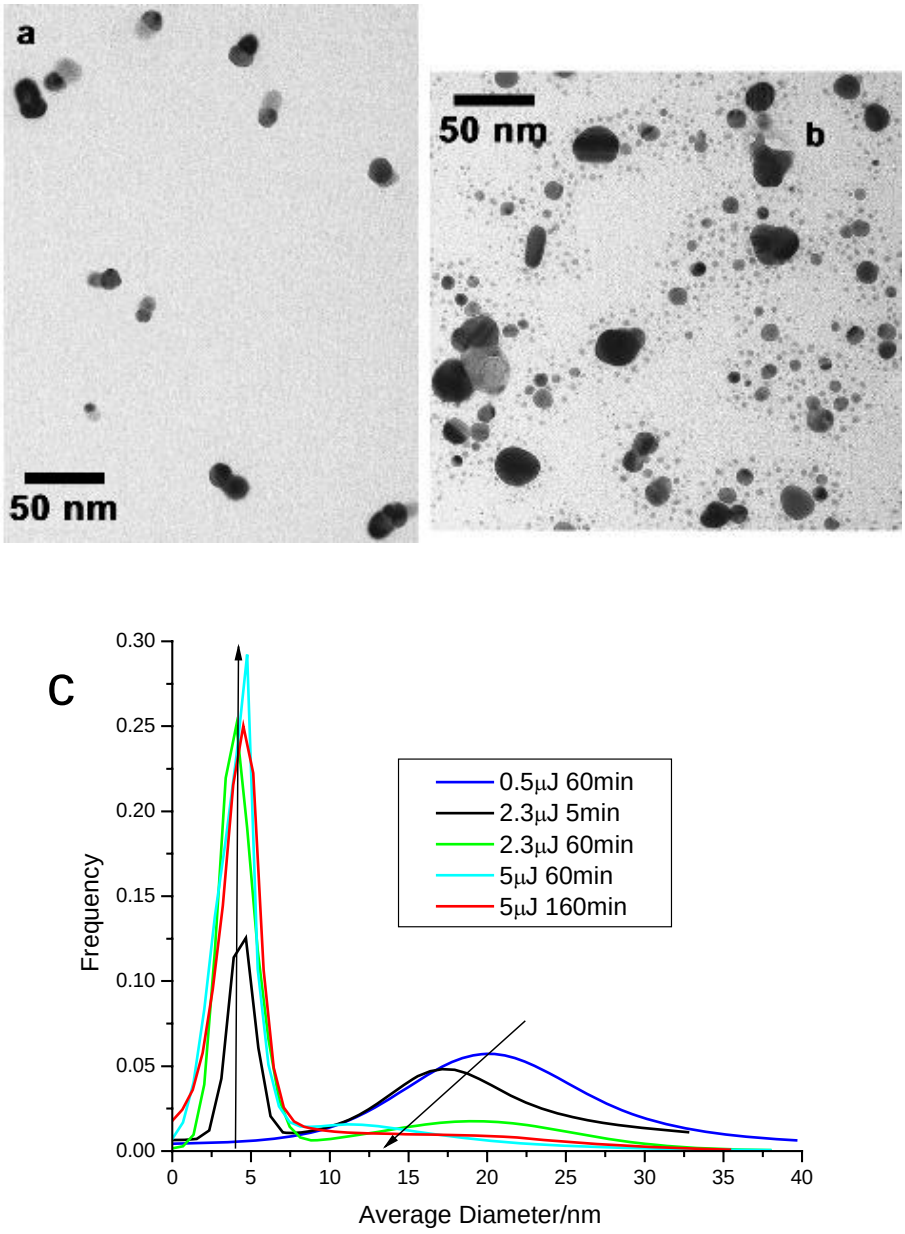

Figure 6-4: *(a) TEM image of 0.5μJ, 60 min femtosecond laser irradiation. (b) TEM image of 5.0μJ, 60 min femtosecond laser irradiation. (c)Gaussian fits to size distribution data for samples from Figure 6-3, femtosecond laser, CTAB stabilizer, at various powers.*

The size of the nanoparticles remains relatively constant for the smaller nanoparticles at ~5nm in diameter. The dominating process at the time of formation determines the sizes generated. The larger nanoparticles are formed first by growth mechanisms, with the size determined by the local concentrations of benzophenone, Ag^+, and the stabilizer. The percentage of large spheres in the sample decreases with increasing laser energy, supporting the mechanism of their ablation or dissociation to form the smaller nanoparticles, as more energy is given to the system. The smaller nanoparticles are proposed to be generated by photo-ablation events of atomic or small clusters from the large particles followed by condensation to form small nanoparticles. Higher powers increase the rate of the ablation events, thus generating more small nanoparticles. At long irradiation time, the loss of the capping material around the nanoparticles (due to the ablation processes, photodecomposition, and increasing surface area) could lead to aggregation and precipitation as reflected by the decline in the optical absorbance observed in Figure 6-2b.

B. C.W. Lamp Irradiation:

In the mercury lamp experiments, different results were obtained from those obtained with the femtosecond laser irradiation as seen in Figure 6-5. The absorption band of the lamp samples is broader than that observed in the laser synthetic method and has a long tail to the red of the plasmon resonance band maximum. The broad distribution is not due to the presence of Ludox in the lamp synthetic method. A control experiment was performed on samples with Ludox using femtosecond laser irradiation. The absorption spectrum in this control sample was narrower than that of the lamp irradiated samples and the sample from the femtosecond laser experiments discussed

previously. In the time dependence experiments, the optical absorbance first grows in intensity and blue shifts, followed by a red shift with decreasing absorbance intensity at longer times. This data suggests separate competing processes are involved. First nanoparticles might grow by Oswald ripening processes, followed by aggregation and precipitation. Lamp irradiation is useful as the source is easily attainable generating nanoparticles with a changing optical absorbance spectrum that is observed with continuous irradiation. After 2 hours of exposure, a new population appears which absorbs at longer wavelengths, characteristic of aggregated nanoparticles. The decrease in the absorption with long irradiation times suggests precipitation of the aggregate. This leaves behind a population of newly formed small nanoparticles.

The TEM results of the produced particles in the mercury lamp irradiation are presented in Figure 6-5c and Table 6-2. The size distribution is broad at short irradiation times, but becomes smaller after 45 minutes of irradiation with an average diameter of 10nm nanoparticles generated. After two hours of irradiation the relative population of the small nanoparticles increases, with a broad distribution of nanoparticles of larger diameter formed due to aggregation. A decrease in the total absorption is also observed after 2 hours suggesting some nanoparticles have already precipitated. Thus, complex kinetics of formation generate different nanoparticle sizes initially. First growth by Oswald ripening, then aggregation and finally precipitation lead first to a broad distribution, and then precipitation of the larger particles leaving the small particles in solution. Lamp irradiation generates nanoparticles using benzophenone sensitization and Ludox as a stabilizer. The polydispersity observed is large in all samples generated with lamp irradiation.

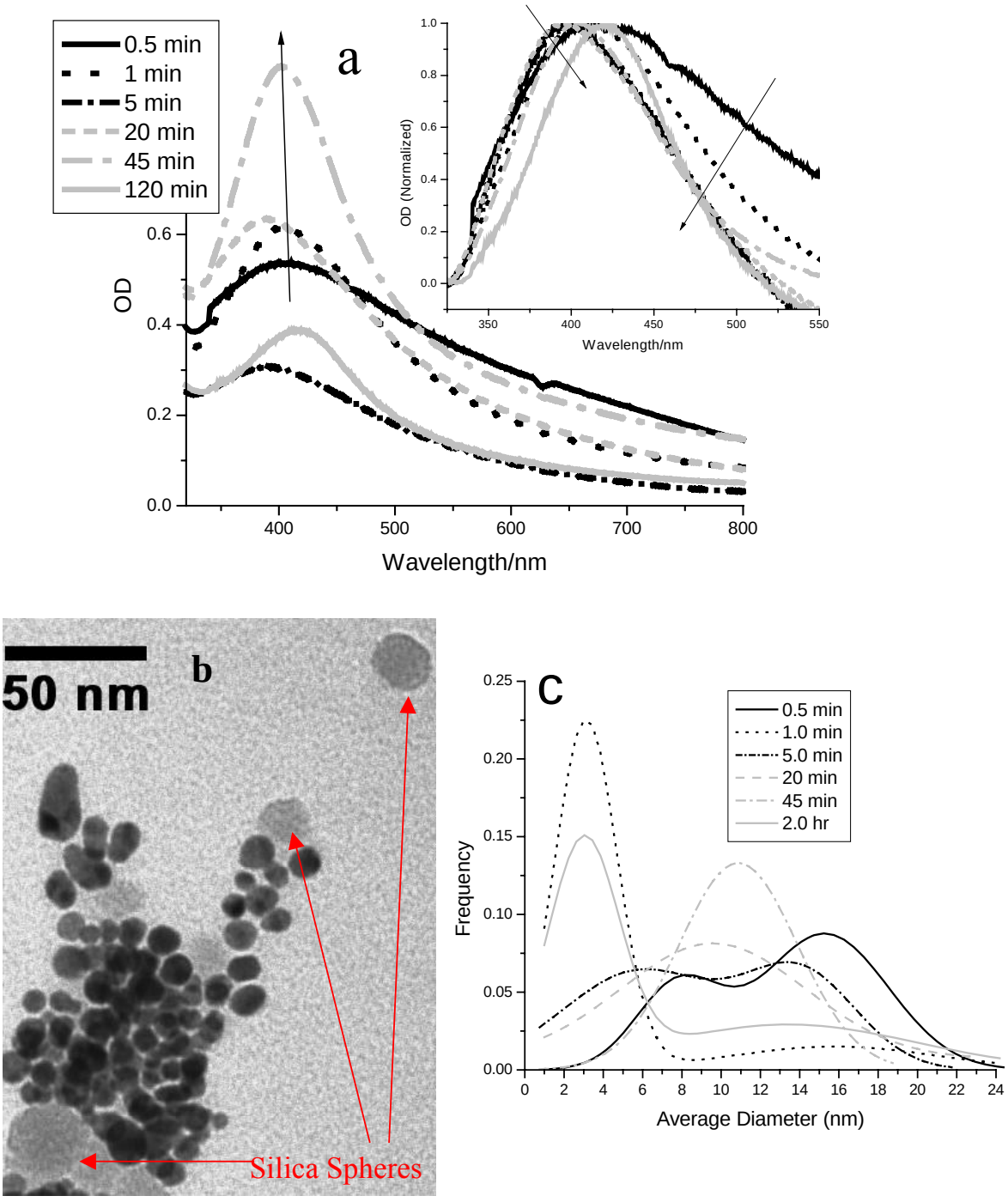

***Figure 6-5**: (a) Optical absorbance of silver/benzophenone solution with mercury lamp irradiation at times indicated. Inset: Absorbance normalized at the peak intensity to observe changes in shape of optical absorbance as a function of irradiation time. (b) TEM image of silver/benzophenone solution after mercury lamp irradiation, 45min. (c) Gaussian fits to size distribution data for the same samples, mercury lamp, Ludox stabilizer, at times indicated.*

Table 6-2: *Mercury lamp irradiation: irradiation time dependence of the position of the two centers (xc1, xc2), the widths (w1, w2), and the percent widths (% width), of the small (subscript 1) and large nanoparticle (subscript 2) distributions obtained from Gaussian fits to size distribution data for samples from Figure 6-5.*

	Small			Large				
Time(min)	Xc1	W1	% width	Xc2	W2	% width	% small	% large
0.5	7.8	4.3	54.9	15.3	6.5	42.2	29.1	70.9
1	3.1	3.2	101.2	15.8	10.4	66.1	82.0	18.0
5	5.8	7.8	134.2	14.1	5.7	40.7	58.9	41.1
20				9.6	9.4	98.1	0.0	100.0
45				10.9	6.0	55.4	0.0	100.0
120	3.0	3.6	118.4	13.4	13.0	97.1	57.2	42.8

C. Proposed Growth Mechanism

The above results can be discussed by use of the following mechanism for particle growth. The benzophenone ketyl radical (BPK), is formed from the abstraction reaction of benzophenone in its triplet state of a hydrogen atom from the solvent, isopropyl alcohol (ROH). This also generates the alcohol radical. The silver atoms are then reduced by the benzophenone ketyl radical to form an atomic nuclus,[22] which can then grow by reducing more silver ions on the surface to form a small particle. More reduction can occur or more atomic silver can condense on the nuclei surface to form $(Ag)_L$. These large silver nanoparticles could also be aggregates of smaller nanoparticles. Capping is also occurring and limits the size of the $(Ag)_L$. At the same time the absorption of photons by the strong absorbing $(Ag)_L$ is continuously occurring, which could leading to the ablation of surface silver atoms. This leaves behind the $(Ag)_S$, small silver nanoparticles, which are observed in the TEM results. The chemical reactions describing this mechanism can be written as:

$$BP + h\upsilon \longrightarrow {}^3BP \quad (6.1)$$

$$^3BP + ROH \longrightarrow BPK^{\bullet} + RO^{\bullet} \quad (6.2)$$

$$Ag^+ + BPK \longrightarrow Ag_0 + BP + H^+, \quad n\,Ag_0 \longrightarrow (Ag_0)_n \quad (6.3)$$

$$(Ag)_nBPK + nAg^+ \longrightarrow (Ag)_L + BP + H^+ \quad \text{(Growth)} \quad (6.4)$$

$$(Ag)_n + (Ag)_m \longrightarrow (Ag)_{n-1} + (Ag)_{m+1} \quad \text{(Oswald ripening)} \quad (6.5)$$

$$b(Ag)_n + c(Ag)_m \longrightarrow (Ag)_L \quad \text{(Aggregation)} \quad (6.6)$$

$$(Ag)_L + n\,h\upsilon \longrightarrow (Ag)_S + m\,Ag \quad \text{(Ablation or dissociation process)} \quad (6.7)$$

This mechanism is able to describe the formation of silver atoms, as well as the growth of the nanoparticles. At long irradiation times, the benzophenone, whose initial concentration is limited by its solubility in the solvent, is consumed. This stops the formation of the larger nanoparticles by the direct mechanism. However, Oswald ripening or aggregation of the small particles causes a shift of the absorption to longer wavelengths. After the benzophenone is consumed, the laser ablation continues to increase as the concentration of the large nanoparticles is at its maximum. Thus the net concentration of the large particles slows down while the ablation rate is at its maximum. This leads to an increase in the relative amounts of the small nanoparticles present in solution.

Summary

The TEM results presented here demonstrate the growth mechanism is followed by ablation for photosensitized metal nanoparticles using benzophenone. Changes are observed in the optical spectra which can be used to follow the generation of nanoparticles, but TEM is required to show the increasing importance of the ablation

mechanism in the laser synthesis as the energy or time of irradiation increases. Nanoparticle growth was observed with mercury lamp and femtosecond laser irradiation with Ludox and CTAB as stabilizers determining the size of nanoparticles generated, respectively. Increasing irradiation time in the lamp synthesis leads to a narrowing of the plasmon resonance band, which could be correlated to a narrowing of the particle distribution observed in TEM for both laser and lamp irradiation due to Oswald ripening mechanisms. Lamp and laser irradiation both generated aggregated nanoparticles after long irradiation times. Laser irradiation also ablated the samples at high laser powers. The systematic changing of the laser power and irradiation time showed that growth of large nanoparticles takes place before benzophenone was consumed, while ablation in the laser experiments takes place throughout the irradiation period. The ablation rate increases as the concentration of the large nanoparticles increases. At longer times or high power, the benzophenone concentration decreases causing a decrease in the rate of formation of the large particles while the rate of ablation is at its maximum.

Acknowledgments: The authors wish to acknowledge the financial support of the Nation Science Foundation, Division of Material Science Grant No. 0138391.

References

1. Yu, Y. Y.; Chang, S. S.; Lee, C. L.; Wang, C. R. C., Gold Nanorods: Electrochemical Synthesis and Optical Properties. *J. Phys. Chem. B* **1997,** 101, (34), 6661-6664.

2. Turkevich, J.; Stevenson, P. C.; Hillier, J., A study of the nucleation and growth processes in the synthesis of colloidal gold. *Discuss. Faraday Soc.* **1951,** 11, 55-75.

3. Petit, C.; Lixon, P.; Pileni, M. P., In Situ Synthesis of Silver Nanocluster in AOT Reverse Micelles. *J. Phys. Chem.* **1993,** 97, (49), 12974-12983.

4. Jana, N. R.; Gearheart, L.; Murphy, C. J., Seeding Growth for Size Control of 5-40nm Diameter Gold Nanoparticles. *Langmuir* **2001,** 17, (22), 6782-6786.

5. Monti, O. L. A.; Fourkas, J. T.; Nesbitt, D. J., Diffraction-limited photogeneration and characterization of silver nanoparticles. *J. Phys. Chem. B* **2004,** 108, (5), 1604-1612.

6. Korchev, A. S.; Bozack, M. J.; Slaten, B. L.; Mills, G., Polymer-initiated photogeneration of silver nanoparticles in SPEEK/PVA films: Direct metal photopatterning. *J. Am. Chem. Soc.* **2004,** 126, (1), 10-11.

7. Weaver, S.; Taylor, D.; Gale, W.; Mills, G., Photoinitiated Reversible Formation of Small Gold Crystallites in Polymer Gels. *Langmuir* **1996,** 12, (20), 4618-4620.

8. Hirose, T.; Omatsu, T.; Sugiyama, M.; Inasawa, S.; Koda, S., Au-nano-particles production by pico-second ultra-violet laser deposition in Au-ion doped PMMA film. *Chem. Phys. Lett.* **2004,** 390, (1-3), 166-169.

9. Kaneko, K.; Sun, H.-B.; Duan, X.-M.; Kawata, S., Two-photon photoreduction of metallic nanoparticle gratings in a polymer matrix. *Appl. Phys. Lett.* **2003,** 83, (7), 1426-1428.

10. Sakamoto, M.; Tachikawa, T.; Fujitsuka, M.; Majima, T., Two-color two-laser fabrication of gold nanoparticles in a PVA film. *Chem. Phys. Lett.* **2006,** 420, (1-3), 90-94.

11. Qiu, J.; Jiang, X.; Zhu, C.; Shirai, M.; Si, J.; Jiang, N.; Hirao, K., Manipulation of Gold Nanoparticles inside Transparent Materials. *Angew. Chem. Int. Ed.* **2004,** 43, 2230-2234.

12. Jiang, X.; Qiu, J.; Zeng, H.; Zhu, C.; Hirao, K., Laser-controlled dissolution of gold nanoparticles in glass. *Chem. Phys. Lett.* **2004,** 391, 91-94.

13. Qiu, J.; Shirai, M.; Nakaya, T.; Si, J.; Jiang, X.; Zhu, C.; Hirao, K., Space-selective precipitation of metal nanoparticles inside glasses. *Appl. Phys. Lett.* **2002,** 81, (16), 3040-3042.

14. Kreibig, U.; Vollmer, M., *Optical Properties of Metal Clusters*. Springer: Berlin, 1995; Vol. 25, p 532.

15. Mulvaney, P., Surface Plasmon Spectroscopy of Nanosized Metal Particles. *Langmuir* **1996,** 12, 788-800.

16. Henglein, A., Physicochemical properties of small metal particles in solution: "microelectrode" reactions, chemisorption, composite metal particles, and the atom-to-metal transition. *J. Phys. Chem.* **1993,** 97, (21), 5457-5471.

17. Henglein, A., Small-particle research: physicochemical properties of extremely small colloidal metal and semiconductor particles. *Chem. Rev.* **1989,** 89, (8), 1861-1873.

18. Bohren, C. F.; Huffman, D. R., *Absorption and Scattering of Light by Small Particles*. Wiley: New York, 1983.

19. Kreibig, U.; Fragstein, C. v., The Limitation of Electron Mean Free Path in Small Silver Particles. *Z. Physik* **1969,** 224, 307-323.

20. Kawabata, A.; Kubo, R., Electronic Properties of Fine Metallic Particles. II. Plasmon Resonance Absorption. *J. Phys. Soc. Japan* **1966,** 21, (9), 1765-1772.

21. Kapoor, S.; Mukherjee, T., Photochemical formation of copper nanoparticles in poly(N-vinylpyrrolidone). *Chem. Phys. Lett.* **2003,** 370, (1-2), 83-87.

22. Kometani, N.; Doi, H.; Asami, K.; Yonezawa, Y., Laser flash photolysis study of the photochemical formation of colloidal Ag nanoparticles in the presence of benzophenone. *Phys. Chem. Chem. Phys.* **2002,** 4, 5142-5147.

23. Kapoor, S., Preparation, characterization, and surface modification of silver particles. *Langmuir* **1998,** 14, (5), 1021-1025.

24. Sato, T.; Maeda, N.; Ohkoshi, H.; Yonezawa, Y., Photochemical Formation of Colloidal Silver in the Presence of Benzophenone. *Bull. Chem. Soc. Japan* **1994,** 67, (12), 3165-3171.

25. Sato, T.; Onaka, H.; Yonezawa, Y., Sensitized photoreduction of silver ions in the presence of acetophenone. *J. Photochem. Photobiol. A* **1999,** 127, (1-3), 83-87.

26. Jin, R. C.; Cao, Y. C.; Hao, E. C.; Metraux, G. S.; Schatz, G. C.; Mirkin, C. A., Controlling anisotropic nanoparticle growth through plasmon excitation. *Nature* **2003,** 425, (6957), 487-490.

27. Jin, R. C.; Cao, Y. W.; Mirkin, C. A.; Kelly, K. L.; Schatz, G. C.; Zheng, J. G., Photoinduced conversion of silver nanospheres to nanoprisms. *Science* **2001,** 294, (5548), 1901-1903.

28. Mafune, F.; Kondow, T., Formation of small gold clusters in solution by laser excitation of interband transition. *Chem. Phys. Lett.* **2003,** 372, 199-204.

29. Mandal, M.; Ghosh, S. K.; Kundu, S.; Esumi, K.; Pal, T., UV photoactivation for size and shape controlled synthesis and coalescence of gold nanoparticles in micelles. *Langmuir* **2002,** 18, (21), 7792-7797.

30. Zhou, Y.; Yu, S. H.; Wang, C. Y.; Li, X. G.; Zhu, Y. R.; Chen, Z. Y., A Novel Ultraviolet Irradiation Photoreduction Technique for the Preparation of Single-Crystal Ag Nanorods and Ag Dendrites. *Adv. Mater.* **1999,** 11, (10), 850-852.

31. Longenberger, L.; Mills, G., Formation of Metal Particles in Aqueous-Solutions by Reactions of Metal-Complexes with Polymers. *J. Phys. Chem.* **1995,** 99, (2), 475-478.

32. Marignier, J. L.; Hickel, B., Pulse Radiolysis Measurements of the Solvation Rate of Benzophenone Anion in Liquid Alcohol: Effect of Temperature. *J. Phys. Chem.* **1984,** 88, (22), 5375-5379.

33. Peters, K. S.; Lee, J., Picosecond Dynamics of the Photoreduction of Benzophenone by DABCO. *J. Phys. Chem.* **1993,** 97, (15), 3761-3764.

34. Miyasaka, H.; Nagata, T.; Kiri, M.; Mataga, N., Femtosecond-Picosecond Laser Photolysis Studies on Reduction Process of Excited Benzophenone with N-Methyldiphenylamine in Acetonitrile Solution. *J. Phys. Chem.* **1992,** 96, (20), 8060-8065.

35. Hoshino, M.; Aral, S.; Imamura, M.; Ikehara, K.; Hama, Y., Mechanism of Benzophenone Ketyl Radical Formation in Acid Alcohols Studied by Pluse-Radiolysis and Rigid-Matrix Techniques. *J. Phys. Chem.* **1980,** 84, (20), 2576-2579.

36. Mural, H.; Jinguji, M.; Obl, K., Activation Energy of Hydrogen Atom Abstraction by triplet Benzophenone at Low Temperature. *J. Phys. Chem.* **1978,** 82, (1), 38-40.

37. Stellacci, F.; Bauer, C. A.; Meyer-Friedrichsen, T.; Wenseleers, W.; Alain, V.; Kuebler, S. M.; Pond, S. J. K.; Zhang, Y.; Marder, S. R.; Perry, J. W., Laser and Electron-Beam Induced Growth of Nanoparticles for 2D and 3D Metal Patterning. *Adv. Mater.* **2002,** 14, (3), 194-198.

38. Eustis, S.; Hsu, H.-Y.; El-Sayed, M. A., Gold Nanoparticle Formation from Photochemical Reduction of Au3+ by Continuous Excitation in Colloidal Solutions. A Proposed Molecular Mechanism *J. Phys. Chem. B* **2005,** 109, (11), 4811-4815.

39. Link, S.; Burda, C.; Nikoobakht, B.; El-Sayed, M. A., Laser-induced shape changes of colloidal gold nanorods using femtosecond and nanosecond laser pulses. *J. Phys. Chem. B* **2000,** 104, (26), 6152-6163.

40. Link, S.; Burda, C.; Mohamed, M. B.; Nikoobakht, B.; El-Sayed, M. A., Laser photothermal melting and fragmentation of gold nanorods: Energy and laser pulse-width dependence. *J. Phys. Chem. A* **1999,** 103, (9), 1165-1170.

41. Hu, M.; Hartland, G. V., Heat dissipation for Au particles in aqueous solution: Relaxation time versus size. *J. Phys. Chem. B* **2002,** 106, (28), 7029-7033.

42. Voisin, C.; Del Fatti, N.; Christofilos, D.; Vallee, F., Ultrafast electron dynamics and optical nonlinearities in metal nanoparticles. *J. Phys. Chem. B* **2001,** 105, (12), 2264-2280.

43. Link, S.; Furube, A.; Mohamed, M. B.; Asahi, T.; Masuhara, H.; El-Sayed, M. A., Hot electron relaxation dynamics of gold nanoparticles embedded in MgSO4 powder compared to solution: The effect of the surrounding medium. *J. Phys. Chem. B* **2002,** 106, (5), 945-955.

44. Kurita, H.; Takami, A.; Koda, S., Size reduction of gold particles in aqueous solution by pulsed laser irradiation. *Appl. Phys. Lett.* **1998,** 72, (7), 789-791.

45. Mafune, F.; Kohno, J. Y.; Takeda, Y.; Kondow, T., Growth of gold clusters into nanoparticles in a solution following laser-induced fragmentation. *J. Phys. Chem. B* **2002,** 106, (34), 8555-8561.

46. Mafune, F.; Kohno, J.; Takeda, Y.; Kondow, T.; Sawabe, H., Formation and size control of sliver nanoparticles by laser ablation in aqueous solution. *J. Phys. Chem. B* **2000,** 104, (39), 9111-9117.

47. Takami, A.; Kurita, H.; Koda, S., Laser-induced size reduction of noble metal particles. *J. Phys. Chem. B* **1999,** 103, (8), 1226-1232.

48. Kamat, P. V.; Flumiani, M.; Hartland, G. V., Picosecond dynamics of silver nanoclusters. Photoejection of electrons and fragmentation. *J. Phys. Chem. B* **1998,** 102, (17), 3123-3128.

49. ImageJ is a public domain Java image processing program inspired by NIH Image. The source code is freely available. Watershead plugin and other plugins also available. http://rsb.info.nih.gov/ij/ Date Accessed (5/23/06).

CHAPTER 7

PHOTOCHEMICAL FORMATION OF METAL NANOPARTICLES WITH SILICA[**]

Abstract

For application of nanoparticles in heterogeneous catalysis, gold and silver nanoparticles have been formed on and in silica surfaces. This chapter presents the photochemical reduction of Au^{3+} and Ag^{1+} using benzophenone. The current study investigates the effect of adsorbing the benzophenone or metal salt on the silica before irradiation to develop methods where the starting material can be separated from the reducing material to enhance stability after irradiation. The use of silica films with adsorbed benzophenone allows the generation of stable gold and silver nanoparticles in solution. Silica films with gold and silver ions impregnated generate metal nanoparticles after irradiation in aqueous solution with benzophenone. These samples allow the photoreduction of the desired species with the ability to selectively remove the product, or the reducing agent. Thus metal nanoparticles are generated that can be used as stable catalytic particles or as a method of removal of metal ions from solution. This technique has the additional advantage of separating the nanoparticles formed from the chemicals used in the solution. A study of the process is discussed.

[**]Eustis, S.; Krylova, G.; Smirnova, N.; Eremenko, A.; Tabor, C.; Huang, W.; El-Sayed, M. A., Using Silica Films and Powders Modified with Benzophenone to Photoreduce Silver Nanoparticles. *J. Photochem. Photobiol. A* **2006,** In press.

Introduction

Silica is an attractive material due to its large abundance, stability, commercial availability, low cost, ease of processing, and its large presence in existing technology.[1-4] Silica can be used to protect the starting material, end material, or as a carrier of either species. It is beneficial to have a large surface area for the photocatalyst and other species to bind. The photochemical reaction of benzophenone (BP) with isopropyl alcohol[5-8] is well known. The formation of the triplet state of benzophenone has been studied on silica surfaces previously.[9, 10] Combining the photochemical reaction with the immobilization on silica surfaces produces a material with a high photoreductive yield. The silica used in current study does not absorb in this region, allowing direct measurement of metal ions and nanoparticles.[11]

Metal nanoparticles have attracted considerable attention due to their interesting optical properties such as large non-linear susceptibility,[12-14] surface enhanced Raman scattering,[15-17] and their use in photophysics[18] and photochemistry.[19] Furthermore, SiO_2-BP systems could become competitive with the widely used photocatalyst TiO_2.[20-22] Initial research into reducing silver and gold in the presence of SiO_2 has previously been presented by various researchers.[14, 23-40] Early work by Breitscheidel et. al.[40] showed the possibility of generating metal nanoparticles in porous silica films. Many researchers have used hydrogen reduction of metal inside a single template to form metal nanoparticles.[38-40] The ability to generate silica in rod geometry as a template for nanoparticle generation has been shown by Han et. al.[38] and Huang et. al.[39]

The ability to add and remove substances from solutions at will is desirable in many synthetic applications. Strong reducing agents are used to reduce metal ion to form

nanoparticles in many syntheses.[38-42] However, concentrations are often higher than a 1:1 mole ratio to insure that all desired atoms are reduced in solution, leaving excess reducing agents in solution with the ability to further reduce products to undesired states.[41] This has been implicated in the destabilization of nanoparticles in solution, and the need to wait before the fabricated nanoparticles can be used for further applications.[41] The ability to separate metal ions and metal nanoparticles from solution is also desired to remove toxic metal ions from environmental sources or chemical processing. The ability to keep nanoparticle catalyst for multiple cycles lead to the desire for easy removal of these substances from solution. Attaching metal nanoparticle or the reducing agent to silica allows for these possibilities.

Increased stability of catalysts while still allowing catalytic activity has been achieved by embedding catalysts in silica.[43] The catalytic properties[36] of silver nanoparticles supported on silica spheres[34] has been shown to increase the stability and the length of the catalytic lifetime of silver nanoparticles by avoiding flocculation of the silver nanoparticles, without reducing the access to the surface with surfactants. The photochemical preparation of silver nanoparticles was recently published[30] using benzophenone as a sensitizing agent and discussed in Chapter 6.

In this work, the photosensitizer benzophenone was adsorbed onto the surface of photochemically inactive silica. Both gold and silver can be reduced to form nanoparticles using the photochemical sensitization of benzophenone and silica to stabilize the nanoparticles. Mesoporous silica films were synthesized via the low-temperature sol-gel process consisting of the acid hydrolysis of tetraethoxysilane in the presence of template agents. Commercially available porous silica powders were also

used. The activity of SiO_2-BP films and powders used as photoreducing agents to generate silver nanoparticles was studied as a function of the substrate structure and BP concentration.

Experimental

Three different types of silica are considered in the following section; mesoporous films, powders and colloidal suspensions. The mesoporous silica films are prepared by by the sol-gel technique where a templating agent is used to obtain an ordered and controlled pore size. The best results were obtained using the non-ionic, tri-block copolymer Pluronic (P123) as described by literature methods.[44-46] Silica gel powders and colloidal silica are purchased from commercial sources and used as received. The experimental conditions have been reported previously for the preparation of the silica films and powders, along with the functionalization with benzophenone.[30] Conditions are identical to those reported previously[29] for photoreduction solutions containing BP with Ludox (colloidal silica) in aqueous solution

The photoreduction solutions containing SiO_2-BP films and powders were used as a removable photoreducing agent. The reaction mixture consisted of a 40 ml aqueous solution of $1.5*10^{-4}$M $AgNO_3$ ($HAuCl_4$), 0.4M isopropyl alcohol (IPA), and 1% Ludox. SiO_2-BP films and 0.5g of SiO_2-BP powder were placed into separate solutions and vigorously stirred for 10 min before irradiation to establish adsorption/desorption equilibrium of BP from the film or powder with the solution. Ludox acted as a stabilizer in this system.

Dissolving metal ion in the silica prior to casting the film creates generation of silica films with embedded silver and gold nanoparticles. SiO_2-Ag (Au) films are

prepared with a 0.1 Ag (Au)/SiO_2 molecular ratio. An aqueous solution of $AgNO_3$ ($HAuCl_4$) was added to hydrolyzed silica sol before film deposition. After calcinations in air at 400^0C, transparent colorless films were produced with no traces of silver nanoparticles and small numbers of gold nanoparticles as observed by optical absorption. Irradiation of the SiO_2-Ag (Au) film was carried out in an aqueous solution of $1.4*10^{-3}$M BP, $1.7*10^{-3}$M SDS, and 1.84M IPA. SDS was used to increase the solubility of BP in the alcohol-water solution. SDS could act as a hydrogen donor in the reaction with the BP triplet.

A monochromatic 1000-W low-pressure mercury lamp connected with a standard cobalt (II) sulfate solution filter was used as a 253.7 nm irradiation source. A 500-W low-pressure mercury lamp combined with the appropriate UV 7-60 filter was used as a source of 365 nm light. A cylindrical quartz vessel with a volume of 40 ml was used as the reaction cell. The incident photon intensity (as determined by a tris(oxalato) ferrate(III) actinometer[47]) is determined at 253.7nm and 365nm to be $2*10^{17}$ and $2.12*10^{15}$ $cm^{-2}s^{-1}$, respectively. Irradiation was carried out while bubbling argon through the solution at room temperature. The absorption spectra of the solutions before and after irradiation were measured with a Lambda UV-Vis spectrophotometer (Perkin Elmer) in a rectangular 1cm thick quartz cuvette. Diffuse reflectance spectra of SiO_2-BP films and powders were also measured with this spectrophotometer.

Results and Discussion

Metal Ions and Benzophenone in Solution

As shown in Chapter 6 aqueous solutions of benzophenone with alcohol can be used to reduce metal ions in solution with the inclusion of colloidal silica. This procedure works for gold as shown in Figure 7-1. The formation of gold nanoparticles is observed by the characteristic plasmon resonance at 520nm. The edge of the absorption of benzophenone is decreasing as the plasmon resonance absorption of the gold nanoparticles is increasing. The size distribution is large due to the size of Ludox particles, and their weak binding to the gold nanoparticle surface. The background of silica particles is seen in the TEM image as the lighter spheres, and always found with the gold nanoparticles, showing the ability to cap the nanoparticles. The width of the plasmon resonance also shows the polydisperisty of the gold nanoparticles obtained by this synthesis method.

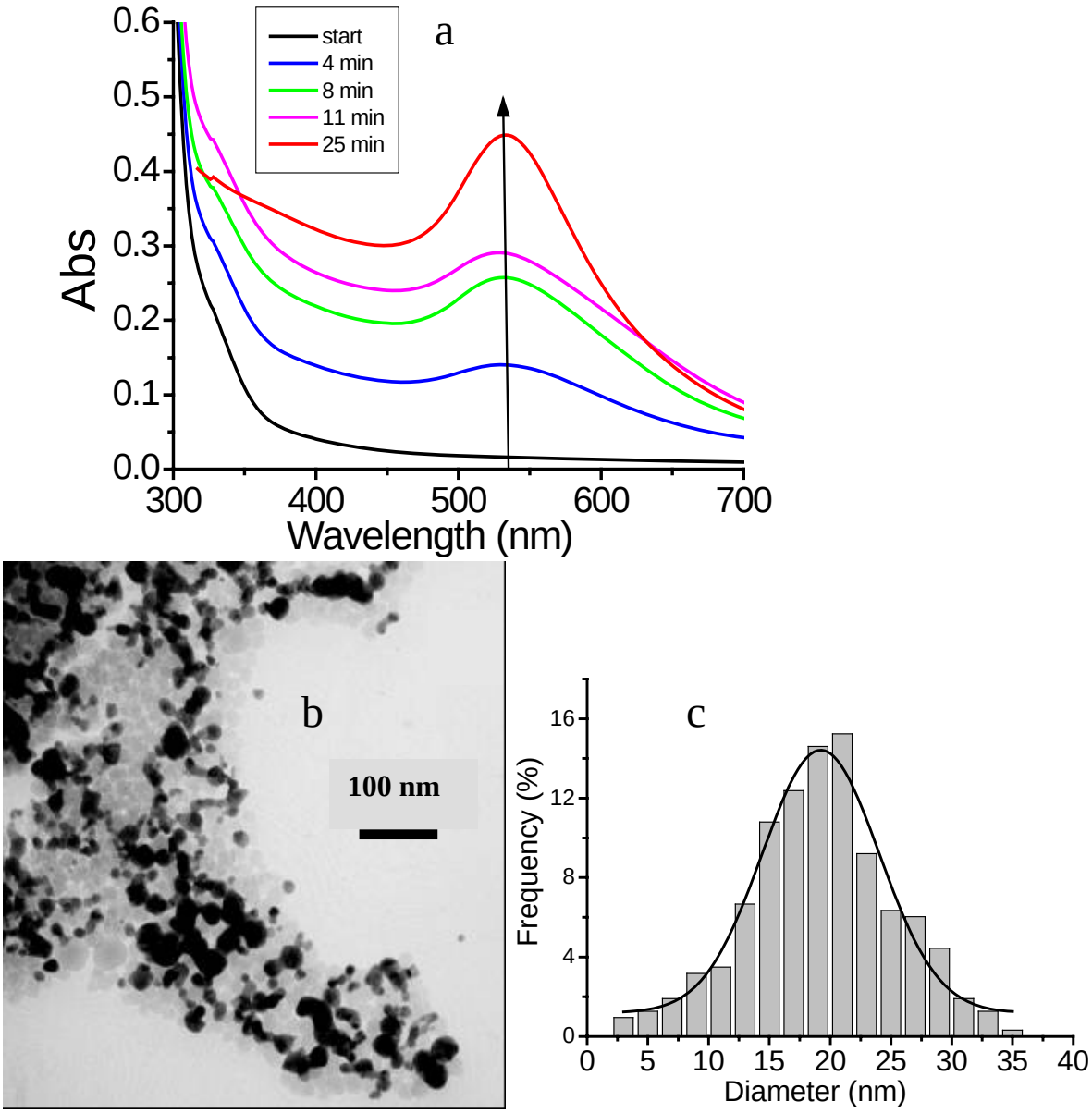

Figure 7-1: *The formation of gold nanoparticle during irradiation with 254 nm light in solution with Ludox. a) with increasing irradiation time, the surface plasmon resonance absorption of the spherical nanoparticles(528nm) increases while the absorption of the benzophenone(>350nm) decreases b) TEM image of sample c) size distribution of the diameter with Gaussian fit (Average diameter 19.2nm)*

Silica Films Modified with BP to Photoreduce Metal Ions

The photochemical reduction of metal ions via SiO_2–BP porous films was investigated in a water-alcohol solution with incident irradiation at 254nm from a mercury lamp. The SiO_2-BP film was removed from solution immediately after irradiation and the absorption spectra of the irradiated solutions were measured. The absorption spectra of reduced silver particles as a function of irradiation time in the presence of a SiO_2-BP film are shown in Figure 7-2a. A broad absorption band from the silver nanoparticles (maximum at 407 nm) increased with irradiation time while in the presence of the stabilizer, Ludox similar to the results obtained when benzophenone is in solution with the metal ions. Figure 7-2b shows the absorption spectrum of gold nanoparticles formed with irradiation of a solution containing IPA and SiO_2-BP film. The absorption of the plasmon resonance increases and slightly blue shifts as irradiation time increases similar to the results of the silver solution. The theoretical absorption maximum of the surface plasmon resonance absorption for silver nanoparticles is located at 360nm in air, at 390nm in water, and at 410nm in glass.[18, 48] The surface plasmon in this experiment was observed between 403-407 nm.

The intensity of the surface plasmon resonance absorption is proportional to the nanoparticle concentration and is plotted versus irradiation time for both gold and silver with the $Si0_2$-BP films and without any BP in Figure 7-2c. The intensities have been normalized to the maximum intensity of the sample with SiO_2-BP film for gold and silver. Photoreduction with 254 nm light is more effective in the presence of the SiO_2-BP film than in the absence of the silica film shown in Figure 7-2c, particularly for the silver solution. While irradiation of the gold solution leads to higher reaction rates with the

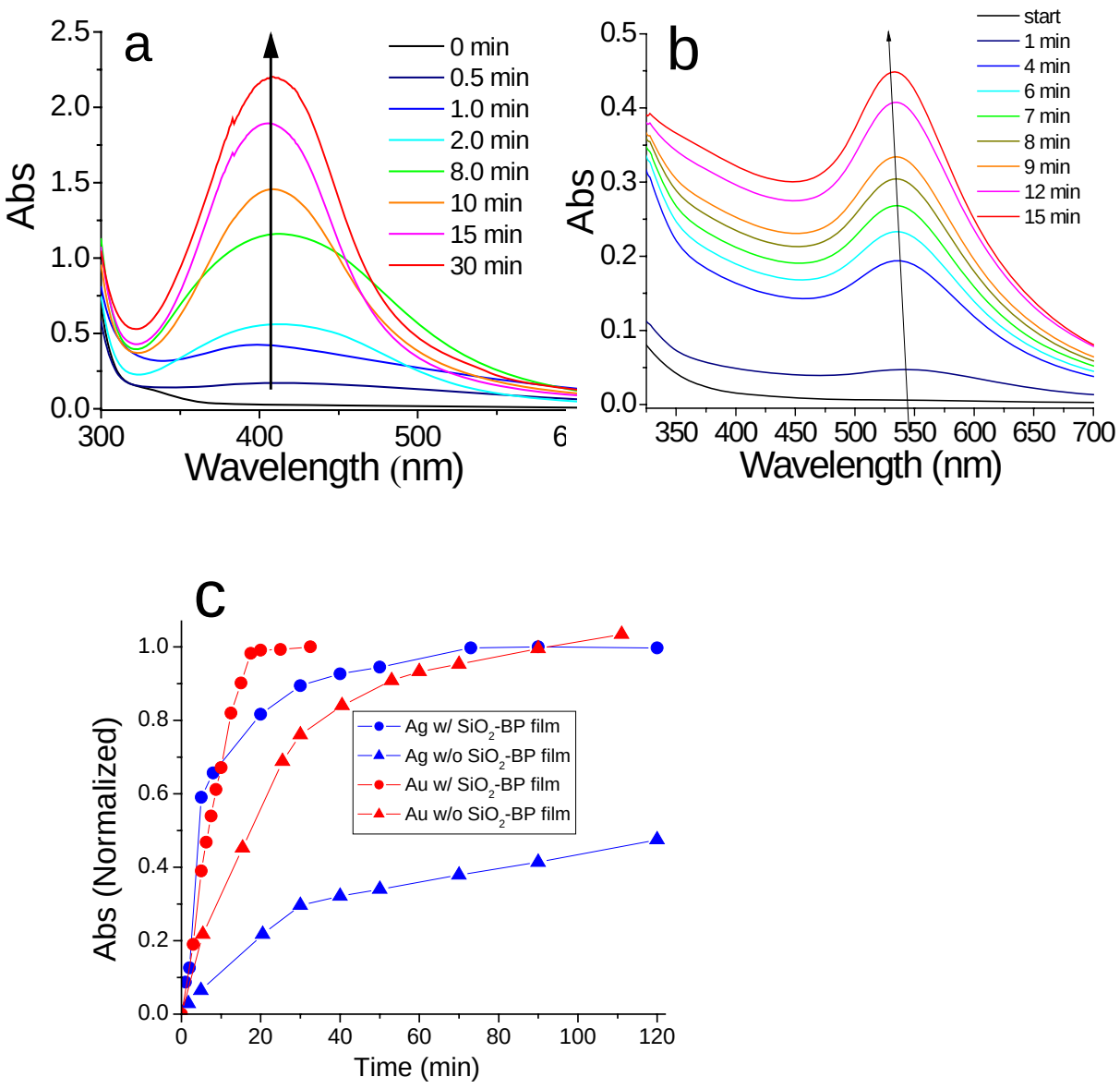

Figure 7-2: *Absorption spectra using 254nm irradiation with SiO_2-BP film at various irradiation times generating a) silver nanoparticles b) gold nanoparticles and c)Kinetics of silver nanoparticle formation (measured by the absorbance intensity as a function of irradiation time) for silver (blue) and gold (red) solutions normalized to the maximum intensity with SiO_2-BP film (,), and without SiO_2-BP film (7)*

inclusion of the SiO_2-BP film, the sample without BP reaches the same intensity. Thus, the presence of SiO_2-BP films is able to catalyse the formation of silver nanoparticles generated at 254nm. However, $HAuCl_4$ is able to absorb the incoming radiation at 254nm without addition of BP, and become photoreduced in alcohol solution as discussed in Chapters 8-10. The addition of BP to the gold solution increases the reduction rate, as it is a better reducing agent for the gold ions than the alcohol to form gold nanoparticles.

Using equations from our previous publication[30] and given in Chapter 6, the quantum yields for formation of gold and silver nanoparticles can be calculated. The photoreduction quantum yields calculated for both silver and gold nanoparticles using SiO_2-BP films are 2.73% and 1.8%, respectively. The conditions of the blank experiment, without silica film are similar to that of Hada et. al.[49] The quantum yield for the blank irradiation was 0.3%, for silver and 0.6% for gold. The value for silver is about 9 times less than in the presence of the SiO_2-BP film. Thus, the SiO_2-BP films were solely responsible for the observed generation of silver nanoparticles in this study. However, the quantum yield for gold is only 3 times more than the blank experiment, showing that gold ions are capable of being reduced in this solution without benzophenone. Other background studies with only BP in solution have already been performed.[6, 7] Silica film alone is not photoactive and can not contribute to the photoreduction process;[25] therefore its presence in solution would lead to similar results as those preformed in water.[49]

Stability of Silver Nanoparticles Irradiated with SiO_2-BP films

Silver nanoparticles were unstable in solution and were observed to precipitate after irradiation had ceased even if solutions were stored in the dark. This was indicated

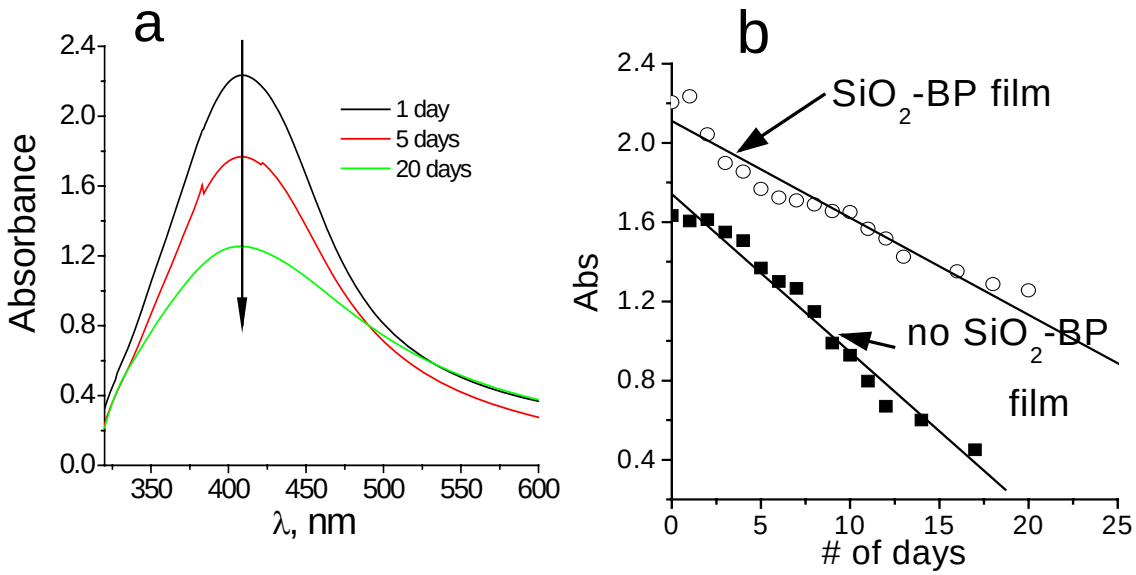

Figure 7-3: *a) Absorption spectra of silver nanoparticles generated using SiO_2-BP film after 30 minutes of irradiation stored in the dark for the indicated time: b) Kinetics of silver nanoparticle SPR absorption at 407nm generated with SiO_2-BP film (–) and without SiO_2-BP film (!).*

by the decrease in the surface plasmon absorbance spectra in Figure 7-3a. The absorption spectra was observed to decrease in intensity with no shifting of the surface plasmon resonance absorption, which confirms the absence of nanoparticle aggregation.[50, 51] The decrease of the maximum absorbance intensity of silver nanoparticles is shown in Figure 7-3b for samples irradiated with SiO_2-BP films and without BP. A slower disappearance rate of silver nanoparticle absorption is observed compared to the sample with no benzophenone. This suggests that the ability to remove BP from contact with solution after irradiation could have a stabilizing effect on the nanoparticles formed. The peptizing action of solution BP ketyl-radicals could have been responsible for the apparent stabilization of Ag colloids as suggested previously:[52-54]

$$(C_6H_5)_2C^{\bullet}OH + (Ag^0)_n \rightarrow (C_6H_5)_2CO + (Ag^0)_n^- + H^+$$

This peptization in the presence of SiO_2-BP films leads to more negatively charged silver nanoparticles than in the experiment without BP, thus enhancing their inter-particle stability due to static repulsion preventing them from aggregation.

Reduction of Silver with SiO_2-BP powders

Solutions of silver nanoparticles generated with SiO_2-BP powder had the largest decrease in the surface plasmon resonance absorption after irradiation due to deposition of the silver particles onto the SiO_2-BP powder surface. Diffuse reflectance spectra of SiO_2-BP powders after the reduction of silver are shown in Figure 7-4 after filtration and drying. The surface plasmon resonance absorption bands of SiO_2-BP powder shown in Figure 7-4 and solution with SiO_2-BP film in Figure 7-2a are similar, suggesting that the silver nanoparticles are located on the SiO_2-BP powders. The importance of Ludox in the solution to stabilize the silver nanoparticles is demonstrated in Figure 7-4 by comparing absorption of the solutions with and without Ludox. The red shift and broadening of the reflectance spectrum without stabilizer is due to aggregation and growth of the silver nanoparticles in the absence of Ludox. SiO_2-BP powder was unable to stabilize the nanoparticles, and the powder was only a method for introduction (and removal) of BP into (and out of) the solution. This suggests that in the absence of Ludox, strong interactions between neighboring silver nanoparticles occurred. Thus, with the SiO_2-BP powders the silver nanoparticles attached to the silica surface, while no nanoparticle attachment was observed on the SiO_2-BP film. This was probably due to the small pore size of the silica films available for embedding silver nanoparticles, and a smaller charge density compared with SiO_2-BP powder.

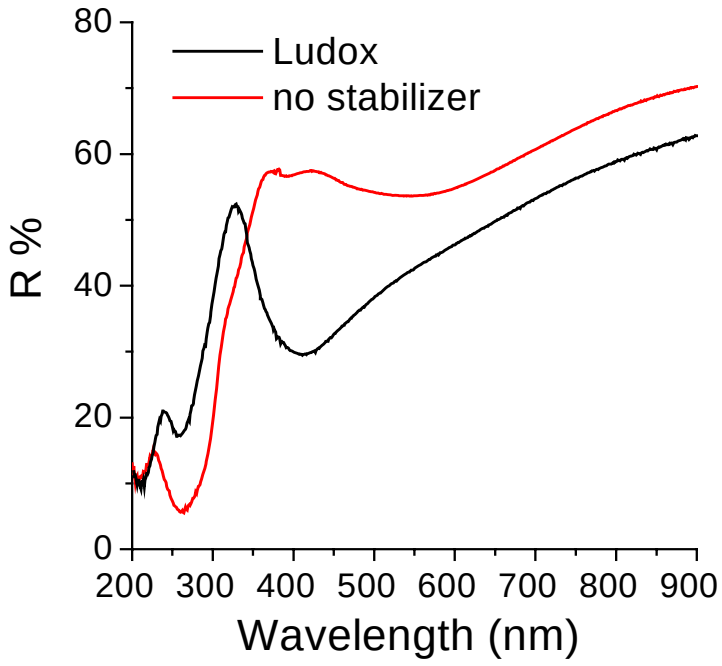

Figure 7-4: *Diffuse reflectance spectra of SiO_2-BP powder after photoreduction of silver in solution with and without Ludox. This clearly shows that the Ludox acts as a stabilizer for the nanoparticles (with a maximum at ~400nm)*

Photoinduced formation of SiO_2-Ag and SiO_2-Au films

Silica films doped with Ag^+ or $Au^{(3+)}Cl_4^-$ were synthesized via the sol-gel route in order to produce a material with a uniform distribution of Ag or Au nanoparticles. Irradiation of the SiO_2-Ag^+ or SiO_2-Au^{3+} film in an aqueous solution of BP, SDS, and IPA resulted in the photoreduction of the embedded silver or gold ions and the appearance of the typical surface plasmon resonance absorption band centered at 408 nm and 514nm from $(Ag)_n$ and $(Au)_n$ nanoparticles seen in Figure 7-5a and 7-5b, respectively. The silver does not form nanoparticles prior to irradiation as shown in Figure 7-5. Twenty minutes of irradiation for the silver film is enough to observe the plasmon resonance and the nanoparticles in the SEM image in Figure 7-5c. However,

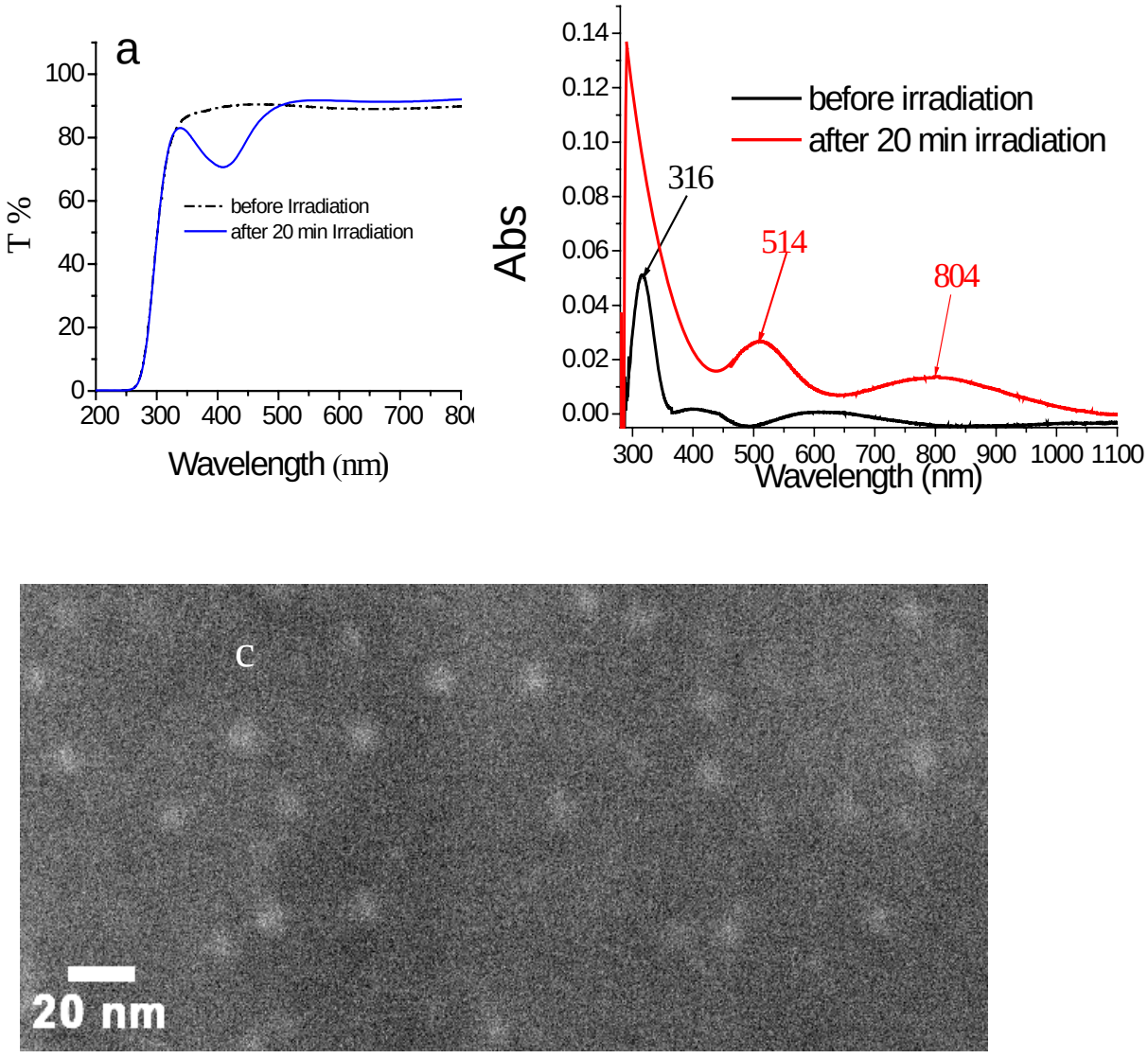

Figure 7-5: *a) Transmittance spectra of SiO_2-Ag films before and after irradiation b) Absorption spectra of SiO_2-Au films before and after irradiation c) SEM image reveals silver particles formed embedded in the porous silica film (Image taken by Wenyu Huang). The light spots are the silver nanoparticles.*

gold nanoparticle formation is observed prior to irradiation as seen by the weak broad absorption peak at 600nm in Figure 7-5b suggesting that the nanoparticles formed are aggregates of many different sizes and shapes. The absorption at 315nm in Figure 7-5b before irradiation is due to unreduced $AuCl_4^-$. This can be reduced by photochemistry directly or by reaction with the BP from the solution.

The XRD pattern of the SiO_2-Ag film consists of Ag(111), Ag(200), Ag(220), and Ag(311) diffraction peaks.[30] The silver nanoparticle diameter calculated by the Scherrer equation[55] is about 7 nm. An SEM image of silver nanoparticles embedded in the silica film after irradiation is shown in Figure 7-5c, confirming the presence of silver nanoparticles on the surface and in the interior of the silica film. Particle size is observed to be 5-10 nm, which is in agreement with the value obtained from XRD. The nanoparticles are embedded in the silica matrix, making it difficult to obtain a clear picture of them. The blurring of the sample is due to the silica-insulating layer between the particles and the electron beam. Similar images are obtained for gold films, with larger variation in the size and shape of the nanoparticles produced as suggested by the appearance of two plasmon resonances after irradiation in solution with BP.

To determine the adhesion of silver nanoparticles to the silica surface after the photoreduction of the SiO_2-Ag film in BP solution, the surface was repeatedly washed with aqueous solution. Absorption measurements were taken of the aqueous solution after washing and no surface plasmon resonance of silver nanoparticles was detected; therefore adhesion is suggested to be good.

Conclusions

The photochemical process allows the generation of gold and silver nanoparticles with silica. The silica is useful for the stability of the nanoparticles and for the addition and removal of desired components from the solution. This offers the ability to combine solution phase synthesis techniques with solid phase transfer agents. The photoreduction using benzophenone is still effective even if the BP has been adsorbed to the solid surface of the silica. This allows for the removal of the excess BP in the solution after the desired reduction has taken place without limiting the initial concentration of BP in solution. This technique also produces silica films and powders with embedded silver and gold nanoparticles. These allow the fabrication of highly conductive materials and firmly anchored nanoparticle catalysts, thereby suppressing loss of catalytic activity due to nanoparticle aggregation or removal.

References

1. Adams, C. R., High Temperature Stability of Silica-Base Gels. *J. Phys. Chem.* **1963,** 67, (2), 313-318.

2. Calvert, J. B. Silicon. http://www.du.edu/~jcalvert/phys/silicon.htm Date Accessed (2/27/2006).

3. Kotz, J. C.; Treichel, P., Jr., *Chemistry & Chemical Reactivity*. 3rd ed.; Saunders College Publishing: Orlando, 1996; p 1018-1024.

4. McQuarrie, D. A.; Rock, P. A., *Descriptive Chemistry*. W.H. Freeman and Co.: New York, 1985.

5. Kapoor, S.; Palit, D. K.; Mukherjee, T., Preparation, characterization and surface modification of Cu metal nanoparticles *Chem. Phys. Lett.* **2002,** 355, (3-4), 383-387.

6. Kometani, N.; Doi, H.; Asami, K.; Yonezawa, Y., Laser flash photolysis study of the photochemical formation of colloidal Ag nanoparticles in the presence of benzophenone. *Phys. Chem. Chem. Phys.* **2002,** 4, 5142-5147.

7. Sato, T.; Maeda, N.; Ohkoshi, H.; Yonezawa, Y., Photochemical Formation of Colloidal Silver in the Presence of Benzophenone. *Bull. Chem. Soc. Japan* **1994,** 67, (12), 3165-3171.

8. Yankov, P.; Nickolov, Z.; Zhelyaskov, V., *J. Photochem. Photobiol.* **1988,** 47, 155-165.

9. Kazanis, S.; Azarani, A.; Johnston, L. J., Diffuse reflectance laser flash photolysis studies of reactions of triplet benzophenone with hydrogen donors on silica. *J. Phys. Chem.* **1991,** 95, (11), 4430 - 4435.

10. Drake, J. M.; Levitz, P.; Turro, N. J.; Nitsche, K. S.; Cassidy, K. F., Benzophenone Triplet Quenchhg by Oxygen at the Gas/Solid Interface: A Target Annihilation Reaction In the Restricted Pore Geometry of Silica. *J. Phys. Chem.* **1988,** 92, (16), 4680-4684.

11. Bronstein, L.; Krämer, E.; Berton, B.; Burger, C.; Förster, S.; Antonietti, M., Successive Use of Amphiphilic Block Copolymers as Nanoreactors and Templates: Preparation of Porous Silica with Metal Nanoparticles. *Chem. Mater.* **1999,** 11, (6), 1402-1405.

12. Hutter, E.; Fendler, J. H., Exploitation of Localized Surface Plasmon Resonance. *Adv. Mater.* **2004,** 16, (19), 1685 - 1706.

13. Drachev, V. P.; Buin, A. K.; Nakotte, H.; Shalaev, V. M., Size Dependent $\chi^{(3)}$ for Conduction Electrons in Ag Nanoparticles. *Nano Lett.* **2004,** 4, (8), 1535-1539.

14. Qu, S.; Zhao, C.; Jiang, X.; Fang, G.; Gao, Y.; Zeng, H.; Song, Y.; Qiu, J.; Zhu, C.; Hirao, K., Optical nonlinearities of space selectively precipitated Au nanoparticles inside glasses. *Chem. Phys. Lett.* **2003,** 368, (3-4), 352-358.

15. Campion, A.; Kambhampati, P., Surface-enhanced Raman scattering. *Chem. Soc. Rev.* **1998,** 27, (4), 241-250.

16. Kneipp, K.; Kneipp, H.; Itzkan, I.; Dasari, R. R.; Feld, M. S., Ultrasensitive Chemical Analysis by Raman Spectroscopy *Chem. Rev.* **1999,** 99, (10), 2957-2976.

17. Nie, S.; Emory, S. R., Probing Single Molecules and Single Nanoparticles by Surface-Enhanced Raman Scattering. *Science* **1997,** 275, (5303), 1102-1106.

18. Bohren, C. F.; Huffman, D. R., *Absorption and Scattering of Light by Small Particles*. Wiley: New York, 1983.

19. Hildebrandt, P.; Stockburger, M., Surface-enhanced resonance Raman spectroscopy of Rhodamine 6G adsorbed on colloidal silver *J. Phys. Chem.* **1984,** 88, 5935-5944.

20. Kamat, P. V., Photochemistry on nonreactive and reactive (semiconductor) surfaces *Chem. Rev.* **1993,** 93, (1), 267-300.

21. Hoffmann, M. R.; Martin, S. T.; Choi, W.; Bahnemann, D. W., Environmental Applications of Semiconductor Photocatalysis. *Chem. Rev.* **1995,** 95, (1), 69-96.

22. Anpo, M.; Takeuchi, M., The design and development of highly reactive titanium oxide photocatalysts operating under visible light irradiation. *J. Catal.* **2003,** 216, (1-2), 505-516.

23. Janata, E.; Henglein, A.; Ershov, B. G., First Clusters of Ag+ Ion Reduction in Aqueous Solution *J. Phys. Chem.* **1994,** 98, (42), 10888-10890.

24. Kamat, P. V.; Flumiani, M.; Dawson, A., Metal-metal and metal-semiconductor composite nanoclusters. *Colloids Surf. A* **2002,** 202, (2-3), 269-279.

25. Lawless, D.; Kapoor, S.; Kennepohl, P.; Meisel, D.; Serpone, N., Reduction and Aggregation of Silver Ions at the Surface of Colloidal Silica *J. Phys. Chem.* **1994,** 98, (38), 9619-9625.

26. Pillai, Z. S.; Kamat, P. V., What Factors Control the Size and Shape of Silver Nanoparticles in the Citrate Ion Reduction Method? . *J. Phys. Chem. B* **2004,** 108, (3), 945-951.

27. Ung, T.; Liz-Marzan, L. M.; Mulvaney, P., Controlled Method for Silica Coating of Silver Colloids. Influence of Coating on the Rate of Chemical Reactions *Langmuir* **1998,** 14, (14), 3740-3748.

28. Henglein, A., Colloidal Silver Catalyzed Multi-Electron Transfer Processes in Aqueous Solution. *Ber. Bunsen-Ges. Phys. Chem.* **1980,** 84, 253-259.

29. Eustis, S.; Krylova, G.; Eremenko, A.; Smirnova, N.; Schill, A. W.; El-Sayed, M. A., Growth and fragmentation of silver nanoparticles in their synthesis with a fs laser and CW light by photo-sensitization with benzophenone. *Photochem. Photobio. Sci.* **2005,** 4, (1), 154-159.

30. Eustis, S.; Krylova, G.; Smirnova, N.; Eremenko, A.; Tabor, C.; Huang, W.; El-Sayed, M. A., Using Silica Films and Powders Modified with Benzophenone to Photoreduce Silver Nanoparticles. *J. Photochem. Photobiol. A* **2006,** In press.

31. Hsia, C. H.; Yen, M. Y.; Lin, C. C.; Chiu, H. T.; Lee, C. Y., In Situ Generation of the Silica Shell Layer - Key Factor to the Simple High Yield Synthesis of Silver Nanowires. *J. Am. Chem. Soc.* **2003,** 125, (33), 9940-9941.

32. Prodan, E.; Nordlander, P.; Halas, N. J., Electronic Structure and Optical Properties of Gold Nanoshells. *Nano Lett.* **2003,** 3, (10), 1411-1415.

33. Salgueirino-Maceira, V.; Caruso, F.; Liz-Marzan, L. M., Coated Colloids with Tailored Optical Properties. *J. Phys. Chem. B* **2003,** 107, (40), 10990-10994.

34. Jiang, Z. j.; Liu, C. y., Seed-Mediated Growth Technique for the Preparation of a Silver Nanoshell on a Silica Sphere. *J. Phys. Chem. B* **2003,** 107, (45), 12411-12415.

35. Dick, K.; Dhanasekaran, T.; Zhang, Z.; Meisel, D., Size-Dependent Melting of Silica-Encapsulated Gold Nanoparticles. *J. Am. Chem. Soc.* **2002,** 124, (10), 2312-2317.

36. Jiang, Z. J.; Liu, C. Y.; Sun, L. W., Catalytic Properties of Silver Nanoparticles Supported on Silica Spheres. *J. Phys. Chem. B* **2005,** 109, (5), 1730-1735.

37. Oldenburg, S. J.; Averitt, R. D.; Westcott, S. L.; Halas, N. J., Nanoengineering of optical resonances. *Chemical Physics Letters* **1998,** 288, (2-4), 243-247.

38. Han, Y.-J.; Kim, J. M.; Stucky, G. D., Preparation of Noble Metal Nanowires Using Hexagonal Mesoporous Silica SBA-15. *Chem. Mater.* **2000,** 12, (8), 2068-2069.

39. Huang, M. H.; Amer, C.; Yang, P., Ag nanowire formation within mesoporous silica. *Chem. Commun.* **2000**, 1063-1064.

40. Breitscheidel, B.; Zieder, J.; Schubert, U., Metal complexes in inorganic matrixes. 7. Nanometer-sized, uniform metal particles in a silica matrix by sol-gel processing of metal complexes. *Chem. Mater.* **1991,** 3, (3), 559-566.

41. Murphy, C. J.; Sau, T. K.; Gole, A. M.; Orendorff, C. J. G., J.; Gou, L.; Hunyadi, S. E.; Li, T., Anisotropic Metal Nanoparticles: Synthesis, Assembly, and Optical Applications *J. Phys. Chem. B* **2005,** 109, (29), 13857-13870.

42. Nikoobakht, B.; El-Sayed, M. A., Preparation and growth mechanism of gold nanorods (NRs) using seed-mediated growth method. *Chem. Mater.* **2003,** 15, (10), 1957-1962.

43. Chisem, J.; Chisem, I. C.; Rafelt, J. S.; Clark, J. H., Liquid phase oxidations using novel surface functionalised silica supported metal catalysts. *Chem. Commun.* **1997**, 2203-2204.

44. Eremenko, A.; Smirnova, N.; Spanhel, L.; Rusina, O.; Linnik, L.; Eremenko, B.; Rechthaler, K., Photophysical properties of organic fluorescent probes on nanosized TiO2/SiO2 systems prepared by the sol-gel method. *J. Molec. Struct.* **2000,** 553, 1-7.

45. Smirnova, N.; Eremenko, A.; Rusina, O.; Hopp, W.; Spanhel, L., Synthesis and characterization of photocatalytic porous Fe3+/TiO2 layers on glass. *J. Sol-Gel Sci. Tech.* **2001,** 21, 109-113.

46. Yamada, T.; Asai, K.; Endo, A.; Zhou, H. S.; Honma, I., Size control of oriented hexagonal mesoporous silicate thin film prepared by triblock copolymer templates. *J. Mater. Sci. Lett.* **2000,** 19, (24), 2167-2169.

47. Hatchard, C. G.; Parker, C. A., A New Sensitive Chemical Actinometer. II. Potassium Ferrioxalate as a Standard Chemical Actinometer *Proc. R. Soc. London, Ser. A* **1956,** 235, (1203), 518-537.

48. Henglein, A.; Mulvaney, P., Chemistry of Agn aggregates in aqueous solution: non-metallic oligomeric clusters and metallic particles. *Faraday Discuss.* **1991,** 92, 31-44.

49. Hada, H.; Yonezawa, Y.; Yoshida, A.; Kurakake, A., Photoreduction of silver ion in aqueous and alcoholic solutions *J. Phys. Chem.* **1976,** 80, (25), 2728-2731.

50. Kreibig, U.; Vollmer, M., *Optical Properties of Metal Clusters*. Springer: Berlin, 1995; Vol. 25, p 532.

51. Zhao, L. L.; Kelly, K. L.; Schatz, G. C., The Extinction Spectra of Silver Nanoparticle Arrays: Influence of Array Structure on Plasmon Resonance Wavelength and Width. *J. Phys. Chem. B* **2003,** 107, (30), 7343-7350.

52. Turro, N., *Modern Molecular Photochemistry*. The Benjamin-Cummings Publishing Co.: CA, 1978.

53. Turro, N. J.; Zimmt, M. B.; Gould, I. R.; Mahler, W., Triplet energy transfer as a probe of surface diffusion rates: time-resolved diffuse reflectance transient absorption spectroscopy study. *J. Am. Chem. Soc.* **1985,** 107, (20), 5826-5827.

54. Boitsova, T. B.; Gorbunova, V. V.; Volkova, E. I., Photochemical Method of Controlling Dispersity of Nanostructures of Transition Metals. *Russ. J. Gen. Chem.* **2002,** 72, (4), 642-656.

55. Hincapie, B.; Garces, L.; Zhang, Q.; Sacco, A.; Suib, L. S., Synthesis of mordenite nanocrystals *Microporous Mesoporous Mater.* **2004,** 67, (1), 19-22.

PART III: MECHANISTIC INVESTIGATIONS OF THE PHOTOCHEMICAL REDUCTION OF AURIC ACID COMPLEXES BY ETHYLENE GLYCOL TO FORM GOLD NANOPARTICLES

CHAPTER 8

CHANGES IN THE OPTICAL ABSORPTION SPECTRUM OF TETRACHLOROAURIC(III) ACID AND TETRABROMOAURIC(III) ACID IN DIFFERENT SOLVENTS

Introduction

The origin of the absorption of $HAuCl_4$ and $HAuBr_4$[1-3] have been known since the early sixties. The absorption is due to a charge transfer between the halide ions and gold ion.[1-3] Crystal field theory has been used with dsp^2 hybridization to explain the transfer of charge from the halide *p* to the gold *d* orbitals.[3] The absorption is used to initiate the photoreduction of gold in alcohol solution by the photoexcitation of $AuCl_4^-$.[4] The reactions that affect the absorption spectrum are important to understand side reactions that affect the starting material.

The hydrolysis equilibrium of $AuCl_4^-$ is well studied.[5-8] The reaction is reported to be:

$$AuCl_4^- + H_2O \overset{K}{\leftrightarrow} AuCl_3OH^- + H^+ + Cl^- \qquad K_{eq} = 7 \times 10^{-7}\ M^2 \quad [5]$$

or

$$AuCl_4^- + H_2O \overset{k_1}{\underset{k_2}{\leftrightarrow}} AuCl_3H_2O^- + Cl^-$$

$$AuCl_3H_2O^- \overset{K}{\leftrightarrow} AuCl_3OH^- + H^+ \qquad K_{eq} = 4.4 \times 10^{-7}\ M^2 \quad [6]$$

The rate of hydrolysis is found to depend on both the chloride and hydrogen ion concentration. High concentrations of either the hydrogen ion or the chloride ion suppress the hydrolysis. As the acid concentration or chloride concentration is decreased,

the hydrolyzed species is expected. This reaction can be followed spectroscopically by observing the shift and decrease in the absorption of $AuCl_4^-$ as the reaction proceeds in the forward direction.[6]

To follow these reactions, the absorption spectrum is measured as a function of concentration. A well-known equation, Beer's law, is used to quantitate the concentrations. It states that the absorption of a solution is equal to the absorption coefficient of the solution times the path length of the sample times the concentration of the solute.

$$A = \varepsilon l c \qquad (8.1)$$

where A is the absorption, ε is the absorption coefficient, l cm is the path length and c is the concentration. Determining the absorption coefficient of different molecules can be used to obtain the concentration of an unknown solution from the absorption of the solution. The extinction coefficient reported for $AuCl_4^-$ is 4800 $M^{-1}cm^{-1}$ (315nm) in acidic solution.[1, 6] The spectrum shifts to the blue as OH^- ions replace Cl^- ions in $AuCl_4^-$.[6] A change to the solvent is expected to slightly alter the observed absorption due to changes in the environment.

All photochemical experiments rely on the absorption of the starting material to initiate the reaction. The absorption of $AuCl_4^-$ in water is well known, but the absorption spectrum has never been reported in other solvents. This section explores how the absorption of the starting material $AuCl_4^-$ changes as a function of solvent, pH, and chloride concentration. As the environment around the molecule changes the observed absorption wavelength shifts due to the interaction of the molecule with the solvent. To further investigate the role of the solvent in shifting the absorption spectrum of $AuCl_4^-$,

the polarity of the solvent is used. Interactions of $AuCl_4^-$ with hydrolysis, hydrogen bonding and the index of refraction of the solvent determine the absorption.

As bromide salt is added to a solution containing $AuCl_4^-$, the absorption spectrum gradually shifts to the red, indicating the presence of mixed chloride and bromide salts.[9, 10] This reaction has been shown to proceed stepwise with the step-by-step replacement of chloride ions with bromide ions.[9, 10] The intermediate complexes with both chloride and bromide ligands bound to a single gold ion have been observed previously and their spectra and equilibrium constants have been published in water.[9-12]

The stepwise replacement of the chloride ions takes place by direct halide displacement, without undergoing intermediate hydrolysis as has been reported by Elding and Gröning[9] and Pouradier and Coquard.[10] With an equal amount of chloride ions added to the bromide complex and bromide ions added to the chloride complex a larger change in the absorption spectra is observed when the bromide ion is added. This shows that the bromide species is the more stable of the two in solution.[5, 9-12] The stability constant of the chloride and bromide complexes have been calculated.[9, 11] The overall stability constant, β_{4X}, for AuX_4^- to dissociate in solution to Au^{3+} and $4X^-$ is expressed as the concentration of the pure salt $[AuX_4^-]$, the naked gold concentration $[Au^{3+}]$, and the counter ion concentration $[X^-]$ as shown below.

$$\beta_{4X} = \frac{[AuX_4^-]}{[Au^{3+}][X^-]^4} \qquad (8.2)$$

For the stepwise replacement of chloride ions with bromide ions the equilibrium constant can be represented as

$$K_n = \frac{[AuCl_{3-n}Br_{n+1}^-][Cl^-]}{[AuCl_{4-n}Br_n^-][Br^-]} \text{ for n=0, 1, 2, and 3} \qquad (8.3)$$

$$AuCl_{4-n}Br_n^- + Br^- \Leftrightarrow AuCl_{3-n}Br_{n+1}^- + Cl^- .$$

The four equilibrium constants for n = 0, 1, 2, and 3 shown above can be used to obtain the ratio of the stability of the bromide complex to the chloride complex.

$$\beta_{4Br} / \beta_{4Cl} = K_0 K_1 K_2 K_3 \qquad (8.4)$$

β_{4Br}/β_{4Cl} is calculated[9] to be 2.0×10^7, showing the larger stability (lower free energy) of the bromine-gold complex over the chloride-gold complex in solution.

The hydrolysis of both the chloride and the bromide ion have been reported previously.[5, 12] The equilibrium constant of replacing the first bromide ion by the hydroxide ion is two orders of magnitude lower for chloride ion.[5]

Experimental

Methanol (MeOH), ethanol (EtOH), isopropyl alcohol (IPA) and ethylene glycol (EG) are reagent grade and used as received. $HAuCl_4$ (trihydrate) and $HAuBr_4$ (trihydrate) are purchased from Aldrich and used as received. Sodium bromide, sodium chloride, and poly (vinylpryloindone) (PVP) (MW=55,000) are used as received. Solutions are placed in 1cm or 1mm cuvettes for measurements. All solutions are made by dissolving $HAuCl_4$ or $HAuBr_4$ in the stated solvent. Concentrated hydrochloric acid and sulfuric acid are used as received. The refractive index of the solvents was obtained from the CRC Handbook of Chemistry and Physics.[13]

For irradiation experiments, solutions in ethylene glycol are made up to contain 0.0023M gold ions, using either the chloride salt or the bromide salt. The concentration of PVP in the final solutions is 0.010M per repeat unit. Then 0.1M solutions of the opposite sodium salt in EG is added. The pH is below 3 in all studies so that the hydrolysis equilibrium may be safely ignored. The sample is placed in a 1cm x 1cm x

3cm quartz cuvette (or a 0.1cm x 1cm x 3cm quartz cuvette for initial decrease of Au^{3+} studies) for irradiation with a xenon lamp (LPI-250, PTI power controller) operated at 50W. In the light path are a lens to focus the light, aluminum screening to control the intensity, and a band pass filter to control the wavelengths of irradiation (Filter A ~250-400nm, Filter B ~350-525nm). The power at the sample is ~45mW.

Effect of Changing the Solvent on the Absorption Spectra of $AuCl_4^-$

Results

The absorption of $AuCl_4^-$ is investigated in water and different alcohols. A 10nm red shift is observed as the solvent is changed from water to ethylene glycol. This shift is observed to be continuous as a function of ethylene glycol content as shown in Figure 1. The intensity of the absorption also increases as ethylene glycol is added to the solution. Solvent mixtures are produced for this binary solvent system with the absorption maximum intensity and wavelength are plotted in Figure 8-1b and 8-1c, respectively. A continuous shift in both the maximum intensity and wavelength are observed as the mole fraction of glycol increased.

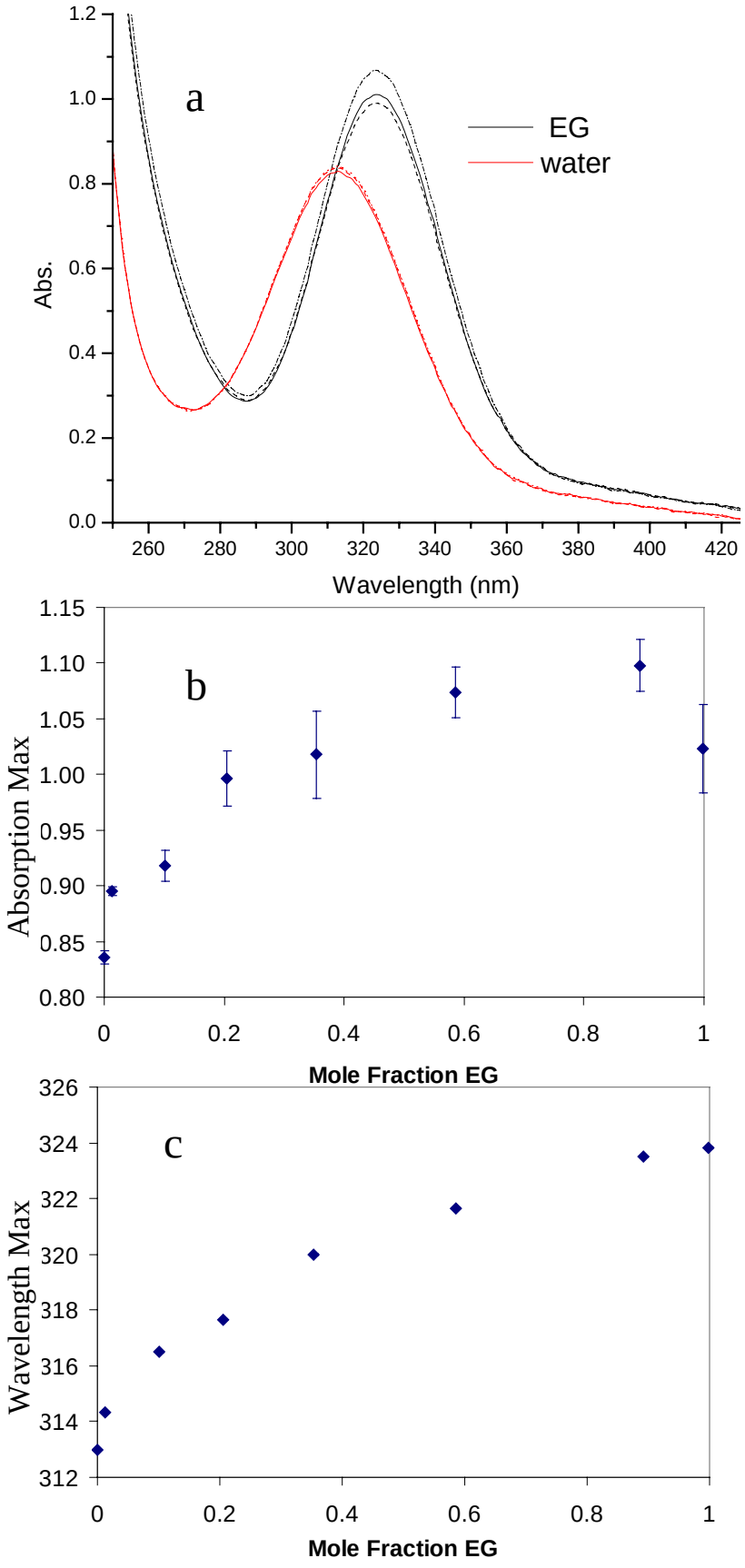

Figure 8-1: *a) Absorption spectra of $2.4x10^{-3}M\ AuCl_4^-$ in water and ethylene glycol. b) Absorption intensity as a function of mole fraction ethylene glycol. c) Wavelength maximum position as a function of mole fraction ethylene glycol.*

To further investigate the absorption spectrum of $HAuCl_4$, the absorption spectrum is measured as a function of gold ion concentration in water and simple alcohol solutions. The absorption spectra of $1.66x10^{-4}$M $HAuCl_4$ with 0.065M HCl in various solvents are shown in Figure 8-2. The absorption spectrum of the aqueous solution is shifted from the absorption spectra of $AuCl_4^-$ in the alcohol solutions. The absorption maximum of the alcohol solutions remained constant as the concentration increased. The intensity of $AuCl_4^-$ absorption is found to linearly increase in the concentration range observed for all of the alcohol solutions, obeying Beer's law. The absorption coefficient, ε of $AuCl_4^-$ is determined by linear fits to the absorption intensity as a function of the gold concentration in different alcohol solvents with the values of the absorption coefficient listed in Table 8-1. The absorption coefficient increased from methanol, ethanol, to ethylene glycol and finally isopropyl alcohol. The absorption coefficient of $AuCl_4^-$ in water from the literature values is between the absorption coefficient in ethanol and ethylene glycol.

Table 8-1: *The absorption coefficient and maximum wavelength for $AuCl_4^-$ in different solvents with the refractive index from CRC.*[13] a) literature values[1, 6]

Solvent	Absorption Coefficient (1/M cm)	Wavelength max (nm)	Refractive Index
MeOH	4900	320.2	1.3288
EtOH	5100	321.1	1.3611
IPA	6100	321.4	1.3776
EG	5900	323.6	1.4318
Water (in Acid) [a]	5500	315	1.33

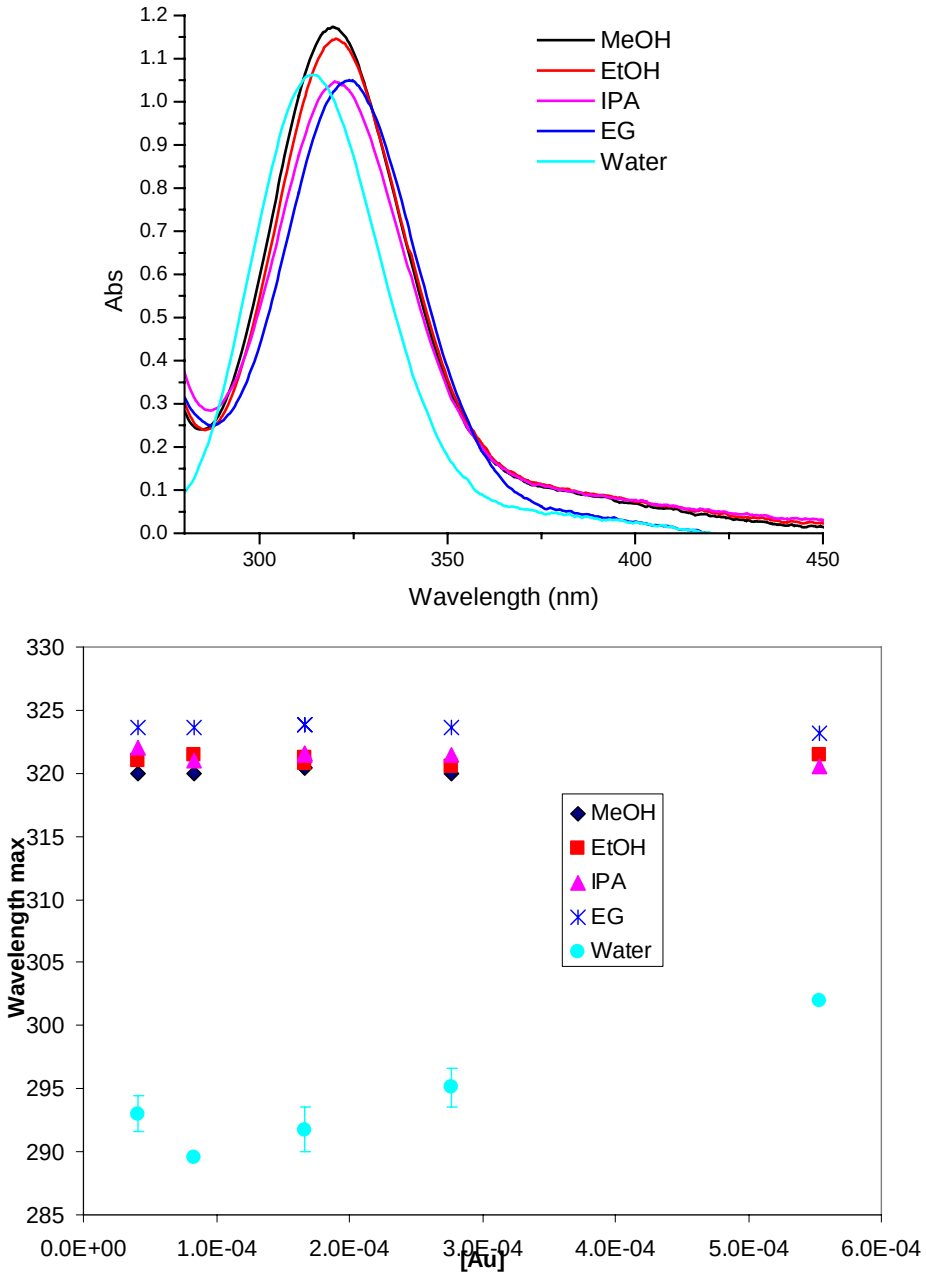

***Figure 8-2**: a) Absorption of 1.66x10^{-4}M $HAuCl_4$ with 0.065M HCl in various solvents (1mm cuvette) b) maximum wavelength of absorption of $AuCl_4^-$ at different concentrations in different solvents.*

The behavior of the absorption spectra of the aqueous solution is different from the absorption spectra observed in alcohol solutions. As the concentration of $HAuCl_4^-$ increased the absorption spectrum of the aqueous solution red shifted and increased in intensity. This is due to the hydrolysis equilibrium, which interacts with the aqueous sample.[5-8]

To investigate the shift in the absorption maximum of $AuCl_4^-$ in water as its concentration changes due to hydrolysis effects, concentrated hydrochloric acid and sulfuric acid are added to $1.66x10^{-4}$M $HAuCl_4$ in different solvents. The intensities and wavelengths of the maximum absorption are plotted in Figure 8-3a and 8-3b, respectively. Adding acid shifts the aqueous absorption spectrum to 315nm, where the spectrum remains constant, as described in the literature.[6] Adding acid to ethylene glycol has very little effect on the maximum wavelength or the intensity. For methanol, ethanol and, isopropyl alcohol solutions the absorption maximum wavelength remained relatively constant while the intensity increased with increasing acid concentration, and a new spectral feature was observable at 270nm at high acid concentrations.

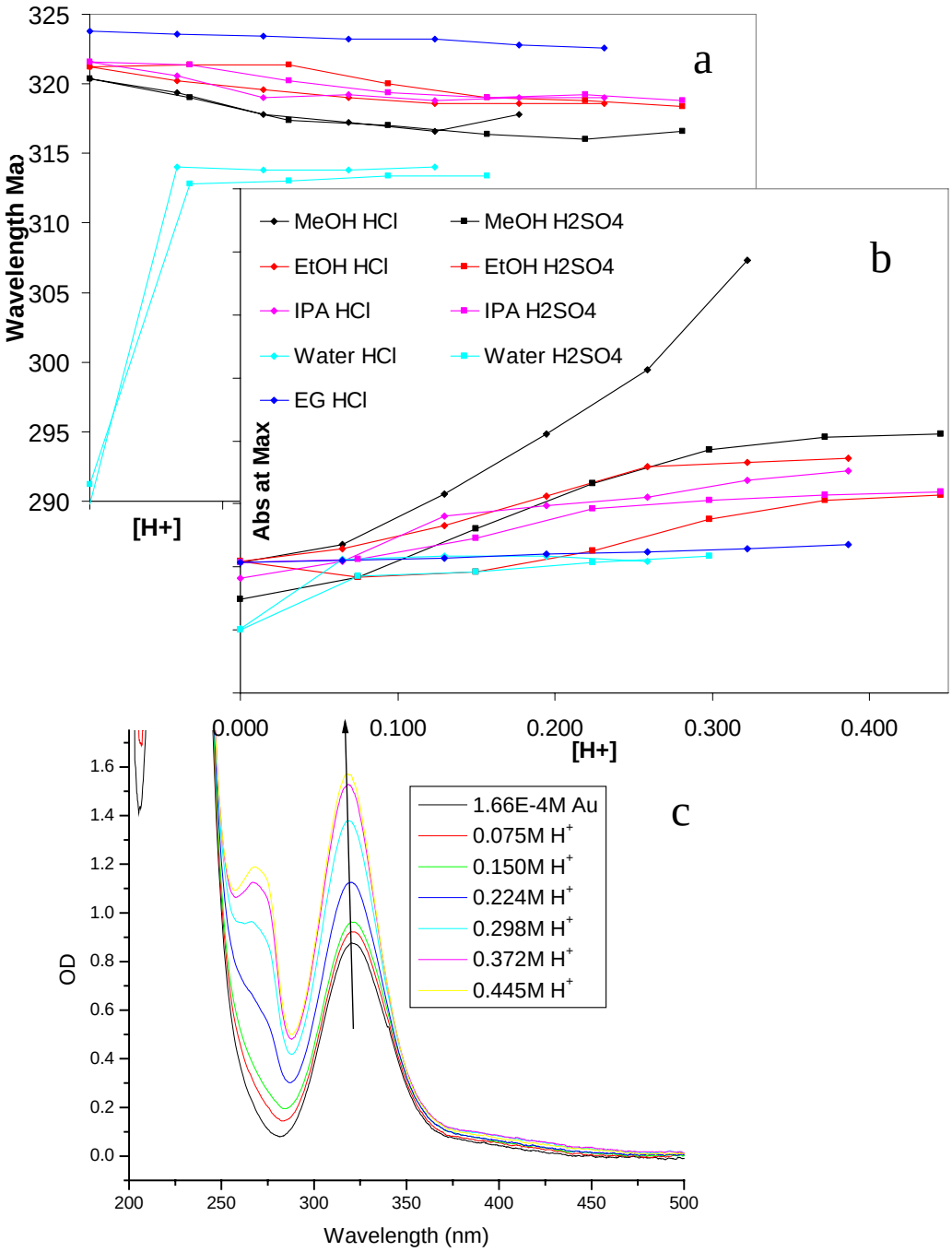

Figure 8-3: *Absorption maximum of 1.66x10^{-4}M $AuCl_4^-$ as a function of the concentration of hydrogen ion added to the solution from HCl or H_2SO_4 a) absorption intensity b) wavelength maximum and c)absorption spectra of 1.66x10^{-4}M $AuCl_4^-$ in ethanol with added acid*

Discussion of Results

The change in the absorption spectrum in water and alcohol solutions show the importance of considering side reactions and solute concentrations in all solutions. The absorption spectrum of $AuCl_4^-$ in water behaves differently than the absorption spectrum in the alcohols. The hydrolysis of $AuCl_4^-$ is a well known reaction occurring at high pH's.[8, 14] The hydrolysis at low chloride and hydrogen ion concentrations in aqueous solutions is observed in the spectra of $AuCl_4^-$ at low concentrations. This is observed by the shift in of the absorption maximum between 290-315 nm and the low absorption intensity. As the concentration of $AuCl_4^-$ increases, so does the pH due to use of the acid as the starting material ($HAuCl_4$). At higher pH's, the hydrolyzed species is the dominant state. The absorption coefficient reported for $AuCl_4^-$ in water is 4800 $M^{-1}cm^{-1}$ (315nm) in acidic solution,[1, 6] This is similar to the ε calculated in all of the alcohols studied seen in Table 8-1. The hydrolysis can explain the shift in the absorption of the aqueous solution shown in Figure 8-3b, and plays a major role in dilute solutions. However, the effect of acid dissociation and hydrolysis are not a large contribution in any alcohol solution.

To understand the shift of the absorption spectra as the solvent is changed, the origin of the absorption spectra is examined. The absorbance of $AuCl_4^-$ is due to charge transfer from the halide ions to the metal ion.[1-3] Thus the amount of charge available for transfer and the field strength around the chloride ions will affect the energy levels of the electrons, and thus the absorption spectrum. The amount of hydrogen bonding available is different for the four different solvents.[15] Water has the largest hydrogen bonding ability of all of the solvents investigated.[15] Thus the hydrogen from the water is more available than hydrogen from the alcohol to transfer charge into the chloride ions. The

reason for the larger hydrogen bonding ability of water is the large electronegativity of the oxygen atom.[15] In alcohols, a carbon is attached to the oxygen atom, which is able to support some of this excess charge. Water only has two hydrogen atoms, which do not stabilize the excess charge from the lone pair of electrons from the oxygen atom. The charge transfer results in a slight shift of the energy levels of the chloride electrons. Thus the absorption of $AuCl_4^-$ in water has larger energy of absorption than in the alcohol solvents as observed from the blue shift of the absorption spectrum.

The hydrogen atom of water is also better hydrogen bonding than the hydrogen atom in R-OH. This is due to the fact that the R groups in the alcohols are better in satisfying the electronegative oxygen atom in the OH bond than the hydrogen atom in H_2O. These two facts make the hydrogen bond between the water hydrogen and the long pairs of electrons of the Cl^- much stronger. This in turn makes the energy required to transfer an electron from the Cl^- to Au^{3+} higher. This is a simple explanation for the observed higher absorption frequency for the complex in water compared to alcohols.

An additional factor could be responsible for the larger energy of absorption of $AuCl_4^-$ in water is that the water can complex with Au^{3+} ion using a pair of its electrons on the oxygen. This makes it more difficult to transfer the electron from Cl^- to the Au^{3+} in water. This electron transfer be should be less efficient for the R-OH than the water molecule due to steric factors.

The concentrations of $HAuCl_4$ used in photochemical experiments are higher than those reported here, safely allowing the hydrolysis of gold chloride to be ignored in future chapters. The pH is found to be very low for solutions used, even in alcohol solutions. The pH for standard conditions in ethylene glycol is >1.

Ethylene glycol is an ideal solvent, due to its insensitivity to hydrolysis or shifting the absorption spectrum of $AuCl_4^-$ due to concentrations of gold, hydrogen or chloride ions. The slight shift from the absorption published for $AuCl_4^-$ in water relative to ethylene glycol is due to the hydrogen bonding of the solvent and refractive index differences from water. These solutions will be used in the following sections as the starting material for direct photochemical reduction.

Calculating Number of Br^- Ions Attached to Gold in Ethylene Glycol

The absorption spectrum of a solution of $HAuCl_4$ shifts to the red as sodium bromide is added to the solution.[9, 10] This is due to the replacement of the chloride ions with bromide ions attached to the gold ion.[9, 10] This reaction proceeds step-wise and can be followed by the absorption spectrum. This section quantifies the shift of the absorption spectrum in ethylene glycol to determine the number of bromide ions attached to a gold cluster.

Due to the difference in the stability of gold chloride and gold bromide in solution, the concentration of opposite salt added to the solution does not give the amount of salt attached to gold ions.[9] Thus a spectroscopic method to determine the number of bromide ions attached to each gold ion is presented. This method takes advantage of the molar absorption spectrum reported previously[9-11] of the mixed chloride and bromide gold complexes in water. The change in solvent is accounted for by the linear fit between the absorption maximum of the two absorption peaks for each $AuCl_4^-$ and $AuBr_4^-$ in water (pH < 3) and ethylene glycol as shown in Figure 8-4.

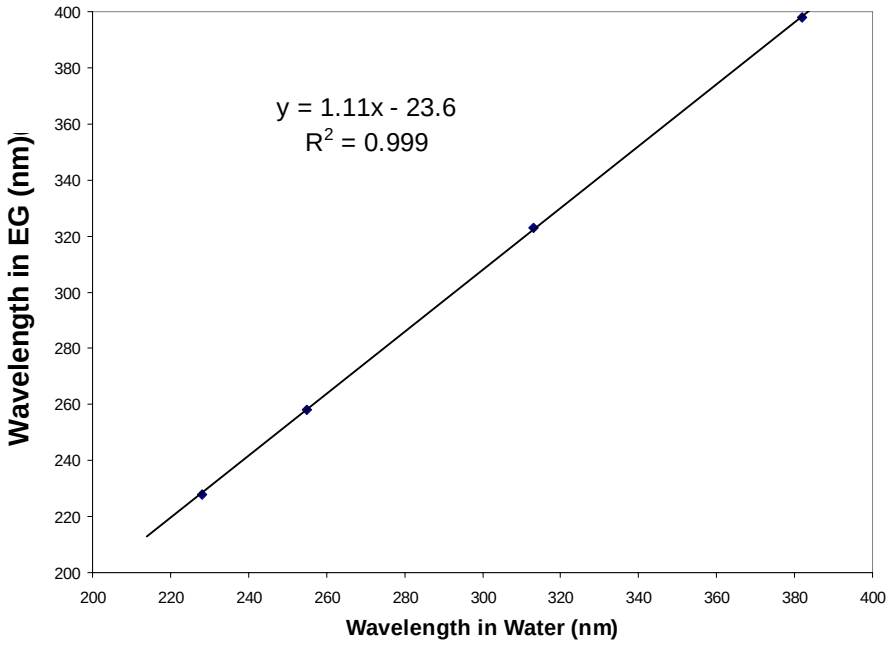

Figure 8-4: *Maximum absorption wavelength of $AuCl_4^-$ and $AuBr_4^-$ in water and ethylene glycol*

The absorption spectrum of $AuCl_4^-$, $AuCl_3Br^-$, $AuCl_2Br_2^-$, $AuClBr_3^-$, and $AuBr_4^-$ have been reported previously in water.[9, 11] To obtain the absorption spectrum of these species in ethylene glycol, the linear relationship obtained in Figure 4 between the absorption wavelength in water and ethylene glycol can be used to obtain the absorption spectrum in ethylene glycol. The results of this are shown in Figure 8-5.

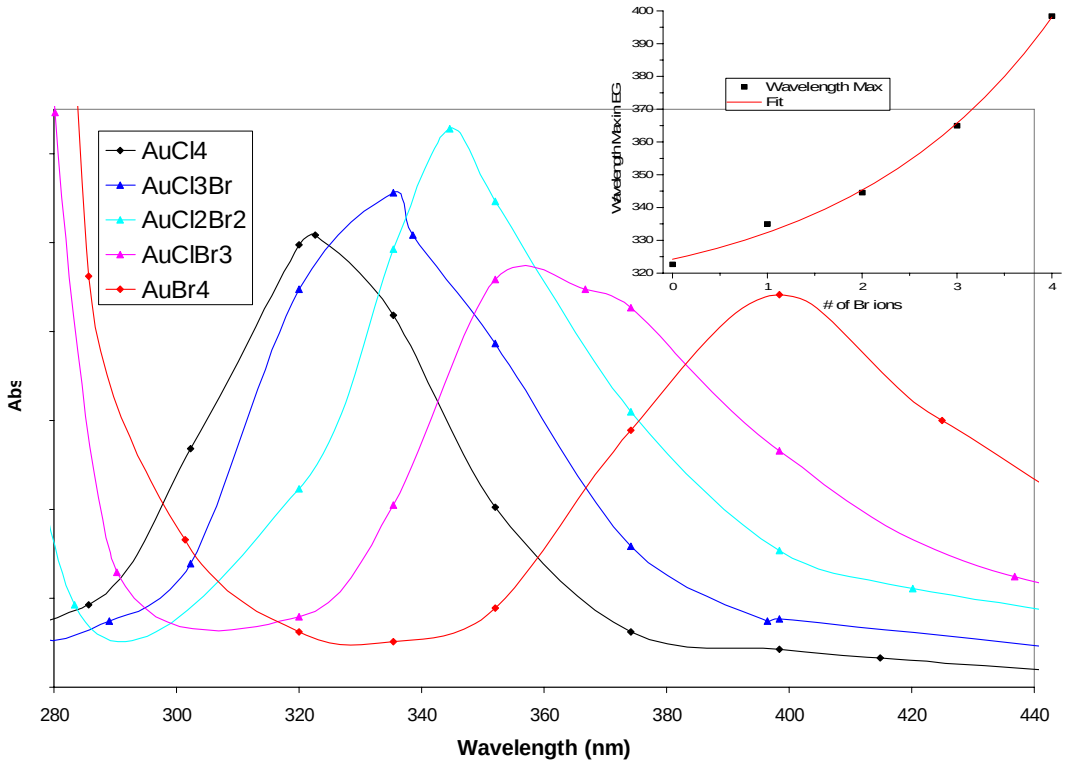

Figure 8-5: *Absorption spectrum calculated from literature values and modified to correct for the ethylene glycol solvent. Inset) fit of the wavelength maximum of each complex taken from the absorption spectrum shown in the main frame as a function of the number of bromide ions in the complex*

These absorption spectra shown in Figure 8-5 can be used to determine which intermediates absorb at different wavelengths in this region and what species are present in a solution. The maximum absorption wavelength of each species can also be used to determine the number of bromide ions attached to a gold ion in solution. The wavelength maximum for each species is plotted against the number of bromide ions in the complex as shown in the inset of Figure 8-5. Then the data is fit with an empirically determined function to enable determination of the number of bromide ions attached to gold ion in solution from the absorption spectrum in ethylene glycol solution. The wavelength

maximum (λ_{max}) and the number of bromine ions (#Br) obtained from Figure 8-5[9-11] are used to obtain the following empirical relationship.

$$\#Br = 14.0 * e^{\lambda_{max}/2.18} + 310 \qquad (8.5)$$

This relationship gives the average number of bromide ions attached to a gold ion from spectroscopic measurements in ethylene glycol.

Investigating Reduction of Complexes with Both Chloride and Bromide Ions

To investigate the effect of the bromide ion on the photoreduction, molecules with both chloride and bromide ions attached to the same gold ion are made by addition of the opposite sodium salt as reported previously.[9-12] The photoreduction of $HAuCl_4$ in ethylene glycol has been reported previously[4] and will be discussed in more detail in Chapter 9. The absorption of $AuCl_4^-$ leads to the ignition of the reduction of the gold ions to form gold nanoparticles after further reduction with the solvent ethylene glycol and disproportionation reactions of the gold ions.[4] The absorption spectra of $AuCl_4^-$ and $AuBr_4^-$ decrease with irradiation at the same rate for all wavelengths. However, the absorption spectra of $AuBr_4^-$decreases with a slower rate than the absorption spectra of $AuCl_4^-$. Irradiation of a solution with both chloride and bromide ions attached to the gold ion decrease the absorption spectra. The blue side of the absorption spectrum decreases faster, resulting in a wavelength maximum that red-shifts, as shown in Figure 8-6a. This red-shifting shows that the chloride species decrease in absorption intensity is faster than the bromide species. Thus species that initially contain more chloride ions attached to the gold atoms are photoreduced faster. The chloride ions liberated during the irradiation do not replace the bromide ions attached to gold atoms in the sample. However, if a solution with the same initial absorption is prepared from the bromine salt, not as much red

shifting is observed. In order to prepare a solution with the same absorption as Figure 8-6a starting from the bromide salt, a large excess of chloride ions is needed because of the large difference in the binding constants of chloride and bromide ions.[9] When the gold ions are reduced in Figure 8-6b there is a large excess of chloride ions in solution available to displace chloride ions, and the absorption spectrum does not shift as much.

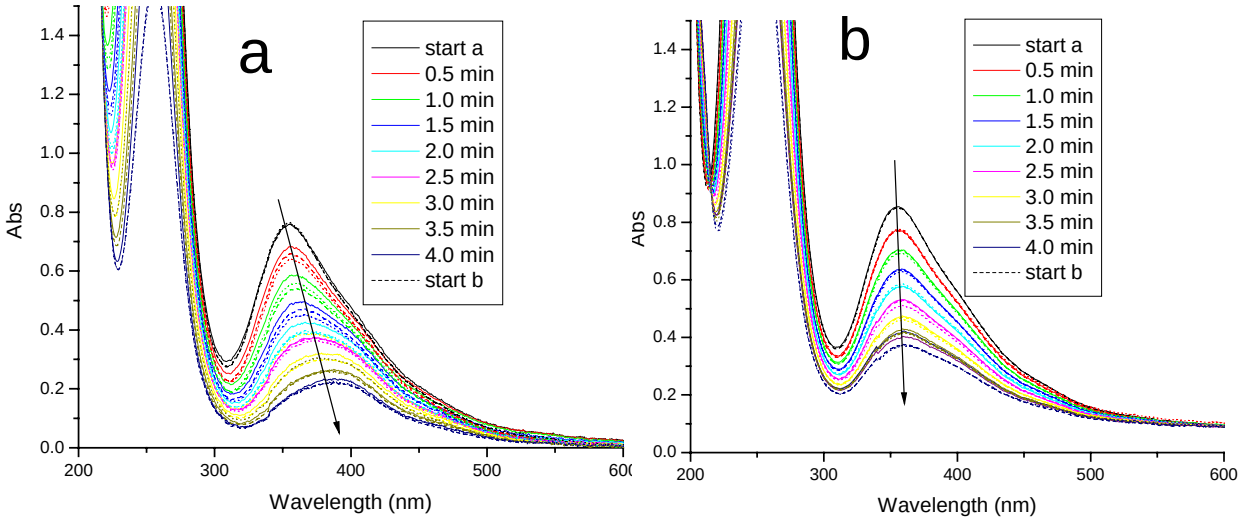

Figure 8-6: *The absorption spectrum during irradiation of a)$HAuCl_4$ + NaBr (#Br = 2.51) b)$HAuBr_4$ + NaCl (#Br = 2.53)*

After irradiation, the halide ions liberated from the gold ions go back into qusi-equilibrium with the bound-species available. If more bromide ions are released during the irradiation, the remaining gold ions bind bromide ions displacing the chloride ions. If enough chloride ions are present in solution to overcome the larger binding energy of bromine, then the chloride ions are able to remain attached to gold ions in the same percentage. This leads to faster overall reduction of the gold complex due to the faster rate of decrease of $AuCl_4^-$.

A number of wavelengths are chosen for rate analysis of samples during irradiation. The wavelengths are chosen to represent the different species present in solution. $AuCl_4^-$ and $AuCl_3Br^-$ are the major components absorbing at 323nm. $AuBr_4^-$ is mostly responsible for the absorption at 425nm. The absorption at 398nm is mostly due to $AuBr_4^-$ and with some absorption from $AuClBr_3^-$. The absorption at 350nm is sensitive to $AuClBr_3^-$, $AuCl_2Br_2^-$ and $AuClBr_3^-$. The absorption at 374nm is more sensitive to $AuCl_2Br_2^-$ and $AuClBr_3^-$, but also due to $AuBr_4^-$ and $AuCl_3Br^-$. By looking at the absorption at all of these wavelengths together the behavior of the sample can be understood.

The rate of decrease for different samples can be compared using the number of bromide ions calculated from equation 8.5 and shown in Figure 8-5. The absorption intensity is normalized to 1 for each wavelength analyzed at time zero. Then the decrease of the absorption is linearly fit for different wavelengths and different samples shown in Figure 8-7 where the maximum absorption wavelength has been used to determine the average number of bromine ions per gold ion using equation 8.5. $HAuCl_4$ and $HAuBr_4$ decrease with the same rate at all wavelengths, and the bromide species reduces slower than the chloride. For samples with mixed populations of chloride and bromide ions, a gradual decrease in the rate is observed as more bromide ions are attached to each gold ion. Thus the wavelengths on the chloride side decrease faster for all of the solutions studied, showing that species the chloride ions continue to be reduced.

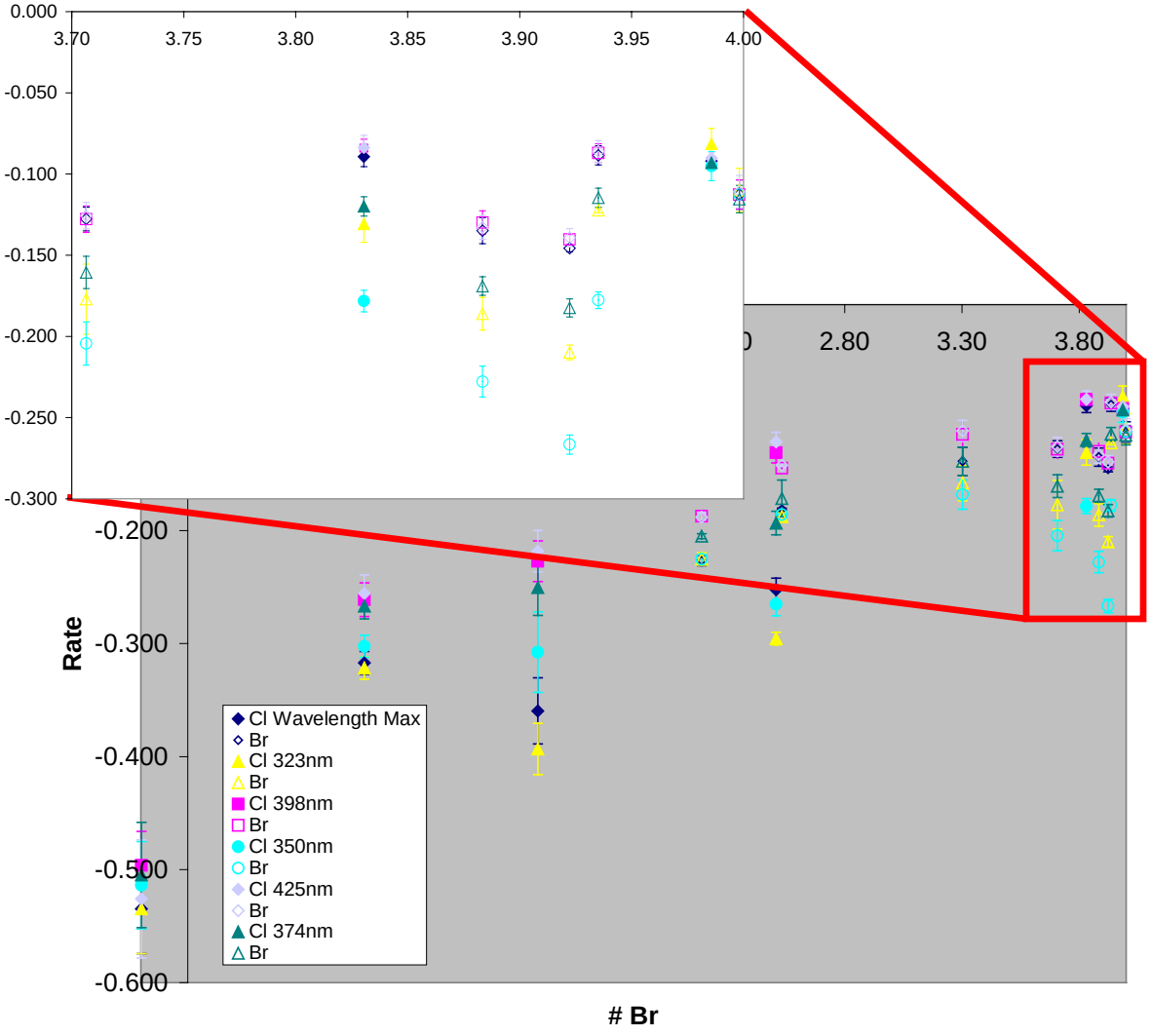

Figure 8-7: *Rate of decrease of absorption at different wavelengths during irradiation with 250-400nm light. Samples starting with $HAuCl_4$ are shown with solid symbols, and samples starting with $HAuBr_4$ are shown with open symbols. Inset: Blow up of high percentage bromide ions.*

The rate of decrease is less when even one bromide ion is added to each gold ion showing the importance of a single bromide ion. This species is still observed to form nanoparticles, but formation of nanoparticles is not observed from solutions with 2 bromide ions for each gold ion. This behavior is not obvious from the rate data, where a continual shift is observed as the number of bromide ions increases. This suggests that a point is reached where the rate of reduction crosses a threshold of generating enough atoms to nucleate nanoparticle growth.

The samples shown in Figure 8-6 with #Br = 2.5 are observed in Figure 8-7 to have the same rates within error bars 398nm and 425nm 375nm. However, the rates 350nm and 323nm are different. Thus once the original species with more than two ions chloride have been reduced there are no new ones to replace them due to the availability of bromide ions to replace them. The absorption is able to decrease faster because it is not being replaced from solution.

Interesting behavior is observed when the number of bromide ions per gold ion is between 3.7 and 4 as shown in the inset of Figure 8-7. In this region the rate at 350nm exhibits a maximum with the number of bromine ions equal to 3.93. Similar behavior is observed from the rates at 323nm and 374nm. As seen in Figure 8-7 this suggests that $AuCl_2Br_2^-$ is being formed even with the majority of the ions bound to gold are bromide as calculated by #Br of 3.93. Similar rates at 350nm are present at a number of bromide ions as 3.93 as 2.5 further suggesting that some $AuCl_2Br_2$ is present in the samples with #Br close to 4.

Summary

The absorption spectrum of $AuCl_4^-$ is due to the charge transfer from the halide ion to the metal ion. The absorption spectrum is sensitive to the solvent and the hydrolysis state of $AuCl_4^-$. Hydrolysis is only an important reaction in water, and not in other solvents. The change in the absorption spectrum is due to the ability of the solvent to hydrogen bond with the $AuCl_4^-$ species. The largest hydrogen bonding is observed in water. The hydrolysis can be overcome by excess hydrogen or chloride ions. These are important conditions for irradiation experiments where the absorption is largest in the un-hydrolyzed species.

When the chloride ions are replaced by bromide ions, the absorption spectrum red shifts depending on the number of bromide ions attached to a gold ion. An equation to determine the number of bromides on a single gold ion is generated allowing the spectroscopic determination of the number of bromide ions complexed to the gold ion. Increasing the number of bromide ions attached to the gold ion slows down the photochemical reaction due to the larger solution stability of this species.

References

1. Chakravorty, A., U.V. Spectrum of $KAuCl_4$. *Naturwissenschaften* **1961,** 48, 375.

2. Chakravorty, A., Comments on the Colour of Alkyl-Gold(III) Complexes. *Naturwissenschaften* **1961,** 48, 643.

3. Gangopadhayay, A. K.; Chakravorty, A., Charge Transfer Spectra of Some Gold (III) Complexes. *J. Chem. Phys.* **1961,** 35, (6), 2206-2209.

4. Eustis, S.; Hsu, H.-Y.; El-Sayed, M. A., Gold Nanoparticle Formation from Photochemical Reduction of Au3+ by Continuous Excitation in Colloidal Solutions. A Proposed Molecular Mechanism *J. Phys. Chem. B* **2005,** 109, (11), 4811-4815.

5. Chateau, H.; Gadet, M.-C.; Pouradier, J., Electrochimie des Sels D'Or III. - Hydrolyse des aurichlorures et des auribromures. *J. Chim. Phys.* **1966,** 63, (2), 269-271.

6. Fry, F. H.; Hamilton, G. A.; Turkevich, J., The Kinetics and Mechanism of Hydrolysis of Tetrachloroaurate(III). *Inorg. Chem.* **1966,** 5, (11), 1943-1946.

7. Rich, R. L.; Taube, H., The Induced Exchange of Cl^- and $AuCl4^-$. Evidence for Au(II). *J. Phys. Chem.* **1954,** 58, (1), 6-11.

8. Robb, W., Kinetics and Mechanisms of Reactions of Gold(III) Complexes. I. The Equilibrium Hydrolysis of Tetrachlorogold(III) in Acid Medium. *Inorg. Chem.* **1967,** 6, (2), 382-386.

9. Elding, L. I.; Gronong, A.-B., Kinetics, Mechanism and Equilibria for Halide Substitution Processes of Chloro Bromo Complexes of Gold(III). *Acta. Chem. Scand. A* **1978,** 32, (9), 867-877.

10. Pouradier, J.; Coquard, M., Électrochimie des sels D'Or V.-Complexes Mixtes Aurichlorobromure. *J. Chim. Phys.* **1966,** 63, (7-8), 1072-1078.

11. Almgren, L., The Stability Constants of Mixed Chloro-Bromo-Aurate (III) Complexes. *Acta. Chem. Scand. A* **1971,** 25, (10), 3713-3720.

12. Louw, W. J.; Robb, W., Kinetics and Mechanism of Reactions of Gold(III) Complexes. II. The Formation and Equilibrum Hydrolysis of Tetrabromoaurate (III). *Inorg. Chim. Acta* **1974,** 9, 33-37.

13. Lide, D. R., *CRC Handbook of Chemistry and Physics*. 80th ed.; CRC Press LLC: Washington, DC, 1999.

14. Mironov, I. V.; Sokolova, N. P.; Makotchenko, E. V., Activities of the Components in the Chloroauric Acid-Perchloric Acid-Water System. *Russian J. Phys. Chem. (translation of Zhurnal Fizicheskoi Khimii)* **1999,** 73, (11), 1780-1784.

15. Taft, R. W.; Kamlet, M. J., The Solvatochromic Comparison Method. 2. The α-Scale of Solvent Hydrogen-Bond Donor (HBD) Acidities. *J. Am. Chem. Soc.* **1976,** 98, (10), 2886-2894.

CHAPTER 9

GOLD NANOPARTICLE FORMATION FROM PHOTOCHEMICAL REDUCTION OF TETRACHLOROAURIC(III) ACID BY CONTINUOUS EXCITATION IN COLLOIDAL SOLUTIONS; A PROPOSED MOLECULAR MECHANISM[††]

Abstract

A photochemical reduction of tetrachloroauric(III) acid with continuous 250-400nm excitation is studied in ethylene glycol and polyvinylpyrrolidone (PVP). PVP is used as the capping material. After the absorption of tetrachloroauric(III) acid disappears, excitation is stopped. The surface plasmon absorption of gold as well as the thermal reappearance of the Au^{3+} absorption are found to increase as a function of time. The rates of these changes are studied as a function of the mole fraction of ethylene glycol in water. Experimental results show that a small amount of ethylene glycol increases the formation of gold nanoparticles, and decreases the reformation of the Au^{3+} absorption after irradiation. Increasing the glycol concentration first increases the rate of formation of gold nanoparticles to a maximum at a mole fraction 0.40. As the glycol concentration is further increased, the rate of formation of the gold nanoparticles and the rate of reformation of Au^{3+} decrease. A mechanism is proposed which involves the reduction of the excited Au^{3+} to Au^{2+} by ethylene glycol. This is followed the

[††] Reproduced with permission from Eustis, S.; Hsu, H.-Y.; El-Sayed, M. A., Gold Nanoparticle Formation from Photochemical Reduction of Au^{3+} by Continuous Excitation in Colloidal Solutions. A Proposed Molecular Mechanism *J. Phys. Chem. B* **2005,** 109, (11), 4811-4815. Copyright 2005 American Chemical Society.

disproportionation of Au^{2+} to Au^{3+} and Au^{1+}. Both the reduction of Au^{1+} by ethylene glycol and its disproportionation lead to the formation of Au^0, which upon nucleation and growth form Au nanoparticles.

Introduction

Many new synthetic methods are being developed to control nanoparticle shape and size.[1-6] However, much remains to be learned about the detailed mechanism of the formation of metal nanoparticles. Considerable attention has been focused on metal nanoparticles because of their optical,[3, 7] catalytic[8] and electronic properties.[8] Gold nanoparticles are known to have a strong plasmon resonance absorption in the visible region due to the collective oscillation of free electrons in the conduction band.[3] Metal nanoparticles are being used for optical sensors,[9, 10] bioconjugation,[11-13] and SERS enhancement.[12, 14] As more is understood about the properties and the mechanism of formation of these nanoparticles, a better control of their size, shape and applications can be achieved.

Most methods of colloidal synthesis use thermal reduction of metal ion salts. Some electrochemical methods have been developed.[6, 15] Recently, photochemical reduction methods have been developed to produce metal nanoparticles.[16-36] Various different approaches are used in photochemical reduction such as use of a photosensitizer,[16-20] use of dendrimers as stabilizers,[21, 22] or placement of metal salts in polymer films.[19, 23-26] Light has also been used to modify the shape of nanoparticles.[27-29] Since both the precursor salt ($AuCl_4^-$)[37-39], and the final product (gold nanoparticles) [3, 7] are colored, the progress of the reaction forming gold nanoparticles can be followed optically. Many researchers have noticed that the color of $AuCl_4^-$ disappears before gold

nanoparticle absorbance appears, indicating the presence of at least one intermediate state.[30-35, 40] Gachard et al[40] describe the stability of Au^{1+} as the only possible intermediate with the appropriate lifetime to explain the observed absorption behavior. Han and Quek attributed formation of gold nanoparticles to the dissociation of $AuCl_4^-$ in the solvent, formamide.[31] Zhao et al[23] attribute formation of nanoparticles to multi-photon process of 800nm fs irradiation light to form electrons capable of reducing $AuCl_4^-$ to Au^0. Kurihara et al[33] generate gold nanoparticles with γ-irradiation, and laser irradiation to study transient absorption spectrum and presence of intermediates. Yonezawa et al[35] show an increase in the region of Au^{3+} absorption for increasing dark times, but fail to recognize the significance. Longenberber and Mills[32] suggest that disproportion of Au^{1+} is responsible for formation of gold nanoparticles, but offer no data to support this mechanism. Malone et al[25] discuss possible mechanisms of formation inside polymer gels by photochemical and solvent reduction. It has also been suggested that the surfactant plays an important role in the formation of nanoparticles through micelle formation.[36] Pre-formed nanoparticles are able to catalyze disproportionation.[40, 41] This chapter hopes to discuss the previous models in light of the new results we obtained to present a mechanism for formation of gold nanoparticles by photochemical reduction.[42]

Ethylene glycol has many attractive properties as a solvent, and has been used extensively for metal nanoparticle formation via the polyol process.[1, 2, 15, 43-47] It is also a viscous solvent slowing down diffusion, and is capable of providing reducing species, without the need for a separate reducing agent.[1, 45, 46] The polyol process uses very high temperatures(160^oC – 280^oC) to achieve reduction of the metal ions.[1, 45, 46]

We show that cw UV irradiation is able to reduce the same species at room temperature. We used cw excitation and ethylene glycol, known to be a reducing agent in the thermal reduction of metal ions, to make metal nanoparticles. The importance of water and ethylene glycol to the rate of formation of metal nanoparticles was studied. The rate of reformation of Au^{3+} absorption is examined in relation to the rate of formation of the nanoparticle absorption after stopping the irradiation. From all of these results, a mechanism is presented in which the gold nanoparticles formed from Au^0, which are proposed to be produced from the disproportionation of the gold in its higher oxidation states as well as by glycol reduction.

Experimental

The sample presented in the first two figures is made up with 82μL of 0.083M $HAuCl_4 \bullet 3H_2O$, 78μL of 0.375M (per repeat unit) polyvinylpyrrolidone (PVP) (55,00 MW), and 0.50mL of water in 2.2mL of ethylene glycol (EG). The total volume of water plus ethylene glycol is kept constant at 2.7mL for all samples. The pH is below 3 in all studies so that the hydrolysis equilibrium may be safely ignored. The sample is placed in a 1cm x 1cm x 3cm quartz cuvette (or a 0.1cm x 1cm x 3cm quartz cuvette for initial decrease of Au^{3+} studies), and irradiated with a xenon lamp (LPI-250, PTI power controller) operated at 54W, with a lens to focus the light, aluminum screening to control the intensity, and a band pass filter to control the wavelengths of irradiation (~250-400nm). The power at the sample is ~50mW. All reactions take place at room temperature, with no heat detected by feel when the solution is removed from irradiation. The optical absorbance spectra were recorded on a Shimadzu UV-3101-PC UV-Vis-NIR scanning spectrometer. The size distribution was determined from TEM images using

100kV on JEOL100 transmission electron microscope (TEM) and Image J (NIH)[48] for image analysis.

The effect of different gasses was carried out by generating the solution, and allowing it to purge in with stated gas for at least 10 minutes prior to irradiation. A volume of 2.7 mL of solution was removed from the purged solution, and placed in a quartz cuvette. Parafilm was used to cover the top of the solution, and the solutions were not purged during irradiation. Three consecutive samples were removed, with the final solution purged for the longest time. Solutions were protected from the light while purged with gasses. The same concentrations of $HAuCl_4$ and PVP are used as described above.

Results and Discussion

Effect of Water on Reaction

The experiments presented here describe the formation of gold nanoparticles using a photochemical reduction in various concentrations of ethane glycol. The irradiation wavelengths were selected with a bandpass filter to match the absorption of the Au^{3+}. The effect of the irradiation on the gold solutions is observed by following the UV/Vis spectrum as shown in Figure 9-1a. The absorbance of the Au^{3+}, centered at 323nm, decreases during irradiation. After all of the Au^{3+} absorbance disappears, a peak is observed to form around 550nm, representing the formation of gold nanoparticles in solution. The irradiation is stopped after 36 minutes, and the solution is left in the dark. The absorption spectrum is followed as a function of time after the irradiation was stopped as shown in Figure 9-1b.

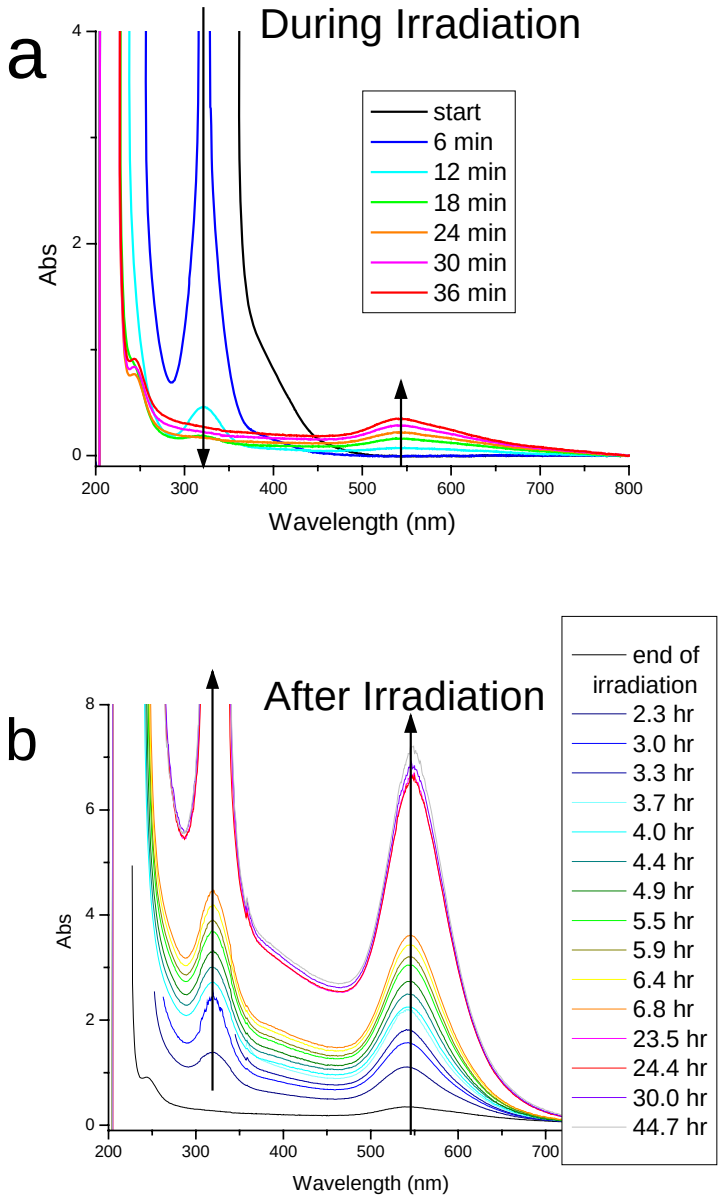

Figure 9-1: *(a) Absorbance of sample during irradiation of gold salt solution with xenon lamp and band pass filter for times listed. (b) Absorbance of sample after irradiation was stopped for times listed. Growth of nanoparticles (545nm) and Au^{3+} (323nm) is observable. Both figures are from a sample that contains 2.4 x 10^{-3}M $HAuCl_4$, 0.010M PVP, and 0.59 mole fraction ethylene glycol.*

As the time increases after irradiation was stopped, the plasmon resonance of gold nanoparticles increases. The absorbance of regenerated Au^{3+} is also found to increase as the time increases, without a shift in the absorption spectra from the starting material. At the end of irradiation there is no absorbance due to Au^{3+}, all of the gold salt initially present is reduced during irradiation. At the end of irradiation a small shoulder is observed at 244nm, very close to the absorption reported for $Au^{(1+)}Cl_2^-$ at 246nm by experimental reports[49] and theoretical predictions.[50, 51] Au^{3+} is reformed during the thermal formation of the gold nanoparticles after irradiation. TEM was used on samples that are spotted immediately after irradiation. This showed the sample in Figure 9-1 contained >90% spheres, with an average size of 7.2nm and a standard deviation of 6nm with over 700 particles counted. The distribution showed a tailing behavior, with the presence of small nanoparticles ~4nm in diameter and a large tail of larger nanoparticles.

Figure 9-2a shows the time dependence of the absorbance of the plasmon resonance absorption of the gold nanoparticles (545nm) and that of the Au^{3+} salt (323nm) after irradiation was stopped. Both of these absorbance's increase linearly with time initially, with initial slopes of 0.510, and 0.245 abs/hr, for the nanoparticles (at 545 nm) and the Au^{3+} (at 323 nm), respectively. The extinction coefficient reported for $AuCl_4^-$ is 4800 $M^{-1}cm^{-1}$ in acidic solution,[38, 52] close to the coefficient reported for Au nanoparticles per Au atom 3200 to 4700 $M^{-1}cm^{-1}$,[40] thus allowing a direct comparison of the absorbance of these two species. The ratio of the initial rate of formation as determined from the initial rate of increases of gold nanoparticles absorbance to Au^{3+} absorbance is 2.08 for this sample.

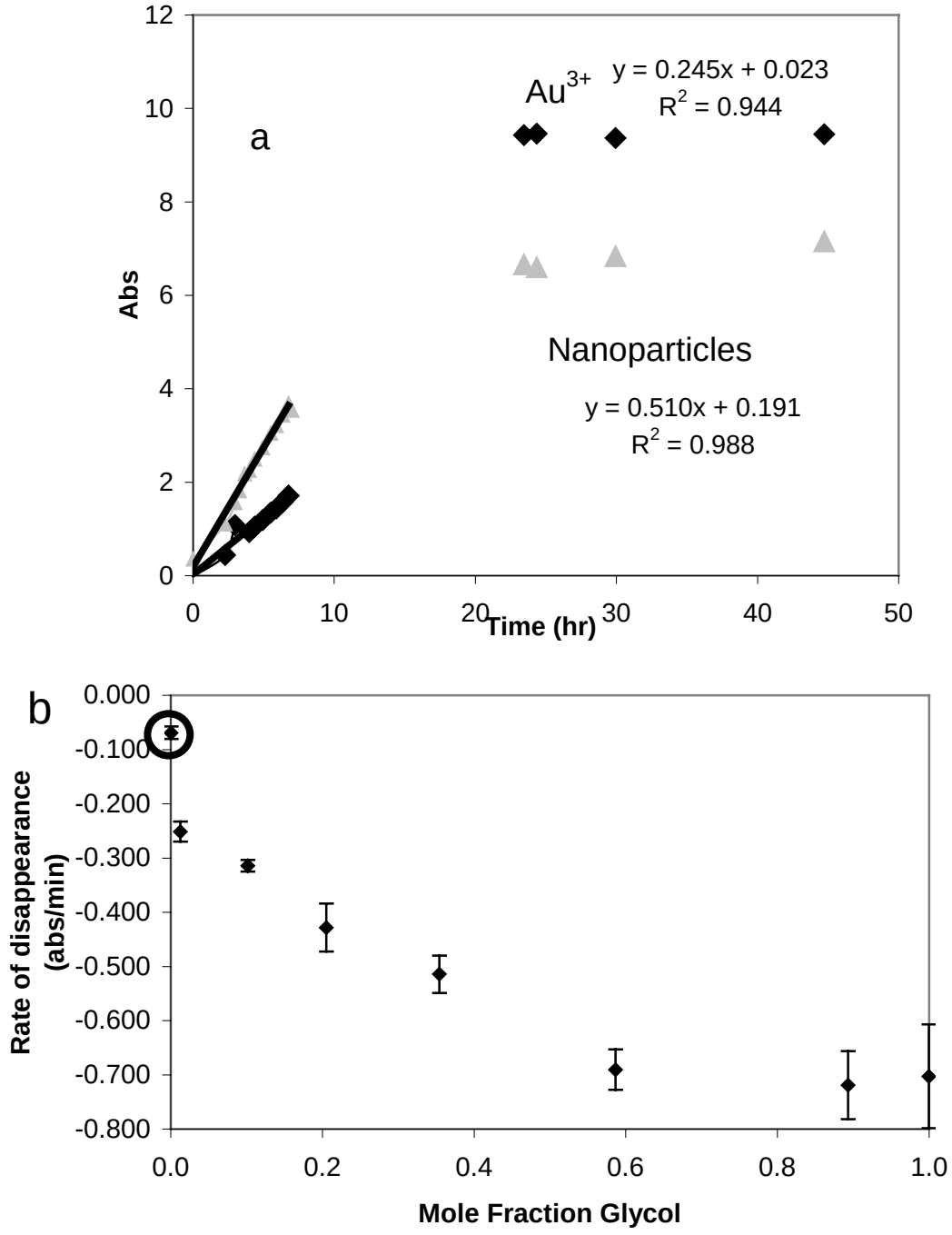

Figure 9-2: *(a) Plot of the absorbance maximum of Au^{3+} and gold nanoparticles as a function of time after the irradiation is stopped. Initially this sample contains 2.4 x 10^{-3}M $HAuCl_4$, 0.010M PVP, and 0.59 mole fraction EG (same sample as Figure 1). (b) Plot of the rate of disappearance of Au^{3+} during initial irradiation as a function of glycol mole fraction. (The sample with no ethylene glycol is circled) These samples contain 2.4x10^{-3}M $HAuCl_4$, 0.010M PVP, and water to replace glycol.*

At a later time the line's slope of the formation of the Au nanoparticle slows down. The rate for the Au nanoparticles absorption decreases faster than that for Au^{3+} due to the fact the gold nanoparticles are found to precipitate out of solution as Au metal powder, as observed visually.

The initial absorption decrease of Au^{3+} during irradiation was followed as a function of glycol concentration in Figure 9-2b. The absorbance of each sample at the maximum of the Au^{3+} charge transfer band was measured, as irradiation proceeded. The initial decrease was measured using a 1 mm cuvette, but the same concentrations. The initial decrease was linearly fit, and the rate of disappearance is taken from the slope of the absorbance decrease. Solutions with high glycol concentrations have large rates of disappearance. The rates of decrease can be measured on the order of minutes; showing not every excited molecule is stable as an intermediate. This suggests that the disproportionation of intermediates is taking place during irradiation, reforming $Au^{(3+)}Cl_4^-$. Adding water decreases the rate of disappearance of the Au^{3+}. When all of the glycol is removed, the reaction became slower, indicating that the glycol is important for the disappearance of Au^{3+} by the direct reduction of Au^{3+} to Au^{2+} by ethylene glycol. This process is diffusion controlled at low glycol concentrations.

Many samples were prepared with different ratios of water to ethylene glycol to study the kinetics after stopping the irradiation. The equations of the initial rate of reformation of Au^{3+} as well as the rate of formation of nanoparticles were calculated. Figure 9-2a presents these results for one sample. The collected rates (taken from the slopes of the observed lines as shown in Figure 9-2a) are found in Figure 9-3a where the formation rates are plotted for the Au^{3+} salt and the nanoparticles for many different

glycol ratios. The maximum intensity of the plasmon resonance absorption of the nanoparticles formed 1 hour after irradiation was stopped is calculated from the fits similar to that shown in Figure 9-2a for a sample with 0.59mole fraction of glycol. This absorbance should be proportional to the yield of nanoparticles 1 hour after irradiation was stopped. This is plotted in Figure 9-3b for different ethylene glycol concentrations. A drastic transition is observed when a small amount of ethylene glycol is added to the system as observed in both Figure 9-3a and 9-3b. The yield of nanoparticles produced during irradiation of the pure water sample is close to zero. Longer irradiation times do produce nanoparticles in pure water, so it is possible to produce nanoparticles in a water solvent system possibly due to reduction by PVP or water itself. However, adding a small percentage of ethylene glycol to the solution produces large amounts of nanoparticles for the same irradiation time. The rate of reformation of Au^{3+} is observed to be much higher in the case of pure water than when a small volume of ethylene glycol is added to the solution. This is most likely due to the higher concentration of gold transients, which have not formed gold nanoparticles. A maximum rate of formation of gold nanoparticles is obtained at 0.40 mole fraction of glycol.

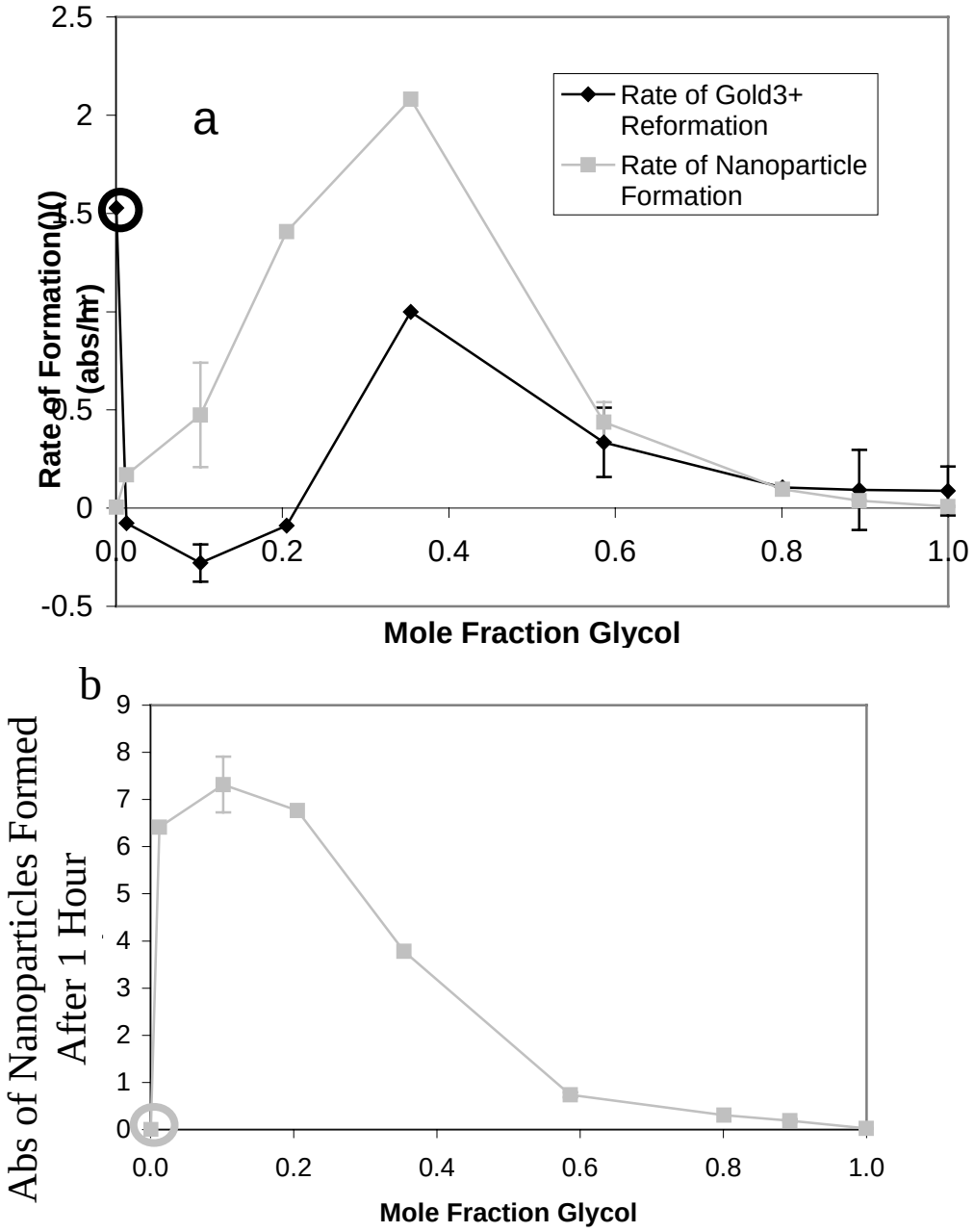

Figure 9-3: *(a) Plot of the initial rate (10-20 hr.) of formation of gold nanoparticles and reformation of Au^{3+} after irradiated is stopped as a function of the glycol mole fraction. The data is taken from fits to data similar to that shown in Figure 9-2a. (b) The intensity at the maximum of nanoparticle plasmon resonance absorption formed 1 hour after irradiation (which is proportional to concentration) from equations similar to those generated in Figure 9-2a plotted as a function of the glycol mole fraction. The sample with no ethylene glycol is circled. The initial samples contain 2.4 x 10^{-3} M $HAuCl_4$, 0.010M PVP, and water to replace glycol.*

These results point to a mechanism underlying the photochemical reduction of Au^{3+} to finally form Au atoms, which nucleate and grow into nanoparticles. Previous mechanisms rely on a transient absorption spectra observed by Ghosh-Mazumdar and Hart[53] which was attributed to Au^{2+} formed as a result of electron-beam radiation. Kurihara et. al.[33] observed similar transient spectra after the photoirradiation of a gold solution. They proposed the following mechanism (a) for the formation of gold nanoparticles in a water-n-hexane solvent mixture using nanosecond laser irradiation:[33]

$(HAu^{3+}Cl_4) \xrightarrow{h\nu} (HAu^{3+}Cl_4)^*$	(9.1a)	excitation
$(HAu^{3+}Cl_4)^* \longrightarrow (HAu^{2+}Cl_3\ldots Cl)$	(9.2a)	reduction
$(HAu^{2+}Cl_3\ldots Cl) \longrightarrow HAu^{2+}Cl_3 + Cl$	(9.3a)	dissociation
$2HAu^{2+}Cl_3 \longrightarrow HAu^{3+}Cl_4 + HAu^{+}Cl_2$	(9.4a)	disproportionation
$HAu^{+}Cl_2 \xrightarrow{h\nu} Au^0 + HCl + Cl$	(9.5a)	photoreduction
$nAu^0 \longrightarrow (Au^0)_n$	(9.6a)	nanoparticle formation

This mechanism suggests that first Au^{3+} is excited by the incoming radiation, and then reduced to form Au^{2+}, which is unstable. Au^{2+} disproportionates to form Au^{+} and Au^{3+} (the starting state). The Au^{+} is then suggested to be photoreduced by absorbing another photon. The gold atoms can then get together to form nuclei and gold nanoparticles.

Earlier, Henglein[34] has proposed a mechanism involving the reduction of gold ions with γ-irradiation. Au^{3+} is proposed to be reduced to Au^{2+} by reaction with the electrons formed in the solutions during γ-irradiation. The Au^{2+} is then proposed to disproportionate to Au^{3+} and Au^{+}. Then more irradiation is necessary to reduce Au^{+} to Au^0, which forms gold nanoparticles. Henglein noted that less irradiation is necessary than predicted based on stoichiometric considerations to form Au^0, suggesting that an

autocatalytic mechanism also plays a part in reducing the Au^{3+}. Thus as gold nanoparticles are formed they may catalyze the further reduction of the remaining Au^{3+} or Au^{1+} without additional γ-irradiation.

Our results can be understood with a mechanism that is sensitive to the glycol concentration because of its reducing property as well as its viscous nature. Furthermore, it does not require radiation after the initial excitation of $AuCl_4^-$ as most of the nanoparticles are formed after the irradiation is ceased. The increase in the rate of the disappearance of Au^{3+} during irradiation, and the acceleration of nanoparticle formation (up to a mole fraction of 0.40 of glycol) as glycol is added to the solution strongly suggests the involvement of the glycol in the reduction. This suggests that in addition to its importance in the reduction of excited Au^{3+}, it is probably needed for the reduction of Au^{2+} and Au^{+}. As the glycol mole fraction increases further, the solution becomes viscous, thus slowing down the diffusion controlled reactions, such as the disproportionation reactions that requires the collisions between multiple gold ions. From all theses results, and the previously proposed mechanisms, the reaction mechanism (b) is proposed as follows:

$Au^{(3+)}Cl_4^- \xrightarrow{h\nu} [Au^{(3+)}Cl_4^-]^*$		(9.1b)	Excitation
$[Au^{(3+)}Cl_4^-]^* \xrightarrow{glycol} Au^{(2+)}Cl_3^- + Cl$		(9.2b)	Reduction
$2\ Au^{(2+)}Cl_3^- \longrightarrow Au^{(1+)}Cl_2^- + Au^{(3+)}Cl_4^-$	fast	(9.3b)	Disproportionation
$4\ Au^{(1+)}Cl_2^- \longrightarrow 2\ Au^{(2+)}Cl_3^- + 2\ Au^0 + 2\ Cl^-$	slow	(9.4b)	Disproportionation
$3\ Au^{(1+)}Cl_2^- \longrightarrow Au^{(3+)}Cl_4^- + 2\ Au^0 + 2\ Cl^-$		(9.5b)	Net Disproportionation
$Au^{+m} \xrightarrow{glycol} Au^0$ (+m: +3,+2,+1)		(9.6b)	Glycol Reduction
$nAu^0 \longrightarrow (Au^0)_n$	rapid	(9.7b)	Nanoparticle Formation

The initial steps are the same as those presented by Kurihara et al[33] where the gold ion absorbs the incoming photon and is reduced to the 2+ state. Previous researchers have suggested that disproportionation reactions are catalyzed by pre-formed nanoparticles in the solution.[40, 41, 54] Whether step 9.4b could be catalyzed to be competitive with step 9.6b in transforming Au^{1+} to Au^{0} is not known.

The results presented in Figure 9-2b and Figure 9-3 suggest that the glycol is able to reduce the excited Au^{3+} ions as shown by the large increase in the yield of formation of gold nanoparticles with a small addition of ethylene glycol to the system. (Ethylene glycol is known to thermally reduce gold to form nanoparticles at elevated temperatures (160-280^{o}C, but not at room temperature.[1, 45, 46]) Thus, the light excites the gold to a state where ethylene glycol can reduce it at room temperature as shown in step 9.2b and 9.6b of our mechanism. This suggests that the excited state is more readily reduced by glycol than the ground state. Au^{2+} is an unstable species,[55] and is not observed at equilibrium, thus it is proposed to disproportionate quickly.[56] Thus the disproportionation of Au^{2+} feeds the disproportionation of Au^{+}, which is a much slower reaction.[41, 57, 58] The cycling of these two disproportionation reactions leads to the net disproportionation reaction shown in equation 9.5b. The reaction rate is known to be slow, due to the stability of the Au^{+} and the need for the combination of multiple species. Equation 9.5b might be the rate-limiting step in the formation of gold nanoparticles. Thus, this is a diffusion-limited process and sensitive to the viscosity of the solution. Ethylene glycol is a viscous liquid, and is miscible with water. Thus, as its mole fraction increases, the solution viscosity increases, and the rate of disproportionation reactions decreases.

The rate of disproportionation increases as the ethylene glycol content decreases due to decreasing the viscosity of the solvent. The rate of reduction by ethylene glycol increases with the increasing concentration of glycol. These two opposite effects of increasing glycol content, taken together, can explain the observed maximum shown in Figure 9-3a. The rate of formation of gold nanoparticles achieves a maximum rate at a glycol mole fraction of 0.40. Glycol seems to reduce Au^{1+} to Au^{0} at room temperature, as glycol is needed to form nanoparticles. The final step in the mechanism is the association of the gold atoms to form gold nanoparticles, which are detected by their plasmon resonance absorbance.

Investigation of the Mechanism

There are two important parameters that determine the rate of reformation of Au^{3+} after irradiation. The concentration of the intermediate present in solution and the viscosity changes in the solution as the percentage of ethylene glycol in the solution is increased. Thus, the concentrations of the intermediate gold species and ethylene glycol are important, as the gold intermediate determines the amount of material available for further reaction. The viscosity is important in diffusion-controlled reactions, such as disproportionation in order to form gold in the neutral state, necessary for the formation of gold nanoparticles.

One of the slow steps in the formation of gold nanoparticles is the disproportionation of Au^{1+} to form gold zero. The disproportionation is a diffusion-limited reaction, which can be modeled by the Stokes-Einstein equation.

$$D = \frac{RT}{6\pi\eta a} \qquad (9.8)$$

Thus the diffusion (D) can be modeled with the temperature (T), the radius of particles diffusing though solution (*a*) and the viscosity of the solution (η). Thus the rate of a diffusion-controlled reaction is changed as the solvent viscosity increases and can be modeled by the inverse of the viscosity of the solvent. The only parameter in this equation that is changing in the current experiment is the viscosity as the atoms involved in the disproportionation are constant as is the temperature, allowing the radius and temperature to be ignored. As water is replaced by ethylene glycol in the solution, the viscosity increases. To determine the viscosity of the different solutions, the viscosity of water and ethylene glycol are used along with the mole fractions of each substance for each solution.

The concentrations of ethylene glycol and Au^{1+} are important parameters of this mechanism. The concentration of EG is determined from the amount of ethylene glycol added to solution. Determining the concentration of Au^{1+} is less strait forward due to the absence of the absorption of this species, and changes with the concentration of ethylene glycol.

In order to determine the concentration of Au^{1+} in these solutions, the amount of Au^{0} and Au^{3+} present are used. The gold atoms do not disappear as the reaction proceeds, so the total number of gold ions and atoms must remain constant in the solution. Thus the total concentration of gold in the solution is a constant throughout the reaction and can used to determine the concentration of intermediates. Both Au^{0} and Au^{3+} have visible absorption, enabling the determination of the concentration of these species in solution. The concentration of Au^{2+} is ignored due to the short lifetime (<μs) compared to the time scale (minutes) investigated in this system. Thus the total

concentration of gold ions in solution $[Au]_t$ must be a sum of the concentration of gold in the neutral state $[Au^0]$, the 1+ state $[Au^{1+}]$, and the 3+ state $[Au^{3+}]$. This expression can be used to obtain the expression for the concentration of Au^{1+} as follows.

$$[Au^{1+}] = [Au]_t - [Au^{3+}] - [Au^0] \qquad (9.9)$$

However, the concentration of the species can be replaced with the integral of the area of the gold absorption to determine the amount of the different species present in solution. Thus the total integrated area of the initial Au^{3+} absorption (~400) is proportional to the total gold concentration, $[Au]_t$. However the maximum observed intensity of gold nanoparticles is around ~900 for many solutions. Thus the area of absorption of the two gold states is not the same for the same number of atoms. In order to calculate the concentration of Au^{1+} at the end of the irradiation, a relationship that insures the integrated area of absorption represents the same number of atoms for all species is required. The amount of integrated area of Au^{3+} absorption is calculated before irradiation is begun and the maximum integrated absorption of gold nanorods after many days is used to obtain a relationship between the intensities. The proportionally constant, α, is used to take into account the larger absorption per atom observed for gold nanoparticles.

$$\alpha = \frac{\left(I_{Au^0}\right)_{final}}{\left(I_{Au^{3+}}\right)_{final}} \qquad (9.10)$$

The integral of the area of the gold nanoparticle absorption and the Au^{3+} absorption are determined at the end of irradiation. The equation for the concentration of Au^{1+} (equation 9.9) can be rewritten in terms of the integrated absorption areas of the total gold (I_{Au_t}), Au^{3+} ($I_{Au^{3+}}$), gold nanoparticles (I_{Au^0}), and the proportionality constant (α),

calculated in equation 9.10 so that all integrated areas are calculated relative to the absorption coefficient of Au^{3+}.

$$I_{Au^+} = I_{Au_t} - I_{Au^{3+}} - \frac{I_{Au^0}}{\alpha} \qquad (9.11)$$

This allows the concentration of Au^{1+} to be determined for each experimental sample. The results of equation 9.11 are shown in Figure 9-4.

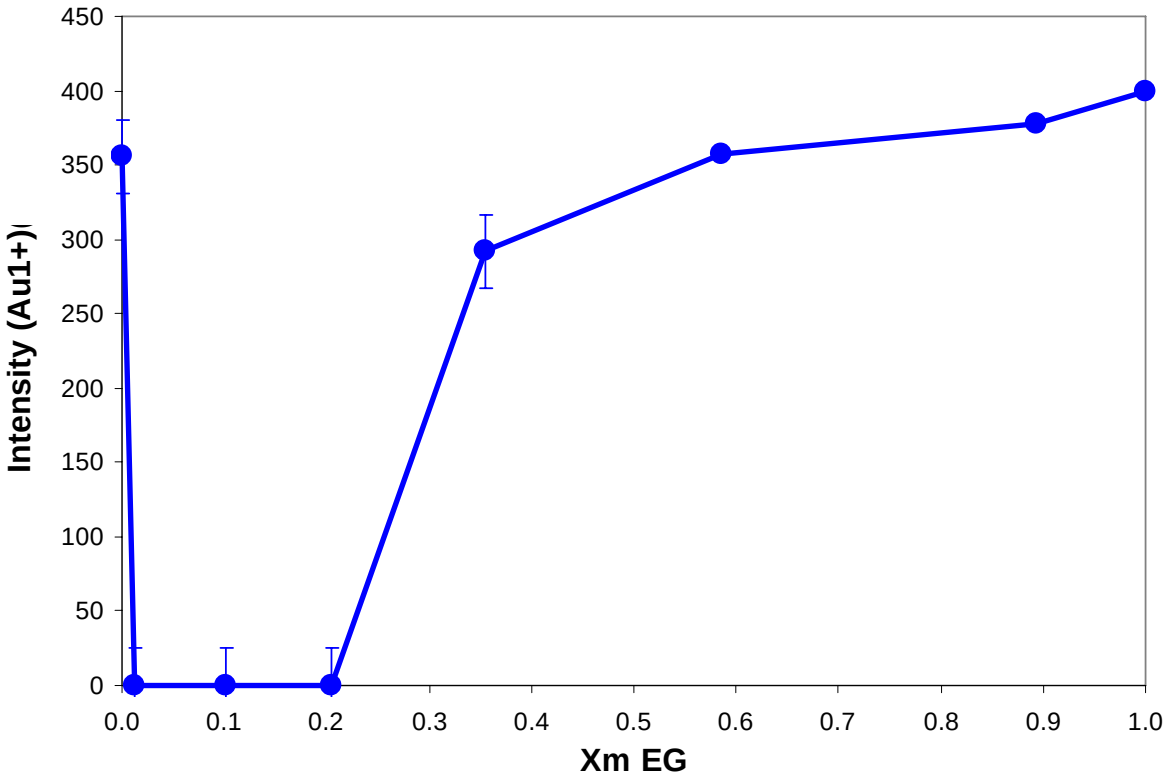

Figure 9-4: *The integrated area of the absorption of Au^{1+} assuming the same integrated absorption area as Au^{3+} as a function of mole fraction ethylene glycol. The concentration decreases with small increases in the glycol concentration as it acts as a reducing agent. Further addition of ethylene glycol slows down the diffusion, and thus fewer nanoparticles are formed, leading to the larger presence of Au^{1+} in the sample.*

As seen from Figure 9-4, the $(Au^{3+})^*$ excited state can be reduced to form Au^{1+} by the alcohol or by water. When no ethylene glycol is present and at high ethylene glycol concentrations, the amount of Au^{1+} is similar to the initial amount of Au^{3+} showing that all of the Au^{3+} has been reduced to Au^{1+}. The irradiation conditions are set up such that all of the Au^{3+} is removed during the irradiation conditions. Thus only a weak reducing agent is necessary to reduce the $(Au^{3+})^*$ excited state to Au^{1+}.

However, after a small amount of ethylene glycol is added to the water sample, the calculations show that there is no free Au^{1+} in solution. This behavior can be explained by comparing Figure 9-4 to Figure 9-3b, showing the amount of nanoparticles formed 1 hour after irradiation. Figure 9-3b shows the large number of nanoparticles formed with the addition of a small amount of ethylene glycol. Thus instead of Au^{1+} reaming in stable in solution as observed in the water solution, nanoparticles are formed from the Au^{1+} with the glycol present. Thus water is not a strong enough reducing agent to form gold nanoparticles from the Au^{1+} salt. This shows the importance of the ethylene glycol to reduce the gold ions to form Au^0. Thus the absence of the Au^{1+} in solution after irradiation is due to the reduction by ethylene glycol to form gold nanoparticles.

This data is also able to explain why the maximum of the rate of reformation of Au^{3+}, the rate of formation of gold nanoparticles and the number of nanoparticles all shown in Figure 9-3 do not appear at the same mole fraction ethylene glycol. If most of the gold ions have already formed nanoparticles, the rate to form more nanoparticles will be less due to the limited supply of starting material or in this case Au^{1+}. As the mole fraction of ethylene glycol increases, the amount of nanoparticles in solution decreases, leaving some Au^{1+} in solution, but still a large amount of mobility leading to large rates

of formation of gold nanoparticles and reformation of Au^{3+}. The maximum rate of formation of nanoparticles and the reformation of Au^{3+} in the sample with 0.40 mole fraction ethylene glycol is expected to be dominated by disproportionation of Au^{1+}.

Increasing the mole fraction ethylene glycol also decreases the rate of the diffusion-controlled reactions, such as disproportionation due to the increase in the viscosity of the solvent with added ethylene glycol. The disproportionation is sensitive to the viscosity due to the need for two metal centers to interact. Thus the disproportionation does not happen until two different metal centers diffuse to the same location. Then the electrons and atoms can rearrange, but fist they must come into contact. Thus the viscosity of the solution is also important in the photochemical formation of gold nanoparticles.

The effect of the absence of ethylene glycol is clearly shown in Figure 9-4 where a small addition of ethylene glycol reduces the concentration of Au^{1+} ions. At higher mole fractions of ethylene glycol the amount of Au^{1+} in solution is similar to the aqueous solution. However, a decreasing rate of formation of gold nanoparticles and reformation of Au^{3+} show the important effect of the increasing viscosity at high glycol concentrations. Thus ethylene glycol has two important roles in this reaction. It reduces the gold ions to generate gold nanoparticles, and it also slows down diffusion-controlled reactions such as disproportionation with its large viscosity.

Effect of Purging with Different Gases

To further investigate this system, the solutions were purged with different gases. The absorption spectrum of the different solutions after 36 minutes of irradiation is shown in Figure 9-5. Experimental conditions are described in the experimental section,

but the irradiation conditions are identical to previous solutions except for that the solutions are purged with the specified gas prior to irradiation. The solution that was heated before irradiation was allowed to cool before irradiation to investigate the effects of mixing. These solutions all contain no water, and thus have a high viscosity, leading to slow mixing at room temperature of the stock solution. Heating the solution had only a small affect on the generation of nanoparticles as observed in Figure 9-5. Saturating the solution with N_2 gas generated more nanoparticles with increasing purging time suggesting that dissolved nitrogen gas affects the solution before irradiation. N_2O and O_2

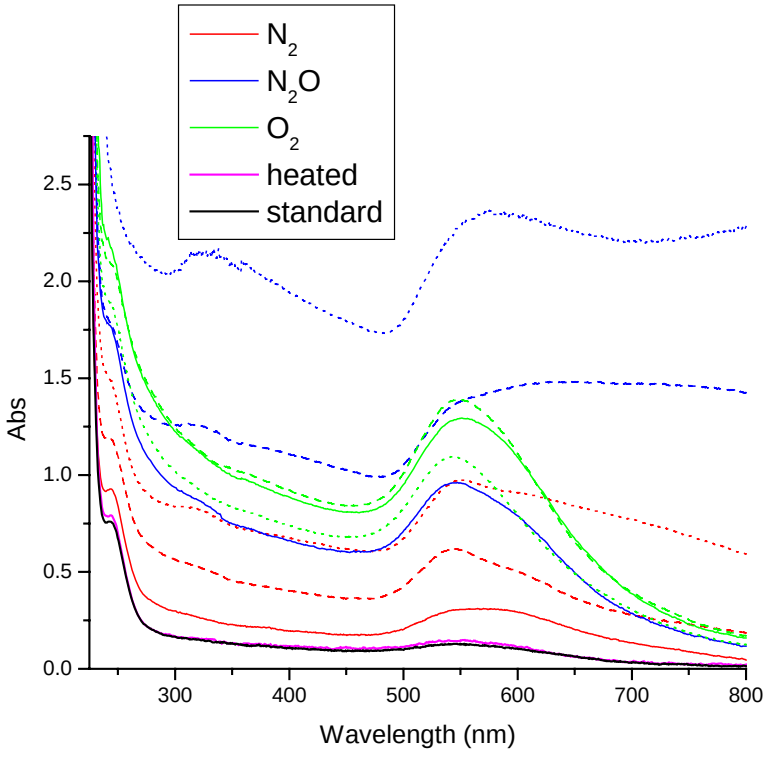

Figure 9-5: *Absorption spectrum after 36 min. irradiation for solutions purged (before irradiation) with different gases. Dotted lines are repeated with longer purging times with the specified gas.*

gases have a similar effect with the ability to generate more nanoparticles with the same amount of irradiation. This suggests that the dissolved gasses can generate nuclei or impurities in solution that are more likely to form gold nanoparticles. It is possible that radicals are created in the solution during irradiation and that can react with O_2 or N_2O in solution to form more radicals similar to that observed with γ-irradiation.[5]

Conclusions

By following the rate of formation of metal nanoparticles and the rate of reformation of Au^{3+}, a mechanism of photochemically synthesized gold nanoparticles is suggested. The reduction of the metal ions by ethylene glycol after photoexcitation is important to drive the formation of gold nanoparticles. The presence of Au^{1+} is suggested by the absence of absorbance of Au^{3+} and gold nanoparticles. The concentration of Au^{1+} is determined from the absorption intensities of Au^{3+} and gold nanoparticles. The disproportionation is also shown to be important in this reaction, as nanoparticles and Au^{3+} are formed after irradiation has stopped. This mechanism is used to generate a model that accounts for the dual effect of ethylene glycol in solution as a reducing agent, and a viscous solvent to slow down disproportionation. Purging the solution with different gases suggest that nuclei or impurities are generated which increase the yield of nanoparticles after photoexcitation of gold ions.

Acknowledgments: The authors wish to acknowledge the financial support of the Nation Science Foundation, Division of Material Research Grant No. 0138391.

References

1. Kim, F.; Connor, S.; Song, H.; Kuykendall, T.; Yang, P. D., Platonic gold nanocrystals. *Angew. Chem. Int. Ed.* **2004,** 43, (28), 3673-3677.

2. Sun, Y. G.; Xia, Y. N., Shape-controlled synthesis of gold and silver nanoparticles. *Science* **2002,** 298, (5601), 2176-2179.

3. El-Sayed, M. A., Some interesting properties of metals confined in time and nanometer space of different shapes. *Acc. Chem. Res.* **2001,** 34, (4), 257-264.

4. Turkevich, J.; Stevenson, P. C.; Hillier, J., A study of the nucleation and growth processes in the synthesis of colloidal gold. *Discuss. Faraday Soc.* **1951,** 11, 55-75.

5. Henglein, A.; Meisel, D., Radiolytic control of the size of colloidal gold nanoparticles. *Langmuir* **1998,** 14, (26), 7392-7396.

6. Yu, Y. Y.; Chang, S. S.; Lee, C. L.; Wang, C. R. C., Gold Nanorods: Electrochemical Synthesis and Optical Properties. *J. Phys. Chem. B* **1997,** 101, (34), 6661-6664.

7. Mulvaney, P., Surface Plasmon Spectroscopy of Nanosized Metal Particles. *Langmuir* **1996,** 12, 788-800.

8. Kamat, P. V., Photophysical, photochemical and photocatalytic aspects of metal nanoparticles. *J. Phys. Chem. B* **2002,** 106, (32), 7729-7744.

9. Ghosh, S. K.; Nath, S.; Kundu, S.; Esumi, K.; Pal, T., Solvent and ligand effects on the localized surface plasmon resonance (LSPR) of gold colloids. *J. Phys. Chem. B* **2004,** 108, (37), 13963-13971.

10. Haes, A. J.; Stuart, D. A.; Nie, S. M.; Van Duyne, R. P., Using solution-phase nanoparticles, surface-confined nanoparticle arrays and single nanoparticles as biological sensing platforms. *J. Fluorescence* **2004,** 14, (4), 355-367.

11. Frederix, F.; Friedt, J. M.; Choi, K. H.; Laureyn, W.; Campitelli, A.; Mondelaers, D.; Maes, G.; Borghs, G., Biosensing based on light absorption of nanoscaled gold and silver particles. *Analytical Chemistry* **2003,** 75, (24), 6894-6900.

12. Cao, Y. C.; Jin, R. C.; Nam, J. M.; Thaxton, C. S.; Mirkin, C. A., Raman dye-labeled nanoparticle probes for proteins. *J. Am. Chem. Soc.* **2003,** 125, (48), 14676-14677.

13. Park, S. J.; Lazarides, A. A.; Storhoff, J. J.; Pesce, L.; Mirkin, C. A., The structural characterization of oligonucleotide-modified gold nanoparticle

networks formed by DNA hybridization. *J. Phys. Chem. B* **2004,** 108, (33), 12375-12380.

14. Doering, W. E.; Nie, S. M., Spectroscopic tags using dye-embedded nanoparticles and surface-enhanced Raman scattering. *Anal. Chem.* **2003,** 75, (22), 6171-6176.

15. Bonet, F.; Guery, C.; Guyomard, D.; Urbina, R. H.; Tekaia-Elhsissen, K.; Tarascon, J.-M., Electrochemical reduction of noble metal compounds in ethylene glycol. *Int. J. Inorg. Mater.* **1999,** 1, 47-51.

16. Mandal, M.; Ghosh, S. K.; Kundu, S.; Esumi, K.; Pal, T., UV photoactivation for size and shape controlled synthesis and coalescence of gold nanoparticles in micelles. *Langmuir* **2002,** 18, (21), 7792-7797.

17. Kapoor, S., Preparation, characterization, and surface modification of silver particles. *Langmuir* **1998,** 14, (5), 1021-1025.

18. Kometani, N.; Doi, H.; Asami, K.; Yonezawa, Y., Laser flash photolysis study of the photochemical formation of colloidal Ag nanoparticles in the presence of benzophenone. *Phys. Chem. Chem. Phys.* **2002,** 4, 5142-5147.

19. Korchev, A. S.; Bozack, M. J.; Slaten, B. L.; Mills, G., Polymer-initiated photogeneration of silver nanoparticles in SPEEK/PVA films: Direct metal photopatterning. *J. Am. Chem. Soc.* **2004,** 126, (1), 10-11.

20. Eustis, S.; Krylova, G.; Eremenko, A.; Smirnova, N.; Schill, A. W.; El-Sayed, M. A., Growth and fragmentation of silver nanoparticles in their synthesis with a fs laser and CW light by photo-sensitization with benzophenone. *Photochem. Photobio. Sci.* **2005,** 4, (1), 154-159.

21. Esumi, K.; Suzuki, A.; Aihara, N.; Usui, K.; Torigoe, K., Preparation of Gold Colloids with UV Irradiation Using Dendrimers as Stabilizer. *Langmuir* **1998,** 14, 3157-3159.

22. Zhou, Y.; Yu, S. H.; Wang, C. Y.; Li, X. G.; Zhu, Y. R.; Chen, Z. Y., A Novel Ultraviolet Irradiation Photoreduction Technique for the Preparation of Single-Crystal Ag Nanorods and Ag Dendrites. *Adv. Mater.* **1999,** 11, (10), 850-852.

23. Zhao, C. J.; Qu, S. L.; Qiu, J. R.; Zhu, C. S., Photoinduced formation of colloidal Au by a near-infrared femtosecond laser. *J. Mater. Res.* **2003,** 18, (7), 1710-1714.

24. Hirose, T.; Omatsu, T.; Sugiyama, M.; Inasawa, S.; Koda, S., Au-nano-particles production by pico-second ultra-violet laser deposition in Au-ion doped PMMA film. *Chem. Phys. Lett.* **2004,** 390, (1-3), 166-169.

25. Malone, K.; Weaver, S.; Taylor, D.; Cheng, H.; Sarathy, K. P.; Mills, G., Formation Kinetics of Small Gold Crystallites in Photoresponsive Polymer Gels. *J. Phys. Chem. B* **2002,** 106, (30), 7422-7431.

26. Stellacci, F.; Bauer, C. A.; Meyer-Friedrichsen, T.; Wenseleers, W.; Alain, V.; Kuebler, S. M.; Pond, S. J. K.; Zhang, Y.; Marder, S. R.; Perry, J. W., Laser and Electron-Beam Induced Growth of Nanoparticles for 2D and 3D Metal Patterning. *Adv. Mater.* **2002,** 14, (3), 194-198.

27. Jin, R. C.; Cao, Y. C.; Hao, E. C.; Metraux, G. S.; Schatz, G. C.; Mirkin, C. A., Controlling anisotropic nanoparticle growth through plasmon excitation. *Nature* **2003,** 425, (6957), 487-490.

28. Jin, R. C.; Cao, Y. W.; Mirkin, C. A.; Kelly, K. L.; Schatz, G. C.; Zheng, J. G., Photoinduced conversion of silver nanospheres to nanoprisms. *Science* **2001,** 294, (5548), 1901-1903.

29. Callegari, A.; Tonti, D.; Chergui, M., Photochemically Grown Silver Nanoparticles with Wavelength-Controlled Size and Shape. *Nano Lett.* **2003,** 3, (11), 1565-1568.

30. Bronstein, L.; Chernyshov, D.; Valetsky, P.; Tkachenko, N.; Lemmetyinen, H.; Hartmann, J.; Forster, S., Laser photolysis formation of gold colloids in block copolymer micelles. *Langmuir* **1999,** 15, (1), 83-91.

31. Han, M. Y.; Quek, C. H., Photochemical synthesis in formamide and room-temperature Coulomb staircase behavior of size-controlled cold nanoparticles. *Langmuir* **2000,** 16, (2), 362-367.

32. Longenberger, L.; Mills, G., Formation of Metal Particles in Aqueous-Solutions by Reactions of Metal-Complexes with Polymers. *J. Phys. Chem.* **1995,** 99, (2), 475-478.

33. Kurihara, K.; Kizling, J.; Stenius, P.; Fendler, J. H., Laser and Pulse Radiolytically Induced Colloidal Gold Formation in Water and in Water-in-Oil Microemulsions. *J. Am. Chem. Soc.* **1983,** 105, (9), 2574-2579.

34. Henglein, A., Radiolytic preparation of ultrafine colloidal gold particles in aqueous solution: Optical spectrum, controlled growth, and some chemical reactions. *Langmuir* **1999,** 15, (20), 6738-6744.

35. Yonezawa, Y.; Kawabata, I.; Sato, T., Photochemical Formation of Colloidal Gold Particles in Chitosan Films. *Ber. Bunsen-Ges. Phys. Chem.* **1996,** 100, (1), 39-45.

36. Leontidis, E.; Kleitou, K.; Kyprianidou-Leodidou, T.; Bekiari, V.; Lianos, P., Gold colloids from cationic surfactant solutions. 1. Mechanisms that control particle morphology. *Langmuir* **2002,** 18, (9), 3659-3668.

37. Chakravorty, A., Comments on the Colour of Alkyl-Gold(III) Complexes. *Naturwissenschaften* **1961,** 48, 643.

38. Chakravorty, A., U.V. Spectrum of $KAuCl_4$. *Naturwissenschaften* **1961,** 48, 375.

39. Gangopadhayay, A. K.; Chakravorty, A., Charge Transfer Spectra of Some Gold (III) Complexes. *J. Chem. Phys.* **1961,** 35, (6), 2206-2209.

40. Gachard, E.; Remita, H.; Khatouri, J.; Keita, B.; Nadjo, L.; Belloni, J., Radiation-induced and chemical formation of gold clusters. *New. J. Chem.* **1998**, 1257-1265.

41. Gammons, C. H.; Yu, Y.; Williams-Jones, A. E., The disproportionation of gold(I) chloride complexes at 25 to 200^{o}C. *Geochim. Cosmochim. Acta* **1997,** 61, (10), 1971-1983.

42. Eustis, S.; Hsu, H.-Y.; El-Sayed, M. A., Gold Nanoparticle Formation from Photochemical Reduction of Au3+ by Continuous Excitation in Colloidal Solutions. A Proposed Molecular Mechanism *J. Phys. Chem. B* **2005,** 109, (11), 4811-4815.

43. Bonet, F.; Delmas, V.; Grugeon, S.; Urbina, R. H.; Silvert, P. Y.; Tekaia-Elhsissen, K., Synthesis of monodisperse Au, Pt, Pd, Ru and Ir nanoparticles in ethylene glycol. *Nanostruct. Mater.* **1999,** 11, (8), 1277-1284.

44. DucampSanguesa, C.; HerreraUrbina, R.; Figlarz, M., Synthesis and Characterization of Fine and Monodisperse Silver Particles of Uniform Shape. *J. Solid State Chem.* **1992,** 100, (2), 272-280.

45. Fievet, F.; Lagier, J. P.; Blin, B.; Beaudoin, B.; Figlarz, M., Homogeneous and Heterogeneous Nucleations in the Polyol Process for the Preparation of Micron and Sub-Micron Size Metal Particles. *Solid State Ionics* **1989,** 32-3, 198-205.

46. Silvert, P. Y.; Tekaiaelhsissen, K., Synthesis of Monodisperse Submicronic Gold Particles by the Polyol Process. *Solid State Ionics* **1995,** 82, (1-2), 53-60.

47. Wiley, B.; Herricks, T.; Sun, Y. G.; Xia, Y. N., Polyol synthesis of silver nanoparticles: Use of chloride and oxygen to promote the formation of single-crystal, truncated cubes and tetrahedrons. *Nano Lett.* **2004,** 4, (9), 1733-1739.

48. ImageJ is a public domain Java image processing program inspired by NIH Image. The source code is freely available. Watershead plugin and other plugins also available. http://rsb.info.nih.gov/ij/ Date Accessed (5/23/06).

49. Kunkely, H.; Vogler, A., Photooxidation of dichloro- and dibromoaurate(1-) induced by ds excitation *Inorg. Chem.* **1992,** 31, (22), 4539-4541.

50. Savas, M. M.; Mason, W. R., Electronic and MCD spectra of linear two-coordinate dihalo-, halo(trialkylphosphine)-, and bis(triethylphosphine)gold(I) complexes *Inorg. Chem.* **1987,** 26, (2), 301-307.

51. Koutek, M. E.; Mason, W. R., Electronic structure and spectra of linear dihaloaurate(I) ions *Inorg. Chem.* **1980,** 19, (3), 648-653.

52. Fry, F. H.; Hamilton, G. A.; Turkevich, J., The Kinetics and Mechanism of Hydrolysis of Tetrachloroaurate(III). *Inorg. Chem.* **1966,** 5, (11), 1943-1946.

53. Ghosh-Mazumdar, A. S.; Hart, E. J., A Pulse Radiolysis Study of Bivalent and Zerovalent Gold in Aqueous Solutions. *Adv. Chem. Ser.* **1968,** 81, 193-209.

54. Kissner, R.; Welti, G.; Geier, G., The hydrolysis of gold(I) in aqueous acetonitrile solutions. *J. Chem. Soc., Dalton Trans.* **1997**, 1773-1777.

55. Rich, R. L.; Taube, H., The Induced Exchange of Cl^- and $AuCl4^-$. Evidence for Au(II). *J. Phys. Chem.* **1954,** 58, (1), 6-11.

56. Baxendale, J. H.; Koulkrd-Pujo, A. M., Une Etude Par Radiolyse Pulsee Sur L'Espece Transitoire Au II. *J. Chim. Phys.* **1970,** 67, 1602-1607.

57. Bard, A. J.; Parsons, R.; Jordan, J., *Standard Potentials in Aqueous Solution*. Marcel Dekker, Inc.: New York, 1985.

58. Lingane, J. J., Standard Potentials of Half-Reactions Involving +1 and +3 Gold in Chloride Medium. Equilibrium Constant of the Reaction AuCl4- +2Au +Cl- = 3AuCl2-. *J. Electroanal. Chem.* **1962,** 4, 332-342.

CHAPTER 10

MOLECULAR MECHANISM OF THE PHOTOCHEMICAL GENERATION OF GOLD NANOPARTICLES IN ETHYLENE GLYCOL: SUPPORT FOR THE DISPROPORTIONATION MECHANISM[‡‡]

Abstract

It is found that replacement of the chloride ions in tetrachloroauric acid with bulky bromide ions inhibits the formation of gold nanoparticles in the photochemical reduction in ethylene glycol. However, the addition of silver ions to either the bromide or the chloride auric acid solution is found to enhance the rate of gold nanoparticle formation. These results are found to be accounted for by the previously proposed mechanism (Eustis, S.; Hsu, H.-Y.; El-Sayed, M. A., *J. Phys. Chem. B* **2005,** 109, 4811) which involves disproportionation of the chloroauric complexes to generate free gold atoms and chloride ions. The steric effects of the bulky bromide ions inhibit the formation of Au-Au bonds needed in the electron transfer process are involved in the disproportionation reaction. The addition of Ag^+ ions results in the formation of insoluble silver halide, which shifts the disproportion reaction towards the formation of gold atoms and thus the formation of gold nanoparticles.

[‡‡] Reproduced with permission from *J. Phys. Chem. B,* submitted for publication. Unpublished work copyright 2006 American Chemical Society.

Introduction

As shown in a previous publication[1] and Chapter 9, a simple mechanism is proposed for the photochemical synthesis of gold nanoparticles from the photoreduction of tetrachloroauric acid in ethylene glycol. The mechanism involves the photoexcitation of the starting material, $[Au^{(3+)}Cl_4]^-$. This starting material is then reduced to the unstable[2] $[Au^{(2+)}Cl_3]^-$ by the solvent, ethylene glycol.[1] This is followed by two disproportionation reactions.[1, 3-6] The $[Au^{(2+)}Cl_3]^-$ is unstable[2] and rapidly forms[1, 3-6] $[Au^{(1+)}Cl_2]^-$ and $[Au^{(3+)}Cl_4]^-$. The $[Au^{(1+)}Cl_2]^-$ is a metastable species,[7] which can then undergo further disproportionation to form $[Au^{(3+)}Cl_4]^-$ and neutral gold, which forms gold nanoparticles in solution. Support for this mechanism came from the observed effect of changing the water-ethylene glycol solvent composition from pure water to pure ethylene glycol on the rate of formation of gold nanoparticles. This allowed the determination of the effect of the reducing power of ethylene glycol, as well as its control of the diffusion controlled disproportionation reaction due to its high viscosity.

To further investigate the mechanism of formation of gold nanoparticles, the effect of substituting the chloride ions in the tetrachloroauric acid by bromide ions as well as the effect of adding silver ions are examined on the rate of the gold nanoparticle formation. Also the effect of adding silver ions to the solution to determine their effect on the nanoparticle formation is examined.

The origin of the absorption of $HAuCl_4$ and $HAuBr_4$ has been studied previously.[8-10] The absorption is due to charge transfer between the chloride (or bromide) ions and gold ion.[8-10] Crystal field theory has been used to calculate the spectrum using dsp^2 hybridization where the electron charge transfer is from the chloride *p* orbital to the

gold *d* orbitals.[10] There are two bands in the absorption spectrum which are assigned to $p_\sigma \rightarrow d_{x^2-y^2}$ and $p_\pi \rightarrow d_{x^2-y^2}$ for the high and low energy transitions, respectively.[8-10] These two absorption bands are used to initiate the photoreduction of gold in alcohol solution by the photoexcitation of $[AuX_4]^-$. Further characterization is presented in Chapter 8.

It is observed that while the tetrachloride complex produces gold nanoparticles the tetrabromide complex does not. The influence of the excited state of gold is found not to be the determining factor in the photochemical formation of gold nanoparticles. We propose that the replacement of the chloride ions with bromide ions sterically slows down the disproportionation processes. This slows down the formation of Au^0 and the subsequent formation of the nanoparticles. We also observed that the addition of silver ions accelerated the formation of gold nanoparticles from either the tetrachloride or the tetrabromide complex. Two possible mechanisms for increasing the rate of formation of gold nanoparticles are proposed. One possible effect is due to the fact that the silver ions shift the disproportion equilibrium forward to favor the formation Au^0 by removing the halide ions (to form insoluble silver halide) that are produced along with the Au^0 in these reactions. The silver ions could also assist in the formation of gold nanoparticles by heterogeneous nucleation.

Experimental

$HAuCl_4$ (trihydrate) and $HAuBr_4$ (trihydrate) are purchased from Aldrich and used as received. Sodium bromide, sodium chloride, silver nitrate, ethylene glycol (EG) and poly (vinylpryloindone) (PVP) (MW=55,000) are used as received. Solutions in ethylene glycol are made up to contain 0.0023M gold ions, using either the chloride salt

or the bromide salt. The concentration of PVP in the final solutions is 0.010M per repeat unit. Silver solutions have 3.50×10^{-4}M $AgNO_3$ for a ratio of Au/Ag ions of 6.81. The pH is below 3 in all studies so that the hydrolysis equilibrium may be safely ignored. The sample is placed in a 1cm x 1cm x 3cm quartz cuvette (or a 0.1cm x 1cm x 3cm quartz cuvette for initial decrease of Au^{3+} studies) for irradiation with a xenon lamp (LPI-250, PTI power controller) operated at 50W. In the light path are a lens to focus the light, aluminum screening to control the intensity, and a band pass filter to control the wavelengths of irradiation (filter ~250-400nm). The power at the sample is ~45mW.

Experimental Results

Comparing the Photochemical Reduction of $HAuCl_4$ and $HAuBr_4$

To further examine the photoreduction of $HAuCl_4$ in ethylene glycol, the chloride ions are replaced with bromide ions. The absorption spectrum red shifts as the chloride is replaced with bromide shown in Figure 10-1. The absorption spectra are similar to those reported previously for $AuCl_4^-$ and $AuBr_4^-$ with the two absorptions due to the electronic transitions of $p_\sigma \rightarrow d_{x^2-y^2}$ at 228nm and 255nm and the $p_\pi \rightarrow d_{x^2-y^2}$ transition at 313nm and 382nm for $AuCl_4^-$ and $AuBr_4^-$, respectively.[8-13] The filter is the same band pass filter used in our previous investigations[1] to allow 250-400nm light to reach the sample. Since the absorption spectrum red shifts in the bromide complex, a different amount of energy is imparted to the gold complex during photoirradiation. The integrated area of $HAuBr_4$ absorbance after correction for the filter is shown in the inset of Figure 10-1, and is 2.3 times larger than the integrated area of the $HAuCl_4$ absorption. Thus the reduction of

$HAuBr_4$ with photoirradiation is expected to be faster than $HAuCl_4$ if it is solely based on absorption probability considerations.

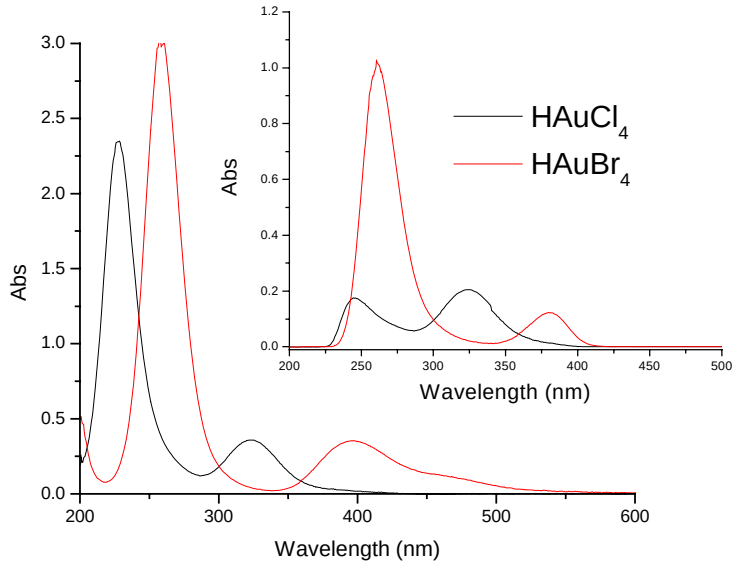

Figure 10-1: *Absorption spectra of $HAuCl_4$ (black) and $HAuBr_4$ (red) (0.023M Au) in ethylene glycol in 1mm cuvette. The inset shows the absorption spectra of the same solutions in the presence of the filter. This shows that in the excitation region used the tetrabromoauric acid absorbs more light than the tetrachloroauric acid.*

Solutions of $HAuBr_4$ are irradiated to determine the effect of replacing chloride with bromide ions. The absorption spectra of this solution are shown in Figure 10-2a as a function of the irradiation time. The reduction is much slower for the bromide complex than for the chloride complex, even though the integrated absorption intensity is larger. If the concentration is increased, the rate of decrease of $AuBr_4^-$ absorption does not change. Furthermore, no nanoparticle absorption is observed as determined from the continuous decrease of the absorbance at all wavelengths, including 500-600nm region where the strong gold nanoparticles plasmon absorption is expected. No nanoparticles

are in TEM of these samples. Longer irradiation times do not generate gold nanoparticles.

The rate of decrease of the absorption spectra due to ligand to metal charge transfer are followed as a function of irradiation time for $HAuCl_4$ and $HAuBr_4$. The rate of the disappearance of the absorption of the complex is calculated from the decrease of the absorption intensity to compare how the concentrations of these two complexes change with irradiation time. As can be seen from Table 10-1, the reaction rate is slower in the bromide complex than the chloride complex. As a larger amount of light is absorbed in the case of the bromide complex, the observed decrease in the rate must then result from the rate of the photoreduction of the Au^{3+} to Au^{2+} in the complex with the solvent. This could also be a result of the steric effect due to the larger size of the bromide ion compared with the chloride ion.

Table 10-1: *Comparison of the reduction rate of Au^{3+} using Filter A in $HAuCl_4$ and $HAuBr_4$*

Species	Rate
$HAuCl_4$	-0.535 ±0.039
$HAuBr_4$	-0.113 ±0.009

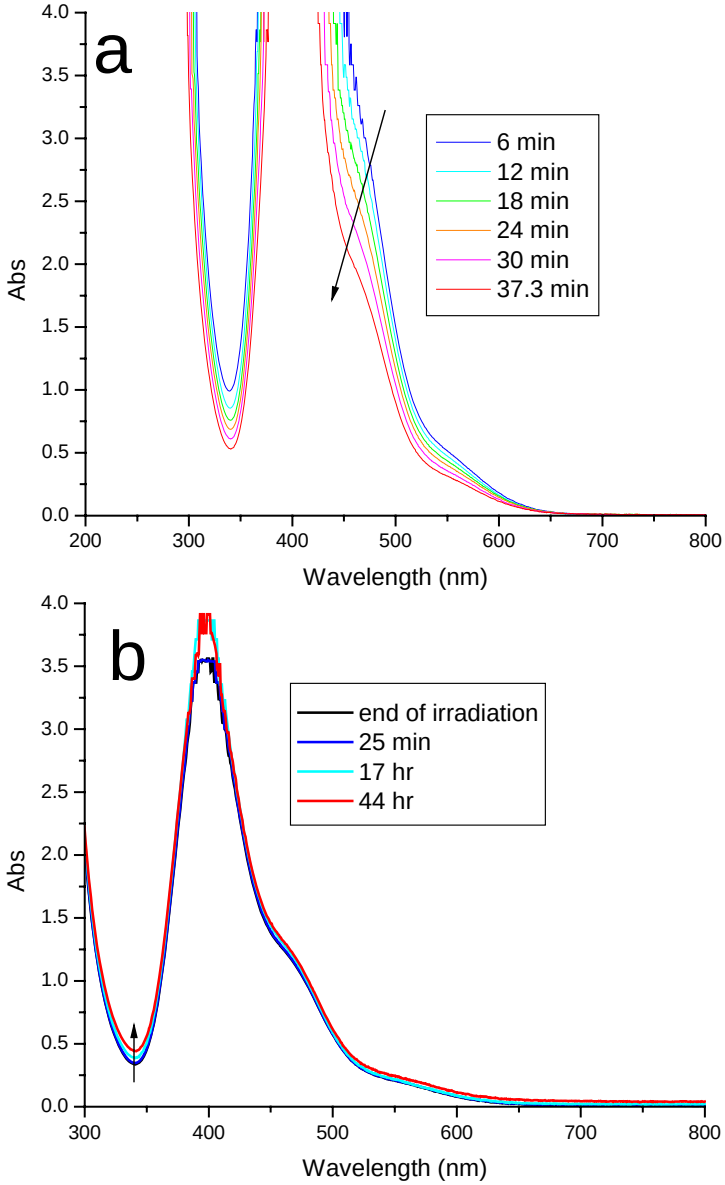

Figure 10-2: *Changes in the absorption spectrum of $HAuBr_4$ solutions with irradiation as a function of time a) during irradiation b) after irradiation. The absence of a surface plasmon absorption in the region from 500-600nm suggests that $HAuBr_4$ does not form gold nanoparticles as rapidly as $HAuCl_4$.*

In the irradiation of $AuCl_4^-$, nanoparticle growth takes place as a function of time after the irradiation is ceased. Figure 10-2b shows the absorption spectrum of $AuBr_4^-$ after irradiation is stopped. The absorption intensity remains relatively constant with only a slight increase that is observed after two days. This strongly suggests that the disproportionation process that is responsible for the reformation of the $[Au^{(3+)}Cl_4]^-$ species absorption in the region is not taking place in the bromide complex. The absence of nanoparticle formation in this solution further confirms the previously proposed mechanism[1] for the chloride complex. Since there is no nanoparticles formed with the bromide complex, no surface acceleration of the different reactions involved in the formation of the nanoparticles takes place.

Effect of the Silver Ion on the Photochemical Reduction

We investigated the effect of adding silver ions before the solution is irradiated. Figure 10-3 shows the absorbance of a $HAuCl_4$ solution both with and without addition of silver ions during irradiation. Figure 10-3a is similar to that reported previously,[1] where the absorbance of $AuCl_4^-$ decreases, and then gold nanoparticles form after most of the $AuCl_4^-$ is reduced, as observed by the small absorption between 300-400nm when the plasmon resonance absorption of gold nanoparticles at 550nm increases. Figure 10-3b shows that when silver ions are added to this solution and the solution is irradiated under the same conditions, the yield of nanoparticles is much larger as measured by the intensity of the plasmon resonance of the gold nanoparticles between 500-600nm. Gold nanoparticles are formed in the first 6 minutes of irradiation with silver ions present instead of after 18 minutes without silver ions as seen in Figure 10-3. This is an increase in the rate by 300%.

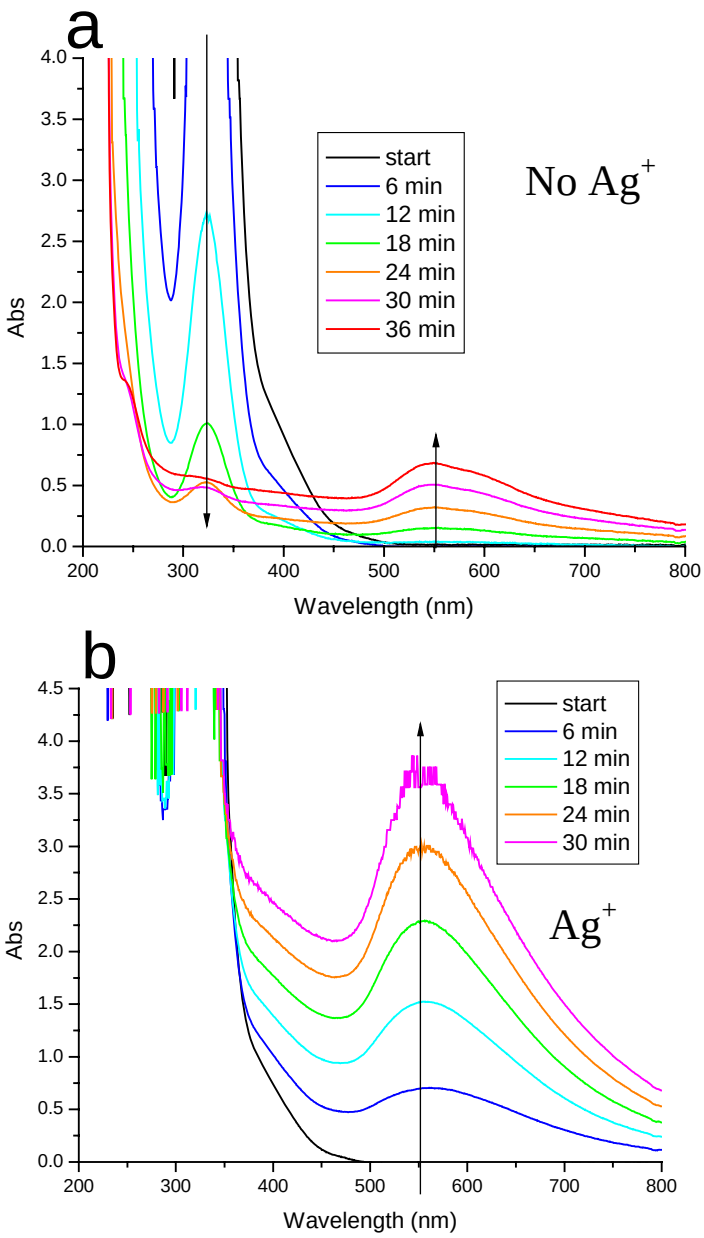

Figure 10-3: *Time dependence of the absorption spectra of $HAuCl_4$ solutions during irradiation a) without silver b) with silver nitrate ($3.5x10^{-4}M$)*

Another important difference in solutions with silver ions present is that the absorption of $[Au^{(3+)}Cl_4]^-$ does not decrease to the same extent as observed without silver ions present. The decrease of the $AuCl_4^-$ absorption is more difficult to detect when silver ions are present in the solution due to the large increase in the baseline absorption from the gold nanoparticles generated. Thus the concentration of $[Au^{(1+)}Cl_2]^-$ in solution is less than under previous conditions to form nanoparticles. This suggests that something is able to further reduce the $[Au^{(1+)}Cl_2]^-$ in solution to form gold nanoparticles with a lower concentration of Au^{1+} when silver ions are present in solution. This data suggests that the amount of gold necessary for nucleation of nanoparticles is different when silver is added to the solution. Silver is known to have a lower reduction potential than gold, [14] leading to the possibility that the silver ions are a source of heterogeneous nucleation.

To further investigate the effect of the silver ion in the gold solution, a solution with silver nitrate, PVP and ethylene glycol is irradiated without gold ions. The solution contains the same amount of silver nitrate as in the above studies. The absorption spectra of the silver ion solution are shown as a function of irradiation time in Figure 10-4a. The initial absorption of silver nitrate at 300nm is observed in Figure 10-4a at time zero. After only 6 minutes of irradiation the characteristic plasmon resonance at ~400nm of silver spheres[15] is observed in the solution. Continuing irradiation increases the intensity of this plasmon resonance absorption, and shifts the absorption spectrum to the blue, as more nanoparticles are nucleated with increasing irradiation time. The absorption spectrum blue-shifts due to the increasing number of small nanoparticles, which have a narrower absorption spectrum.[16] The absorption intensity is very low, due to the small

absorption coefficient of the nitrate group, and the small concentration of silver ions present in solution.

The effect of adding silver ions to a solution of $HAuBr_4^-$ is observed in Figure 10-4b. The first signs of gold nanoparticle formation are observed as the plasmon resonance of gold nanoparticles increases between 550nm and 600nm as opposed the behavior observed in Figure 10-2a, where only a decrease in intensity is observed with the same concentrations of gold. TEM results confirm that gold nanoparticles are formed when $AuBr_4^-$ is irradiated with silver ions in solution.

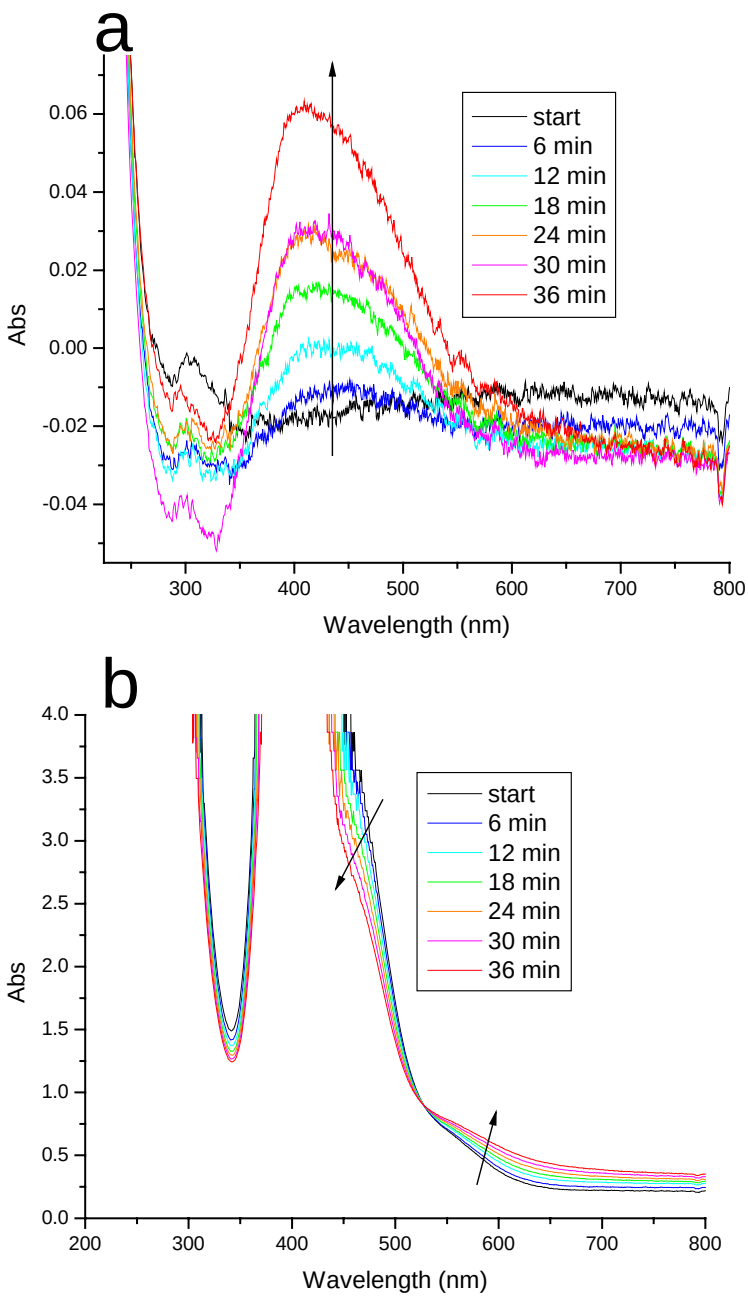

Figure 10-4: *Absorption of ethylene glycol solutions during irradiation of a) silver nitrate solution b) $HAuBr_4$ with the addition of silver nitrate*

Discussion of Results and Proposed Mechanism

The first principle observation is that replacing the Cl^- ions with Br^- ions in the starting material (tetrachloroauric acid) is found to have two effects: 1) to slow down the photoreduction rate of the starting material, and 2) to diminish the rate of nanoparticle formation. The second principle observation is the addition of silver ions is found to accelerate the rate of formation of the gold nanoparticles formed from either the tetrachloroauric acid or tetrabromoauric acid. These observations can be explained in terms of (and thus supports) the previously proposed mechanism[1] shown below.

$Au^{(3+)}X_4^- \xrightarrow{h\nu} [Au^{(3+)}X_4^-]^*$ (10.1) Excitation

$[Au^{(3+)}X_4^-]^* \xrightarrow{glycol} Au^{(2+)}X_3^- + X$ (10.2) Reduction

$2\ Au^{(2+)}X_3^- \longrightarrow Au^{(1+)}X_2^- + Au^{(3+)}X_4^-$ fast (10.3) Disproportionation

$2\ Au^{(1+)}X_2^- \longrightarrow Au^{(2+)}X_3^- + Au^0 + X^-$ slow (10.4) Disproportionation

$3\ Au^{(1+)}X_2^- \longrightarrow Au^{(3+)}X_4^- + 2\ Au^0 + 2\ X^-$ (10.5) Net Disproportionation

$Au^{+m} \xrightarrow{glycol} Au^0$ (+m: +3,+2,+1) (10.6) Glycol Reduction

$nAu^0 \longrightarrow (Au^0)_n$ rapid (10.7) Nanoparticle Formation

where X is either Cl or Br.

The rate of formation of the gold nanoparticles is determined by the rate of formation of the Au^0. This in turn is determined by the rate of the slow disproportionation process given by equation 10.4. The disproportionation reaction involves electron transfer between two gold ions complexed to halide ions. This bimolecular complex must involve a gold-gold bond. For example, the disproportionation reaction in equation 10.4 must involve the following bimolecular complex:

$$2(Au^{(1+)}X_2^-) \longrightarrow \begin{matrix}[^-X\text{-}Au^{(1+)}\text{-}X^-]^- \\ | \\ [^-X\text{-}Au^{(1+)}\text{-}X^-]^-\end{matrix} \longrightarrow X^- + Au^0 + [Au^{(2+)}X_3]^- \qquad (10.8)$$

First, since Br^- ion is larger in size than the Cl^- ion, there will be a large energy barrier to the formation of the gold-gold diamer. This decreases the concentration of the diamer complex and in turn decreases the concentration of bromide ions and Au^0 released through disproportion.

In support of the above explanation is the fact that the species Au_2Cl_6 is well known in the literature.[17-20] Although the Au_2Br_6 is reported to exist, the literature on this complex is less[17] suggesting that it is less stable or there is a larger barrier for its formation. The fact that the generation of a metal-metal bond can be formed even when chloride ions are attached to the gold suggest that a network structure of gold atoms can form which starts the process of nucleation of the metal nanoparticles. This is important in the formation of gold nanoparticles. Thus disproportion and nucleation are inhibited with the tetrabromoauric acid due to the inability of the gold ions to interact due to the large size of the bromide ions.

This mechanism is also useful to explain the effect of the silver ion. There are two possible reasons for the increase in the reduction rate of the gold complex in the presence of silver ions. The silver ions be a source of heterogeneous nucleation to increase the rate of formation of new nanoparticles. The silver ions can also remove the halide ions produced in equation 10.4 by forming insoluble silver halide complexes. This increases the formation of Au^0 due to shifting the equilibrium described in equation 10.4

by the removal of the halide ion from solution. This accelerates the formation of Au^0 and thus the formation of gold nanoparticles.

Figure 10-4a shows that the silver ions are quickly reduced in solution to form silver nanoparticles. This suggests that the silver ions can initiate heterogeneous nucleation by forming nuclei of gold and silver atoms for further generation of gold nanoparticles. No evidence of silver nanoparticle formation is observed in Figure 10-3b or 10-4b, but the intensity of the plasmon of silver nanoparticles is not large enough to be noticed above the baseline of the gold absorption. Silver also has a lower reduction potential,[14] and silver atoms in nanoparticles are known to be replaced by gold ions free in solution.[14, 21-25] Thus the gold ions in solution replace the silver ions to form gold nanoparticles increasing the rate of formation of gold nanoparticles.

The other possible mechanism that could account for the effect of silver ion is as follows. The silver ions can react with the halide ions formed in all the disproportionation reactions to from insoluble $AgCl_{(s)}$ or $AgBr_{(s)}$. The solubility product constant of silver chloride and silver bromide are $1.77x10^{-10}$ and $8.45x10^{-13}$, respectively.[26] This suggests that when silver ions are present in the solution, they complex with free halide ions in solution. When tetrachloroauric acid or tetrabromoauric acid is present in high concentration with the same ratio gold/silver used in this study, cloudy solutions are obtained immediately upon the addition of the silver ions. This confirms occurrence of the interaction of the silver ions and the halide ions in solution. Thus an equation can be added to the mechanism when silver is present in the solution.

$$Ag^+ + X^- \longrightarrow AgX_{(s)} \qquad \text{rapid} \quad (10.9) \quad \text{Precipitation w/ } Ag^+$$

The mechanism of the disproportionation reactions involves the production of halide ions together with the formation Au^0. The addition of Ag^+ ions to the solution removes some of the halide ions from solution, thus driving the equilibrium to the formation of Au^0. This in turns accelerates the formation of gold nanoparticles as observed experimentally.

The optical absorption of the different complexes is not responsible for the differing reaction behavior. Steric repulsion is proposed to lead to the difference in reactivity of the tetrachloroauric acid and tetrabromoauric acid. This also shows that the halide ions are attached to the gold ion throughout the reduction process and the release of the halide ions to the solution to form isolated gold atoms is a necessary step in the reaction to form nanoparticles. Thus, the disproportionation reaction is important not only after irradiation, but during irradiation. Silver ions increase the rate of reaction for the formation of gold nanoparticles. The gold bromide complex prevents the formation of nanoparticles by steric hindrance, which can be overcome by the presence of silver ions either through the presence of catalytic nuclei or by forming insoluble complexes that drive the disproportionation reaction to generate gold atoms.

Conclusions

It is found that the mechanism previously proposed can account for the two important effects observed in this study. The first effect is that while tetrachloroauric acid can photochemically form gold nanoparticles, tetrabromoauric acid cannot. The importance of the steric factor of the larger bromide ions in inhibiting the disproportion reaction is responsible for this observation. The acceleration in the rate of formation of the gold nanoparticle upon the addition of the Ag^+ to the solution is explained by the removal of the halide ions formed in the disproportion reaction. This shifts the equilibria

involved resulting in the formation of more of Au^0. Such increase in the Au^0 leads to a faster rate of formation of gold nanoclusters. It is also possible that the silver and gold atoms are forming nuclei through heterogeneous nucleation, increasing the rate of formation of gold nanoparticles.

References

1. Eustis, S.; Hsu, H.-Y.; El-Sayed, M. A., Gold Nanoparticle Formation from Photochemical Reduction of Au3+ by Continuous Excitation in Colloidal Solutions. A Proposed Molecular Mechanism *J. Phys. Chem. B* **2005,** 109, (11), 4811-4815.

2. Rich, R. L.; Taube, H., The Induced Exchange of Cl^- and $AuCl4^-$. Evidence for Au(II). *J. Phys. Chem.* **1954,** 58, (1), 6-11.

3. Baxendale, J. H.; Koulkrd-Pujo, A. M., Une Etude Par Radiolyse Pulsee Sur L'Espece Transitoire Au II. *J. Chim. Phys.* **1970,** 67, 1602-1607.

4. Bard, A. J.; Parsons, R.; Jordan, J., *Standard Potentials in Aqueous Solution.* Marcel Dekker, Inc.: New York, 1985.

5. Gammons, C. H.; Yu, Y.; Williams-Jones, A. E., The disproportionation of gold(I) chloride complexes at 25 to 200^{o}C. *Geochim. Cosmochim. Acta* **1997,** 61, (10), 1971-1983.

6. Lingane, J. J., Standard Potentials of Half-Reactions Involving +1 and +3 Gold in Chloride Medium. Equilibrium Constant of the Reaction AuCl4- +2Au +Cl- = 3AuCl2-. *J. Electroanal. Chem.* **1962,** 4, 332-342.

7. Gachard, E.; Remita, H.; Khatouri, J.; Keita, B.; Nadjo, L.; Belloni, J., Radiation-induced and chemical formation of gold clusters. *New. J. Chem.* **1998**, 1257-1265.

8. Chakravorty, A., U.V. Spectrum of $KAuCl_4$. *Naturwissenschaften* **1961,** 48, 375.

9. Chakravorty, A., Comments on the Colour of Alkyl-Gold(III) Complexes. *Naturwissenschaften* **1961,** 48, 643.

10. Gangopadhayay, A. K.; Chakravorty, A., Charge Transfer Spectra of Some Gold (III) Complexes. *J. Chem. Phys.* **1961,** 35, (6), 2206-2209.

11. Almgren, L., The Stability Constants of Mixed Chloro-Bromo-Aurate (III) Complexes. *Acta. Chem. Scand. A* **1971,** 25, (10), 3713-3720.

12. Elding, L. I.; Gronong, A.-B., Kinetics, Mechanism and Equilibria for Halide Substitution Processes of Chloro Bromo Complexes of Gold(III). *Acta. Chem. Scand. A* **1978,** 32, (9), 867-877.

13. Pouradier, J.; Coquard, M., Électrochimie des sels D'Or V.-Complexes Mixtes Aurichlorobromure. *J. Chim. Phys.* **1966,** 63, (7-8), 1072-1078.

14. Sun, Y.; Xia, Y., Mechanistic Study on the Replacement Reaction between Silver Nanostructures and Chloroauric Acid in Aqueous Medium. *J. Am. Chem. Soc.* **2004,** 126, (12), 3892-3901.

15. Eustis, S.; El-Sayed, M. A., Why Gold Nanoparticles Are More Precious than Pretty Gold: Noble Metal Surface Plasmon Resonance and its Enhancement of the Radiative and Nonradiative Properties of Nanocrystals of Different Shapes. *Chem. Soc. Rev.* **2006,** 35, (3), 209-217.

16. Kreibig, U.; Fragstein, C. v., The Limitation of Electron Mean Free Path in Small Silver Particles. *Z. Physik* **1969,** 224, 307-323.

17. Cotton, F. A.; Wilkinson, G., *Advanced Inorganic Chemistry*. John Wiley & Sons: New York, 1988; p 948-950.

18. Schulz, A.; Hargittai, M., Structural Variations and Bonding in Gold Halides: A Quantum Chemical Study of Monomeric and Dimeric Gold Monohalide and Gold Trihalide Molecules, AuX, Au_2X_2, AuX_3, and Au_2X_6 (X=F, Cl, Br, I). *Chem. (European)* **2001,** 7, (17), 3657-3670.

19. Janssen, E. M. W.; Pohlmann, F.; Wiegers, G. A., The phase diagram of the gold-chlorine system. *J. Less Common Metals* **1976,** 45, (2), 261-273.

20. Adams, D. M.; Churchill, R. G., Vibrational spectra of halogen-bridged systems. II. Au2Cl6, Al2Br6, Al2I6, and In2I6. *J. Chem. Soc. A Inorg. Phys. Theor.* **1968,** 9, 2141-2144.

21. Sun, Y.; Xia, Y., Increased Sensitivity of Surface Plasmon Resonance of Gold Nanoshells Compared to That of Gold Solid Colloids in Response to Environmental Changes. *Anal. Chem.* **2002,** 74, (20), 5297-5305.

22. Sun, Y. G.; Xia, Y. N., Shape-controlled synthesis of gold and silver nanoparticles. *Science* **2002,** 298, (5601), 2176-2179.

23. Sun, Y.; Mayers, B.; Xia, Y., Metal Nanostructures with Hollow Interiors. *Adv. Mater.* **2003,** 15, (7-8), 641-646.

24. Sun, Y.; Xia, Y., Multiple-Walled Nanotubes Made of Metals. *Adv. Mater.* **2004,** 16, (3), 264-268.

25. Metraux, G. S.; Cao, Y. C.; Jin, R.; Mirkin, C. A., Triangular Nanoframes Made of Gold and Silver. *Nano Lett.* **2003,** 3, (4), 519-522.

26. Lide, D. R., *CRC Handbook of Chemistry and Physics*. 80th ed.; CRC Press LLC: Washington, DC, 1999.

VITA: SUSIE EUSTIS

EDUCATION:

Ph. D*. *Georgia Institute of Technology, Physical Chemistry Major, expected August 2006 GPA: 3.65

B. S. Rochester Institute of Technology (RIT) with Highest Honors, Chemistry Major (American Chemical Society Certified) May 2000 GPA: 3.8

RESEARCH POSITIONS HELD (see publications and presentations at end)

Ph. D. research with ***Dr. M.A. El-Sayed (Georgia Tech)*** 2002-present, focused on synthesis and optical properties of gold and silver nanoparticles of different shapes

Ph. D. research with ***Dr. L.A. Lyon (Georgia Tech)*** 2000-2002, focused on assembly of soft colloidal nanoparticles

Teaching Assistant for quantitative analysis lab 2001 and advanced analytical chemistry lab 2002

Eastman Kodak Company, 2000 research intern, fluorescence spectroscopy of polymer film surfaces

Teaching Assistant for undeclared science seminar (RIT) 1999-2000

Participated in ***REU at CERN (NSF sponsored undergraduate research experience) Summer 1999*** in Geneva Switzerland

B. S. research with ***Dr. A. Langner (RIT)*** on the thermal and kinetic analysis of poly(ethylene glycol) and mechanical and optical properties of PEN 1998-1999

B. S. research with ***Dr. L. Tubbs (RIT)*** and ***Dr. D. Mathiason (RIT)*** on the analysis and applications of chemical decomposition data showing importance of correlations 1998

ACADEMIC AWARDS

Received the House-Flaschka-Ashby Research Award (Georgia Tech Chemistry) 2005

Named RIT Outstanding Scholar (RIT) 1999-2000

Chemistry Achievement Award for Seniors (ACS) 1999-2000

Undergraduate Award in Analytical Chemistry (RIT Chemistry) 1999-2000

Received James Wilson Memorial Scholarship (RIT) 1999-2000

Admitted to Phi Kappa Phi Honorary Society 1999-2000

Nominated for Senior Student Delegate (RIT College of Science) 1999-2000

Received Orange and Black Award (RIT Women's Hockey) 1999-2000

Physical Chemistry Undergraduate Student of the Year (RIT Chemistry) 1998-1999

Admitted to Golden Key National Honors Society 1997

Received Honorable Mention Ellingson Award (Scholastic Achievement by an Athlete, RIT Athletics) 1998-1999

Named to Dean's List Every Academic Quarter at RIT (RIT College of Science) 1996-2000

National Honor Society 1995

RESEARCH INTERESTS

1. Synthesis and properties of gold and silver nanoparticles
2. Understanding the mechanism of photochemical and chemical synthesis of nanoparticles
3. Using analytical tools to determine properties such as TEM, SEM, FTIR, Raman and optical spectroscopy
4. Modeling experimental results
5. Collaboration with international collaborators and undergraduate students

PERSONAL INTERESTS

Varsity Women's Ice Hockey Team (RIT), 1996-1997, 1998-2000
Started Women's Hockey Team at Lexington High School, MA 1994
Captain of Women's Hockey Team (LHS), 1994-1996
Engineering House (RIT), 1997-1999
Viola player-RIT Philharmonic Orchestra 2000
University of Rochester Symphony Orchestra 1997-1998
LHS String Orchestra 1992-1996
Participated in Foreign Exchange to Spain 1994.
Church Choir

SUPERVISED STUDENTS IN RESEARCH LABORATORY

Middle school student, Matlock Rogers, Fall 2003, used FTIR to determine the concentration of DEET in commercial insect repellent, went to national science fair for middle school students

College Undergraduate, Hsan-Yin Hsu (National Nanotechnology Infrastructure Network (NNIN) fellow, Summer 2004) worked on photochemical generation of gold nanoparticles, co-author on published paper

College Undergraduate, Jacob Hughey (National Nanotechnology Infrastructure Network (NNIN) fellow, Summer 2005) worked on synthesis of metal shells on silica nanoparticles by different techniques

OTHER POSITIONS

Member of Board of Directors WinterGreen Research, Inc. 1997-present
Research Associate for WinterGreen Research, Inc. 1992-present

PUBLICATIONS

1. J. D. Debord, S. Eustis, S. B. Debord, M. T. Lofye and L. A. Lyon, "Color-tunable colloidal crystals from soft hydrogel nanoparticles", *Adv. Mater.*, 14(9), **2002**, 658-662.
2. R. P. Apkarian, E. R. Wright, V. A. Seredyuk, S. Eustis, L. A. Lyon, V. P. Conticello and F. M. Menger, "In-lens cryo-high resolution scanning electron microscopy: Methodologies for molecular imaging of self-assembled organic hydrogels", *Microsc. Microanal.*, 9(4), **2003**, 286-295.
3. S. Eustis, G. Krylova, A. Eremenko, N. Smirnova, A. W. Schill and M. A. El-Sayed, "Growth and fragmentation of silver nanoparticles in their synthesis with a fs laser and CW light by photo-sensitization with benzophenone", *Photochem. Photobio. Sci.*, 4(1), **2005**, 154-159.

4. S. Eustis, H.Y. Hsu, and M. A. El-Sayed, "Gold Nanoparticle Formation from Photochemical Reduction of Au^{3+} by Continuous Excitation in Colloidal Solutions; A Proposed Molecular Mechanism" *J. Phys. Chem. B*, 109(11), **2005,** 4811-4815. **#10 most accessed paper Jan.-Jun. 2005 J. Phys. Chem. B**
5. S. Eustis, M. A. El-Sayed, "The Aspect Ratio Dependence of the Enhanced Fluorescence Intensity of Gold Nanorods: Experimental and Simulation Study" *J. Phys. Chem. B* 109(34), **2005,** 16350-16356.
6. G. V. Krylova, A. M. Eremenko, N. P. Smirnova, S. Eustis, "Photochemical Preparation of Nanoparticles of Ag in Aqueous-Alcoholic Solutions and on the Surface of Mesoporous Silica" *Theor. Exper. Chem.* **2005,** 41, (2), 105-110.
7. G. Krylova, A. Eremenko, N. Smirnova, S. Eustis, "Structure and Spectra of Photochemically Obtained Nanosized Silver Particles in Presence of Modified Porous Silica" *Intern. J. Photoenergy* **2005,** 7, (4), 193-198.
8. S. Eustis, and M.A. El-Sayed, "The Aspect Ratio Dependence of the Fluorescence of Gold Nanorods: An Experimental and Theoretical Study" *MRS Proceedings Fall 2005*, **2005**. Accepted.
9. S. Eustis, G. Krylova, N. Smirnova, A. Eremenko, C. Tabor, W. Huang, and M.A. El-Sayed, "Using Silica Films and Powders Modified with Benzophenone to Photoreduce Silver Forming Nanoparticles" *J. Photochem. Photobiol. A,* **2006**. In press.
10. S. Eustis, and M.A. El-Sayed, "Why Gold Nanoparticles Are More Precious than Pretty Gold: Noble Metal Surface Plasmon Resonance and its Enhancement of the Radiative and Nonradiative Properties of Nanocrystals of Different Shapes" *Chem. Soc. Rev.*, **2006,** 35, (3), 209-217.

LIST OF PRESENTATIONS

1. Gordon Research Conference: Electronic Processes In Organic Materials, August 2006, Poster: Molecular mechanism of gold nanoparticle formation by photochemical reduction of Au3+ in ethylene glycol: Disproportionation reactions, Susie Eustis and Mostafa El-Sayed
2. KAKENHI International Symposium on "Molecular Nano Dynamics", June 2006, Poster: Dependence of the Enhanced Fluorescence Emission on the of Size Gold Nanorods: Experimental and Simulation Study, Susie Eustis and Mostafa El-Sayed
3. ACS National Meeting, March 2006, Poster: Enhanced Fluorescence from Gold Nanorods: Experimental and Simulation Study, Susie Eustis and Mostafa El-Sayed
4. MRS National Meeting, November 2005, Oral: The Aspect Ratio Dependence of the Fluorescence of Gold Nanorods: An Experimental and Theoretical Study, Susie Eustis and Mostafa A. El-Sayed
5. Gordon Research Conference: Clusters, Nanocrystals & Nanostructures, August 2005, Poster: Surface Plasmon Enhancement of the Fluorescence of Gold Nanorods of Different Aspect Ratios, Susie Eustis and Mostafa El-Sayed
6. Georgia Tech Conference on Nanoscience and Nanotechnology, November 2004, Poster: Photochemical Reduction of Metal Salt in Ethylene Glycol with Control Over Nanoparticle Shape, Susie Eustis, Hsan-Yin Hsu, and Mostafa El-Sayed

7. SERMACS, November 2003, Poster: The Dependence of Laser Photothermal Melting Energy Threshold and the Fluorescence of Gold Nanoparticles, Susie Eustis and Mostafa El-Sayed
8. Mostafa El-Sayed's Birthday, May 2003, Poster: Laser Melting of Gold Nanorods, Susie Eustis, Stephan Link and Mostafa El-Sayed
9. SERMACS, September 2001, Poster: Optical Properties of Wavelength Tunable Colloidal Crystals, Susie Eustis, Saet Byul Kong, Justin D. Debord and L. Andrew Lyon
10. Georgia Tech Conference on Nanoscience and Nanotechnology, September 2001, Poster: Optical Properties of Wavelength Tunable Colloidal Crystals, Susie Eustis, Justin D. Debord, Saet Byul Kong, and L. Andrew Lyon

Presenting Author